DEPARTAMENTO DE BIOLOGÍA CELULAR Y ANATOMÍA PATOLÓGICA
FACULTAD DE MEDICINA

IMPLICACIÓN DE LOS FILAMENTOS DE ACTINA EN LA ARQUITECTURA, HOMEOSTASIS Y TRÁFICO DE SALIDA DEL APARATO DE GOLGI
Y
ESTUDIO DE LA FORMACIÓN Y DEGRADACIÓN DE UN AGRESOMA DE ACTINA

El director — Gustavo Egea

El autor — Francisco Lázaro Diéguez

Tesis presentada por Francisco Lázaro Diéguez
dirigida por el Dr. Gustavo Egea
para optar al título de Doctor por la Universidad de Barcelona

Barcelona, Marzo de 2008

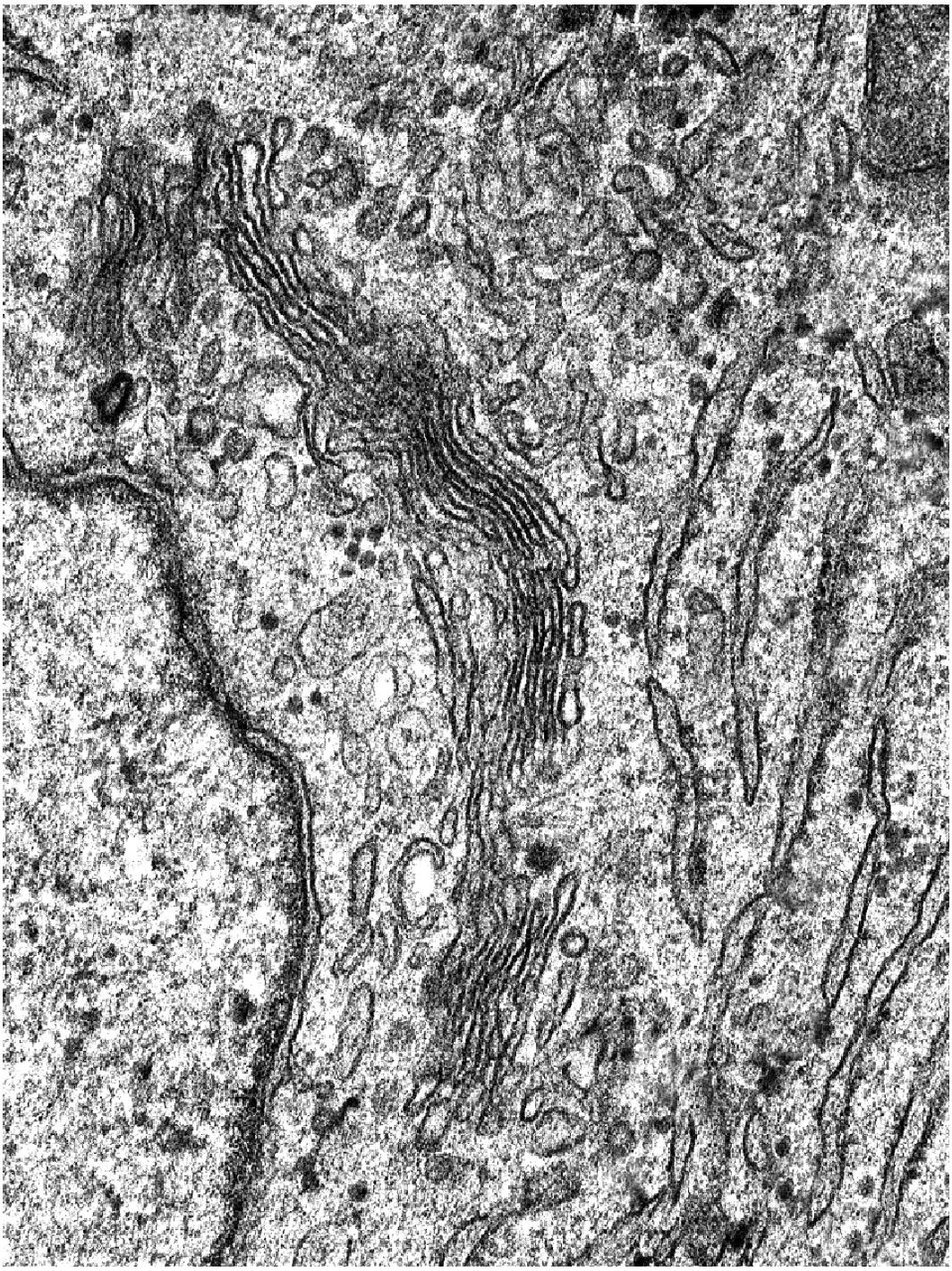

- RESULTADOS -

Trabajo 1

ESTUDIO COMPARATIVO DEL IMPACTO DEL CITOESQUELETO DE ACTINA SOBRE LA MORFOLOGÍA Y SUPERFICIE CELULAR EN CÉLULAS DE MAMÍFERO EN RESPUESTA A LAS TOXINAS DE ACTINA

El citoesqueleto de actina está directamente implicado en la determinación y mantenimiento de la morfología celular. Las toxinas de actina provocan un cambio drástico en la morfología celular, así cuando las células cultivadas en monocapa son expuestas a estas toxinas invariablemente pierden la adhesión al sustrato y se produce un cambio en su fenotipo, pasando de una morfología extendida fusiforme a una morfología esférica. Una de las toxinas utilizadas frecuentemente para interferir en procesos celulares en los que intervienen los MFs es la CyD, la cual produce su despolimerización. En los últimos años se han descubierto multitud de nuevas toxinas que bloquean/despolimerizan los MFs (LtB, MyB y C2) y otras que los polimerizan/estabilizan (Jpk). Estás toxinas son de gran utilizad para realizar estudios de la implicación del los MFs en distintos procesos biológicos como la formación de filopodios y lamelipodios en células en movimiento/migración, tráfico de membrana, adhesión celular o infección por patógenos.

En este trabajo realizamos un estudio comparativo mediante epifluorescencia y microscopia electrónica de barrido en distintos tipos celulares (Hela, NRK y Vero) de las alteraciones provocadas por distintas toxinas de actina sobre la organización del citoesqueleto de actina y la morfología celular. Se observó que tanto las alteraciones de la red de MFs como los cambios morfológicos y perturbación de la superficie celular son variables y dependientes del tipo celular, toxina de actina utilizada y concentración/tiempo de exposición a ésta. Estos resultados implican con claridad a los MFs en el mantenimiento de la morfología celular.

Comparative study of the impact of the actin cytoskeleton on cell shape and membrane surface in mammalian cells in response to actin toxins

Francisco Lázaro-Diéguez and Gustavo Egea*

Dept. de Biologia Cel·lular i Anatomia Patològica, Facultat de Medicina, and Instituts de Nanociències i Nanotecnologia (IN^{2}UB) and d'Investigacions Biomèdiques August Pi i Sunyer (IDIBAPS), Universitat de Barcelona, 08036 Barcelona (Spain).

We performed a correlative epifluorescence and scanning electron microscopy study of the morphological alterations, both in the actin cytoskeleton organization and in the cellular shape and surface morphology of HeLa, NRK and Vero cells, caused by a variety of actin toxins. To this end, we used actin toxins that depolymerize (cytochalasin D, latrunculin B, and Clostridium botulinum C2 toxin) or stabilize (jasplakinolide) filamentous actin. By immunofluorescence we observed that the resulting actin cytoskeleton alterations were cell type- and toxin-dependent. Analysis of the cell shape and membrane surface by scanning electron microscopy also showed that the actin disruption produced variable changes depending on the cell type and the actin toxin used. Therefore, our results indicate that actin directly participates both in the maintenance of cell shape and in membrane surface morphology, revealing significant differences depending on the actin toxin and cell type involved.

Keywords: Actin, cytoskeleton, actin toxins, cell surface, scanning electron microscopy

1. Introduction

The mechanical properties of the cytoskeleton (actin, microtubules and intermediate filaments), as well as its organization, largely determine the morphology and machinery of animal cells [1]. The most direct evidence that the cytoskeleton is necessary for the establishment and maintenance of cell morphology stems from the utilization of various pharmacological agents and natural toxins. This is particularly true for actin filaments. Thus, it has long been known that the use of cytochalasin B induces the reversible loss of cell shape in mouse salivary gland epithelial cells, with the consequent abrogation of gland morphogenesis [2]. Another pioneering example involved the same toxin in cultured neurons, wherein it halted axon elongation as growth cones rounded up [3].

Numerous new actin-disrupting agents or actin toxins have been reported in recent years. [4,5,6]. Moreover, they have been used extensively in a variety of studies examining the potential involvement of either the actin cytoskeleton organization (see below) or actin dynamics (depolymerization/polymerization cycle), or both, in various biological functions, including the formation of filopodia and lamellipodia in cell movement [7], membrane trafficking [8,9,10], podosome and invadopodium formation [11,12,13], cell adhesion [14,15,16], pathogen infection [17,18], neurite extension, and spine formation [19,20,21,22,23].

In animal cells there are several organizational levels of actin filaments or microfilaments: (i) antiparallel arrays, which occur in stress fibres, and which are homologous to the myofibrillar organization seen in skeletal and cardiac muscles; (ii) parallel arrays, which form cell surface protrusive structures such as microspikes and filopodia; (iii) dendritic arrays, which form polarized and branched short actin filaments that give rise to plasma membrane extension(s) known as lamellipodium (a); and (iv) isotropic microfilament arrays localized beneath the plasma membrane and attached to

* Tel.: (+34)93-4021909. Fax: (+34)93-4021907. E-mail: gegea@ub.edu

transmembrane proteins via actin-binding proteins. The usual and most characteristic actin cytoskeleton organization observed in a steady state in animal cells is stress fibre organization (see Fig. 1), which can be easily observed by using phalloidin tagged to tetramethyl rhodamine isothiocyanate (TRITC) or fluorescein isothiocyanate (FITC) [24].

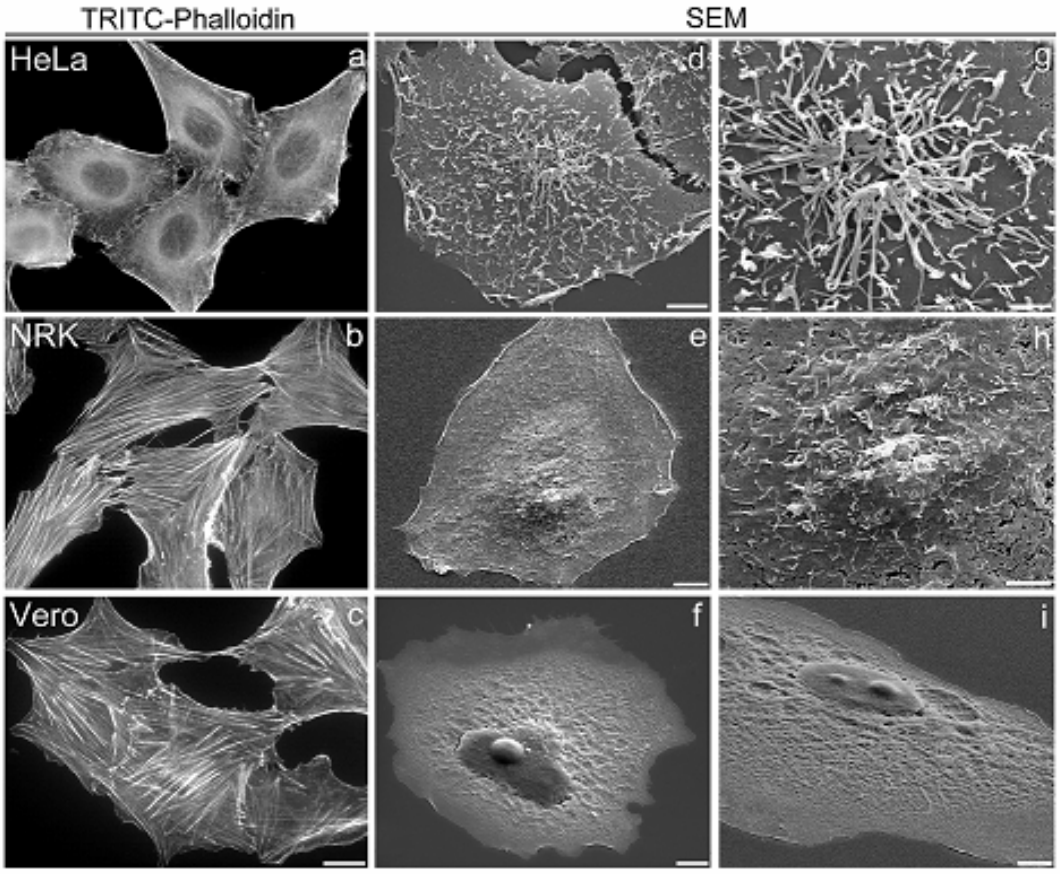

Fig. 1. Fluorescence (a-c) and scanning electron microscopy (SEM) (d-i) imagery of the actin stress fibre organization stained with TRITC-phalloidin (a-c), as well as of the cell shape and cell membrane surface (d-i) in HeLa (a, d, g), NRK (b, e, h), and Vero (c, f, i) cells. Scale bar, 10 μm (a-c), 5 μm (d-f, i) 2 μm (g,h).

Whereas cell shape was long thought to be determined by the (actin) cytoskeleton crossing the cytoplasm and undergoing translocation to the underside of the cellular membrane, this hypothesis has now been complemented not only by the recent discovery of BAR- or F-BAR/EFC-domain-containing membrane-deforming proteins, for example, WASP-WIP complex [25], but also by the contribution of endocytosis, exocytosis and cytokinesis processes.

The present study comprises a comparative examination of how actin cytoskeleton organization, as well as cell shape and the membrane surface, undergo alterations in different mammalian culture cell lines as a result of various natural toxins that depolymerize or stabilize the filamentous actin. The actin-depolymerizing toxins we used include cytochalasin D (CyD), latrunculin B (LtB), and botulinum C2 toxin (C2). Cytochalasins block the barbed-end of actin filaments, thereby preventing microfilament growth [26]. However, latrunculins and botulinum C2 toxin sequester [27,28] and ADP-rybosylates [29,30] G-actin monomers, respectively, giving rise to G-actin monomers that cannot be incorporated into the growing microfilament without altering the intrinsic depolymerization activity that occurs in the pointed-end of the filament [31]. Consequently, microfilaments depolymerize and the actin cytoskeleton

collapses. At the same time, we have used the actin-stabilizing toxin jasplakinolide (Jpk), which binds to the filamentous actin competing with phalloidin for the same location [32].

2. Procedures

2.1. Cell cultures

NRK, HeLa, and Vero cells were grown in Dulbecco's modified Eagle's medium (DMEM). This was supplemented with 10 % foetal bovine serum (FBS), penicillin (100 U/ml), streptomycin (100 µg/ml), L-glutamine (2 mM), and MEM sodium pyruvate (1 mM). Cell cultures were maintained at 37 °C in a humidified CO_2 (5%) atmosphere.

2.2. Actin toxin treatments

Cells were grown on 10 mm diameter glass coverslips at a density of 2 x 10^6 cell/ml. CyD was used at 1 µM for 60 min, LtB at 500 nM for 45 min, and Jpk at 500 nM for 45 min; all were diluted in supplemented DMEM at 37 ºC. The binary botulinum C2 toxin contains two compounds: the membrane-binding subunit (C2II) and the ADP-ribosylation enzyme subunit (C2I). Thus, for C2 toxin experiments, cells were first rinsed twice with DMEM without FBS, and then incubated with 200 ng/ml of C2II plus 100 ng/ml of C2I diluted in DMEM with low FBS (0.5 %) at 37 ºC for several hours. At the end of each actin toxin treatment, cells were quickly rinsed, fixed, and stained for filamentous actin as described above.

2.3. TRITC-phalloidin staining

Visualization of the actin cytoskeleton was performed using TRITC-phalloidin. Control and toxin-treated cells (see above) were quickly rinsed in warm phosphate buffer saline (PBS; 0.01 M phosphate buffer, 0.15 M NaCl, pH 7.4) and fixed with 4 % paraformaldehyde in PBS for 15 min at room temperature. Thereafter, cells were washed with PBS and permeabilized for 10 min at room temperature with 0.1 % saponin in PBS containing 1 % BSA. Cells were incubated for 20 min at room temperature with 10 µg/ml TRITC-phalloidin in PBS containing 1 % BSA, extensively washed with PBS, and mounted in Mowiol. Cells were observed with a BX60 Olympus epifluorescence microscope equipped with an Orca-ER cooled CCD Hamamatsu camera.

2.4. Scanning electron microscopy

Control and actin toxin-treated NRK, HeLa, or Vero cells were quickly rinsed in cacodylate buffer (0.1 M, pH 7.4) and fixed with 2.5% glutaraldehyde in cacodylate buffer for 60 minutes at room temperature. Cells were then thoroughly washed with cacodylate buffer and incubated for 5 min with tannic acid (1 %) in cacodylate buffer. Subsequently, cells were dehydrated in a graded series of ethanol, critical point dried with a Polaron CPD 7501 system, mounted, and coated with gold in a Bio-Rad SC510 sputter coater. All samples were observed under the same kilovolt and electron beam current conditions using an Hitachi S-2300 scanning electron microscope.

3. Results

HeLa, NRK, and Vero cells are three well-known cultured mammalian cells widely used to explore the potential contribution of both the actin cytoskeleton organization and actin dynamics in cellular functions; e.g., in our particular case, vis-a-vis membrane trafficking and organelle architecture [8]. Therefore, we first examined alterations in actin cytoskeleton organization and cell shape change using a

panel of actin toxins. To this end, we combined fluorescence and scanning electron microscopy techniques. Control HeLa, NRK, and Vero cells stained with TRITC-phalloidin showed a high density of actin stress fibres (Fig. 1, a-c), although these were thicker and more densely packed in NRK and Vero cells (Fig. 1, b and c, respectively). In the case of HeLa cells, the density and organization of stress fibres depended on the source of the cell line and on the passing number (not shown). In contrast, NRK and Vero cells were much more consistent in this respect.

We then examined cell shape and membrane surface morphology utilizing a scanning electron microscope (SEM) (Fig. 1, d-i). While the cell shape of the three cell lines was very similar (Fig. 1, d-f), cell surface morphology displayed significant differences (Fig. 1, g-i). For example, HeLa cells showed numerous long and thin filopodia-like structures, which accumulated to a significant degree in the membrane surface located just above the nucleus (Fig. 1, g). The membrane surface of NRK cells also exhibited extensions of the plasma membrane, although these were significantly shorter and more evenly distributed throughout the cell surface (Fig. 1, h). Conversely, Vero cells showed a smooth cell surface, in which the prominence of nucleus and nucleoli were easily observable (Fig. 1, f and i). Moreover, SEM also revealed that Vero cells were flatter than NRK and HeLa cells (compare panels d, e and f in Fig. 1), which correlated with recorded levels of actin stress fibre organization (Fig. 1, a, b, and c, respectively).

Thereafter, HeLa, NRK and Vero cells were treated with actin-depolymerising agents. Cytochalasin D (CyD)-treated cells (Fig. 2A) typically already exhibited dissolution of actin stress fibres after 10 min of treatment, proving even more severe over longer time periods (60 min). After 10 min of treatment, both NRK and Vero cells still contained some stress fibres but HeLa cells did not (for a comparison, see Fig. 2A; a, e and i). After 60 min, stress fibres were no longer visible, although numerous small and highly fluorescent cytoplasmic structures could be seen (Fig. 2A; b, f and j). Unlike NRK and Vero cells, the shape of HeLa cells remained relatively intact, with numerous small and variable sized globular structures or blebs appearing at the cell surface (Fig. 2A; c and d). Such a structure represents, in fact, a ballooning out of the plasma membrane when it detaches from the actin cortex [33]. Their appearance occurred concomitantly with the disappearance of short and long filopodia-like structures characteristic of untreated cells (Fig. 1; d and g). NRK cells showed blebs at the cell surface after 60 min of CyD treatment (Fig. 2A; h), although they were much smaller than those seen in HeLa cells (Fig. 2A; c, d). Strikingly, Vero cells displayed no particularly remarkable structures at the cell surface (Fig. 2A; k, l). Moreover, the cellular body retracted these leading thin and longer extensions as the toxin treatment was extended (compare at 10 and at 60 min), with Vero cells proving the more affected than NRK cells (Fig. 2A; k, l, and g, h, respectively).

Unlike the CyD treatment, the use of LtB or C2 toxin resulted in significant differences between NRK and Vero cells (Fig. 2B). Compared with the CyD treatment, LtB was more potent, since a similar depolymerized actin cytoskeleton organization, cell shape, and membrane surface alterations were already evident after 30 min, whereas CyD required 60 min (compare Fig. 2A; f and j with Fig. 2B; m and q). Strikingly, Vero cells showed several small lamellipodia (arrows in Fig. 2B; q and r, respectively). The formation of lamellipodia was practically absent in HeLa (not shown) and NRK cells. The depolymerization of the actin cytoskeleton by the C2 toxin required much longer time periods (2-4 h, depending on the toxin concentration used and the batch) (Fig. 2B; o, p, s, t), since this toxin slowly internalizes to endosomes and subsequently translocates to the cytosol, where it ADP-rybosylates G-actin. Vero cells seem to be more sensitive than NRK cells to C2 toxin, as the latter still contained some actin stress fibre after 3 h of C2 internalization (compare o and s in Fig. 2B,). Moreover, numerous C2 toxin-treated NRK cells displayed a long and large lamellipodium (arrow in Fig. 2B; o). In contrast, Vero cells collapsed with no stress fibres and exhibiting a general diffuse cytoplasmic fluorescent staining (Fig. 2B; s). Moreover, some thin and long extensions were easily recognizable in the SEM images (Fig. 2B; t). The body retraction in C2 toxin-treated Vero cells was extreme compared to that seen in NRK cells (compare panels p and t in Fig. 2B).

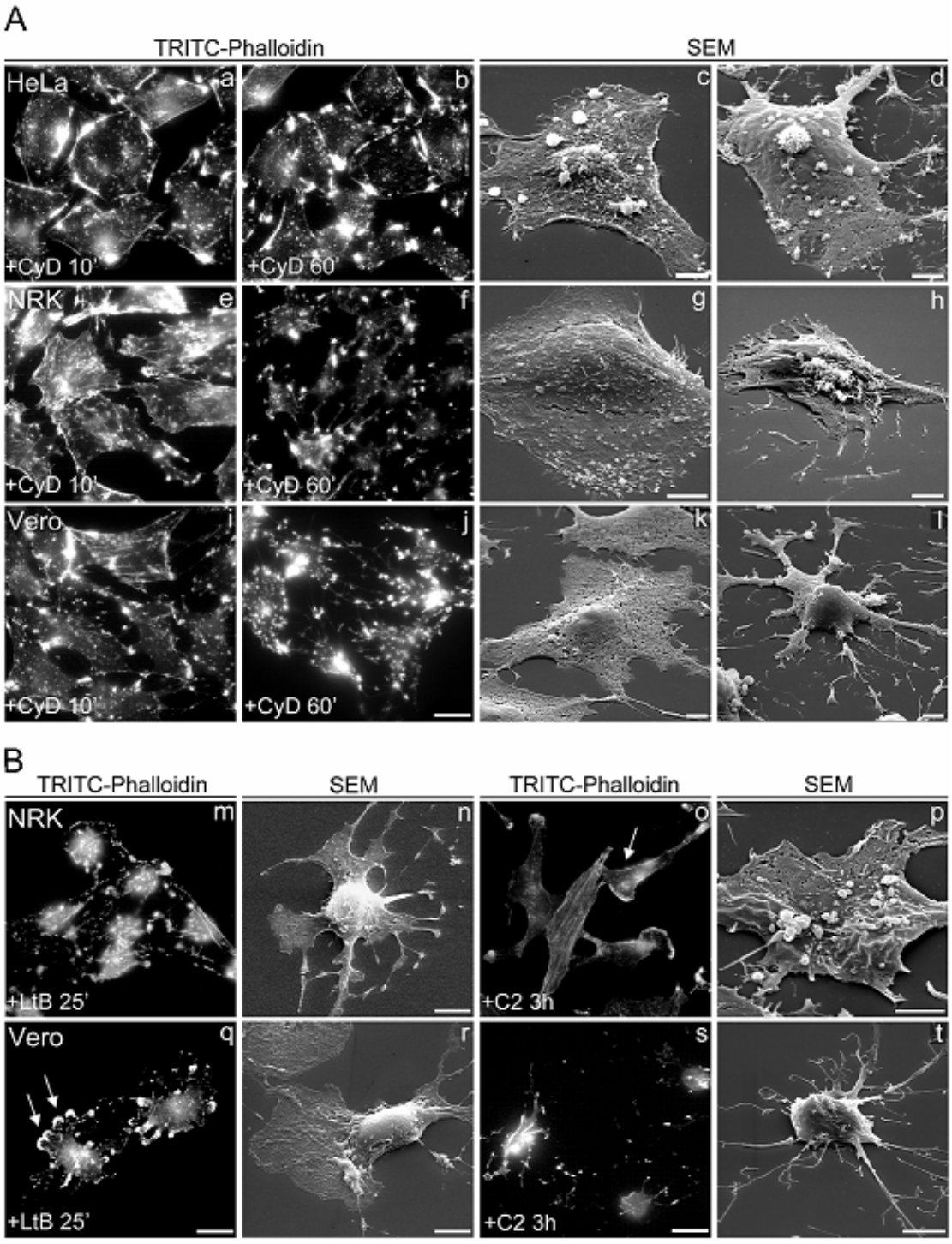

Fig. 2. (A) Actin cytoskeleton organization after staining with TRITC-phalloidin, and SEM images of HeLa, NRK and Vero cells treated with cytochalasin D (CyD) for 10 and 60 min. **(B)** The same procedure described in (A) though here NRK and Vero cells were treated with latrunculin B (LtB) for 25 min, or botulinum C2 toxin (C2) for 3 h. Scale bar, 10 μm (a,b,e,f,i,j,m,o,q,s), 5 μm (c,d,g,h,k,l,n,p,r,t).

Finally, we used jasplakinolide (Jpk) as an actin-stabilizing toxin (Fig. 3). Jpk-treated HeLa cells displayed a rapid dissolution of actin stress fibres after 30 min of toxin treatment (Fig. 3; a). After 60 min, the phalloidin staining was difficult to visualize due to the fact that Jpk occupied the same binding site as phalloidin in the actin filament (Fig. 3; b). HeLa cells maintained their cell shape relatively well; in addition, they displayed dorsal ruffles when viewed by SEM (Fig. 3; c and d, respectively), which can also be seen as strong fluorescent lines corresponding to the plasma membrane (Fig. 3; a). After short incubation periods with Jpk (30 min), both NRK and Vero cells still exhibited some stress fibres (Fig. 3; e and i, respectively), as well as changes in cell shape (Fig. 3; g and k, respectively). At longer incubation times (60 min), phalloidin staining was weak (Fig. 3; f, j) while cell shape was severely affected. Moreover, there were numerous globular membrane structures or blebs of variable size in both HeLa and NRK cells (Fig. 3; c, d, g, h), though none were ever noted in Vero cells (Fig. 3; k, l).

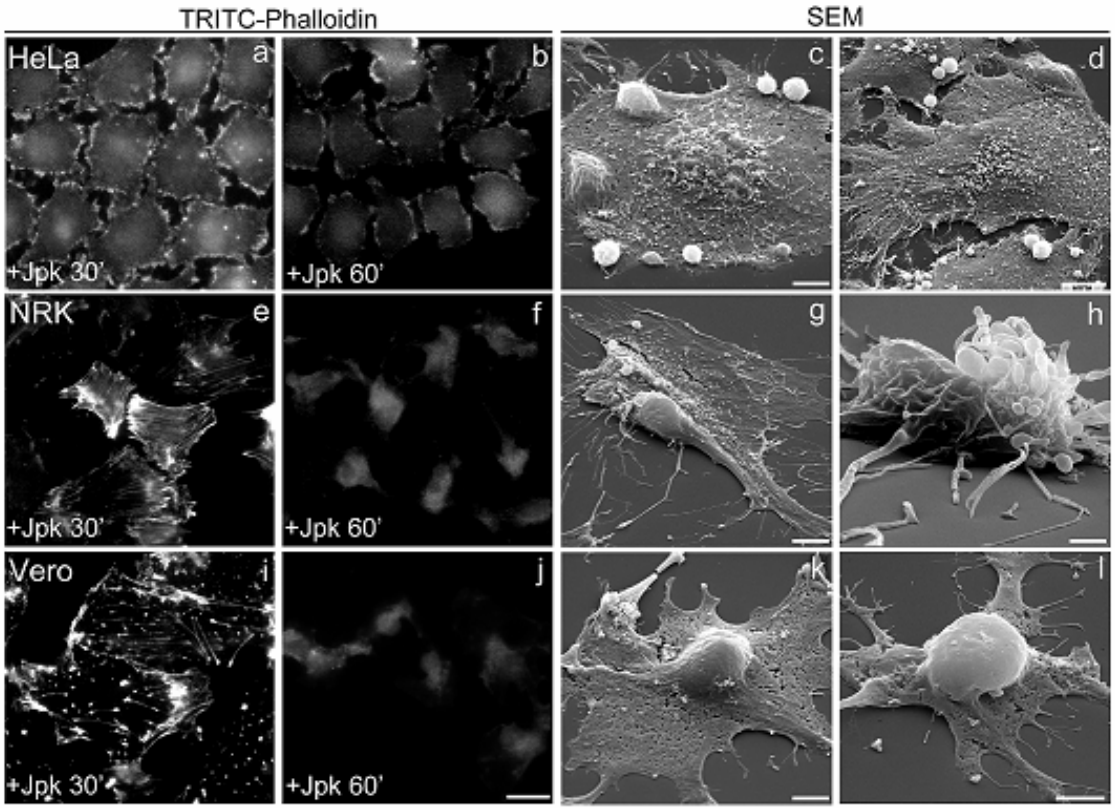

Fig. 3. Actin cytoskeleton organization after staining with TRITC-phalloidin, and SEM images of HeLa, NRK, and Vero cells treated with jasplakinolide (Jpk) for 30 or 60 min. Scale bar, 10 μm (a,b,e,f,i,j), 5 μm (c,d,g,k,l), 2 μm (h).

4. Concluding remarks

The experiments presented in this chapter resulted in the following findings: (i) actin poisons have different effects both on actin cytoskeleton organization and on cellular shape and membrane surface morphology; (ii) the severity of the alterations caused by actin toxins depends on the cell type used. As reported here, some mammalian cell lines are more sensitive to these actin toxins than others. We recommend the use of at least two actin-depolymerizing toxins (CyD and LtB), as well as one actin-stabilizer (Jpk) when investigating the potential contribution of actin on a determined cellular function.

Acknowledgements. We thank the Serveis Científico-Tècnics of the University of Barcelona (campus Casanova) for help with SEM. This work was supported by grants from MEC (BMC2006-00867/BMC and CONSOLIDER CSD2006-00012) to G.E.

References

[1] J. Howard. Mechanics of Motor Proteins and the Cytoskeleton Mechanics of Motor Proteins and the Cytoskeleton. Sinauer Associates, Sunderland, Massachusetts (2001).
[2] B.S. Spooner and N.K. Wessells. Effects of cytochalasin B upon microfilaments involved in morphogenesis of salivary epithelium. Proc Natl. Acad. Sci. U.S.A. Vol. 66 (1970), p. 360-361.
[3] N.K. Wessells, B.S. Spooner, J.F. Ash, M.O. Bradley, M.A. Luduena, E.L. Taylor, J.T. Wrenn and K. Yamaa. Microfilaments in cellular and developmental processes. Science Vol. 171(1971), p. 135-143.
[4] I. Spector, F. Braet, N.R. Shochet and M.R. Bubb. New anti-actin drugs in the study of the organization and function of the actin cytoskeleton. Microsc. Res. Tech. Vol. 47 (1999), p. 18-37.
[5] J.T. Barbieri, M.J. Riese and K. Aktories. Bacterial toxins that modify the actin cytoskeleton. Annu. Rev. Cell Dev. Biol. Vol. 18 (2002), p. 315-344.
[6] J.S. Allingham, V.A. Klenchin and I. Rayment I. Actin-targeting natural products: structures, properties and mechanisms of action. Cell Mol. Life Sci. Vol. 63 (2006), p. 2119-2134.
[7] J.A. Theriot and T.J. Mitchison. Actin microfilament dynamics in locomoting cells. Nature Vol. 352 (1991), p. 126-131.
[8] G. Egea, F. Lazaro-Dieguez, and M. Vilella. Actin dynamics at the Golgi complex in mammalian cells. Curr. Opin. Cell Biol. Vol. 18 (2006), 168-178.
[9] M. Kaksonen, H.B. Peng and H, Rauvala. Association of cortactin with dynamic actin in lamellipodia and on endosomal vesicles. J. Cell Sci. Vol. 113 Pt 24 (2000), p. 4421-4426.
[10] E. Smythe, K.R. Ayscough. Actin regulation in endocytosis. J. Cell Sci. Vol. 119 (2006), p. 4589-4598.
[11] Linder S, Aepfelbacher M. Podosomes: adhesion hot-spots of invasive cells. Trends Cell Biol. Vol. 13 (2003), p. 376-385.
[12] A.M. Weaver. Invadopodia: specialized cell structures for cancer invasion. Clin. Exp. Metastasis Vol. 23 (2006), p. 97-105.
[13] H. Yamaguchi and J. Condeelis. Regulation of the actin cytoskeleton in cancer cell migration and invasion. Biochim. Biophys. Acta Vol. 1773 (2007), p. 642-665.
[14] J. Gates and M. Peifer. Can 1000 reviews be wrong? Actin, alpha-Catenin, and adherens junctions. Cell Vol. 123 (2005), p. 769-772.
[15] P.J. Reddig and R.L. Juliano. Clinging to life: cell matrix adhesion and cell survival. Cancer Metastasis Rev. Vol. 24 (2005), p. 425-439.
[16] I. Delon and N. H. Brown. Integrins and the actin cytoskeleton. Curr Opin Cell Biol Vol. 19 (2007), p. 43-50.
[17] J.C. Patel and J.E. Galan. Manipulation of the host actin cytoskeleton by Salmonella--all in the name of entry. Curr. Opin. Microbiol. Vol. 8 (2005), p. 10-15.
[18] J. Pizarro-Cerda and P. Cossart. Subversion of cellular functions by Listeria monocytogenes. J. Pathol. Vol. 208 (2006), p. 215-223.
[19] J.S. da Silva and C.G. Dotti. Breaking the neuronal sphere: regulation of the actin cytoskeleton in neuritogenesis. Nat. Rev. Neurosci. Vol. 3 (2002), p. 694-704.
[20] M.D. Ledesma and C.G. Dotti. Membrane and cytoskeleton dynamics during axonal elongation and stabilization. Int. Rev. Cytol. Vol. 227 (2003), p. 183-219.
[21] P.D. Sarmiere and J.R. Bamburg. Regulation of the neuronal actin cytoskeleton by ADF/cofilin. J. Neurobiol. Vol. 58 (2004), p. 103-117.
[22] I. Majoul, T. Shirao, Y. Sekino and R. Duden. Many faces of drebrin: from building dendritic spines and stabilizing gap junctions to shaping neurite-like cell processes. Histochem. Cell Biol. Vol. 127 (2007), p. 355-361.
[23] S. Yamada and W. J. Nelson. Synapses: Sites of Cell Recognition, Adhesion, and Functional Specification. Annu. Rev. Biochem. (2007). In press.
[24] J. Small, K. Rottner, P. Hahne and K.I. Anderson. Visualising the actin cytoskeleton. Microsc. Res. Tech. Vol. 47 (1999), p. 3-17.
[25] T. Takenawa and S. Suetsugu. The WASP-WAVE protein network: connecting the membrane to the cytoskeleton. Nat. Rev. Mol. Cell Biol. Vol. 8 (2007), p. 37-48.
[26] JA. Cooper. Effects of cytochalasin and phalloidin on actin. J. Cell Biol. Vol. 105 (1987), p. 1473–1478

[27] I. Spector, N.R. Shochet, Y. Kashman and A. Groweiss. Latrunculins: novel marine toxins that disrupt microfilament organization in cultured cells. Science Vol. 219 (1983), p. 493-495.
[28] M. Coue, S.L. Brenner, I. Spector and E.D. Korn, Inhibition of actin polymerization by latrunculin A. FEBS Lett. Vol. 213 (1987), p. 316-318.
[29] K. Aktories, M. Barmann, I. Ohishi, S. Tsuyama, K.H. Jakobs and E. Habermann. Botulinum C2 toxin ADP-ribosylates actin. Nature Vol. 322 (1986), p. 390-392.
[30] K. Aktories and H. Barth, Clostridium botulinum C2 toxin--new insights into the cellular up-take of the actin-ADP-ribosylating toxin. Int. J. Med. Microbiol. Vol. 293 (2004), p. 557-564.
[31] T.D. Pollard, and W.C. Earnshaw. Cell Biology. Second Edition. W.B. Saunders, New York, NY. (2007).
[32] M.R. Bubb, A.M. Senderowicz, E.A. Sausville, K.L. Duncan and E.D. Korn. Jasplakinolide, a cytotoxic natural product, induces actin polymerization and competitively inhibits the binding of phalloidin to F-actin. J. Biol. Chem. Vol. 269 (1994), p. 14869-14871.
[33] G.T. Charras, J.C. Yarrow, M.A. Horton, L. Mahadevan and T.J. Mitchison. Non-equilibration of hydrostatic pressure in blebbing cells. Nature Vol. 435 (2005), p. 365-369.

Trabajo 2

LOS FILAMENTOS DE ACTINA ESTÁN IMPLICADOS EN EL MANTENIMIENTO DE LA MORFOLOGÍA DE LAS CISTERNAS Y EL pH INTRA-GOLGI

En los últimos años gran cantidad de evidencias experimentales han implicado a los MFs en las distintas rutas del tráfico intracelular. Nuestro laboratorio ha descrito como la perturbación de los MFs altera la morfología del AG provocando su compactación (observada mediante microscopia óptica) y la dilatación de sus cisternas (observada mediante TEM) en células tratadas con CyD. También hemos detectado la presencia de β/γ actina en la zona distal/lateral no compacta de las cisternas del AG y en los ITs de tipo COPI o bien de las proteínas implicadas en la regulación de la dinámica del citoesqueleto de actina Cdc42, N-WASP y Arp2/3. Todo ello indica que los MFs son necesarios para el mantenimiento de la morfología de AG. Sin embargo desconocemos con exactitud el tipo de alteraciones provocadas en la arquitectura del AG y estructuras derivadas como los ITs por toxinas de actina que bloquean/desestabilizan o polimerizan/estabilizan los MFs así como si existen diferencias en función la toxina utilizada, concentración y tiempo de exposición a ésta.

En este trabajo examinamos la contribución de los MFs a la arquitectura del AG utilizando toxinas de actina como herramienta para perturbar la dinámica del citoesqueleto de MFs. El análisis del AG mediante TEM y tomografia electrónica/reconstrucción 3D de células expuestas a las toxinas de actina nos muestra como las cisternas del AG sufren una serie de alteraciones secuenciales en su morfología que van desde la perforación/fragmentación hasta la dilatación y desorganización/colapso de las mismas, incrementándose en todos los casos el número de ITs en la periferia del AG. Por otra parte, se detectó como la despolimerización de los MF provocaba un incremento del pH_G. Las mismas alteraciones se observaron al inhibir específicamente la H^+-ATPasa vacuolar que participa en la regulación del pH intracelular. Teniendo en cuenta que los MFs interaccionan con elementos de la maquinaria molecular implicada en el mantenimiento de la homeostasis del pH de los compartimentos. Proponemos un modelo por el cual los cambios fenotipicos observados en el AG al perturbar los MFs serían consecuencia de una alteración en la función de los elementos implicados en la homeostasis del pH_G.

Cell Motility and the Cytoskeleton 63:778–791 (2006)

Actin Filaments Are Involved in the Maintenance of Golgi Cisternae Morphology and Intra-Golgi pH

Francisco Lázaro-Diéguez,[1,2,3] Nuria Jiménez,[4] Holger Barth,[5] Abraham J. Koster,[4] Jaime Renau-Piqueras,[6] Juan L. Llopis,[7] Koert N. J. Burger,[8] and Gustavo Egea[1,2,3]*

[1]*Departament de Biologia Cel·lular i Anatomia Patològica, Facultat de Medicina, and*
[2]*Instituts de Nanociències i Nanotecnologia (IN²UB), and*
[3]*d'Investigacions Biomèdiques August Pi i Sunyer (IDIBAPS), Universitat de Barcelona, 08036 Barcelona, Spain*
[4]*Department of Molecular Cell Biology, Institute of Biomembranes, Utrecht University, 3584 CH Utrecht, The Netherlands*
[5]*Institute of Pharmacology and Toxicology, University of Ulm, 89081 Ulm, Germany*
[6]*Centro de Investigación, Hospital La Fe, 46009 Valencia, Spain*
[7]*Facultad de Medicina, CRIB, Universidad de Castilla-La Mancha, 02006 Albacete, Spain*
[8]*Department of Biochemical Physiology, Institute of Biomembranes, Utrecht University, 3584 CH Utrecht, The Netherlands*

Here we examine the contribution of actin dynamics to the architecture and pH of the Golgi complex. To this end, we have used toxins that depolymerize (cytochalasin D, latrunculin B, mycalolide B, and *Clostridium botulinum* C2 toxin) or stabilize (jasplakinolide) filamentous actin. When various clonal cell lines were examined by epifluorescence microscopy, all of these actin toxins induced compaction of the Golgi complex. However, ultrastructural analysis by transmission electron microscopy and electron tomography/three-dimensional modelling of the Golgi complex showed that F-actin depolymerization first induces perforation/fragmentation and severe swelling of Golgi cisternae, which leads to a completely disorganized structure. In contrast, F-actin stabilization results only in cisternae perforation/fragmentation. Concomitantly to actin depolymerization-induced cisternae swelling and disorganization, the intra-Golgi pH significantly increased. Similar ultrastructural and Golgi pH alkalinization were observed in cells treated with the vacuolar H^+-ATPases inhibitors bafilomycin A1 and concanamycin A. Overall, these results suggest that actin filaments are implicated in the preservation of the flattened shape of Golgi cisternae. This maintenance seems to be mediated by the regulation of the state of F-actin assembly on the Golgi pH homeostasis. Cell Motil. Cytoskeleton 63:778–791, 2006. © 2006 Wiley-Liss, Inc.

The supplemental materials described in this article can be found at http://www.interscience.wiley.com/jpages/0886-1544/suppmat

Contract grant sponsor: DGCYT; Contract grant numbers: BCM2006-00867; Contract grant sponsor: Consejería de Sanidad, Junta de Comunidades de Castilla-La Mancha; Contract grant numbers: 04007-00, GC04-005; Contract grant sponsor: European Community's Human Potential Programme; Contract grant number: HPRN-CT-2002-00259.

© 2006 Wiley-Liss, Inc.

*Correspondence to: Gustavo Egea, Department de Biologia Cel·lular i Anatomia Patològica, Facultat de Medicina, Universitat de Barcelona, C/Casanova 143, 08036 Barcelona, Spain. E-mail: gegea@ub.edu

Received 3 April 2006; Accepted 26 July 2006

Published online 7 September 2006 in Wiley InterScience (www.interscience.wiley.com).
DOI: 10.1002/cm.20161

Key words: cytoskeleton; actin; pH; electron tomography; Golgi apparatus

INTRODUCTION

Membrane trafficking to and from the Golgi complex is clearly associated with the cytoskeleton in eukaryotic cells. Whereas this association was initially established only for microtubules [Thyberg and Moskalewsky, 1999; Allan et al., 2002; Rios and Bornens, 2003], results from several laboratories have also demonstrated the involvement of microfilaments in mammalian cells [Stamnes, 2002; Egea et al., 2006]. Moreover, a role for actin dynamics is strongly suggested by the involvement of some actin cytoskeleton regulatory molecules and actin-binding or actin-associated proteins in the formation and/or movement of transport intermediates. Those include Cdc42 and some downstream signalling effectors such as N-WASP, Arp2/3, and LIMK1 [Erickson et al., 1996; Fucini et al., 2002; Luna et al., 2002; Carreno et al., 2004; Chen et al., 2004a; Matas et al., 2004; Rosso et al., 2004], Cdc42-GAP protein [Dubois et al., 2005], the Cdc42-related protein TC10 [Kanzaki et al., 2002], mAbp1 [Fucini et al., 2002; Kessels and Qualmann, 2002], non-muscle myosin II [Heimann et al., 1999; Duran et al., 2003], Golgi-specific spectrin and ankyrin isoforms [Beck et al., 1994, 1997; Deverajan et al., 1996], the spectrin family member syne-1 [Gough et al., 2003, 2004], syndapins [Kessels and Qualmann, 2002, 2004], the Sla2/Huntingtin-interactin protein 1 member Hip1R [Carreno et al., 2004] and cortactin [Cao et al., 2005]. Collectively, these data indicate that a complex molecular machinery regulates actin dynamics in Golgi membranes, which seems to be involved in Golgi-associated transport events.

As an initial step, the use of actin toxins is extremely useful for the examination of the putative involvement of the actin cytoskeleton in various cellular events (endo/exocytosis, cell motility and migration, cell polarity and differentiation, axonal transport and neuritogenesis, amongst many others). Cytochalasins are widely used to study the putative involvement of F-actin in the cellular process of interest. However, it is important to utilize more than one actin toxin because depending on the anti-actin agent used, disparate results are obtained. For instance, on the basis of results obtained using cytochalasin D (CyD) we initially reported that membrane dynamics at the ER/Golgi interface was actin-independent [Valderrama et al., 1998]. In contrast, in a subsequent study, using latrunculin B (LtB) or *Clostridium botulinum* C2 toxin (C2 toxin), we reported that microfilaments were involved in the retrograde (Golgi-to-ER) but not anterograde (ER-to-Golgi) membrane pathway [Valderrama et al., 2001]. These disparate results are due to the fact that, unlike LtB and C2 toxin, CyD does not appear to produce a significant net depolymerization of F-actin [Morris and Tannenbaum, 1980]. However, when examining the effect of actin toxins on Golgi morphology, these three F-actin disrupters (CyD, LtB and C2 toxin) caused the same compaction of the Golgi complex [Valderrama et al., 2001], which occurred before the rounding up of cells [Valderrama et al., 1998, 2001]. Thus, results obtained with these three F-actin depolimerizing agents indicate that there is a high sensitivity of the Golgi shape to changes in the organization of the actin cytoskeleton but it is not always necessarily followed by alterations in the Golgi-associated membrane dynamics or protein transport [di Campli et al., 1999].

Here we examine the contribution of actin filaments to the architecture of the Golgi complex by comparing the effect of several F-actin depolimerizing and stabilizing drugs. Our data unravel an interesting new functional link between actin filaments, Golgi cisternae morphology and intra-Golgi pH homeostasis.

MATERIALS AND METHODS

Antibodies, Reagents and cDNAS

Mouse monoclonal antibodies to giantin were kindly provided by H.-P. Hauri (Biozentrum, Basel University, Switzerland). Goat anti-mouse-FITC was from Jackson ImmunoResearch (West Baltimore, PA, USA). Latrunculin B (LtB), mycalolide B (MyB), bafilomycin A1 (Baf), concanamycin A (ConcA), and nocodazole (NZ) were from Calbiochem (EMD Biosciences, Darmstadt, Germany), and TRITC-phalloidin, cytochalasin D (CyD), monensin and nigericin were from Sigma (St. Louis, MO, USA). Jasplakinolide (Jpk) was from Molecular Probes (Eugene, OR, USA). C2I and C2IIa components of *Clostridium botulinum* C2 toxin (C2 toxin) were obtained as described [Barth et al., 2000] cDNAs encoding the N-terminal of human β1,4-GT fused enhanced mutants GFP (EGFP), CFP (EGFP) or YFP (EYFP) mutants were used as described [Llopis et al., 1998]. EMbed-812 embedding media kit and the reagents used in electron microscopy experiments were from Electron Microscopy Sciences (Hatfield, PA, USA). Colloidal gold was purchased from J. Slot (Utrecht University, Utrecht).

Cell Culture and Actin Toxins Treatments

NRK, HeLa, and Vero cells were grown in Dulbecco's modified Eagle's medium (DMEM) from Gibco/Brl

Life Technologies (Paisley, UK) supplemented with fetal bovine serum (FBS) from Gibco, penicillin (100 U/ml), streptomycin (100 μg/ml), L-glutamine (20 mM) and MEM sodium piruvate (10 mM). Cell cultures were maintained at 37°C in a humidified 5% CO_2 atmosphere.

Actin toxins were diluted in DMEM supplemented with FBS (10%) with the exception of C2 toxin. In these experiments, cells were rinsed twice with DMEM without FBS and then incubated with C2 toxins diluted in DMEM with the presence of low FBS (0.5%).

Indirect Immunofluorescence

Indirect immunofluorescence was carried out as described previously [Valderrama et al., 1998, 2000] with the following antibody dilutions: anti-giantin, 1:500 and goat anti-mouse FITC, 1:50. TRITC-phalloidin was used at 1:500. Coverslips were mounted on microscope slides using Mowiol (Calbiochem, EMD Biosciences, Darmstadt, Germany). Microscopy and imaging were performed with a B ×60 epifluorescence microscope (Olympus, Tokyo, Japan) with an Orca-ER cooled CCD camera (Hamamatsu Photonics, Japan) or with a TCS-NT confocal microscope (Leica Microsystems, Heerbrugg, Switzerland). The images were processed using Adobe Photoshop CS software (Adobe Systems, San Jose, CA).

Transmission Electron Microscopy

NRK, HeLa, or Vero cells were rapidly fixed with 1.25% glutaraldehyde in PIPES buffer (0.1 M, pH 7.4) containing sucrose (2%) and Mg_2SO_4 (2 mM) for 60 min at 37°C. Cells were then gently scraped, pelleted at 100 g 10 min, rinsed in PIPES buffer solution (3 × 5 min) and postfixed with 1% (wt/vol) OsO_4, 1% (wt/vol) $K_3Fe(CN)_6$ in PIPES buffer for 1 h at room temperature in the dark. After cells were treated for 5 min with tannic acid (0.1%) in PIPES buffer, rinsed in distilled water, block-stained with 1% uranyl acetate in 70% ethanol for 1 h, dehydrated with graded ethanol solutions and finally embedded in Epon plastic resin. Ultrathin sections (50–70 nm thick) were stained with lead citrate and observed on a JEOL 1010 electron microscope. Micrographs of randomly selected areas were obtained with a Gatan Bioscan digital camera at the same final magnification (50,000×) and analyzed using point-counting procedures. The stereological parameters were determined using standard procedures [Weibel, 1979]. The minimum sample size of each stereological parameter was determined by the progressive mean technique (confidence limit of 5%).

Electron Tomography and 3D Modeling

Sections (250 nm) of chemically fixed (2% glutaraldehyde plus 1% formaldehyde in 0.1 M cacodylate buffer, pH 7.4), Epon-embedded Hela cells were transferred to Butvar-coated copper slot grids. Colloidal gold particles (10 nm) were added to one side of the grid to serve as fiducial markers for aligning the series of tilted images. Tilt series of representative Golgi stacks were automatically recorded [Ziese et al., 2002] at 200 kV using a Tecnai20 electron microscope (FEI/Philips Electron Optics, Eindoven, The Netherlands) equipped with a slow-scan CCD camera (TemCam F214, TVIPS GmbH, Germany) and a motorized goniometer. Every specimen was tilted about two orthogonal axes from -65° to $+65^\circ$ at 1° intervals, resulting in two datasets of 131 high-resolution digital images. Using the program package IMOD [Kremer et al., 1996], images were then aligned and a tomogram was computed from each tilt series. The two single-axis tomograms were merged into one [Mastronade, 1997] and the tomographic dual-axis reconstruction was interpreted and modeled using IMOD software.

Gene Transfection

HeLa cells grown in glass coverlisps at 200,000 cells/ml were transiently co-transfected with FuGene (Roche Diagnostics) containing GT-EGFP and GT-ECFP or GT-EYFP and GT-ECFP cDNAs (0.5 μg each), which were expressed for 24 h.

Calibration Protocols, Intra-Golgi and Cytoplasmic pH Determinations, and Live Cell Imaging

Co-transfected HeLa cells expressing GT-EGFP and GT-ECFP or GT-EYFP and GT-ECFP were first treated with the respective anti-actin agent, or vacuolar H^+-ATPase inhibitor at 37°C. Thereafter, cells were rinsed in HBSS medium supplemented with 24 mM $NaHCO_3$, 50 mM HEPES and 10 mM glucose at 22°C and under a continuous flow of 5% CO_2. At this point, in situ Golgi-associated GT-EGFP/GT-ECFP or GT-EYFP/GT-ECFP ratiometric fluorescence intensities were measured. Then, these cells were quickly rinsed and incubated with at least three different pH calibration buffers resulting from the mixture of different volumes of two solutions (A and B) which contained 70 mM NaCl, 70 mM KCl, 1.5 mM K_2HPO_4, 1 mM $MgSO_4$, 2 mM $CaCl_2$, nigericin and monensin (10 μM each) and 10 mM HEPES (Solution A; pH 8.0) or 10 mM MES (Solution B; pH 5.0). These three ratio measurements established a linear regression from which initial in situ pH_G measurement was extrapolated.

For estimation of cytoplasmic pH (pH_C), control and LtB-treated cells were loaded with 5 μM BCECF-AM (Molecular Probes) for 15 min at 37°C. Thereafter, cells were rinsed in HBSS medium supplemented with

24 mM $NaHCO_3$, 50 mM HEPES and 10 mM glucose at 22°C and under a continuous flow of 5% CO_2. At this point, BCECF ratiometric fluorescence intensities were measured. Then, cells were treated with the different pH calibration buffers as mentioned above and in situ pH_C was extrapolated from the linear regression obtained from three BCECF ratio measurements.

Both pH_G and pH_C ratiometric measurements were obtained with the Aquacosmos software (Hamamatsu Photonics, Japan) from live fluorescence images captured with an Orca-ER cooled CCD camera (Hamamatsu Photonics, Japan) coupled to an epifluorescence microscopy (Leica DM-IRB). The excitation and emission interference filters (Omega Optical, Brattleboro, VT and Chroma Technology Corp. Rockingham, VT) used for Golgi-associated fusion proteins were respectively 430 ± 12.5 nm and 470 ± 17.5 nm for ECFP and 495 ± 10 nm and 535 ± 15 nm for EGFP and EYFP. In the case of BCECF, excitation was performed with 495 ± 10 nm (pH-sensitive) and 430 ± 12.5 nm (pH-insensitive) filters, and emission filter was at 535 ± 15 nm.

RESULTS

All Anti-Actin Agents Induce Compaction of the Golgi Complex But Vary in Their Ultrastructural Effects

We have previously reported that the disruption of actin filaments causes compaction of the Golgi complex in NRK cells [Valderrama et al., 1998, 2001]. However, it is not known (i) whether this unusual Golgi morphology is generated in other mammalian cell lines when the actin cytoskeleton is disrupted by actin toxins and (ii) whether different toxins cause equivalent alterations of Golgi ultrastructure. To address these issues, NRK, HeLa, and Vero cells were treated with several anti-actin agents that depolymerize or stabilize actin filaments. Regardless of the cell line used, treatment with F-actin depolimerizing agents such as CyD, LtB, mycalolide B (MyB) and C2 toxin on one hand, and the actin-stabilizing agent jasplakinolide (Jpk) on the other, resulted in the loss of the normal actin stress fibre organization (Supplementary Figs. 1A–1R and Supplementary Table). Irrespective of the toxin used, the Golgi complex showed an identical compact shape when examined under epifluorescence microscope (Supplementary Figs. 1A–1R). When this Golgi compaction was examined at ultrastructural level by transmission electron microscopy (TEM) (Fig. 1), NRK cells treated with CyD (Fig. 1B), MyB (Fig. 1D) or LtB (Fig. 1F) showed partially fragmented and large swollen Golgi cisternae. Cells treated with C2 toxin showed disorganized cisternae in which the limits of membranes (and lumen) were difficult to distinguish (Fig. 1E, asterisks). Although Jpk-treated cells showed extensively fragmented Golgi stacks, cisternae remained flat (Fig. 1C). All actin toxins consistently induced an increase in peri-Golgi coated and non-coated vesicular (round) profiles. Identical ultrastructural alterations were also viewed in Golgi mini-stacks when cells were treated first with NZ and then with actin toxins (Supplementary Fig. 2).

Thus, the ultrastructural alterations produced by C2 toxin in the Golgi complex differed from those produced by the others F-actin depolimerizing agents. We reasoned that these disparate changes in Golgi cisternae induced on the one hand by CyD, LtB, and MyB (swollen cisternae) and on the other hand by C2 toxin (disorganized cisternae) could simply reflect different stages of a common and continuous sequence of ultrastructural changes in this organelle. To address this hypothesis, NRK cells were treated longer with LtB to induce a larger extent of actin filament depolymerization and then processed for TEM. These cells displayed Golgi stacks containing both a mixture of swollen and disorganized cisternae while others showed only disorganized cisternae (Fig. 1G), which were indistinguishable from those observed in C2 toxin-treated cells (Fig. 1E).

The actin toxin-induced ultrastructural observations were quantified by stereological analysis (Table I). Consistently with the qualitative observations, the volume density of cisternae with respect to the Golgi stack ($Vv_{cist\text{-}G}$) showed a significant increase in LtB-, CyD-, and MyB-treated cells, but remained unaltered in those treated with Jpk. These changes in volume density were accompanied by a significant increase in surface density with respect to the Golgi stack ($Sv_{cist\text{-}G}$), indicating that these anti-actin agents cause an increase in the amount of cisternae membrane. Finally, actin toxins also induced a significant increase in the numerical density of vesicle profiles ($Nv_{ves\text{-}G}$).

To gain further insight into the diverse ultrastructural changes of the Golgi apparatus caused by actin toxins, tomograms of Golgi stacks were obtained from untreated and LtB- and Jpk-treated cells. Figure 2A shows a tomographic slice from a dual-axis tomogram containing a representative Golgi stack (movie 1). The Golgi cisternae in the tomogram of control HeLa cells, appeared similar to the conventional ultrathin sections of NRK cells (compare Fig. 2A with 1A). As previously reported for NRK cells [Ladinsky et al., 1999], a representative 3D model of the Golgi stack of HeLa cells consisted of seven stacked cisternae (C1–C7; Fig. 2C and movie 2). Individual cisterna displayed a continuous, smooth membrane surface (Fig. 2D; movie 2). *Trans*-cisternae (C6–C7) were identified by their tight association with clathrin-coated vesicles (recognized by the

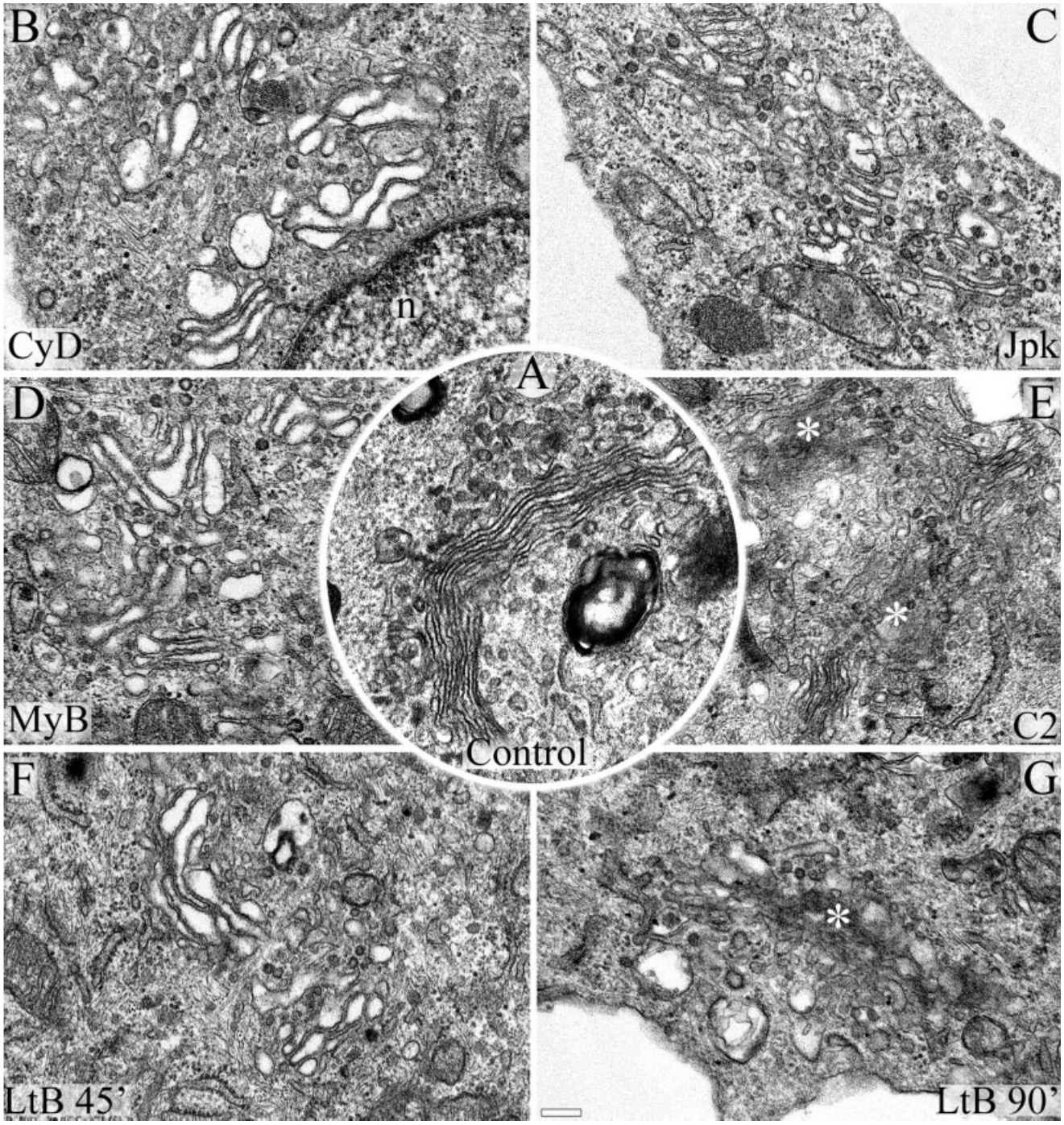

Fig. 1. Ultrastructural alterations of the Golgi complex induced by actin toxins. Control (**A**), CyD- (1 μM/60 min; **B**), Jpk- (500 nM/45 min; **C**), MyB- (100 nM/60 min; **D**), C2 toxin- (100 ng/ml C2I plus 200 ng/ml C2IIa/4 h; **E**), and LtB- (500 nM/45 min, **F**; 500 nM/90 min, **G**) treated NRK cells were processed for TEM. Note that the F-actin disrupters CyD (B), MyB (D), and LtB (500 nM/45 min; F) caused some fragmentation and large swelling of Golgi cisternae, whilst C2 toxin (E) or longer incubation times of LtB (500 nM/90 min; G) produced a disorganized cisternae (membrane limits and lumen were not distinguished; asterisks). In contrast, Jpk treatment (C) only induced fragmentation of the Golgi cisternae. All the actin toxins also induced an increase in peri-Golgi coated and non-coated vesicle profiles. n; nuclei, Bar, 200 nm.

presence of a lattice on their surface and their large size) (Figs. 2B and 2C, pink). Some buds (grey) and vesicles (white; 50–70 nm) showed no preferential association with any cisterna although most of them tended to be located in the lateral regions (Fig. 2C). Analysis of tomograms and 3D models of Golgi stacks of HeLa cells

TABLE I. Stereological Analysis of the Golgi Complex in NRK Cells Treated With Actin Toxins

Experimental condition	Stereological parameter		
	$Vv_{cist\text{-}G}$	$Sv_{cist\text{-}G}$	$Nv_{ves\text{-}G}$
Control	40.5 ± 2.6	16.9 ± 1.6	274.1 ± 37.3
+ LtB (500 nM/45 min)	51.4 ± 3.9*	23.9 ± 4.3*	391.8 ± 45.5*
+ LtB (500 nM/90 min)	–	–	431.7 ± 41.7*
+ CyD (1 μM/1 h)	48.2 ± 3.4*	22.0 ± 2.4*	374.9 ± 49.8*
+ C2 (100 ng/mL/4 h)	–	–	478.9 ± 31.6*
+ MyB (100 nM/60 min)	47.9 ± 3.9*	21.0 ± 3.3*	369.4 ± 47.2*
+ Jpk (500 nM/45 min)	41.4 ± 3.9	17.5 ± 4.3	494.3 ± 46.2*

Actin toxins: latrunculin B (LtB), cytochalasin D (CyD), *C. botulinum* C2 toxin (C2), mycalolyde B (MyB), and jasplakinolide (Jpk). Stereological parameters: $Vv_{cist\text{-}G}$, volume density (%); $Sv_{cist\text{-}G}$, surface density (μm^{-1}) of cisternae with respect to the Golgi stack; $Nv_{ves\text{-}G}$, numerical density (μm^{-3}) of peri-Golgi vesicle profiles with respect to the Golgi stack. Data represents means ± SD of three independent experiments.

*Significant differences with respect to the control; Student's *t* test ($P \leq 0.01$).

treated with LtB (movies 3 and 4, respectively), Jpk (movies 5 and 6, respectively) revealed significant differences compared with untreated cells. LtB (500 nM/45 min) induced significant swelling of stacked cisternae and an increase in the number of associated vesicles, which were preferentially accumulated in the lateral portions of swollen cisternae (Fig. 2E and inset). Cisternae viewed in the *z*-axis showed perforations/fragmentations that interrupted the continuity of stacked cisternae (Fig. 2F). Unlike LtB, Jpk-treated cells displayed flattened cisternae although they showed numerous perforations/fragmentations (Figs. 2G and 2H). Interestingly, vesicles were nonuniformly distributed, being mostly located in the lateral portions of stacked cisternae (Fig. 2G) and between the perforation/fragmentation of *trans*-cisternae (C5–C7) (Fig. 2G, arrow). EM-tomography and complete stereological data of Golgi stacks in LtB (500 nM/90 min)- and C2 toxin-treated cells (Table II) was hampered by the fact that the cisternae membrane was poorly resolved in numerous zones (asterisks in Figs. 1E and 1G).

Collectively, ultrastructural results indicate that F-actin depolymerization first induces severe swelling of partially perforated/fragmented Golgi cisternae, which leads to a completely disorganized structure. In contrast, the stabilization of F-actin produces a large cisternae perforation/fragmentation without significant swelling. These different actin toxin-induced alterations in cisternae morphology are microtubule-independent.

Both Golgi Complex and Actin Cytoskeleton Alterations Induced by Actin Toxins Are Reversible

Next, we examined whether these ultrastructural Golgi alterations are reversible after withdrawal of the actin toxins (Fig. 3). In every cell line examined, we found that the reformation of actin stress fibre organization and normal perinuclear and reticular Golgi complex morphology was also different for each actin toxin (Supplementary Table). For example, in CyD- or LtB-treated Vero cells, some actin stress fibres were already seen at 15 min (Fig. 3A) but a completely normal actin stress fibre organization and Golgi complex morphology only took place respectively after 60 and 90 min of the drug withdrawal (Fig. 3B). However, in cells previously treated MyB or Jpk, a normal actin cytoskeleton did not appear until 48 h (Fig. 3E) or 32 h (Fig. 3H) after their removal from the medium. In contrast, C2 toxin-induced alterations of the actin cytoskeleton and Golgi complex were both irreversible (data not shown). After the withdrawal of MyB or Jpk, there were marked differences in the process of recovery of Golgi morphology and, more significantly, in the actin organization. In MyB-washout Vero cells, the Golgi complex was reconstituted in the expected juxtanuclear position and located between accumulations of small F-actin spots (Fig. 3D, arrowheads and inset). In the case of Jpk, the actin cytoskeleton was still significantly disassembled 4 h after withdrawal (data not shown) but after 8 h, although actin stress fibre density and organization was practically normal, the Golgi complex was always localized to the vicinity of a single, large and well delimited F-actin aggregate (Fig. 3G and inset). This large F-actin aggregate disappeared 32 h after the drug removal, at which time both the actin cytoskeleton and Golgi complex morphology were normal (Fig. 3H). Ultrastructural analysis of the Golgi complex in LtB-, MyB- and Jpk-washout Vero cells showed a normal flattened cisternae morphology (Figs. 3C, 3F, and 3I, respectively), which was indistinguishable from that seen in untreated NRK or HeLa cells (Figs. 1A and 2A, respectively) and, moreover, regardless of their association with F-actin inclusion bodies (-MyB and -Jpk). Like in Vero, NRK cells showed similar results (Supplementary Fig. 3).

Depolymerization But Not Stabilization of F-Actin Raises Intra-Golgi pH

The molecular basis of the maintenance of the characteristic flattened Golgi architecture is unknown and can only be speculated on. However, we reasoned that by analogy to what has been reported at the plasma membrane, it might be linked to the maintenance of intra-Golgi ion and pH homeostasis by the regulation of the actin cytoskeleton on Golgi-associated vacuolar H^+-

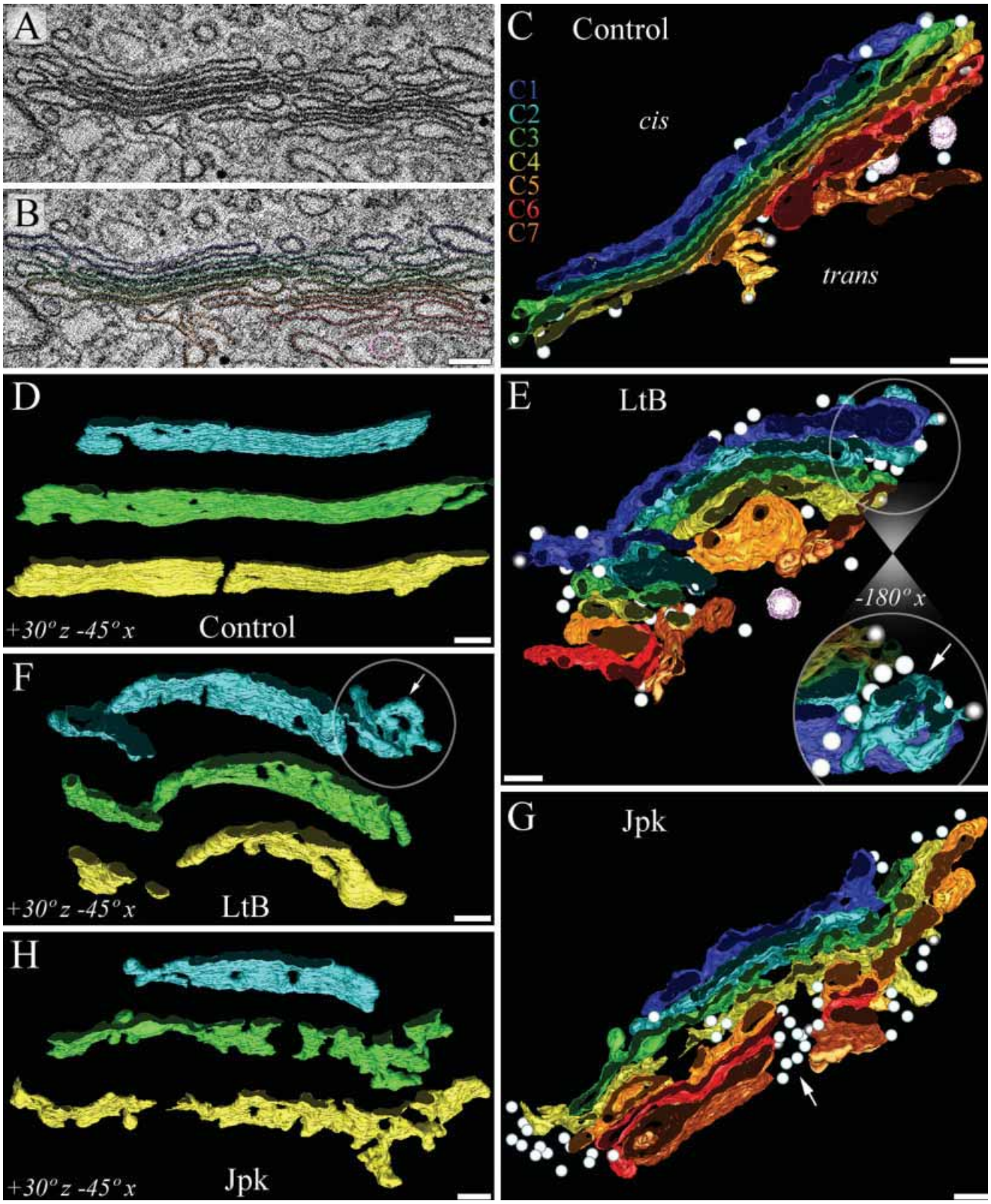

Fig. 2. Electron tomography and 3D modelling of the Golgi complex of HeLa cells treated with actin toxins. (**A**) Virtual slide ($\sim$ 6 nm) obtained from a tomogram of a representative Golgi stack of a control HeLa cell. The stack is composed of seven flattened cisternae. (**B**) The *cis*-to-*trans* cisternae, vesicles, and buds are outlined with different colours (*cis*-C1, blue; C2, light blue; C3, green; C4, yellow; C5, orange; C6, red; *trans*-C7, brown; non-clathrin-coated vesicles, white; buds, grey; clathrin-coated vesicles, pink) to generate a 3D model (**C**). (**D**) A $+30^{\circ}$ *z*-axis with -45° *x*-axis rotation of the C2, C3, and C4 cisternae from the 3D model shown in C. Note that the cisternae are flattened and show few fenestrations. The lateral view of the C2, C3, and C4 cisternae modelled from Golgi stacks of LtB- and Jpk-treated cells (F and H respectively) shows perforations that differ in size. In Jpk-treated cells (H), cisternae perforations are numerous and large, explaining the fragmented appearance of the Golgi in conventional TEM images (see Fig. 1C). Note also the increased number of vesicles seen in the 3D models of both LtB- and Jpk-treated cells (E and G respectively; arrow in G). In LtB-treated cells, the lateral portion of the C2 cisterna shows extensive branching that overlaps with the swollen lateral portion of the C1 cisterna (white arrow in F and inset in E which is magnified and rotated -180° around the *x*-axis). Bars, 200 nm.

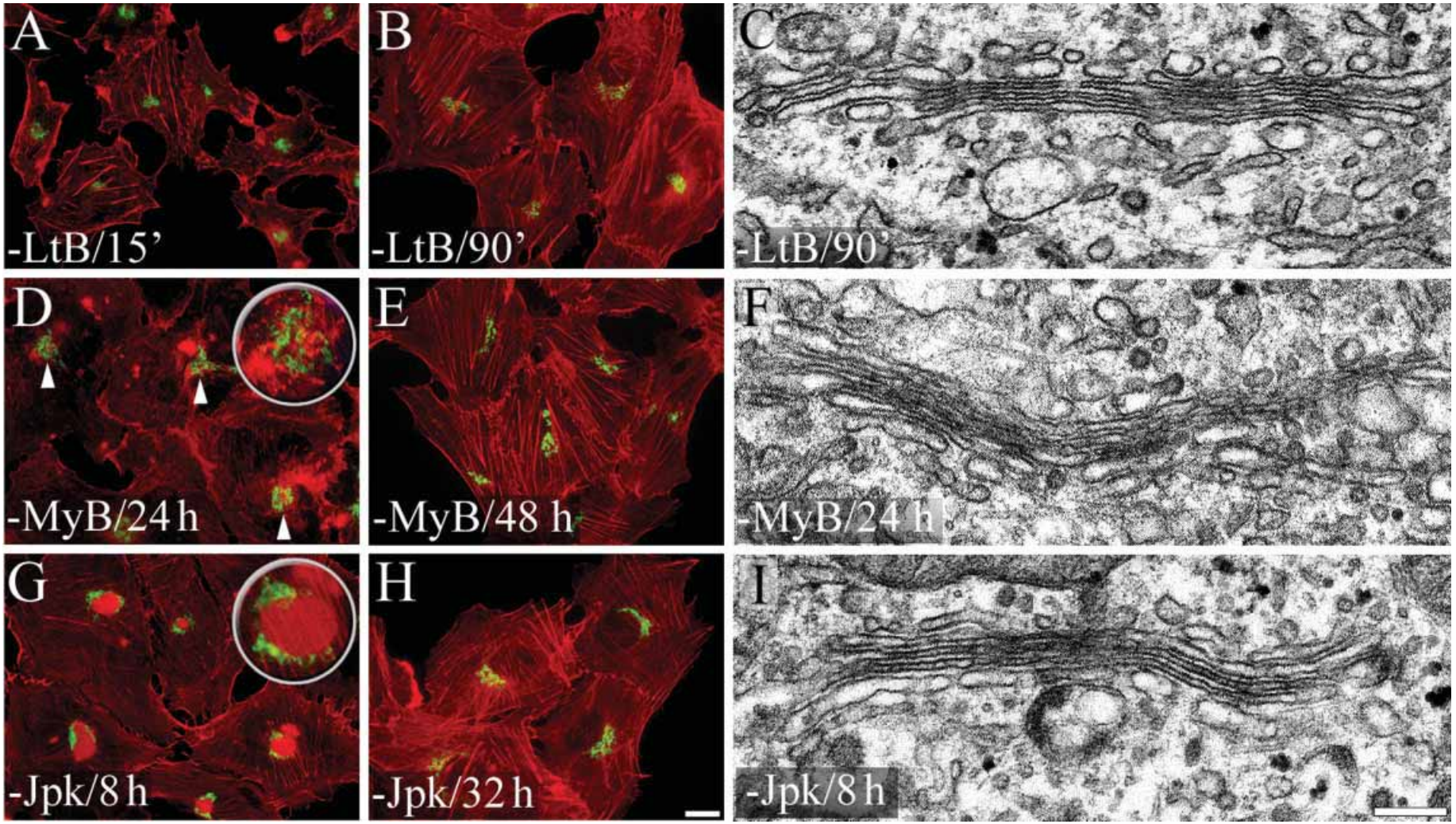

Fig. 3. Reversibility of the effects of actin toxins on the Golgi complex morphology and actin cytoskeleton organization. Vero cells first treated with LtB (500 nM/45 min), MyB (100 nM/60 min) or Jpk (500 nM/45 min) were subsequently deprived of actin toxins (-LtB, **A–C**; -MyB, **D–F**; -Jpk; **G–I**) for varying lengths of time (indicated in the respective panels) and co-stained for actin cytoskeleton with TRITC-phalloidin (red) and for the Golgi complex with anti-giantin antibodies (green). LtB-, MyB-, and Jpk-washout cells were also processed for TEM (C, F and I, respectively). Depending of the actin toxin used, actin cytoskeleton is directly recovered forming either actin stress fibres (-LtB) or differently F-actin inclusion bodies (-MyB and -Jpk). In the case of -MyB and -Jpk, the Golgi complex invariablely associates with these F-actin inclusion bodies. Ultrastructuraly normal flat Golgi cisternae were observed after the removal of actin toxins (C, F, I). Bars, 10 μm (A, B, D, E, G, H) and 200 nm (C, F, I).

TABLE II. Effects of a Variety of Actin Toxins and Vaculolar H^+-ATPase Inhibitors on the Intra-Golgi pH

	Intra-Golgi pH (pH_G)			
Experimental condition	GT-EGFP/GT-ECFP	*n*	GT-EYFP/GT-ECFP	*n*
Control	6.36 ± 0.11	21	6.40 ± 0.09	22
+ LtB (500 nM/45 min)	6.64 ± 0.08*	18	6.81 ± 0.20*	22
+ LtB (500 nM/90 min)	6.69 ± 0.05*	18	7.11 ± 0.11*	21
− LtB (90 min)	6.44 ± 0.04	17	6.41 ± 0.08	19
+ CyD (100 nM/1 h)	6.59 ± 0.11*	20	6.77 ± 0.18*	27
+ C2 (100 nM/4 h)	6.71 ± 0.06*	18	7.04 ± 0.14*	21
+ Jpk (500 nM/45 min)	6.43 ± 0.09	22	6.48 ± 0.12	22
+ Baf (100 nM/3 h)	7.24 ± 0.07*	18	7.27 ± 0.13*	17
+ ConA (100 nM/3 h)	7.20 ± 0.07*	19	7.25 ± 0.09*	20

Actin toxins: latrunculin B (LtB), cytochalasin D (CyD), *C. botulinum* C2 toxin (C2), mycalolyde B (MyB), and jasplakinolide (Jpk). Vaculolar H^+-ATPase inhibitors: Bafilomycin A1 (Baf) and Concanamycin A (ConA). Ratiometric measurements of pH_G obtained in the Golgi region of the same co-transfected HeLa cell expressing GT-EGFP and GT-ECFP or GT-EYFP and GT-ECFP. Data represents means ± SD of three independent experiments. Number of cells, *n*.
*Significant differences with respect to the control using Student's *t* test ($P \leq 0.01$).

ATPases and ion exchangers [Glickman et al., 1983; Al Awqati, 1995; Demareux et al., 1998; Thompson et al., 2002; Nakamura et al., 2005]. Therefore, we examined whether the actin toxin-induced alterations of Golgi cisternae ultrastructure were accompanied by changes in intra-Golgi pH (pH_G). To this end, HeLa cells were co-transfected with cDNAs encoding N-terminal 81 aa residues of the Golgi-resident integral membrane protein GT fused to EYFP, EGFP or ECFP [Llopis et al., 1998]. It is important to highlight that (i) both EGFP and EYFP fluorescence intensities are highly pH-sensitive, (ii) ECFP, which is much less sensitive to pH that either of the others, is used as a reference to correct putative changes in the cell focussing that could modify fluorescence emission only due to expected pH changes, and (iii) only EGFP but no EYFP has been found to be insensitive to chloride concentration [Wachter and Remington, 1999; Wachter et al., 2000]. GT-EGFP, GT-EYFP and GT-ECFP mostly localized to the Golgi complex (middle/*trans* cisternae) of HeLa cells [Llopis et al., 1998]. Single wavelength fluorescence intensities of both GT-EGFP (or GT-EYFP) and GT-ECFP were simultaneously measured in the Golgi region of the same co-transfected cell. Then, the ratios of GT-EGFP/GT-ECFP or GT-EYFP/GT-ECFP (pH_G sensor/reference) were calculated pixel by pixel. Ratio images were calibrated in terms of pH values by using the proton ionophores monensin and nigericin with extracellular solutions of know pH values. Importantly, EGFP/ECFP or EYFP/ECFP ratiofluorescence is insensitive to toxin-induced cell volume changes, movements, or changes in focus that could happen during pH calibration measurements, since both sensor and reference were diluted to the same extent.

As previously reported [Llopis et al., 1998], control HeLa cells showed an average pH_G of 6.4 (Table II). When cells were treated with LtB, CyD or C2 toxin, intra-Golgi pH significantly raised (Table II). Note that the intra-Golgi increase was usually higher in cells measured with GT-EYFP/GT-ECFP than with GT-EGFP/GT-ECFP ratios. This increase is most likely due to the added sensitivity of EYFP fluorescence intensity to a possible perturbed flow of chloride ion across Golgi membranes in F-actin depolymerized cells (see discussion). When LtB was removed from the culture medium (-LtB/90 min) a normal resting pH_G value was obtained. Note that in CyD (not shown) and LtB-washout cells (-LtB), both pH_G (Table II) and flattened Golgi cisternae ultrastructure normalization (Fig. 3C and Supplementary Fig. 3C) occurred simultaneously. Strikingly, the pH_G measured in Jpk-treated cells showed no change. Finally, to rule out that the pH_G increase associated to the F-actin depolymerization was a mere consequence of pH changes occurring in the cytoplasm (pH_C), cells were loaded with the intracellular pH fluorescent indicator BCECF [Llopis et al., 1998]. Both control and LtB (500 nM/90 min)-treated cells showed very similar pH_C values 7.21 ± 0.10 and 7.25 ± 14, respectively (total $n =$ 50 cells in three experiments). Therefore, the results show that F-actin depolymerization perturbs the pH_G but not the pH_C.

Like F-Actin Depolymerization Agents, Vacuolar H^+-ATPase Inhibitors Bafilomycin A1 and Concanamycin A Also Alkalinize Intra-Golgi pH and Induce Similar Cisternae Ultrastructural Alterations

As a hallmark of actin depolymerization is the elevation of Golgi lumen pH, we next examined whether other well-known components that raise Golgi pH might also induce similar Golgi ultrastructural changes to those observed with F-actin depolymerization agents such as CyD, LtB or C2 toxin. With this aim, NRK cells were treated with the naturally occurring plecomacrolides

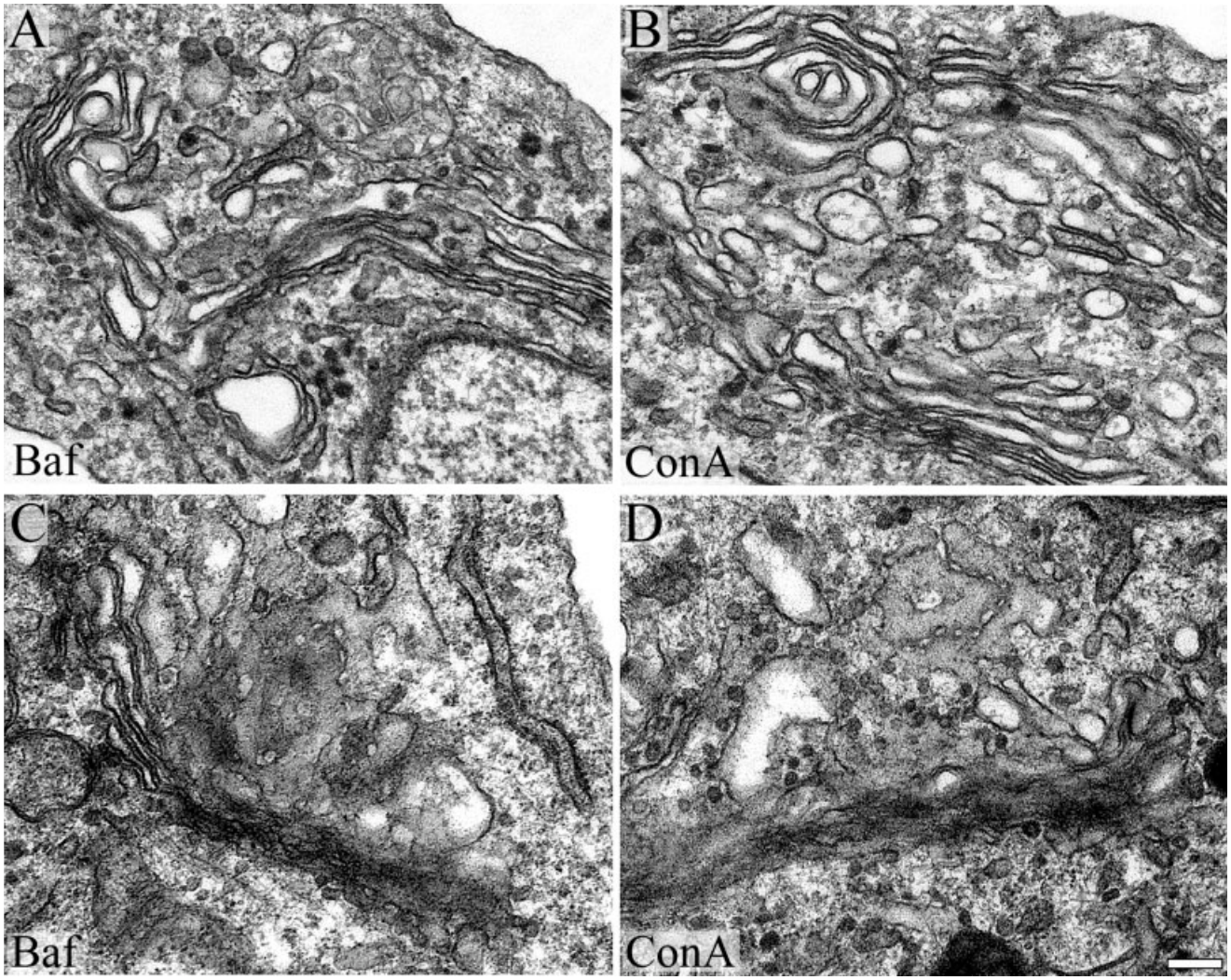

Fig. 4. Golgi complex ultrastructural alterations induced by bafilomycin A1 and concanamycin A treatments. Bafilomycin A1 (100 nM/3 h)- (**A** and **C**) and concanamycin A (100 nM/3 h)-treated (**B** and **D**) NRK cells were processed for TEM. Note that both H^+-ATPase inhibitors produce both swelling (A and B) and the complete disorganization (C and D) of Golgi cisternae, which are reminiscent of those ultrastructural alterations seen in cells treated with LtB (500 nM/45 and 90 min) or C2 toxin (see Figs. 1F, 1G and 1E, respectively). Bar, 200 nm.

bafilomycin A1 (Baf) or concanamycin A (ConcA), which have been shown to be potent and selective inhibitors of the vacuolar H^+-ATPase [Drose and Altendorf, 1997]. As expected, pH_G was severely alkalanized to values that were similar to those of the cytoplasm [Llopis et al., 1998] (Table II). When Baf- or ConcA-treated cells were examined at EM level (Fig. 4), the Golgi ultrastructure showed similar impairments to those observed in LtB (500 nm/45 and 90 min)- or C2 toxin-treated cells (compare Figs. 4A–4D with Figs. 1E–1G). In particular, some cisternae were swollen (Figs. 4A and 4B) and some other (usually from the same stack) showed a diffused morphology (Figs. 4C and 4D). No ultrastructural differences were observed between Baf and ConcA treatments.

DISCUSSION

Here, we have performed a comparative study to assess the participation of actin dynamics in the characteristic stacked and flattened Golgi architecture and pH using a variety of actin toxins to depolymerize or stabilize actin filaments. In summary, F-actin depolymerization first induces perforation/fragmentation and severe swelling of Golgi cisternae, which ends with a complete cisternae disorganization. In contrast, F-actin stabilization does not produce cisternae swelling but their large perforation/fragmentation. In both cases, cisternae remain stacked. Looking for the molecular basis of these morphological alterations, we tested whether the interference in actin dynamics perturbed the Golgi pH home-

ostasis, which in turn is determined by the appropriate ion and H^+ inflow and outflow occurring in cisternae. The correlation between cisternal morphological alterations and intra-Golgi pH alkalinization seen in F-actin depolymerised cells, on one hand, and the similar Golgi-associated ultrastructural changes caused by the inhibition of vacuolar H^+-ATPases, on the other hand, suggest that the involvement of actin in the Golgi complex architecture could be in part mediated through the regulation of cisternal ion and H^+ homeostasis.

How Could Actin Dynamics Be Coupled to the Maintenance of the Characteristic Flattened Morphology of Golgi Cisternae?

Analysis of the alterations of Golgi morphology and positioning caused by actin toxins shows that, unlike what happens with microtubule toxins, the pericentriolar location of the Golgi ribbon is maintained. However, the unique flattened morphology of cisternae is lost. Interestingly, the usual experimental treatments with F-actin disrupters (CyD, LtB and MyB) induce a severe swelling of Golgi cisternae. However, following longer incubation times (LtB and C2 toxin) this swelling is hardly visible and cisternae membrane and lumen limits appear diffused. It is likely that these different Golgi complex alterations induced by depolymerization of actin filaments are representative of a sequential process that begins with the swelling of cisternae (Figs. 1B, 1D and 1F) and ends with a disorganized morphology (Figs. 1E and 1G). The latter may simply represent the final cisternae morphological collapse caused by the complete loss of Golgi-associated filamentous actin, which is an essential component to maintain the functional integrity of the Golgi-associated cytoskeletal scaffolding [Beck, 2005].

The actin depolymerization induced cisternae swelling may be attributable to at least two mutually non-exclusive mechanisms. First, actin filaments (probably together with the Golgi-associated spectrin and ankyrin isoforms) would provide mechanical stability to cisternae, and thus prevent the swelling of cisternae as a result of the hyperosmotic protein content present in the Golgi lumen. The depolymerization of microfilaments would decrease the mechanical stability of the cisterna membrane, leading to its perforation/fragmentation (see 3D models in Fig. 2) or swelling (see ultrathin sections and tomograms in Figs. 1 and 2, respectively). Note, however, that Jpk, an actin stabilizer, induces cisternae perforation/fragmentation but not swelling, suggesting that these two morphological alterations are not necessarily linked. Depolymerization of actin filaments and the subsequent osmotic swelling may also increase membrane tension in the Golgi complex [Morris and Homann, 2001; Sheetz, 2001] and thus decrease the reported differences in tension between the ER and Golgi [Upadhyaya and Sheetz, 2004] slowing down Golgi-to-ER membrane flow. Consistent with this hypothesis is the observation that LtB and C2 toxin treatments reduce the rate of the Golgi disassembly induced by brefeldin A [Valderrama et al., 2001]. Secondly, cisternae swelling could be also generated by the functional uncoupling of actin filaments with ion exchangers and/or vacuolar H^+-ATPases ($(V)H^+$-ATPases). The former are electrochemically neutral because exchanges cations (NHEs) or anions (AEs), whilst the latter actively pumps H^+ resulting in lumen or extracellular acidification. Ion exchangers and $(V)H^+$-ATPases can be both Golgi-resident and en route to the plasma membrane [Kellokumpu et al., 1988; Kopito, 1990; Moriyama and Nelson, 1998; Nishi and Forgac, 2002; Vitavska et al., 2003; Chen et al., 2004b]. By analogy to NHEs isoforms localized to the plasma membrane (NHE1) and endocytic compartments (NHE3 and NHE5) [Szaszi et al., 2000; Denker and Barber, 2002], Golgi-associated NHEs isoforms (NHE7 and NHE8) [Nakamura et al., 2005] might be regulated by the state of F-actin in the Golgi complex. In the plasma membrane of red blood cells, an ankyrin/spectrin meshwork associates with anion exchanger 1 (AE1 or Band 3). This interaction is essential for the maintenance of the characteristic flattened shape of the cell and its mechanical stability [Marchesi, 1985; Nishi and Forgac, 2002]. Hence, in the Golgi complex, the potential ankyrin-interacting Golgi membrane protein anion exchanger 2 (AE2) [Holappa et al., 2001; Holappa and Kellokumpu, 2003] could provide a functional membrane anchorage site for the Golgi-associated spectrin/ankyrin/actin cytoskeleton [De Matteis et al., 2000; Valderrama et al., 2000]. The structural role of the AE2 protein in the Golgi complex would be linked to its function (the reversible electroneutral exchange of Cl^- for HCO_3^-), thus contributing to the regulation of intracellular pH, organelle volume, and chloride concentration. Strikingly, in AE2-depleted cells, Golgi stacks display numerous fenestrations and swollen cisternae [Holappa et al., 2004]. On the other hand, it has also been reported that actin-binding activity is a requirement for transport of $(V)H^+$-ATPase to and from the plasma membrane [Vitavska et al., 2003; Chen et al., 2004b] and therefore, it is reasonable to assume a role for microfilaments and actin dynamics in the delivery and/or activation of $(V)H^+$-ATPase in endomembrane systems, including the Golgi complex. To this respect, Baf and ConcA treatments induced very similar cisternae ultrastructural alterations (Fig. 4), which were undistinguishable from those seen in LtB- or C2 toxin-treated cells (Fig. 1). As expected and concomitantly to these Baf/ConcA-induced Golgi alterations, intra-Golgi pH raised to values that however were higher than those obtained in F-actin

depolymerised cells. Therefore, the similar morphological and physiological effects on the Golgi complex produced by actin depolymerising agents and inhibitors of $(V)H^+$-ATPase suggest that actin regulation of a Golgi-associated $(V)H^+$-ATPase [Moriyama and Nelson, 1998] could be involved in the maintenance of flattened cisternae whilst being coupled to the regulation of an osmotically active molecule exchanger. Actin depolymerization may impair this functional coupling and generate an inappropriate gradient formation (and intra-Golgi pH), which at ultrastructural level would initially lead to cisternae swelling and then to their collapse. Abnormal ion gradients and pH coupled to the loss of actin cytoskeleton integrity in the Golgi complex could impair both protein transport- and non-transport-associated functions (for instance, protein and lipid glycosylation) [Axelsson et al., 2001; Kellokumpu et al., 2002]. In line with this hypothesis, interference with either the activity of $(V)H^+$-ATPase [Yilla et al., 1993] or with actin polymerization [Hirschberg et al., 1998; Jacob et al., 2003; Cobbold et al., 2004] results in an altered post-Golgi transport. Consistently with these observations, there is an increase in the surface membrane area of the Golgi (Table I) and an abnormal accumulation of peri-Golgi transport carriers in actin toxins-treated cells (Figs. 1 and 2, Table I). Strikingly, unlike F-actin depolymerization, the Jpk-induced F-actin stabilisation produces neither cisternae swelling nor changes in the intra-Golgi pH.

In conclusion, our data point to a new functional coupling at the Golgi between microfilaments, the maintenance of flattened cisternae and intra-Golgi pH homeostasis.

ACKNOWLEDGMENTS

The authors thank Shannon Holliday (University of Florida College of Dentistry) and John Cox (University of Tennessee Health Science Ctr) for helpful discussions. We also thank Willie J.C. Geerts (Utrecht University) for expert advice on electron tomography, Serveis Cientifico-Tècnics of the University of Barcelona (SCT-UB, Campus Casanova) for technical support with electron and confocal microscopes, and Robin Rycroft for his editorial assistance.

REFERENCES

Al Awqati Q. 1995. Chloride channels of intracellular organelles. Curr Opin Cell Biol 7:504–508.

Allan VJ, Thompson HM, McNiven MA. 2002. Motoring around the Golgi. Nat Cell Biol 4:E236–E242.

Axelsson MA, Karlsson NG, Steel DM, Ouwendijk J, Nilsson T, Hansson GC. 2001. Neutralization of pH in the Golgi apparatus causes redistribution of glycosyltransferases and changes in the *o*-glycosylation of mucins. Glycobiology 11:633–644.

Barth H, Blocker D, Behlke J, Bergsma-Schutter W, Brisson A, Benz R, Aktories K. 2000. Cellular uptake of *Clostridium botulinum* C2 toxin requires oligomerization and acidification. J Biol Chem 275:18704–18711.

Beck KA. 2005. Spectrins and the Golgi. Biochim Biophys Acta 1744:374–382.

Beck KA, Buchanan JA, Malhotra V, Nelson WJ. 1994. Golgi spectrin: Identification of an erythroid β-spectrin homolog associated with the Golgi complex. J Cell Biol 127:707–723.

Beck KA, Buchanan JA, Nelson WJ. 1997. Golgi membrane skeleton: Identification localization and oligomerization of a 195 kDa ankyrin isoform associated with the Golgi complex. J Cell Sci 110:1239–1249.

Cao H, Weller S, Orth JD, Chen J, Huang B, Chen JL, Stamnes M, McNiven MA. 2005. Actin and Arf1-dependent recruitment of a cortactin-dynamin complex to the Golgi regulates post-Golgi transport. Nat Cell Biol 7:483–492.

Carreno S, Engqvist-Goldstein AE, Zhang CX, McDonald KL, Drubin DG. 2004. Actin dynamics coupled to clathrin-coated vesicle formation at the trans-Golgi network. J Cell Biol 165:781–788.

Chen JL, Lacomis L, Erdjument-Bromage H, Tempst P, Stamnes M. 2004a. Cytosol-derived proteins are sufficient for Arp2/3 recruitment and ARF/coatomer-dependent actin polymerization on Golgi membranes. FEBS Lett 566:281–286.

Chen SH, Bubb MR, Yarmol EG, Zuo J, Jian J, Lee BS, Lu M, Gluck SL, Hurst IR, Holliday LS. 2004b. Vacuolar H^+-ATPase binding to microfilaments: Regulation in response to phosphatidylinositol 3-kinase activity and detailed characterization of the actin-binding site in subunit B. J Biol Chem 279:7988–7998.

Cobbold C, Coventry J, Ponnambalam S, Monaco AP. 2004. Actin and microtubule regulation of trans-Golgi network architecture and copper-dependent protein transport to the cell surface. Mol Membr Biol 21:59–66.

De Matteis MA, Morrow JS. 2000. Spectrin tethers and mesh in the biosynthetic pathway. J Cell Sci 113:2331–2343.

Demaurex N, Furuya W, D'Souza S, Bonifacino JS, Grinstein S. 1998. Mechanism of acidification of the trans-Golgi network (TGN): In situ measurements of pH using retrieval of TGN38 and furin from the cell surface. J Biol Chem 273:2044–2051.

Denker SP, Barber DL. 2002. Cell migration requires both ion translocation and cytoskeletal anchoring by the Na-H exchanger NHE1. J Cell Biol 159:1087–1096.

Devarajan P, Stabach PR, Mann AS, Ardito T, Kashgarian M, Morrow JS. 1996. Identification of a small cytoplasmic ankyrin (AnkG119) in the kidney and muscle that binds β I σ spectrin and associates with the Golgi apparatus. J Cell Biol 133:819–830.

di Campli A, Valderrama F, Babia T, De Matteis MA, Luini A, Egea G. 1999. Morphological changes in the Golgi complex correlate with actin cytoskeleton rearrangements. Cell Motil Cytoskeleton 43: 334–348.

Drose S, Altendorf K. 1997. Bafilomycins and concanamycins as inhibitors of V-ATPases and P-ATPases. J Exp Res 200:1–8.

Dubois T, Paleott O, Mironov AA, Fraisier V, Stradal TE, De Matteis MA, Franc M, Chavrier P. 2005. Golgi-localized GAP for Cdc42 functions downstream of ARF1 to control Arp2/3 complex and F-actin dynamics. Nat Cell Biol 7:353–364.

Duran JM, Valderrama F, Castel S, Magdalena J, Tomas M, Hosoya H, Renau-Piqueras J, Malhotra V, Egea G. 2003. Myosin motors and not actin comets are mediators of the actin-based

Golgi-to-endoplasmic reticulum protein transport. Mol Biol Cell 14:445–459.

Egea G, Lazaro-Dieguez F, Vilella M. 2006. Actin dynamics at the Golgi complex in mammalian cells. Curr Opin Cell Biol 18(2): 168–178.

Erickson JW, Zhang C, Kahn RA, Evans T, Cerione RA. 1996. Mammalian Cdc42 is a brefeldin A-sensitive component of the Golgi apparatus. J Biol Chem 271:26850–26854.

Fucini RV, Chen JL, Sharm C, Kessels MM, Stamnes M. 2002. Golgi vesicle proteins are linked to the assembly of an actin complex defined by mAbp1. Mol Biol Cell 13:621–631.

Glickman J, Croen K, Kelly S, Al Awqati Q. 1983. Golgi membranes contain an electrogenic H^+ pump in parallel to a chloride conductance. J Cell Biol 97:1303–1308.

Gough LL, Beck KA. 2004. The spectrin family member Syne-1 functions in retrograde transport from Golgi to ER. Biochim Biophys Acta 1693:29–36.

Gough LL, Fan J, Chu S, Winnick S, Beck KA. 2003. Golgi localization of Syne-1. Mol Biol Cell 14:2410–2424.

Heimann K, Percival JM, Weinberger R, Gunning P, Stow JL. 1999. Specific isoforms of actin-binding proteins on distinct populations of Golgi-derived vesicles. J Biol Chem 274:10743–10750.

Hirschberg K, Miller CM, Ellenberg J, Presley JF, Siggia ED, Phair RD, Lippincott-Schwartz J. 1998. Kinetic analysis of secretory protein traffic and characterization of golgi to plasma membrane transport intermediates in living cells. J Cell Biol 143: 1485–1503.

Holappa K, Kellokumpu S. 2003. Targeting of the AE2 anion exchanger to the Golgi apparatus is cell type-dependent and correlates with the expression of Ank(195), a Golgi membrane skeletal protein. FEBS Lett 546:257–264.

Holappa K, Suokas M, Soininen P, Kellokumpu S. 2001. Identification of the full-length AE2 (AE2a) isoform as the Golgi-associated anion exchanger in fibroblasts. J Histochem Cytochem 49:259–269.

Holappa K, Munoz MT, Egea G, Kellokumpu S. 2004. The AE2 anion exchanger is necessary for the structural integrity of the Golgi apparatus in mammalian cells. FEBS Lett 564:97–103.

Jacob R, Heine M, Alfalah M, Naim HY. 2003. Distinct cytoskeletal tracks direct individual vesicle populations to the apical membrane of epithelial cells. Curr Biol 13:607–612.

Kanzaki M, Watson RT, Hou JC, Stamnes M, Saltiel AR, Pessin JE. 2002. Small GTP-binding protein TC10 differentially regulates two distinct populations of filamentous actin in 3T3L1 adipocytes. Mol Biol Cell 13:2334–2346.

Kellokumpu S, Neff L, Jamsa-Kellokumpu S, Kopito R, Baron R. 1988. A 115-kD polypeptide immunologically related to erythrocyte Band 3 is present in Golgi membranes. Science 242: 1308–1311.

Kellokumpu S, Sormunen R, Kellokumpu I. 2002. Abnormal glycosylation and altered Golgi structure in colorectal cancer: Dependence on intra-Golgi pH. FEBS Lett 516:217–224.

Kessels MM, Qualmann B. 2002. Syndapins integrate N-WASP in receptor-mediated endocytosis. EMBO J 21:6083–6094.

Kessels MM, Qualmann B. 2004. The syndapin protein family: Linking membrane trafficking with the cytoskeleton. J Cell Sci 117: 3077–3086.

Kopito RR. 1990. Molecular biology of the anion exchanger gene family. Int Rev Cytol 123:177–199.

Kremer JR, Mastronarde DN, McIntosh JR. 1996. Computer visualization of three-dimensional image data using IMOD. J Struct Biol 116:71–76.

Ladinsky MS, Mastronarde DN, McIntosh JR, Howell KE, Staehelin LA. 1999. Golgi structure in three dimensions: Functional insights from the normal rat kidney cell. J Cell Biol 144:1135–1149.

Llopis J, McCaffery JM, Miyawaki A, Farquhar MG, Tsien RY. 1998. Measurement of cytosolic, mitochondrial, and Golgi pH in single living cells with green fluorescent proteins. Proc Natl Acad Sci USA 95:6803–6808.

Luna A, Matas OB, Martinez-Menarguez JA, Mato E, Duran JM, Ballesta J, Way M, Egea G. 2002. Regulation of protein transport from the Golgi complex to the endoplasmic reticulum by Cdc42 and N-WASP. Mol Biol Cell 13:866–879.

Marchesi VT. 1985. Stabilizing infrastructure of cell membranes. Annu Rev Cell Biol 1:531–561.

Mastronarde DN. 1997. Dual-axis tomography: An approach with alignment methods that preserve resolution. J Struct Biol 120: 343–352.

Matas OB, Martinez-Menarguez JA, Egea G. 2004. Association of Cdc42/N-WASP/Arp2/3 signaling pathway with Golgi membranes. Traffic 5:838–846.

Moriyama Y, Nelson N. 1998. H^+-translocating ATPase in Golgi apparatus: Characterization as vacuolar H^+-ATPase and its subunit structures. J Biol Chem 264:18445–18450.

Morris A, Tannenbaum J. 1980. Cytochalasin D does not produce net depolymerization of actin filaments in HEp-2 cells. Nature 287: 637–639.

Nakamura N, Tanaka S, Teko Y, Mitsui K, Kanazawa H. 2005. Four Na^+/H^+ exchanger isoforms are distributed to Golgi and post-Golgi compartments and are involved in organelle pH regulation. J Biol Chem 280:1561–1572.

Nishi T, Forgac M. 2002. The vacuolar (H^+)-ATPases—Nature's most versatile proton pumps. Nat Rev Mol Cell Biol 3:94–103.

Rios RM, Bornens M. 2003. The Golgi apparatus at the cell centre. Curr Opin Cell Biol 15:60–66.

Rosso S, Bollati F, Bisbal M, Peretti D, Sumi T, Nakamura T, Quiroga S, Ferreira A, Caceres A. 2004. LIMK1 regulates Golgi dynamics traffic of Golgi-derived vesicles and process extension in primary cultured neurons. Mol Biol Cell 15:3433–3449.

Sheetz MP. 2001. Cell control by membrane-cytoskeleton adhesion. Nat Rev Mol Cell Biol 2:392–396.

Stamnes M. 2002. Regulating the actin cytoskeleton during vesicular transport. Curr Opin Cell Biol 14:428–433.

Szaszi K, Grinstein S, Orlowski J, Kapus A. 2000. Regulation of the epithelial Na(+)/H(+) exchanger isoform by the cytoskeleton. Cell Physiol Biochem 10:265–272.

Szaszi K, Paulsen A, Szabo EZ, Numata M, Grinstein S, Orlowski J. 2002. Clathrin-mediated endocytosis and recycling of the neuron-specific Na+/H+ exchanger NHE5 isoform: Regulation by phosphatidylinositol 3′-kinase and the actin cytoskeleton. J Biol Chem 277:42623–42632.

Thompson RJ, Nordeen MH, Howell KE, Caldwell JH. 2002. A large-conductance anion channel of the Golgi complex. Biophys J 83:278–289.

Thyberg J, Moskalewski S. 1999. Role of microtubules in the organization of the Golgi complex. Exp Cell Res 246:263–279.

Upadhyaya A, Sheetz MP. 2004. Tension in tubulovesicular networks of Golgi and endoplasmic reticulum membranes. Biophys J 86:2923–2928.

Valderrama F, Babia T, Ayala I, Kok JW, Renau-Piqueras J, Egea G. 1998. Actin microfilaments are essential for the cytological positioning and morphology of the Golgi complex. Eur J Cell Biol 76:9–17.

Valderrama F, Luna A, Babia T, Martinez-Menarguez JA, Ballesta J, Barth H, Chaponnier C, Renau-Piqueras J, Egea G.

2000. The Golgi-associated COPI-coated buds and vesicles contain β/γ-actin. Proc. Natl Acad Sci USA 97:1560–1565.

Valderrama F, Duran JM, Babia T, Barth H, Renau-Piqueras J, Egea G. 2001. Actin microfilaments facilitate the retrograde transport from the Golgi complex to the endoplasmic reticulum in mammalian cells. Traffic 2:717–726.

Vitavska O, Wieczorek H, Merzendorfer H. 2003. A novel role for subunit C in mediating binding of the H^+-V-ATPase to the actin cytoskeleton. J Biol Chem 278:18499–18505.

Wachter RM, Remington SJ. 1999. Sensitivity of the yellow variant of green fluorescent protein to halides and nitrate. Curr Biol 9: R628–R629.

Wachter RM, Yarbrough D, Kallio K, Remington SJ. 2000. Crystallographic and energetic analysis of binding of selected anions to the yellow variants of green fluorescent protein. J Mol Biol 301: 157–171.

Weibel ER. 1979. Practical Methods for Biological Morphometry, Vol. 1. New York: Academic Press.

Yilla M, Tan A, Ito K, Miwa K, Ploegh HL. 1993. Involvement of the vacuolar H(+)-ATPases in the secretory pathway of HepG2 cells. J Biol Chem 268:19092–19100.

Ziese U, Janssen AH, Murk JL, Geerts WJ, Van der Krift KT, Verkleij AJ, Koster AJ. 2002. Automated high-throughput electron tomography by pre-calibration of image shifts. J Microsc 200: 187–200.

Supplemetary Figures

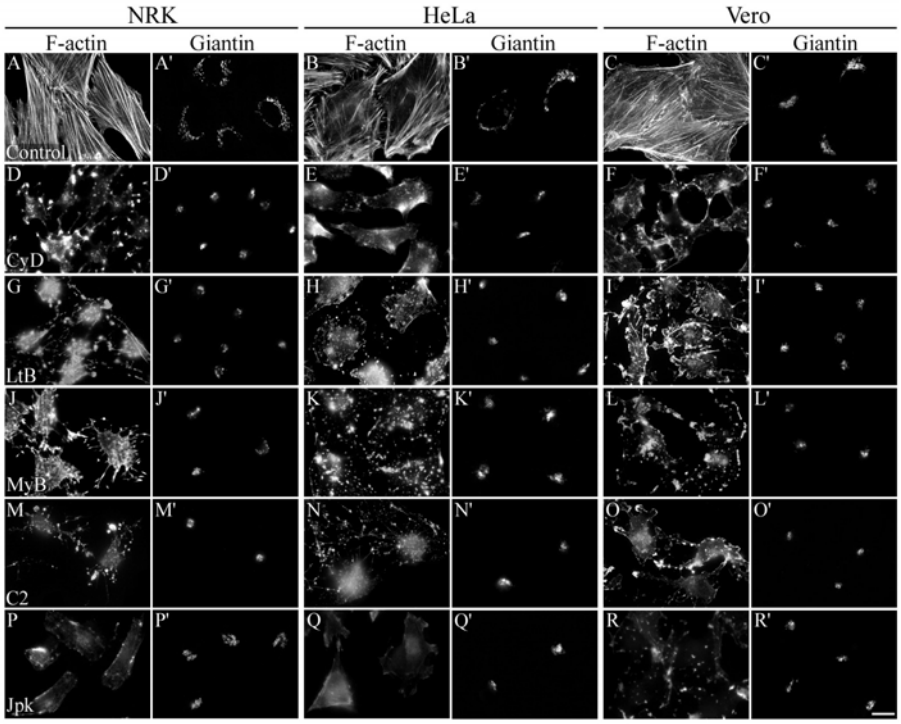

Supplementary Fig. 1. F-actin depolimerizing and stabilizing agents both induce compaction of the Golgi complex. NRK, HeLa, and Vero cells were incubated with the F-actin depolimerizing agent cytochalasin D (CyD; 1 μM/60 min; D-D', E-E', F-F'), latrunculin B (LtB; 500 nM/45 min; G-G',H-H',I-I'), mycalolide B (MyB; 100 nM/60 min; J-J', K-K', L-L'), or C2 toxin (C2; 100 ng/ml C2I plus 200 ng/ml C2IIa/4 h each; M-M', N-N', O-O') or the F-actin stabilizing agent jasplakinolide (Jpk; 500 nM/45 min; P-P', Q-Q', R-R'). Thereafter, cells were fixed and co-stained for actin cytoskeleton with TRITC-phalloidin (A-R) and for the Golgi complex with anti-giantin antibodies (A'-R'). Although the toxins produced diverse alterations of actin organization, all of them induced the Golgi complex compaction. Bar, 10 μm.

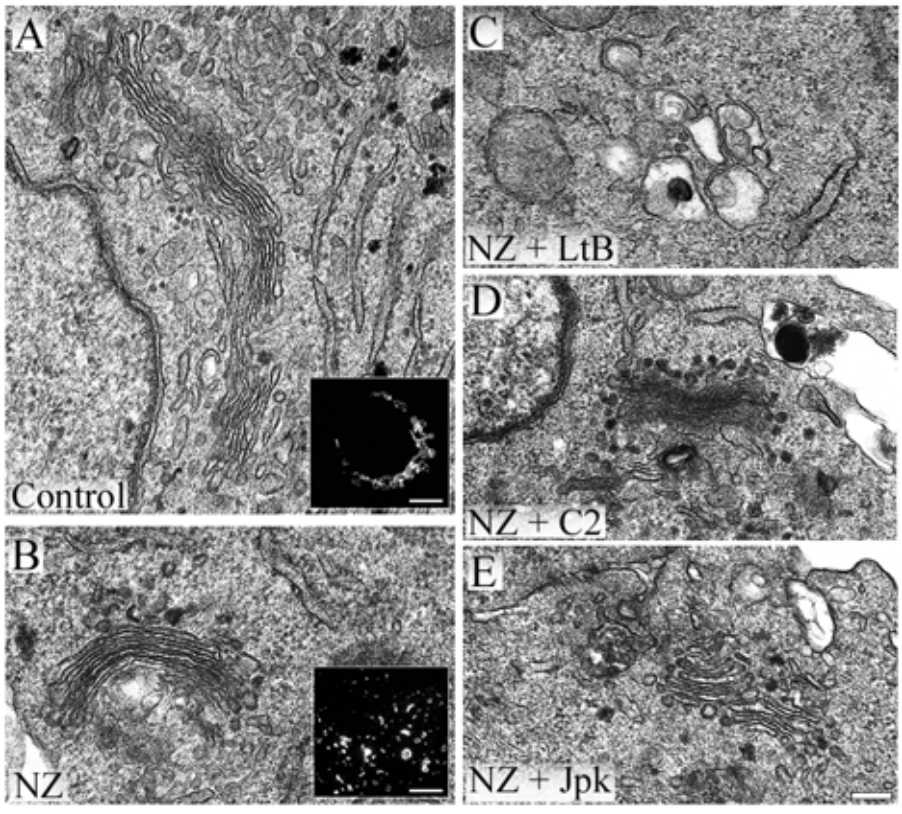

Supplementary Fig. 2. Golgi ultrastructural changes in cells with disrupted microtubule and actin cytoskeletons. NRK cells were first treated with nocodazole (NZ; 33 μM/3 h) (B) and subsequently with LtB (500 nM/45 min), C2 toxin (4 h) or Jpk (500 nM/45 min) in the continuous presence of NZ (C, D, and E, respectively). Panel A shows a representative Golgi complex in untreated cells. Insets in A and B shows the characteristic morphology of the Golgi stained to giantin in untreated (A; a single perinuclear Golgi ribbon) and nocodazole (B; numerous cytoplasmic dispersed mini-stacks)-treated cells. Note that the Golgi mini-stacks morphological alterations induced by the different actin toxins (C, LtB; D, C2 toxin; E, Jpk) are similar to those observed in treated cells with an intact microtubular cytoskeleton (see Fig. 1). Bar in insets and in EM pictures represent 5 μm and 200 nm, respectively.

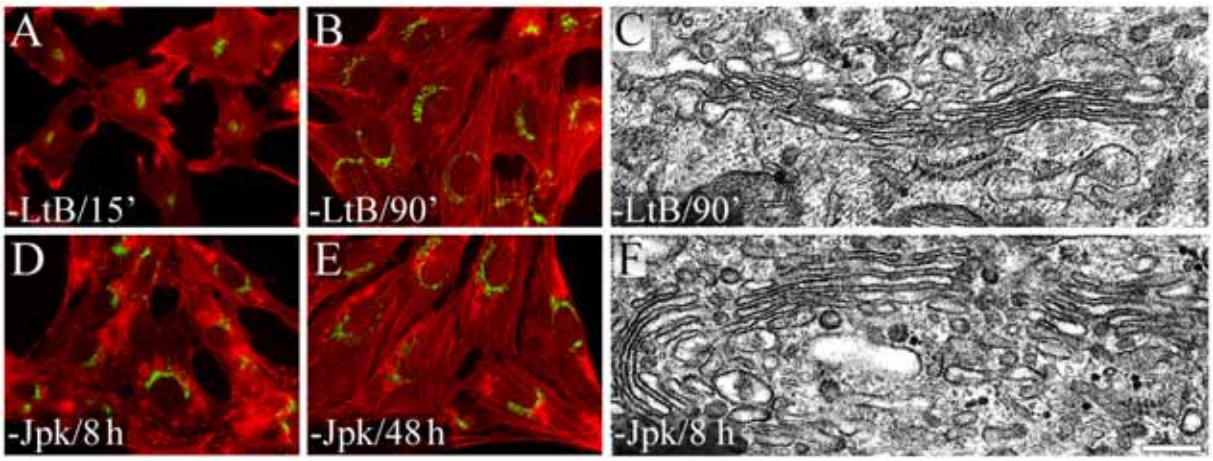

Supplementary Fig. 3. Reversibility of the effects of actin toxins on the Golgi complex morphology and actin cytoskeleton organization in NRK cells. Cells first treated with LtB (500 nM/45 min) or Jpk (500 nM/45 min) which subsequently deprived of actin toxins (-LtB, A-C; -Jpk, D-F) for varying lengths of time (indicated in the respective panels) and co-stained for actin cytoskeleton with TRITC-phalloidin (red) and for the Golgi complex with anti-giantin antibodies (green). LtB- and Jpk-washout cells were also processed for TEM (C and F, respectively). Depending on the actin toxin used, actin cytoskeleton is directly recovered forming either actin stress fibres (-LtB) or differently structured F-actin inclusion bodies (-Jpk). Ultrastructurally, normal flat Golgi cisternae were observed after the removal of actin toxins (C, F). Bars, 10 μm (A, B, D, E) and 200 nm (C, F).

Supplementary Table

		Treatment			Removal		
Actin toxin	***Working concentration***	***T(+)***	***F-actin***	***GC***	***T(-)***	***F-actin***	***GC***
CyD	1μM	+60/90'	D	c	-15' -60' -90'	d n n	c c, n n
LtB	500 nM	+30/45'	D	c	-15' -60' -90'	d n n	c c, n n
MyB	100 nM	+45/60'	D	c	-1/6 h -24/32 h -48/56 h	D d, Fas n	c f-Fas n
C2	C2I +C2IIa (100+200 ng/ml, respectively)	+2/4 h	D	c	n.d.	n.d.	n.d.
Jpk	500 nM	+45/60'	D	c	-1/2 h -6/8 h -24/32 h	D d, Faa n	c n-Faa n

Supplementary Table. Effects of treatment and subsequent withdrawal of actin toxins on actin cytoskeleton organization (F-actin) and the Golgi complex morphology (GC). Actin toxins: F-actin depolimerizing agent: cytochalasin D (CyD), latrunculin B (LtB), mycalolyde B (MyB) and C. botulinum C2 toxin (C2); F-actin stabilizing agent: jasplakinolide (Jpk); T(+) or T(-): respective time or time interval (/) in minutes (') or hours (h) of treatment with (+) or after the removal of (-) anti-actin agent; F-actin: actin stress fibres organization (n, normal; D, totally disrupted; d, partially disrupted) and F-actin inclusion bodies (Fas, numerous small F-actin spots; Faa, single large F-actin aggregate). GC: Golgi complex morphology (n, normal; c, compact; f-Fas, fragmented and intercalated between F-actin spots; n-Faa, normal and associated with the F-actin aggregate). n.d., not determined because the irreversibility of C2 toxin alterations.

Supplementary Movies

Movie 1: Dual-axis tomogram obtained from a 250 nm semithin section containing a representative Golgi stack of a HeLa cell.
Movie 2: 3D model of a representative Golgi stack of a HeLa cell.
Movie 3: Dual-axis tomogram obtained from a 250 nm semithin section containing a representative Golgi stack of a LtB-treated HeLa cell.
Movie 4: 3D model of a representative Golgi stack of an LtB-treated HeLa cell.
Movie 5: Montage of two dual-axis tomograms obtained from 250 nm semithin sections containing a representative Golgi stack of a Jpk-treated HeLa cell.
Movie 6: 3D model of a representative Golgi stack of a Jpk-treated HeLa cell.

Trabajo 2

RESULTADOS ADICIONALES NO PUBLICADOS

2.1. Análisis de la cinética de acción de la latrunculina B y el jasplakinolide sobre el citoesqueleto de actina y el aparato de Golgi

Teniendo en cuenta que los tratamientos con LtB provocan un fenotipo del AG variable en función del tiempo de exposición a la toxina, nos planteamos que este fenómeno es consecuencia del grado de despolimerización de los MFs. Con la finalidad de ratificar esta hipótesis estudiamos la cinética de acción de la LtB en células NRK. A nivel de microscopía óptica se observa como la LtB provoca rápidamente tanto la perturbación del citoesqueleto de actina como la compactación de AG. A nivel ultraestructural, las cisternas del AG aparecen muy dilatadas y fragmentadas (A, +LtB 15 y 45 min). A tiempos más largos de exposición a LtB, se observa una mayor desorganización/colapso de la estructura del AG ,el cual aparece como una estructura difusa electrodensa (A, +LtB 90 min). Paralelamente realizamos la cuantificación del contenido de F-actina en las células tratadas con LtB. Tanto la ratio entre F/G-actina obtenida a partir de *western blot* (B) como el porcentaje de fluorescencia emitida por la F-actina-faloidina-TRITC detectada por espectrofluorimetría (C) disminuyen significativa y progresivamente a lo largo del tratamiento con la LtB. Por lo tanto la variación fenotípica del AG observada por TEM entre los tratamientos con LtB 15-45 min y 90 min en los sería consecuencia del distinto grado de despolimerización de los MFs. Por otro lado, observamos que las alteraciones provocadas por el Jpk sobre la ultraestructura del AG se mantienen constantes en el tiempo (D).

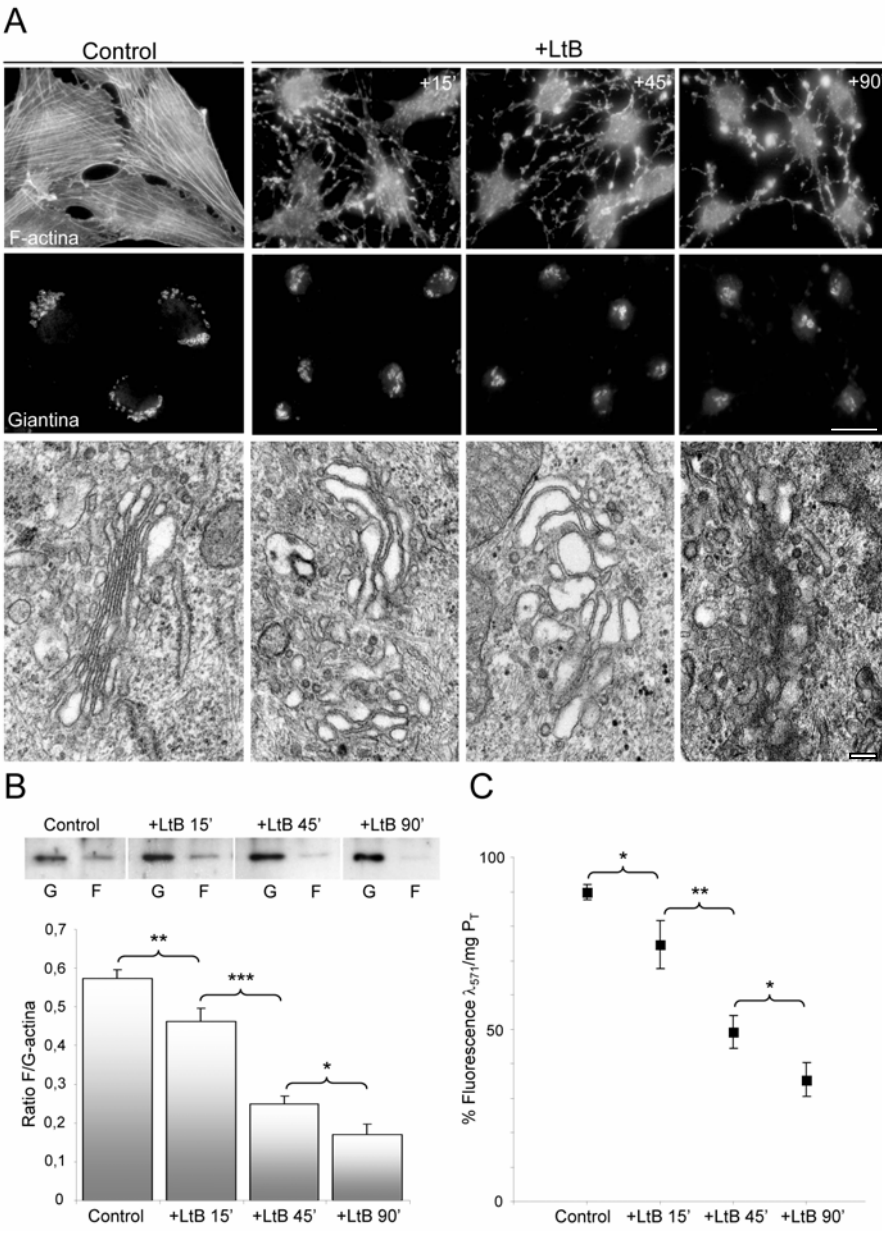

Estudio cinético de las alteraciones provocadas sobre el citoesqueleto de actina y el aparato de Golgi por la latrunculina B. (A) Células NRK tratadas con LtB (500 nM/15, 45 y 90 min), se fijaron y marcaron con faloidina-TRITC (panel superior) y anti-giantin (panel medio) para visualizar el citoesquelto de actina y el AG, respectivamente. Paralelamente, células sometidas a los mismos tratamientos se procesaron para TEM (panel inferior). Barras: Inmunoflurescencia 10 μm, TEM 200 nm. **Cuantificación de los niveles de F-actina después del tratamiento con LtB. (B)** Células NRK tratadas con LtB (500 nM/15, 45 y 90 min), se lisaron en presencia de faloidina-TRITC, separando posteriormente la fracción G-actina de la F-actina y se procesaron para *western-blot* (panel superior). El histograma representa los valores de la relacción entre la actina filamentosa (F-actina) y la globular (G-actina) cociente entre la F/G-actina (ver Material y Métodos) **(C)** Paralelamente la fracción de F-actina también se cuantificó mediante espectrofluorimetría. El gráfico representa el porcentaje de emisión de fluorescencia de la F-actina-faloidina-TRITC respecto a la cantidad de proteína total del lisado celular (ver Material y Métodos). Los resultados corresponden a la media ± s.d. de tres experimentos independientes. Las diferencias entre el control y los tratamientos presentan una significación de $p \leq 0.5$ (**) $p \leq 0.01$ (**) y $p \leq 0.001$ (***) empleando el test de la *t*-Student.

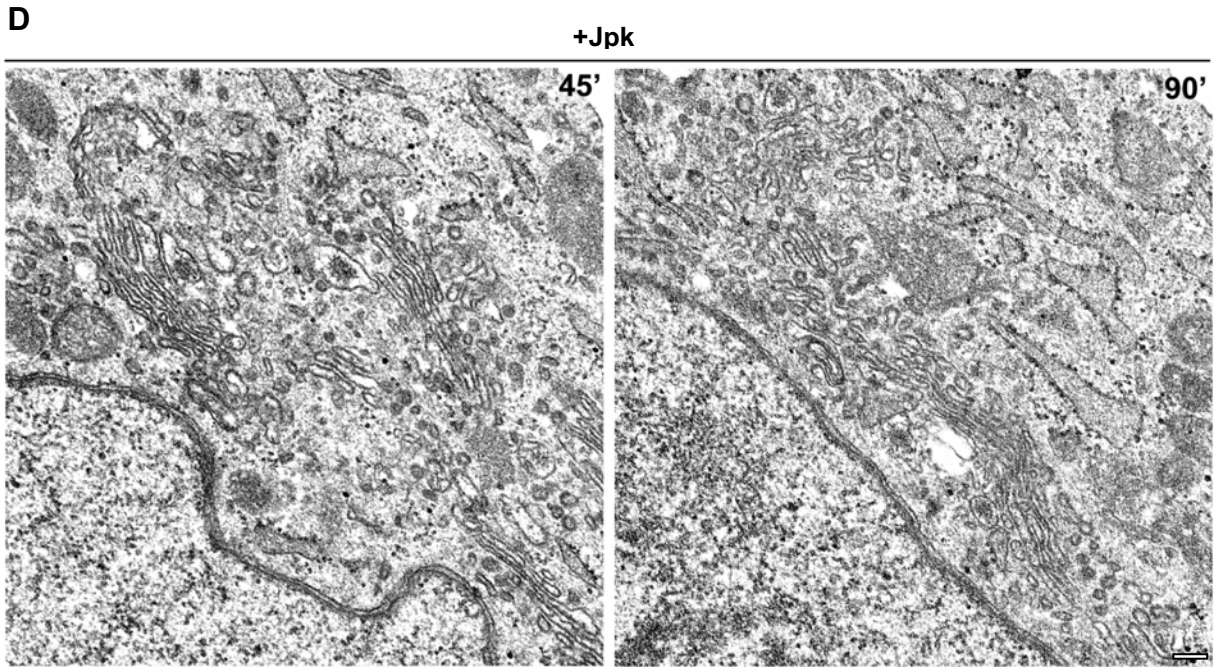

Estudio cinético de las alteraciones provocadas sobre el aparato de Golgi por el jasplakinolide. (D) Células NRK fueron incubadas con Jpk (500 nM/45 y 90 min) tras lo cual se fijaron y procesaron para TEM. Barra: 200 nm.

2.2. Distribución subcelular de la H^+-ATPasa vacuolar y de los intercambiadores iónicos AE2 (aniónico) y NHE7 (catiónico)

Según nuestra hipótesis de trabajo, las variaciones fenotípicas observadas en el AG al despolimerizar MFs podrían estar provocadas por una perturbación de la función de los elementos integrantes en maquinaria implicada en la regulación de la homeostasis iónica intracelular. Teniendo en cuenta que ciertos elementos implicados en la regulación del pH como las H^+-ATPasa vacuolares y los intercambiadores iónicos AE2 y NHE7 interaccionan con los MFs, nos planteamos estudiar su localización subcelular mediante inmunofluorescencia. Como marcadores de compartimentos ácidos subcelulares se utilizaron el GM130 localizado en las cisternas cis-Golgi, la giantina en la zona *cis*- *mid*-Golgi, el TGN38 o TGN46 como marcadores de la red TGN, EEA1 como marcador de endosomas tempranos y las glicoproteínas de membrana lgp-120 y lamp-2 como marcadores lisosomales. Los resultados muestran que la H^+-ATPasa vacuolar se localiza preferentemente en la zona *cis*- *mid*-Golgi, aunque también en el TGN y los lisosomas. El AE2 se encuentra mayoritariamente en la zona *cis*-Golgi mientras que el NHE7 mayoritariamente en la zona *mid*-Golgi y TGN.

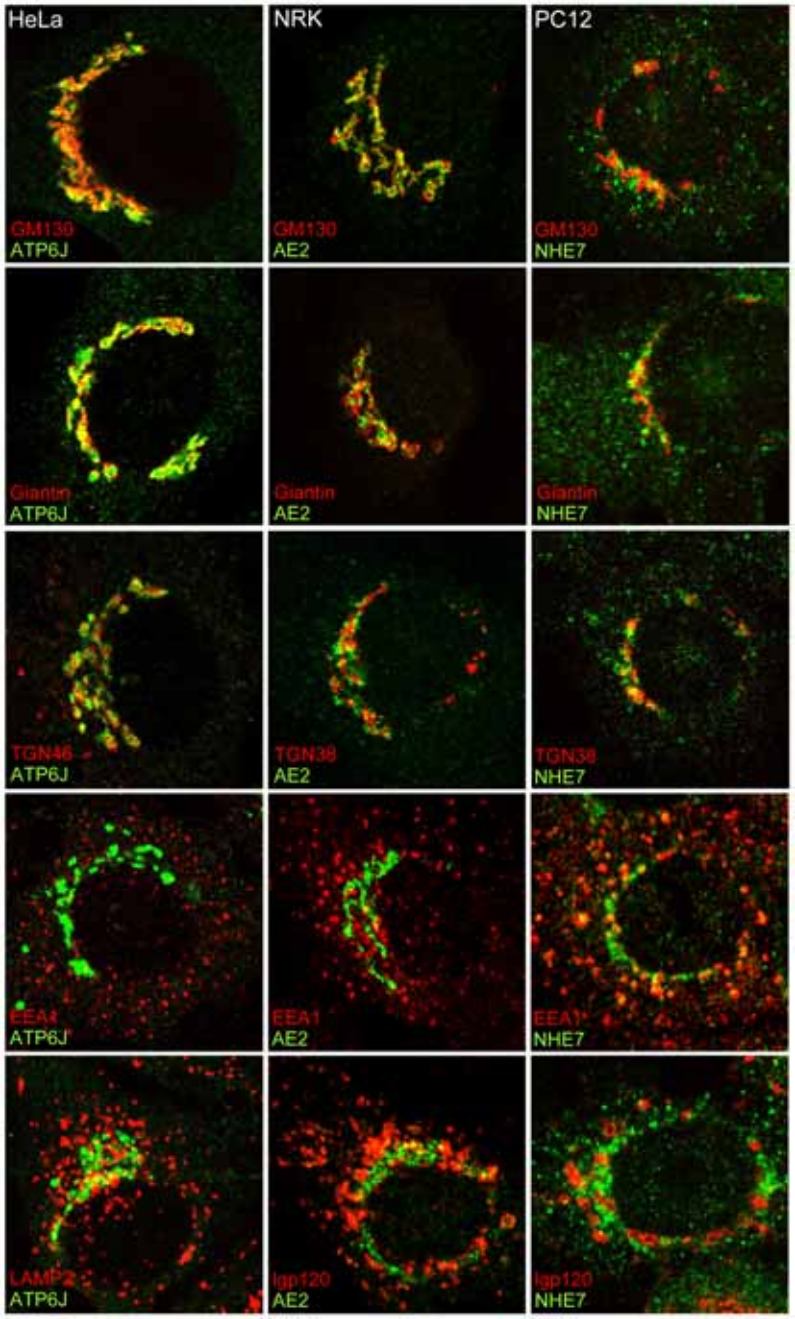

Localización subcelular de elementos implicados en la regulación del pH de compartiemtos intracelulares Células HeLa (izquierda), NRK (centro) o PC12 (derecha), fueron fijadas y teñidas realizando un doble inmunomarcaje frente a la subunidad G de la H^+ ATPasa vacuolar o ATP6J (HeLa), el intercambiador aniónico AE2 (NRK) y el intercambiador catiónico NHE7 (PC12) con distintos marcadores correspondientes al AG (GM130 y Giantina), al TGN (TGN46 y TGN38), a los endosomas tempranos (EEA1) o a los lisosomas (LAMP2 y lgp120). Barra 5 μm.

2.3. Análisis del flujo de membrana inducido por brefeldina A y distribución subcelular del receptor KDEL en la región retículo endoplasmático-aparato de Golgi en células con alteraciones en la homeostasis iónica intracelular

Una forma sencilla de detectar alteraciones en el flujo retrógrado de membranas en la zona RE-AG se consigue mediante el empleo de la droga BfA. La incubación de las células con esta droga provoca un aumento del flujo retrógrado desde AG al RE mediante la emisión de túbulos que se fusionan con el RE, lo que conlleva finalmente a la redistribución completa de las proteínas residentes en el AG al RE. Aprovechando este fenómeno, nos propusimos explorar los efectos que tendrían diferentes drogas que alteran la homeostasis iónica intracelular sobre la cinética de la redistribución del AG hacia el RE inducida por BfA. Como inhibidores de la H^+-ATP vacuolar utilizamos Baf y ConA, la actividad de los intercambiadores aniónicos se alteró con el NaGlu y los intercambiadores catiónicos se inhiben con el Benz. En primer lugar, se valoró el impacto de estas drogas sobre el citoesqueleto con la finalidad de descartar una posible alteración del trasporte retrógrado o anterógrado como consecuencia de una perturbación del citoesqueleto. Observamos como la Baf, la ConA (no presentado), el NaGlu y el Benz a aquellas concentraciones de uso para los experimentos con la BfA no provocan alteraciones en la red de MTs, MFs o FIs (A). La redistribución de membranas desde el AG al ER inducida por la BfA está retrasada por la Baf, ConA, NaGlu y Benz (B). Respecto al reensamblaje del AG al retirar la BfA, observamos un claro retraso en la formación del AG en las células tratadas con NaGlu y Benz pero no con Baf o ConA (C). Por último se analizó la distribución subcelular del KDELr (ver apartado 2.2). Observamos una ligera acumulación de esta proteína en el AG en las células expuestas a la Baf. Por el contrario, el NaGlu y Benz provocan que el KDELr se redistribuya al ERGIC-RE (D). En resumen, la Baf provoca una alteración en la vía retrógrada mientras que el NaGlu y Benz perturban tanto la vía anterógrada como retrógrada.

A

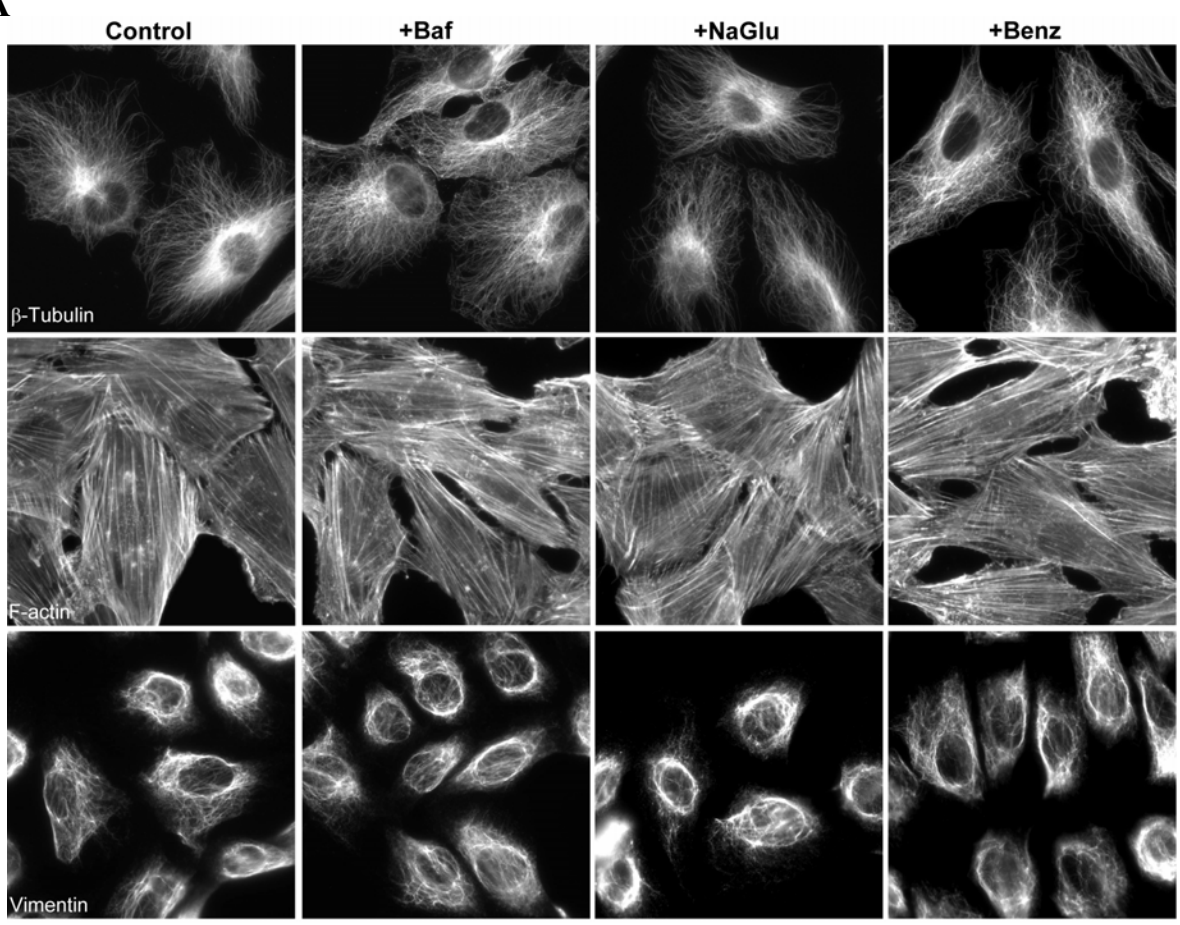

A. Estudio de las alteraciones provocadas sobre el citoesqueleto por agentes que alteran la homeostasis del pH intracelular. Células NRK se incubaron con Baf (100 nM/1 h), NaGlu (50 mM/1 h) o Benz (100 nM/1 h) fijadas y marcadas con β-tubulina, (panel superior) faloidina-TRITC (panel medio) y vimentina (panel inferior) para visualizar la red de MTs, MFs y FIs respectivamente. Barra: 10 μm.

B

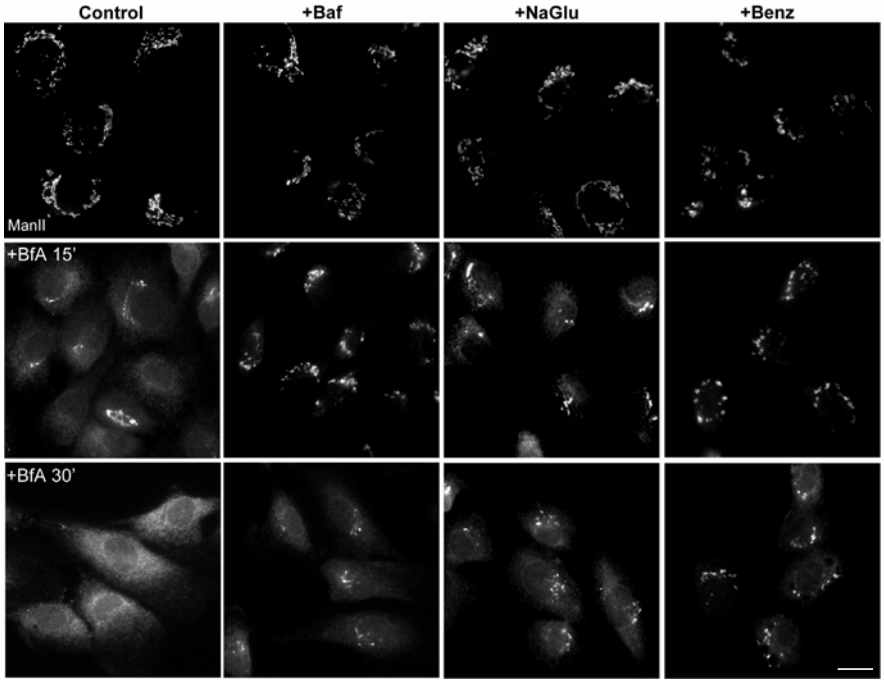

B. Cinética del desensamblaje del AG inducido por la BfA en células incubadas con agentes que alteran la homeostasis iónica intracelular. Células NRK se incubaron con Baf (100 nM/30 min), NaGlu (50 mM/30 min) o Benz (100 nM/30 min) tras lo cual se incubaron con BfA 1 μg/ml 15 y 30 min. El desensamblaje del AG fue visualizado mediante anticuerpos frente a la manosidasa II. Barra: 10 μm.

C

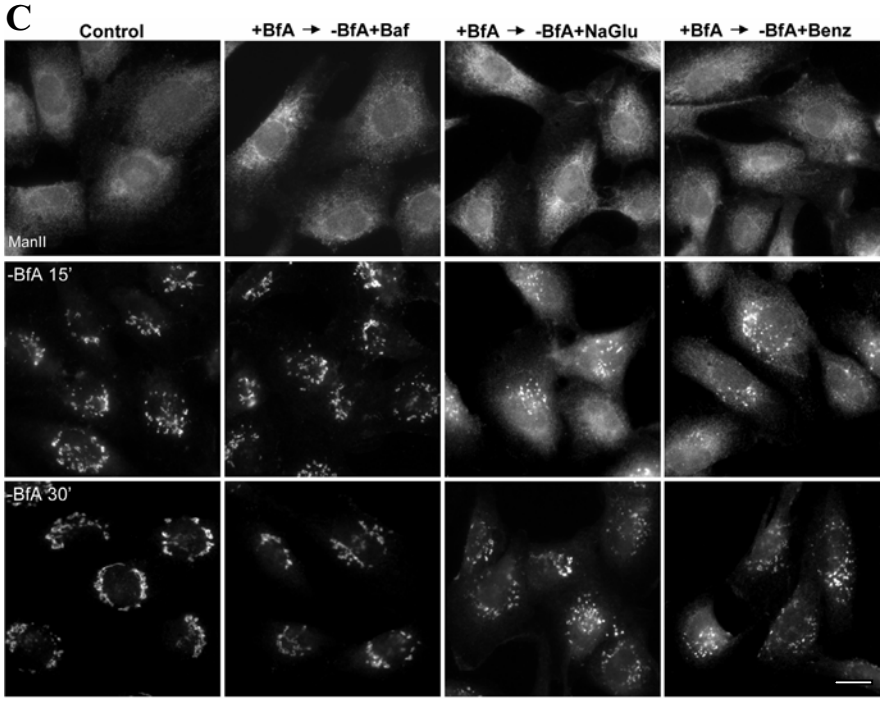

C. Cinética del reseensamblaje del AG tras la retirada de la BfA en células incubadas con agentes que alteran la homeostasis del iónica intracelular. Células NRK previamente tratadas BfA 1 μg/ml 30 min se coincubaron con Baf (100 nM/30 min), NaGlu (50 mM/30 min) y Benz (100 nM/30 min) tras lo cual fueron lavadas e incubadas únicamente con Baf, NaGlu o Benz 15 y 30 min. El reensamblaje del AG fue visualizado mediante anticuerpos frente a la manosidasa II. Barra: 10 μm.

D

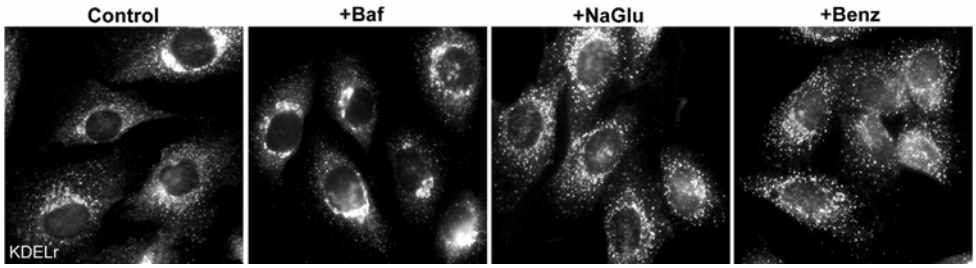

D. Distribución subcelular del receptor KDEL en células incubadas con agentes que alteran la homeostasis iónica intracelular. Células NRK se incubaron con Baf (100 nM/1 h), NaGlu (50 mM/1 h) y Benz (100 nM/1 h) tras lo cual se lavaron y fueron expuestas a la Baf, el NaGlu o el Benz 1 h. Tras ello, se fijaos y tiñeron con anticuerpos frente al receptor de KDEL (KDELr). Barra: 10 μm.

2.4. Ultraestructura del aparato de Golgi en células que presentan alteraciones en la homeostasis iónica intracelular

Teniendo en cuenta que la Baf, la ConA, el NaGlu y el Benz perturban el flujo de membranas entre el RE y AG era de esperar que estas drogas alterasen la morfología de las cisternas del AG. Con la finalidad de detectar dichas alteraciones incubamos células NRK con estos agentes y se procesaron para TEM. El análisis de la ultraestructura de los dictiosomas en las células incubadas con Baf revela una intensa fragmentación y dilatación de cisternas. En el caso del NaGlu observamos un menor número de cisternas. Mientras que el Benz prococa la fragmentación de las cisternas y una ligera dilatación de las mismas. En todos los casos se aprecia un incrementro en el número de perfiles túbulo-vesiculares alrededor de las cisternas del AG.

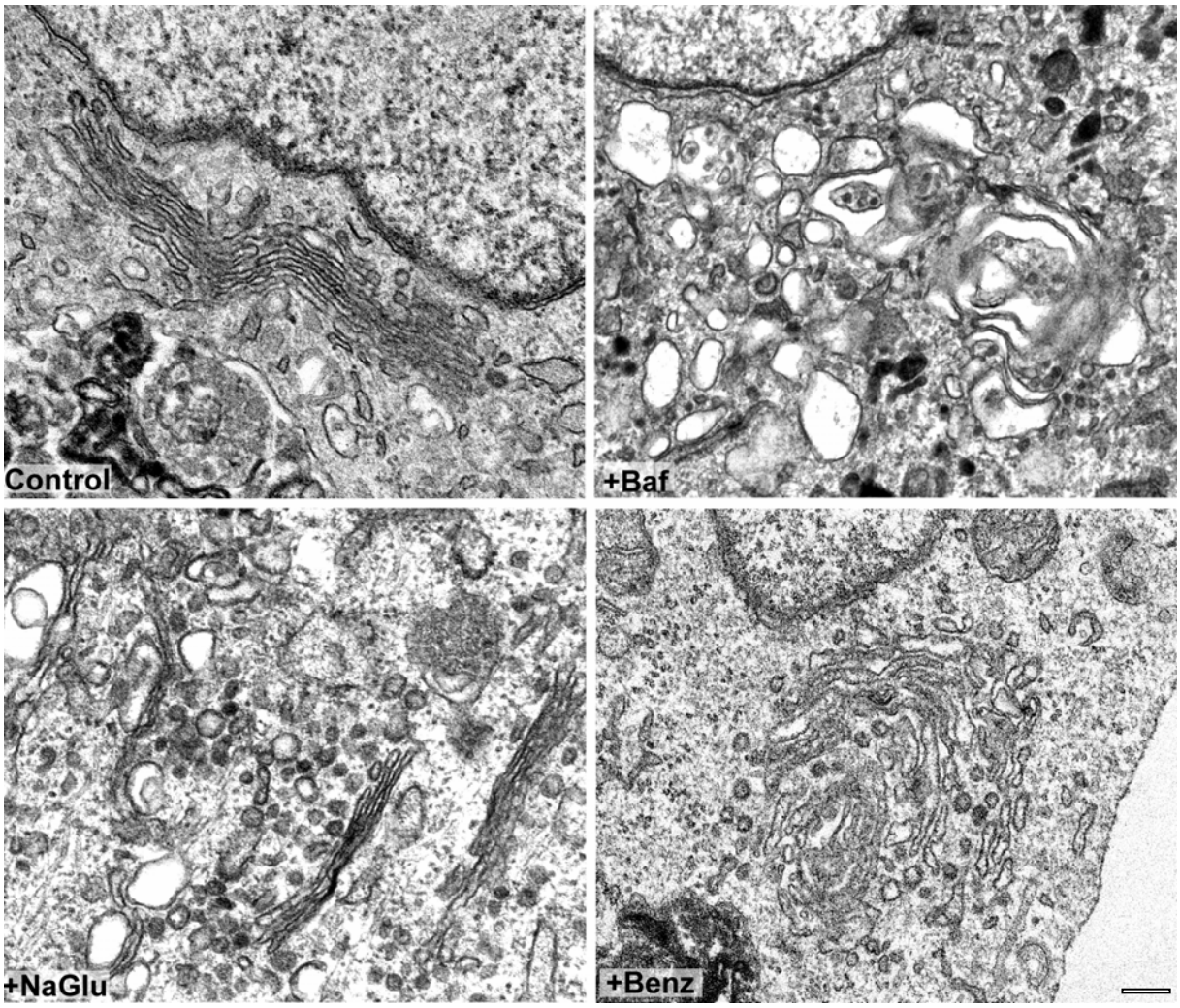

Alteraciones ultraestructurales en el aparato de Golgi inducidas por agentes que alteran la homeostasis iónica intracelular. Células NRK fueron incubadas con Baf (100 nM/1 h), NaGlu (50 mM/1 h) y Benz (100 nM/1 h) tras lo cual fueron fijadas y procesadas para TEM. Barra: 200 nm.

Trabajo 3

REQUERIMIENTO VARIABLE DE LA DINÁMICA DE ACTINA PARA LA SALIDA DE *CARGO* DE LA RED *TRANS* DEL APARATO DE GOLGI

El citoesqueleto de actina no solo tiene un papel estructural en el mantenimiento de la morfología del AG sino que también participa en la funcionalidad del mismo en cuanto al tráfico intracelular. En este sentido, nuestro laboratorio ha implicado a los MFs y una de sus proteínas motoras (la miosina II no muscular) en el transporte retrógrado. A partir de este resultado nos planteamos estudiar si la perturbación de los MF altera también el tráfico intracelular en cuanto al transporte post-Golgi a nivel de la salida de *cargo* del AG y si los posibles efectos son dependientes de la naturaleza del *cargo* y su destino intracelular.

En este trabajo analizamos *in vivo* mediante FRAP inverso la implicación de los MFs en la salida del AG/TGN de *cargo* con destino apical o basolateral asociado o no a balsas lipídicas. Observamos cómo la perturbación del citoesqueleto de actina altera la salida del *cargo* con destino basolateral y apical no asociado a balsas lipídas de una forma variable en función de la proteína estudiada o bien dependiendo del estado en que se encuentren los MFs (despolimerizados con LtB o estabilizados/polimerizados de forma aberrante con Jpk). Por el contrario, la salida de *cargo* con destino apical asociado a balsas lipídicas no se vió afectada por la pertubación de la dinámica del citoesqueleto de actina. Según estos resultados los MFs participan en la salida de *cargo* no asociado con balsas lipídicas del AG con destino basolateral y apical pero sin embargo, son prescindibles para la salida de *cargo* asociado balsas lipídicas.

FEBS Letters 581 (2007) 3875–3881

Variable actin dynamics requirement for the exit of different cargo from the *trans*-Golgi network

Francisco Lázaro-Diéguez[a,b,c,1], Cecilia Colonna[a,1], Miguel Cortegano[a], María Calvo[d], Susana E. Martínez[a,b], Gustavo Egea[a,b,c,*]

[a] *Departament de Biologia Cel·lular i Anatomia Patològica, Facultat de Medicina, Universitat de Barcelona, C/Casanova 143, E-08036 Barcelona, Spain*
[b] *Institut d'Investigacions Biomèdiques August Pi i Sunyer (IDIBAPS), Universitat de Barcelona, C/Casanova 143, E-08036 Barcelona, Spain*
[c] *Institut de Nanociència i Nanotecnologia (IN²UB), Universitat de Barcelona, 08036 Barcelona, Spain*
[d] *Serveis Cientifico-Tècnics (SCT-UB), Universitat de Barcelona, 08036 Barcelona, Spain*

Received 25 April 2007; revised 6 July 2007; accepted 8 July 2007

Available online 17 July 2007

Edited by Felix Wieland

Abstract Efficient post-Golgi trafficking depends on microtubules, but actin filaments and actin-associated proteins are also postulated. Here we examined, by inverse fluorescence recovery after photobleaching, the role of actin dynamics in the exit from the TGN of fluorescent-tagged apical or basolateral and raft or non-raft-associated cargoes. Either the actin-stabilizing jasplakinolide or the actin-depolymerising latrunculin B variably but significantly inhibited post-Golgi traffic of non-raft associated apical p75NTR and basolateral VSV-G cargoes. The TGN-exit of the apical-destined VSV-G mutant was impaired only by latrunculin B. Strikingly, the raft-associated GPI-anchor protein was not affected by either actin toxin. Results indicate that actin dynamics participates in the TGN egress of both apical- and basolateral-targeted proteins but is not needed for apical raft-associated cargo.
© 2007 Federation of European Biochemical Societies. Published by Elsevier B.V. All rights reserved.

Keywords: Actin; Cytoskeleton; Golgi apparatus; Raft; Polarized transport; iFRAP

1. Introduction

The *trans*-Golgi network (TGN) is defined as the major sorting compartment of the secretory pathway of synthesized proteins upon recognition of specific apical or basolateral sorting signals [1–3]. Tightly associated with the TGN is the cytoskeleton, in particular microtubules [4], whereas actin filaments have also recently attracted increasing attention [5,6]. Thus, a variety of actin-regulatory/binding proteins have been implicated in post-Golgi trafficking such as Arp2/3, spir1, myosins II and VI, cortactin, Cdc42, huntingtin related protein 1 (see [5] and references herein), and huntingtin [7]. In addition, the role of actin filaments has also been tested in the transport from the Golgi to the plasma membrane [8–10] and to early/late endosomes [11–13] with a variety of results in some cases. This might be attributable to the use of only one actin-depolymerizing agent (usually cytochalasins) or to utilize different cargoes or both. In any case, the substantial homology between the protein-sequestration and sorting machinery acting at the plasma membrane and the TGN [6,14] points to a significant role of actin filaments or actin dynamics (actin depolymerization/polymerization cycle) at the TGN as occurs at the plasma membrane, but it remains to be established whether actin acts at the level of cargo sorting, in membrane budding/scission, or in the subsequent locomotion of TGN-derived transport carriers or both [5]. As a first approach to this end, we here explore how actin dynamics participates in the exit from the TGN of a variety of cargo proteins using in vivo inverse fluorescence recovery after photobleaching (iFRAP) analysis. This technique allows analysis of the kinetic parameters of the exit of a fluorescently-tagged cargo protein from a subcellular compartment (the Golgi stack/TGN in our case). Furthermore, our study is focused on the potential role of actin dynamics in post-Golgi egress regardless of the intrinsic molecular mechanisms that determine the sorting and subsequent polarized transport of these cargoes. Thus, basolateral sorting is mediated by peptide sequences containing tyrosine- and dileucine motifs [15]. In contrast, apical sorting is facilitated by one of two mechanisms: either by lipid-lipid and lipid-protein interactions within the transmembrane or luminal domains, given by N- and O-glycans [16], or by such interactions within the glycosylphosphatidylinositol (GPI) anchor domain, which is invariably associated with lipid rafts [17,18]. Recent lines of evidence indicate that oligomerization of membrane proteins at the TGN is an important sorting determinant for apical transport of raft-associated proteins [19]. Therefore, apical sorting and transport can be mediated by raft-dependent and raft-independent mechanisms. It is important to highlight that both polarized and non-polarized epithelial cells share molecular mechanisms in the sorting of secretory cargo, the formation of transport carriers and their subsequent transport to the plasma membrane. This validates the utilization of non-polarized cell lines, for instance COS-1 or non-polarized MDCK cells [20,21] to address the aforementioned questions. In this respect, non-epithelial cells are capable of packaging and transporting secretory cargo selectively in distinct types of Golgi-derived carriers like fully-polarized cells do [22].

In this study we examined how actin toxins that depolymerize (latrunculin B/LtB) or stabilize (jasplakinolide/Jpk) actin filaments impair the TGN-exit of non-raft-associated apical

*Corresponding author. Address: Departament de Biologia Cel·lular i Anatomia Patològica, Facultat de Medicina, Universitat de Barcelona, C/Casanova 143, E-08036 Barcelona, Spain. Fax: +34 93 4021907.
E-mail address: gegea@ub.edu (G. Egea).

[1]These authors equally contributed to this study.

0014-5793/$32.00 © 2007 Federation of European Biochemical Societies. Published by Elsevier B.V. All rights reserved.
doi:10.1016/j.febslet.2007.07.015

(p75NTR)- or basolateral (VSV-G)-targeted proteins. At the same time, we also examined whether actin dynamics is needed for the exit of raft-associated GPI from the TGN. Lipid rafts are membrane platforms enriched in sphingomyelin, cholesterol and phosphatidylinositol 4,5-biphosphate (PIP_2). The latter has a tight relationship with the actin cytoskeleton since it promotes actin assembly into filaments [23]. We observed that actin dynamics participates in the exit of both non-raft-associated apical and basolateral-targeted cargo, but it was not needed for the TGN exit of raft-anchored GPI. This indicates that actin does not functionally associate with raft-associated GPI anchored proteins at the TGN.

2. Materials and methods

2.1. Cell culture and reagents

COS-1 cells were grown at 37 °C in complete DMEM culture medium, which consisted of DMEM (Gibco BRL, Eggestein, Germany) supplemented with penicillin (100 i.u./ml), streptomycin (100 mg/ml), L-glutamine (2 mM), MEM sodium pyruvate (1 mM) and fetal calf serum (10%). Latrunculin B was purchased from Calbiochem (EMD Biosiences, Inc., darnstadt, Germany) and Jasplakinolide from Molecular probes (Eugene, OR, USA). Monoclonal antibodies to giantin were kindly provided by H.P. Hauri (Biozentrum, Basel University) and those to TGN46 were purchased from Serotec (Oxford, UK). Secondary Alexa Fluor 546 donkey anti-sheep IgG (H + L) and Alexa Fluor 647 goat anti-mouse was from Invitrogen (Carlsbad, CA, USA).

2.2. Plasmids

GFP-tagged wild type and apical-targeted GFP-VSV-G mutant cDNAS, as well as the CFP-tagged VSV-G wild type cDNA were kindly provided by Kai Simons (Max Planck Institute of Molecular Cell Biology and Genetics, Dresden, Germany), and GFP-p75NTR and YFP-GPI cDNAs were kindly supplied by Roman Polishchuk (CMNS, Chieti, Italy).

2.3. Transient transfection

COS-1 cells were grown on coverslips in a 35 mm Petri dish and transiently transfected with the corresponding cDNA using Effectene, in accordance with the manufacture's instructions (Qiagen) for 16 h at 37 °C in complete DMEM.

2.4. Actin toxins treatments and inversal FRAP experiments

To synchronize post-Golgi traffic at the TGN, transfected cells were incubated at 19.5 °C for 2 h in the presence of cycloheximide (100 μm/ml). Cells were subsequently treated for 20 min at 19.5 °C with LtB or Jpk (500 nM each) (see the experimental scheme in Fig. 1A).

Inverse fluorescence recovery after photobleaching (iFRAP) experiments were carried out using a Leica TCS SL laser scanning confocal spectral microscope (Leica Microsystems Heidelberg GmbH, Manheim, Germany) with Argon and HeNe lasers attached to a Leica DMIRE2 inverted microscope equipped with an incubation system with temperature and CO_2 control. All experiments were performed at 32 °C and 5% CO_2. For visualization of GFP/YFP, images were acquired using a 63× oil immersion objective lens (NA 1.32), 488 nm laser line, excitation beam splitter RSP 500, emission range detection: 500–600 nm with the confocal pinhole set at 4.94 Airy units to minimize changes in fluorescence due to protein-GFP moving away from the plane of focus. The whole cytoplasm, except the Golgi, of GFP-fusion protein transfected cell was photobleached using 50–80 scans with the 488 nm laser line at full power. Postbleach images were monitored at 5 s intervals for 15 min. The excitation intensity was attenuated to approximately 5% of the half laser power to avoid significant photobleaching. Longer recording times were also performed to check the arrival of cargo at the plasma membrane and the subsequent absence of fluorescence in the Golgi.

2.5. Inverse FRAP analysis

To evaluate the results of photobleaching experiments, the observed fluorescence equilibration in the unbleached region (the Golgi complex) was quantified using the Image Processing Leica Confocal Software. Background fluorescence was measured in a random field outside of cells. All experiments were background substracted, corrected and normalized using the equation described below. For each time point the relative loss of total fluorescent intensity in the unbleached region of interest was calculated as:

$$I_{rel} = (I_t)/(I_o) \times (T_{mean}/T_t)$$

where I_t is the average intensity of the unbleached region of interest at time point t, I_o is the average pre-bleach intensity of the region of interest and T_{mean} and T_t are the total mean cell intensity of the whole postbleach period and average total cell intensity at each time of postbleach, respectively. Fitting of iFRAP curves was performed with Graphpad Prism Software v.3.0 (Graphpad Software, San Diego, CA) and modelled assuming two-phase exponential decay iFRAP, whereas they were equally well modelled with the one-phase exponential decay equation:

$$Y(\text{fluorescence decay}) = \text{Span} \cdot \exp(-K \cdot X) + \text{Plateau}$$

where Y started at span + plateau and decayed to plateau with a rate constant K. Half-time was calculated as: $0.69/K$. Afterwards, data plotted as fluorescence intensity that remained in the Golgi vs. time. Mobile fraction (MF) was calculated as:

$$\text{MF} = (F_{pre} - F_{end})/F_{pre}$$

where F_{pre} was the initial fluorescence intensity and F_{end} the final recovered fluorescence intensity. Statistical analysis was performed by non-parametric ANOVA post-test Bonferroni.

2.6. Immunofluorescence

Indirect immunofluorescence was carried out as previously described [7] with the following antibody dilutions: anti-giantin, 1:500 and anti-TGN46, 1:100. Secondary antibodies were used at 1:250.

3. Results and discussion

We analyzed the fluorescence decay curves of a variety of green or yellow fluorescent protein (GFP/YFP)-tagged cargoes from the *trans*-Golgi network (TGN) by iFRAPs in single living mammalian cells. This technique allows us to measure the time of association of the different GFP/YFP-tagged cargoes within the TGN, and their dissociation is then reflected by the loss of fluorescence from this region over time monitored by confocal microscopy.

We performed experiments for three types of GFP/YFP-tagged proteins: either raft-associated and apical-targeted such as GPI, or non-raft-associated and basolateral-targeted like VSV-G protein, or apical-targeted such as p75NTR and VSV-G mutant. All these proteins have been reported in apical- and basolateral-like transport carriers in non-polarized [24] and fully-polarized MDCK cells [2,25–28], Vero, BHK and CHO cell lines [22,29]. Taking this into account, we utilized COS-1 cells (a non-polarized cell line), which are highly suitable to be transfected, in contrast to MDCK cells which usually require microinjection. For quantitative analysis, we chose those cells that express relatively low levels of GFP/YFP-tagged proteins to overcome potential toxicity of overexpression and, furthermore, those with identical Golgi-associated basal fluorescence to render the data comparable.

We analyzed the kinetics of the TGN-exit of membrane cargo by plotting Golgi fluorescence intensity over time and by determining, for each condition, the mobile fraction, which is defined as the amount of cargo that has left the Golgi after 15 min at 32 °C and the halftime point ($T_{1/2}$), which is defined as the time at which 50% of the mobile fraction has been lost (Fig. 1A). COS-1 cells were then transfected with the corre-

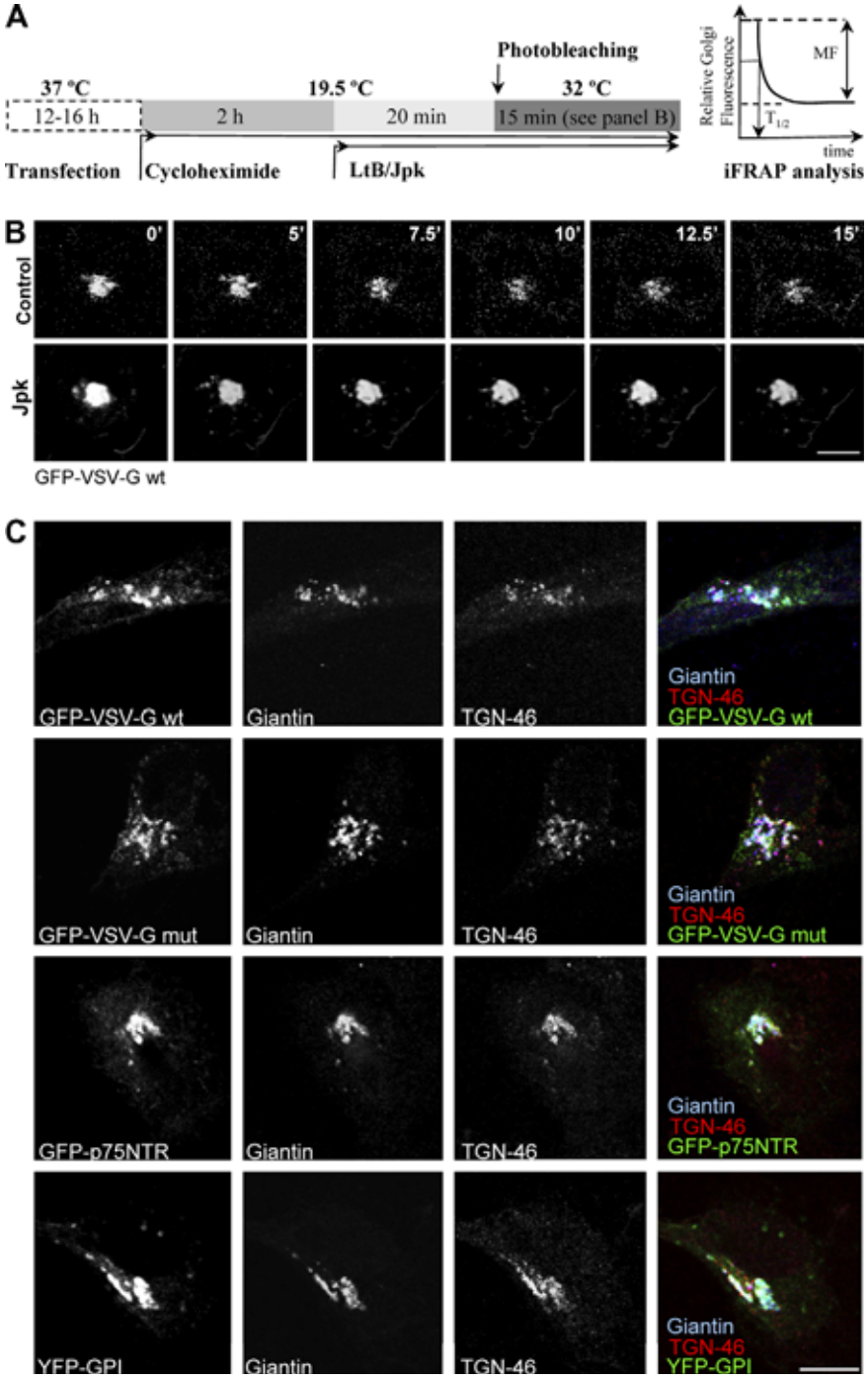

Fig. 1. (A) Scheme of the experimental design used in this study. (B) Representative frames obtained from time-lapse iFRAP confocal microscopy experiments in transiently transfected COS-1 cells expressing wild-type basolateral GFP-VSV-G. Note that in control cells, the Golgi-associated fluorescence of GFP-VSV-G decays over time, whereas in cells treated with the actin-stabilizing toxin jasplakinolide (Jpk; 500 mM) the fluorescence remains virtually unaltered. (C) Colocalization experiments in COS-1 cells of GFP-tagged cargoes used in this study with the Golgi stack marker giantin and the TGN marker TGN-46 in COS-1 cells incubated at 19.5 °C in the presence of cycloheximide. Bar, 10 μm.

sponding plasmids and left overnight at 37 °C. Before the in vivo recording, cargo was allowed to accumulate at the Golgi/TGN by culturing cells at 19.5 °C for 2 h in the presence of cycloheximide. Cells were treated with the corresponding actin toxin (LtB or Jpk) for the last 20 min at 19.5 °C. We confirmed that LtB and Jpk significantly disrupted the actin cytoskeleton at this time and temperature (data not shown). Subsequently, cells were placed in the confocal chamber at 32 °C and iFRAP was carried out (Fig. 1A). When transfected cells were cultured at 19.5 °C, GFP/YFP-tagged proteins invariably accumulated in the Golgi, which was distinguishable because of the high fluorescence accumulated in a peri-nuclear structure (Fig. 1B) and by double-labeling experiments using well-established Golgi stack and TGN markers such as giantin and

TGN46, respectively (Fig. 1C). Moreover, reticular and punctate cytoplasmic fluorescence pools were also observed, which corresponded to proteins located in the endoplasmic reticulum and transport carriers in transit to the Golgi or the plasma membrane, respectively. A characteristic morphological visualization of an iFRAP experiment for untreated (control) and Jpk-treated COS-1 cells expressing GFP-VSV-G is shown in Fig. 1B. In contrast to the control cell, the Golgi-associated fluorescence corresponding to VSV-G was virtually unaltered over time as a consequence of Jpk treatment. The kinetics of Golgi release followed by VSV-G showed a rapid decrease (Figs. 1B and 2A, red), indicating that protein was released up to 56% with a $T_{1/2}$ of 3.0 min in untreated cells (Fig. 2A, red; Table 1). In the presence of Jpk, VSV-G release from the Golgi was robustly inhibited (Fig. 1B), resulting in a fall of the mobile fraction after 15 min which was only of ~10% (Fig. 2A, blue; Table 1). When cells were treated with the actin-depolymerizing toxin LtB (Fig. 2A, green), the mobile fraction was also significantly reduced to ~27% ($T_{1/2}$ of 5.7 min) but to a lesser extent than Jpk treatment (Fig. 2A; Table 1). These results indicate that VSV-G exit from the TGN is significantly reduced by either the stabilization or depolymerization of actin filaments, which suggests that actin dynamics (for example, a rapid actin turnover coupled to the formation of the transport carrier [5]) is necessary for its post-Golgi transport.

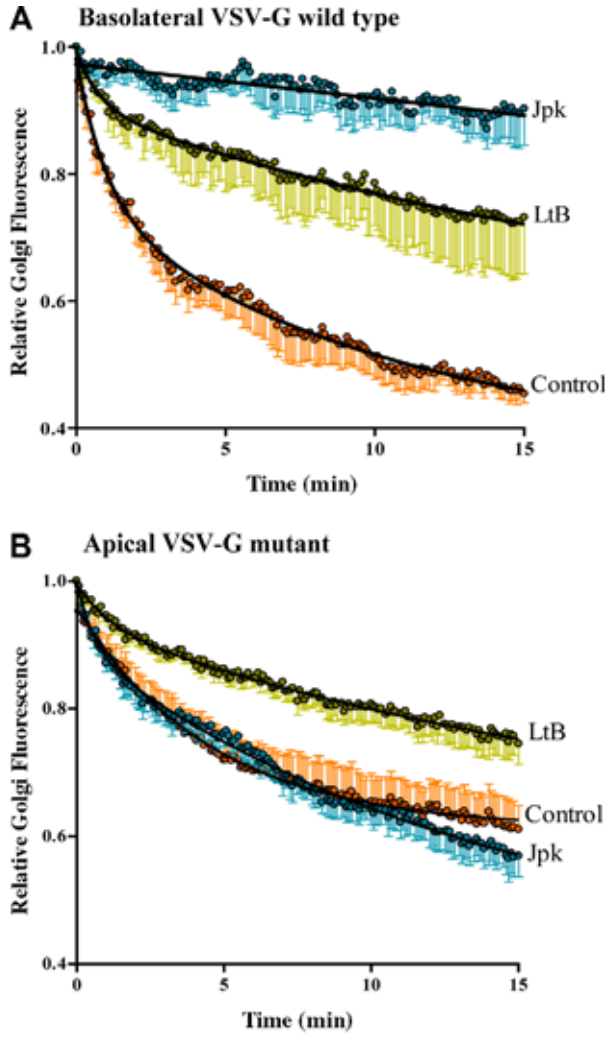

Fig. 2. Inverse FRAP decay curves of basolateral GFP-VSV-G (A) and apical GFP-VSV-G mutant (B) in COS-1 cells. Results are the means ± S.E.M. from *n* cells indicated in Table 1.

In order to test whether this actin dynamics-dependence was in turn dependent on the intrinsic basolateral destination of the VSV-G, we used an apical-destined VSV-G mutant in which the tyrosine-based motif is masked [30]. We reasoned that since the post-Golgi exit of VSV-G involving actin dynamics is also signal-mediated, we would expect differences in the TGN exit kinetic parameters in the apical-targeted mutant in comparison to the basolateral wild-type form. We observed that the apical VSV-G mutant (Fig. 2B, red) showed a lower mobile fraction than that of the basolateral VSV-G (~36% and ~56%, respectively; Table 1) whereas the $T_{1/2}$ was practically the same (3.2 min and 3.0 min, respectively; Table 1). Unexpectedly, the apical VSV-G mutant was only sensitive to LtB (Fig. 2B, green), giving rise to a significant reduction of the mobile fraction (~25%; Table 1) and a larger $T_{1/2}$ (6.2 min). This indicates that cargo transport was slowed-down but, as occurred in control cells, the $T_{1/2}$ of LtB-treated cells expressing either wild-type or mutant VSV-G displayed no significant difference (5.7 min and 6.2 min, respectively; Table 1). In contrast, Jpk-treated cells showed no changes in the shape of the decay curve, the mobile fraction, or the $T_{1/2}$ in comparison to control cells (Fig. 2B, blue; Table 1).

The delay in the VSVG-GFP egress from the Golgi in LtB-treated cells implies the involvement of actin in protein export from the TGN. This result is consistent with previous observations in which VSV-G exit from the TGN was lower in cells treated with cytochalasin-B than in untreated cells [8]. These authors also reported morphological changes in cargo-containing tubules, which suggested that actin and actin-based cytoskeleton components are involved in the detachment of TGN-derived transport carriers. The arrival of VSV-G at the basolateral plasma membrane also decreased in LtB-treated non-polarized MDCK cells [31]. Several groups have found that interfering with interactions between dynamin II and syndapin II in living cells caused an inhibition of VSV-G exit from the TGN [32], and the overexpression of a dominant-interfering mutant of actin nucleator Spir-1 also strongly inhibited post-Golgi VSV-G transport to the plasma membrane [33]. Not only actin but also actin regulators such as Cdc42 participate in the appropriate sorting at the TGN. Thus, VSV-G and LDL receptor were missorted to the apical membrane in cells expressing mutants of Cdc42 [31]. Therefore, our results indicate that actin depolymerization/polymerization cycle controls the exit of basolateral VSV-G protein from the TGN rather than the presence of filamentous actin alone, whose involvement in apical VSV-G mutant transport seems to be more direct according to the inhibitory effects caused only by LtB.

Next, we tested the effect of both actin toxins on post-Golgi traffic of membrane protein p75 neurotrophin receptor (p75NTR) coupled to GFP [9,31]. In stably transfected polarized and non-polarized MDCK cells, p75NTR is a non-raft-associated protein that is exclusively transported to the apical plasma membrane via apical sorting signals contained within the O-glycosylated stalk [9,27]. As shown in Fig. 3A, in control cells the decay curve shape for GFP-p75NTR was similar to those observed for both VSV-Gs. However, the mobile fraction (~46%) was greater than in the apical VSV-G mutant

Table 1
Mobile fraction (MF; in %) and $T_{1/2}$ (in min) values for each GFP/YFP-tagged cargo exiting from the TGN examined by iFRAP in control and actin toxin-treated cells

	Basolateral VSV-G		Apical VSV-G		p75NTR		GPI	
	MF	$T_{1/2}$	MF	$T_{1/2}$	MF	$T_{1/2}$	MF	$T_{1/2}$
Control	56 ± 1.9 (n = 6)	3.0	36.6 ± 3.4 (n = 10)	3.2	46.1 ± 4.5 (n = 8)	7.1	44.8 ± 2.9 (n = 11)	4.1
Jpk	9.5 ± 4.2*** (n = 6)	>10	41.2 ± 3.5 (n = 6)	4.6	28.4 ± 6.0* (n = 7)	3.5	41.8 ± 4.5 (n = 6)	3.1
LtB	26.8 ± 8.9** (n = 6)	5.7	25.2 ± 3.7* (n = 7)	6.2	26.9 ± 3.6** (n = 9)	2.1	38.7 ± 4.9 (n = 8)	3.0

Results are the means ± S.E.M. Statistical significance: * $P \leqslant 0.05$, ** $P \leqslant 0.01$, *** $P \leqslant 0.001$.

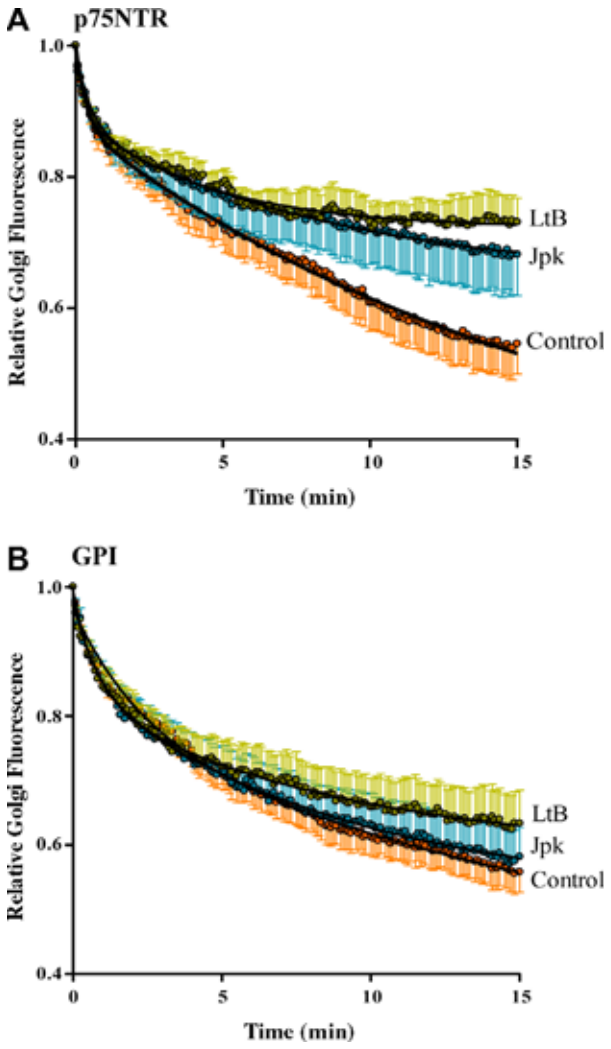

Fig. 3. Inverse FRAP decay curves of non-raft-associated apical-targeted GFP-p75NTR (A) and raft-associated apical YFP-GPI-anchored protein (B). Results are the means ± S.E.M. from n cells indicated in Table 1.

(~36%) but lower than that obtained for the wild-type basolateral VSV-G (~56%) (Table 1). The exit of p75NTR from the Golgi was significantly inhibited when cells were treated with Jpk or LtB (Fig. 3A), which resulted in a significant decrease in their respective protein mobile fractions (~28% and ~27%, respectively) (Table 1). These results are inconsistent with those obtained with the apical VSV-G mutant protein, which is also non-raft-associated, since their respective sensitivity to Jpk appears to be different. In contrast, both are equally sensitive to LtB, whose use and sensitivity for p75NTR was previously reported [9]. Note that the decay curve for p75NTR during the first 3 min at 32 °C was the same in both control and treated cells, and that the differences caused by actin toxins appeared later (Fig. 3A). This behavior indicates that actin dynamics is not required for molecular processes that lead to the immediate egress of cargo from the TGN (for instance, the formation of the transport carrier). In other words, actin toxins do not appear to alter the initial mobile fraction. In contrast, actin dynamics might be necessary for earlier molecular processes (for instance, cargo sorting) and any alterations would then affect the immobile fraction. Previous results showed that p75NTR transport to the membrane is altered by expression of Cdc42 mutants, but both constitutive active and inactive mutants differentially altered the exit of apical and basolateral proteins from the TGN in vitro [31]. The sensitivity to Jpk treatment could be a particularity of p75NTR, suggesting that actin cytoskeleton dynamics would mediate different effects depending on the apically-destined cargo examined. p75NTR contains three dileucine motifs that might represent a type of basolateral sorting signal [34], but that are present on naturally occurring membrane proteins targeted basolaterally because they lack apical sorting information.

Finally, an unconventional (non-sorting-receptor mediated) mechanism for apical sorting is the association with lipid rafts [35]. A role for rafts in protein sorting was first described for apical sorting of GPI-anchored proteins in polarized epithelial cells, where these proteins associate with detergent-resistant microdomains (DRMs) during their passage through the Golgi apparatus [36]. Therefore, to explore whether the actin dynamics actively participates in post-Golgi traffic of raft-associated proteins, we examined the raft-associated glycosylphosphatidylinositol (GPI)-anchored protein tagged to YFP, which is sorted to the apical surface [26,29,37]. The release of YFP-GPI from the Golgi in untreated COS cells showed a similar decay curve to those observed for other cargoes but, notably, after the release from the 19.5 °C blockage (Fig. 3B) and conversely to the other examined apical-targeted proteins, GPI was totally unaffected by actin toxins (Fig. 3B; Table 1). Moreover, the final YFP-GPI subcellular destination was the plasma membrane and equally occurred both in treated and untreated cells (not shown). In fact, all this was unexpected taking into account the attributed role of lipid rafts and actin cytoskeleton polymerization occurring in the plasma membrane [23]. It could be postulated that this occurs since GPI, unlike the other examined cargoes, accumulates in a different perinuclear compartment upon 20 °C incubation and, therefore, we were monitoring its exit from another subcellular compartment in which actin dynamics is irrelevant. This possibility was discarded since cells co-expressing YFP-GPI and

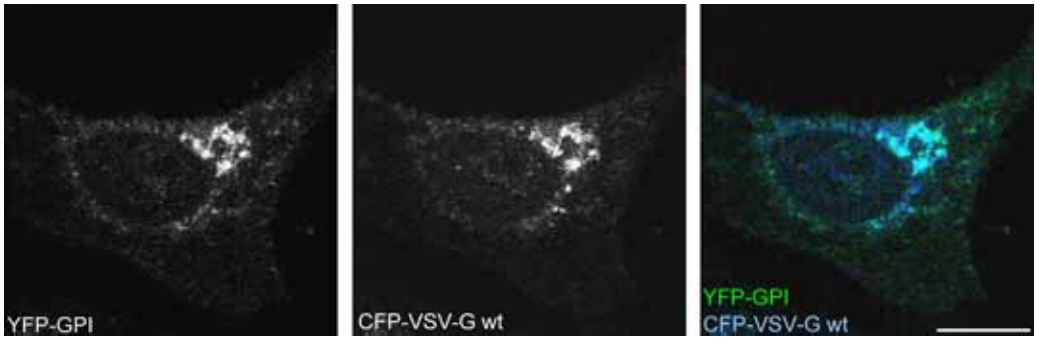

Fig. 4. Colocalization of YFP-GPI and the CFP-VSV-G wild-type form in the Golgi complex of COS-1 cells incubated at 19.5 °C in the presence of cycloheximide. Bar, 10 μm.

CFP-VSV-G showed that both proteins largely colocalized in the same compartment upon 19.5 °C accumulation (Fig. 4). An alternative and more probable explanation is that Golgi-associated lipid rafts are not enriched with PIP_2 like those in the plasma membrane. In this respect, it is known that PIP_2 levels at the Golgi are very low [38]. Recent data have provided additional clues on how rafts might participate in apical sorting, regardless of the putative participation of actin filaments. These authors demonstrated that protein oligomerization is a specific requirement for apical sorting of GPI-tagged apical proteins in MDCK and Fischer rat thyroid (FRT) cells, and is not used by transmembrane, non-raft-associated apical proteins [19]. Association with rafts in the Golgi seems to be insufficient for this process and an additional step that concentrates the proteins into large complexes is required, as suggested by the fact that this behavior is not observed for basolateral GPI-proteins [39].

The results reported here indicate that transport carriers that contain raft-associated GPI anchored proteins are primarily sorted or formed at the TGN independently of actin. This is not the case for those non-raft-associated cargoes destined to apical or basolateral plasma membrane domains. Moreover, data suggest that actin dynamics is particularly relevant to cargo targeted to the basolateral plasma membrane domain.

Acknowledgements: We thank Inés Fernández-Ulibarri and Emma Martínez-Alonso for critical reading of the manuscript, Maite Muñoz and Anna Bosch for technical support and Robin Rycroft for editorial assistance. This work has been supported by Grants BFU2006-876/BMC and European Commission RTN2002-00252 to G.E.

References

[1] Griffiths, G. and Simons, K. (1986) The trans-Golgi network: sorting at the exit site of the Golgi complex. Science 234, 438–443.
[2] Wandinger-Ness, A., Bennett, M.K., Antony, C. and Simons, K. (1990) Distinct transport vesicles mediate the delivery of plasma membrane proteins to the apical and basolateral domains of MDCK cells. J. Cell Biol. 11, 987–1000.
[3] Keller, P., Toomre, D., Diaz, E., White, J. and Simons, K. (2001) Multicolour imaging of post-Golgi sorting and trafficking in live cells. Nat. Cell Biol. 3, 40–149.
[4] Musch, A. (2004) Microtubule organization and function in epithelial cells. Traffic 5, 1–9.
[5] Egea, G., Lázaro-Diéguez, F. and Vilella, M. (2006) Actin dynamics at the Golgi complex in mammalian cells. Curr. Opin. Cell Biol. 18, 168–178.
[6] McNiven, M.A. and Thompson, H.M. (2006) Vesicle formation at the plasma membrane and trans-Golgi network: the same but different. Science 313, 1591–1594.
[7] del Toro, D., Canals, J.M., Ginés, S., Kojima, M., Egea, G. and Alberch, J. (2006) Mutant huntingtin impairs the post-Golgi trafficking of brain-derived neurotrophic factor but not its Val66Met polymorphism. J. Neurosci. 26, 12748–12757.
[8] Hirschberg, K., Miller, C.M., Ellenberg, J., Presley, J.F., Siggia, E.D., Phair, R.D. and Lippincott-Schwartz, J. (1998) Kinetic analysis of secretory protein traffic and characterization of Golgi to plasma membrane transport intermediates in living cells. J. Cell Biol. 143, 1485–1503.
[9] Musch, A., Cohen, D., Kreitzer, G. and Rodriguez-Boulan, E. (2001) Cdc42 regulates the exit of apical and basolateral proteins from the TGN. EMBO J. 20, 2171–2179.
[10] Cao, H., Weller, S., Orth, J.D., Chen, J., Huang, B., Chen, J.L., Stamnes, M. and McNiven, M.A. (2005) Actin and Arf1-dependent recruitment of a cortactin-dynamin complex to the Golgi regulates post-Golgi transport. Nat. Cell Biol. 7, 483–492.
[11] Apodaca, G. (2001) Endocytic traffic in polarized epithelial cells: role of the actin and microtubule cytoskeleton. Traffic 2, 149–159.
[12] Brown, B.K. and Song, W. (2001) The actin cytoskeleton is required for the trafficking of the B cell antigen receptor to the late endosomes. Traffic 2, 414–427.
[13] Mundy, D.I., Machleidt, T., Ying, Y.S., Anderson, R.G. and Bloom, G.S. (2002) Dual control of caveolar membrane traffic by microtubules and the actin cytoskeleton. J. Cell Sci. 115, 4327–4339.
[14] Traub, L.M. (2005) Common principles in clathrin-mediated sorting at the Golgi and the plasma membrane. Biochim. Biophys. Acta 1744, 415–437.
[15] Bonifacino, J.S. and Traub, L.M. (2003) Signals for sorting of transmembrane proteins to endosomes and lysosomes. Annu. Rev. Biochem. 72, 395–447.
[16] Potter, B.A., Ihrke, G., Bruns, J.R., Weixel, K.M. and Weisz, O.A. (2004) Specific N-glycans direct apical delivery of transmembrane, but not soluble or glycosylphosphatidylinositol-anchored forms of endolyn in Madin-Darby canine kidney cells. Mol. Biol. Cell 15, 1407–1416.
[17] Muñiz, M. and Riezman, H. (2000) Intracellular transport of GPI-anchored proteins. EMBO J. 19, 10–15.
[18] Schuck, S. and Simons, K. (2004) Polarized sorting in epithelial cells: raft clustering and the biogenesis of the apical membrane. J. Cell Sci. 117, 5955–5964.
[19] Paladino, S., Sarnataro, D., Tivodar, S. and Zurzolo, C. (2007) Oligomerization is a specific requirement for apical sorting of glycosyl-phosphatidylinositol-anchored proteins but not for non-raft-associated apical proteins. Traffic 8, 251–258.
[20] Keller, P. and Simons, K. (1997) Post-Golgi biosynthetic trafficking. J. Cell Sci. 110, 3001–3009.
[21] Rodríguez-Boulán, E., Kreitzer, G. and Musch, A. (2005) Organization of vesicular trafficking in epithelia. Nat. Rev. Mol. Cell. Biol. 6, 233–247.
[22] Rustom, A., Bajohrs, M., Kaether, C., Keller, P., Toomre, D., Corbeil, D. and Gerdes, H.H. (2002) Selective delivery of secretory cargo in Golgi-derived carriers of nonepithelial cells. Traffic 3, 279–288.
[23] Caroni, P. (2001) New EMBO members' review: actin cytoskeleton regulation through modulation of $PI(4,5)P_2$ rafts. EMBO J. 20, 4332–4336.

[24] Musch, A., Xu, H., Shields, D. and Rodríguez-Boulán, E. (1996) Transport of vesicular stomatitis virus G protein to the cell surface is signal mediated in polarized and nonpolarized cells. J. Cell Biol. 133, 543–558.
[25] Rindler, M.J., Ivanov, I.E., Plesken, H., Rodríguez-Boulán, E. and Sabatini, D.D. (1984) Viral glycoproteins destined for apical or basolateral plsma membrane domains traverse the same Golgi apparatus during their intracellular transport in doubly infected Madin-Darby canine kidney cells. J. Cell Biol. 98, 1304–1319.
[26] Lisanti, M.P., Caras, I.W., Davitz, M.A. and Rodríguez-Boulán, E. (1989) A glycophospholipid membrane anchor acts as an apical targeting signal in polarized epithelial cells. J. Cell Biol. 109, 2145–2156.
[27] Yeaman, C., Le Gall, A.H., Baldwin, A.N., Monlauzeur, L., Le Bivic, A. and Rodriguez-Boulan, E. (1997) The *O*-glycosylated stalk domain is required for apical sorting of neurotrophin receptors in polarized MDCK cells. J. Cell Biol. 139, 929–940.
[28] Keller, P., Toomre, D., Diaz, E., White, J. and Simons, K. (2001) Multicolour imaging of post-Golgi sorting and trafficking in live cells. Nat. Cell Biol. 3, 140–149.
[29] Yoshimori, T., Keller, P., Roth, M.G. and Simons, K. (1996) Different biosynthetic transport routes to the plasma membrane in BHK and CHO cells. J. Cell Biol. 133, 247–256.
[30] Schuck, S., Gerl, M.J., Ang, A., Manninen, A., Keller, P., Mellman, I. and Simons, K. (2007) Rab10 is involved in basolateral transport in polarized Madin-Darby Canine Kidney cells. Traffic 8, 47–60.
[31] Cohen, D., Musch, A. and Rodríguez-Boulán, E. (2001) Selective control of basolateral membrane protein polarity by Cdc42. Traffic 2, 556–564.
[32] Kessels, M.M., Dong, J., Leibig, W., Westermann, P. and Qualmann, B. (2006) Complexes of syndapin II with dynamin II promote vesicle formation at the trans-Golgi network. J. Cell Sci. 119, 1504–1516.
[33] Kerkhoff, E., Simpson, J.C., Leberfinger, C.B., Otto, I.M., Doerks, T., Bork, P., Rapp, U.R., Raabe, T. and Pepperkok, R. (2001) The Spir actin organizers are involved in vesicle transport processes. Curr. Biol. 11, 1963–1968.
[34] Johnson, D., Lanahan, A., Buck, C.R., Sehgal, A., Morgan, C., Mercer, E., Bothwell, M. and Chao, M. (1986) Expression and structure of the human NGF receptor. Cell 47, 545–554.
[35] Helms, J.B. and Zurzolo, C. (2004) Lipids as targeting signals: lipid rafts and intracellular trafficking. Traffic 5, 247–254.
[36] Brown, D.A. and Rose, J.K. (1992) Sorting of GPI-anchored proteins to glycolipid-enriched membrane subdomains during transport to the apical cell surface. Cell 68, 533–544.
[37] Paladino, S., Pocard, T., Catino, M.A. and Zurzolo, C. (2006) GPI-anchored proteins are directly targeted to the apical surface in fully polarized MDCK cells. J. Cell Biol. 172, 1023–1034.
[38] De Matteis, M.A. and Godi, A. (2004) Protein-lipid interactions in membrane trafficking at the Golgi complex. Biochim. Biophys. Acta 1666, 264–274.
[39] Sarnataro, D., Paladino, S., Campana, V., Grassi, J., Nitsch, L. and Zurzolo, C. (2002) PrPC is sorted to the basolateral membrane of epithelial cells independently of its association with rafts. Traffic 3, 810–821.

Trabajo 4

DINÁMICA DE LA ACTINA EN EL COMPLEJO DE GOLGI DE LAS CÉLULAS DE MAMÍFERO

Este trabajo revisamos ampliamente la integración de los MFs y su dinámica en la morfo-funcionalidad del AG en las células de mamífero, centrándonos en el papel de los MFs en el mantenimiento de la arquitectura del AG y en la maquinaria molecular que promueve y regula la biogénesis de los ITs. Proponemos un modelo de actuación conjunta entre MFs y MTs para explicar la formación, fisión y transporte de los ITs generados en el AG. *Grosso modo*, los MFs y proteínas asociadas participarían en la formación, fisión y transporte inicial de los ITs mediado por miosinas o por la polimerización focalizada de actina (microcometas de actina) para facilitar su llegada a los MTs a través de los cuales los ITs serían transportados hasta su destino final.

Full text provided by www.sciencedirect.com
SCIENCE DIRECT®

ELSEVIER

Actin dynamics at the Golgi complex in mammalian cells

Gustavo Egea, Francisco Lázaro-Diéguez and Montserrat Vilella

Secretion and endocytosis are highly dynamic processes that are sensitive to external stimuli. Thus, in multicellular organisms, different cell types utilize specialised pathways of intracellular membrane traffic to facilitate specific physiological functions. In addition to the complex internal molecular factors that govern sorting functions and fission or fusion of transport carriers, the actin cytoskeleton plays an important role in both the endocytic and secretory pathways. The interaction between the actin cytoskeleton and membrane trafficking is not restricted to transport processes: it also appears to be directly involved in the biogenesis of Golgi-derived transport carriers (budding and fission processes) and in the maintenance of the unique flat shape of Golgi cisternae.

Addresses
Departament de Biologia Cel·lular i Anatomia Patològica, Facultat de Medicina and Instituts de Nanociències i Nanotecnologia (IN^{2}UB) and d'Investigacions Biomèdiques August Pi i Sunyer (IDIBAPS), Universitat de Barcelona, E-08036 Barcelona, Spain

Corresponding author: Egea, Gustavo (gegea@ub.edu)

Current Opinion in Cell Biology 2006, **18**:168–178

This review comes from a themed issue on
Cell regulation
Edited by Claude Prigent and Bruno Goud

Available online 20th February 2006

0955-0674/$ – see front matter
© 2006 Elsevier Ltd. All rights reserved.

DOI 10.1016/j.ceb.2006.02.007

Introduction

Historically, the first cytoskeletal element to be clearly linked to membrane trafficking and, in particular, to the Golgi complex was the microtubules. There are extensive data and excellent reviews about the role of microtubules and their associated motor and non-motor proteins in the positioning, structure and transport functions of the Golgi complex [1–6]. In addition, actin filaments have also been implicated in trafficking along the endocytic [7] and secretory pathways, and particularly at the Golgi complex [8]. As happens at the plasma membrane during endocytosis, actin filaments and associated co-factors (components, effectors and regulators) are localised to or interact with Golgi membranes both *in vivo* and *in vitro* (Table 1). Besides microtubules and microfilaments, vimentin intermediate filaments also seem to be associated with Golgi membranes [9,10], but this potential interaction will not be discussed here. Here we provide an overall review of the functional coupling of the actin dynamics in the Golgi complex structure and function in mammalian cells. Readers who are more interested in the role of actin in endo/exocytosis in mammalian cells [7,11–13], or in other cellular systems such as yeast [14] and plant cells [15,16], are referred to these reviews.

The contribution of the actin cytoskeleton to the unique architecture of the Golgi complex

Most cellular organelles in mammalian cells are individualized membrane entities that often acquire a spherical shape. Conversely, the ER consists of arrays of parallel cisternae (with or without associated ribosomes), which form a continuous membranous system; the Golgi complex is a ribbon-like system of stacks comprising closely apposed flattened cisternae and vesicles usually localized in the juxtanuclear area around the centrosome [17]. Therefore, the Golgi apparatus is an organelle with several hierarchical levels of architectonic assembly. The first maintains the stacks together and thus gives rise to a single ribbon-like Golgi structure; the second maintains the Golgi stack structure in a tight and parallel arrangement of cisternae, which is made up of a poorly fenestrated central (compact) region and a highly fenestrated lateral (non-compact) region; and the third makes cisternae very flat in the central compact region, whereas in the lateral portion they tend to be more spherical.

When actin dynamics is impaired by a variety of actin toxins that depolymerise (cytochalasins like CyD; latrunculins like LtB; mycalolide B, MyB) or stabilize (jasplakinolide; Jpk) actin filaments, the Golgi complex invariably acquires a compact morphology when examined under the epifluorescence microscope (Figure 1) [18,19]. However, when examined at the EM level, this compact Golgi shows significant structural differences depending on whether the cells are treated with actin toxins that depolymerise or stabilise microfilaments (F Lázaro-Diéguez *et al.*, unpublished). CyD, LtB or MyB induce a large swelling of the cisternae, whereas Jpk produces an extensive fragmentation of the Golgi stack, whilst cisternae remain flat (Figure 1). These ultrastructural changes were equally observed in cells that were treated with nocadozole and CyD, LtB or Jpk, which indicates that microtubules are not involved in the maintenance of the flatness and continuity of cisternae. Therefore, the contribution of the cytoskeleton to the steady-state structural organization of the Golgi apparatus could be as follows: first, microtubules (and microtubule-associated proteins) determine the localization of the Golgi ribbon around the centrosome, and second, the actin cytoskeleton maintains the continuity and flatness of cisternae in conjunction with other

Table 1

Actin filaments components, effectors and regulators at the Golgi complex in mammalian cells

	Role (or attributed role) at the Golgi	Ref.
β/γ-actin	Golgi-derived transport carrier biogenesis and Golgi-to-ER protein transport	[19,24,25]
Short actin filaments	Transport carrier biogenesis	[59••]
Spectrin βIII	ER-to-Golgi protein transport and Golgi architecture. It binds to the Arp1 subunit of the dynactin complex	[97,98]
Syne 1B (Nesprin 1B)	Spectrin family member involved in Golgi-to-ER protein transport	[99]
Ankyrins G119 and G195	Golgi organization and the ER-to Golgi protein transport	[100,101]
Hip1r (Huntingtin interacting related protein 1)	Actin assembly in clathrin-mediated Golgi-to-lysosomes protein transport	[55••]
Tropomyosin isoform Tm5NM-2 (γ-Tm)	Cell-cycle-dependent Golgi association to the Golgi, and involvement in Golgi-derived transport carrier biogenesis	[24,59••]
MACF1b (Microtubule actin cosslinking factor 1b)	Maintenance of Golgi morphology	[102]
p230/Golgi 245-MACF1	Post-Golgi transport of GPI anchored proteins	[103]
mAbp1 (mouse actin binding protein 1 or SH3p7)	Plasma membrane and Golgi located protein with potential coupling between vesicle translocation and targeting and Golgi-associated actin polymerization. It interacts directly with Fgd1and cortactin	[75,76]
Drebrin	Actin binding protein that together with spectrin is recruited to Golgi membranes in an ARF1-dependent manner	[104]
Neurabins I and II	Actin binding proteins that directly interact with TGN38	[105]
ARP1 (Centractin)	Component of the dynactin complex that contributes to transport carrier locomotion and to Golgi positioning	[106]
Dynamin2/cortactin/Arp2/3	Post-Golgi protein transport regulation	[42•]
Syndapins/dynamins Syndapins/N-WASP/Arp2/3	Actin polymerization and transport carrier fission coupling at the plasma membrane and at the Golgi	[56]
Spir 1	Actin polymerization and vesicle transport at the TGN/endosome interface	[90]
Non-muscle myosin II	Non-processive actin motor involved in the Golgi-to ER protein transport and TGN-derived transport carrier biogenesis	[24,56,107]
Myosin VI	Processive actin motor moving toward the minus-end of microfilaments located in the Golgi and involved in both Golgi and endocytic trafficking	[108,109]
Scar2/Arp2/3	Cell type-dependent Golgi polarization in migrating cells	[110]
Coronin 7 (crn7)	Golgi trafficking regulation	[111]
Cdc42	Rho GTPase recruited and activated at the Golgi and involved in polarized secretory protein transport. It directly interacts with COPI regulating transport carrier formation and dynein motor-based microtubule translocation	[40••,41,50••, 111–116]
Cdc42/N-WASP/Arp2/3	Actin polymerization at the Golgi and Golgi-to-ER protein transport	[39•,40••,41]
Cdc42/Par6/αPKC	Golgi and centrosome polarity in migrating cells	[117]
Cdc42/αPAK/Cdk5-p35	Post-Golgi protein transport regulation in neuronal cells	[87]
PAK4	Cdc42 interacting serine/threonine kinase located at the Golgi. When overexpressed it induces Golgi-associated actin polymerisation	[85]
Fgd1	Cdc42 GEF protein located at the Golgi	[74]
ARHGAP4	Cdc42, Rac and Rho GAP protein located in neuronal Golgi membranes	[72]
ARHGAP10	Cdc42 GAP protein that regulates Arp2/3 complex activity and F-actin dynamics at the Golgi	[73]
RhoA/Citron-N/RockII/profilin	Signalling pathway that regulates actin assembly in neuronal Golgi membranes	[81]
LIMK1	PAK4/PAK1-interacting kinase located in neuronal Golgi membranes, and involved in the axon outgrowth	[83,84]
AKAP350/CIP4	Centrosomal- and Golgi-associated proteins that interact with N-WASP and microtubules. Golgi morphology and trafficking regulation through actin and microtubules	[92]
TC10	Closely related Cdc42 member of the Rho family GTP-binding proteins present in adipocytes. It induces actin polymerisation at the Golgi region through N-WASP and directly interacts with COPI coat proteins, regulating COPI-mediated protein transport	[118]

Figure 1

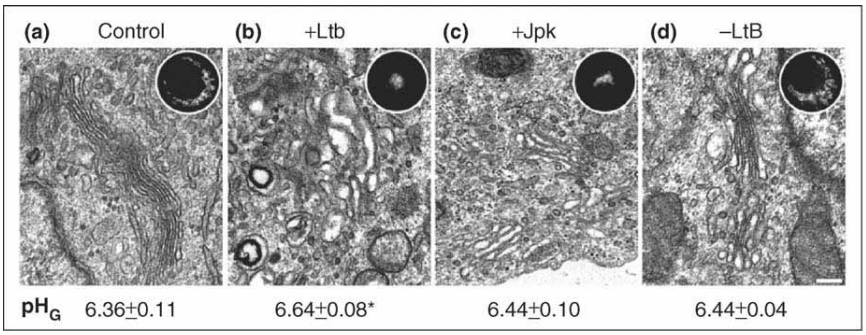

Concomitant ultrastructural alterations of the Golgi architecture and changes in the Golgi pH by the impairment of actin dynamics. Under the immunofluorescence microscope, the disruption (with latrunculin B, LtB) or stabilization (with jasplakinolide, Jpk) of the actin cytoskeleton invariably leads to a compact Golgi morphology — see insets in (b) and (c). However, when examined under the electron microscope, the characteristic flat cisternae seen in control cells **(a)** become largely swollen by the LtB treatment **(b)**. Conversely, in Jpk-treated cells, cisternae are extensively fragmented but remain flat **(c)**. Parallel measurements of Golgi pH (pH_G) in these cells show that only LtB induces a significant increase in the intra-Golgi pH (asterisk: $p \leq 0.01$ using Student's *t* test). Normal flattened cisternae and intra-Golgi pH are obtained after LtB removal **(d)**. Scale bar, 200 nm.

members of the Golgi-associated spectrin-based cytoskeleton. Unfortunately, their specific contribution to the Golgi architecture remains unknown. A detailed analysis of the Golgi ultrastructure in cells depleted of Golgi spectrin or ankyrin by siRNA could clarify this question. At the same time, what has hitherto been considered the fundamental contribution of the coiled-coil Golgi matrix proteins to the Golgi structure [20] should be reconsidered as cells depleted of some of their relevant members (GM130 or giantin) unexpectedly showed a completely normal Golgi complex morphology [21]. Nonetheless, it is possible that Golgi matrix proteins carry out their structural function via direct or indirect interaction with actin and/or other actin players.

As the Golgi apparatus is located at the meeting point between the secretory and endocytic pathways, the Golgi complex morphology at the steady-state is the result of a fine and highly regulated balance between the amount of membrane that is constantly internalised at the cell surface and that generated at the ER. Any significant imbalance between these two membrane trafficking pathways will affect the structure and function of the Golgi [22,23]. Interestingly, cisternae are always kept flat, despite the huge amount of cargo that is continuously crossing the Golgi stack. The aforementioned ultrastructural results using actin toxins indicate that actin filaments provide Golgi cisternae with the necessary mechanical stability to prevent their expected spontaneous swelling as a result of the hyperosmotic protein content. By analogy with red blood cells, the unique flat morphology of Golgi cisternae could result from the structural organization of the Golgi's actin–spectrin-based cytoskeleton. Actin [24,25], spectrin and ankyrin [26], anion exchangers [27] and the protein 4.1 (Isabel Correas, personal communication) are present in Golgi membranes. Ionic regulatory molecules, such as vacuolar H^+-ATPases and anion and cation exchangers (AEs and NHEs) in the Golgi and in transit to the plasma membrane contribute to this postulated actin-associated mechanical stability of cisternae by providing the appropriate intra-Golgi ion and pH homeostasis [28]. This homeostasis is necessary for the Golgi-associated post-translational protein and lipid modifications [29] and for the maintenance of the flattened cisternae morphology [30]. Through analogy with the AE1 (band 3) of the red blood cell plasma membrane, the Golgi-associated AE2 [27] reversibly exchanges chloride for bicarbonate, taking chloride in to the cisternal lumen and expelling bicarbonate into the cytoplasm. This contributes to the regulation of the cisternal chloride concentration [31] and Golgi morphology. In this respect, cells depleted of AE2 show a variable degree of cisternal swelling [32]. It is possible that the actin cytoskeleton disruption impairs AE2 activity in Golgi cisternae, leading to the extrusion of chloride from the lumen and the entrance of bicarbonate (accompanied by water), which, together, lead to the observed cisternal swelling [18] (F Lázaro-Diéguez *et al.*, unpublished) (Figure 1). Likewise, the Golgi-resident anion channels GOLAC-1 and GOLAC-2 [33,34] together with H^+ leak and K^+ conductance could all contribute to the acidification and osmotic balance of the Golgi complex, providing counter anions for H^+-ATPases. By analogy with plasma membrane vacuolar H^+-ATPases, it is possible that the Golgi-associated H^+-ATPase(s) [35] coupled to osmotically active AEs [27] and NHEs [36] could be regulated by the actin cytoskeleton assembly state, which could therefore indirectly contribute in this way to the maintenance of the unique flat morphology of cisternae. Thus, the disruption of Golgi-associated actin dynamics could impair this functional coupling, generating an altered ionic gradient that could lead to the observed cisternal swelling and

changes in intra-Golgi pH. In this respect, the treatment with LtB induces a significant increase in the intra-Golgi pH, whereas Jpk neither produces cisternal swelling nor induces any change in the intra-Golgi pH (Figure 1) (F Lázaro-Diéguez *et al*., unpublished). Furthermore, the disruption of actin filaments and the concurrent cisternal osmotic swelling decreases the differences in membrane tension between the ER and the Golgi [37]. This induces a slowing-down of the Golgi-to-ER membrane flow [19].

Actin-based cytoskeleton and transport carrier biogenesis at different Golgi complex compartments

In common with what occurs during endocytosis, there is also physiological coupling at the Golgi complex between molecular components that directly or indirectly trigger actin recruitment/polymerisation (Cdc42, N-WASP, cortactin, syndapin, Arp2/3, Spir1) and some of those that determine transport carrier budding (COPI and clathrin coats) and fission (dynamin II) (Box 1). One possibility is that actin might provide structural support that facilitates transport carrier (vesicle or tubule) formation at the lateral portions (rims) of Golgi cisternae by generating force either through a highly controlled *de novo* actin polymerisation activity or through actin motors (myosins). With respect to the former, the actin nucleators Arp2/3 complex and Spir1 (but not formins) are recruited to the Golgi, where they stimulate actin nucleation/polymerisation [38,39•,40••]. The upstream effectors that mediate this Golgi-associated actin polymerization are diverse. For the Arp2/3 complex, the more consistent mediators located in the Golgi are Cdc42/N-WASP [39•,40••,41] and dynamin II/cortactin [42•]. Arp2/3-induced Golgi actin nucleation is linked to the dynamin-mediated transport carrier fission process at the *trans*-Golgi network (TGN). Thus, the interference with dynamin II/cortactin [42•] or syndapin II/dynamin II [43•] interactions impairs post-Golgi protein transport. Like the Arp2/3 complex, Spir1 is also involved in the post-Golgi protein transport [38].

Unlike what it has been reported at the TGN [44–46], the potential coupling between membrane fission and actin-based mechanisms at the ER/Golgi interface and early Golgi compartments has not yet been clearly established. Nonetheless, this is also a possibility for a number of reasons: first, the low-temperature-induced formation of Golgi-derived tubules is dependent not only on microtubules but also on microfilaments [47]; second the membrane fissioning protein CtBP3/BARS [48] is required for the formation of COPI transport carriers [49]; and third, there is a functional connection between actin polymerisation governed by Cdc42, COPI transport carrier formation, and its subsequent microtubule-motor-mediated locomotion [50••]. With respect to the latter, Stamnes' laboratory shows that the Cdc42 activation inhibits the recruitment of dynein to COPI-coated transport carriers, whereas preventing the COPI–Cdc42 interaction stimulates their dynein/dynactin binding. However, this study does not clarify how is possible that the characteristic ER-to-Golgi-directed microtubule motor dynein moves COPI transport carriers, which mediate the retrograde (Golgi-to-ER) protein transport [51], which is structurally supported by both microtubules [6] and actin filaments [19].

Whereas actin polymerisation and transport carrier biogenesis seem to occur in all Golgi compartments, some of the molecular mediators that regulate both processes are located in Golgi cisternae. In contrast to Cdc42 and the Arp2/3 complex, N-WASP is absent from the TGN and is restricted to *cis*/middle cisternae [40••]. Whereas cortactin is directly involved in post-Golgi transport, it is visualized at both the *cis*- and the *trans*-Golgi faces (predominantly at the tips and buds of cisternae) [42•]. In the absence of double immunogold electron microscopy experiments with well-established *cis*- and/or *trans*-Golgi-resident pro-

Box 1 Brief description of some important molecular components involved in Golgi transport carrier biogenesis and F-actin dynamics

Arp2/3
Multiprotein complex located in regions of rapid actin filament turnover. It is a characteristic actin nucleator as it nucleates the polymerization of actin in a dendritic manner and promotes accumulation of actin filaments on the surface of some pathogens and endomembrane systems.

Clathrin coat
Protein that assembles into a polyhedral cage on the cytosolic side of the plasma membrane and the trans/trans-Golgi network (TGN).

COPI coat (coatomer)
Complex of seven polypeptides that assembles on the cytosolic side of the lateral regions of Golgi cisternae and tubulovesicular structures at the ER/Golgi interface.

Cortactin
F-actin and dynamin-binding protein that associates with the C-terminal praline-rich domain of dynamins.

CtBP3/BARS (BARS or BARS50)
Protein member of the CtBP family of proteins that was initially identified as the 50-kDa substrate of brefeldin A (BFA)-dependent ADP-ribosylation. This protein has fissiogenic activity and participates in the fragmentation of the Golgi complex during mitosis and
during intracellular membrane transport.

Dynamins
GTPases that oligomerise into tubular structures around lipids. Dynamins are crucial factors for transport carrier formation at the plasma membrane (dynamin I and II) and the Golgi (dynamin II).

Formins
Actin nucleators that generate long and parallel actin filaments. They contribute to the generation of the specific actin-based structures (contractile ring in cytokinesis, actin stress fibers in animal cells, and yeast actin cables).

N-WASP (Neural Wiskott-Aldrich syndrome protein)
Cdc42-, intersectin- and syndapin-interacting protein that mediates the actin polymerization induced by the Arp2/3 complex.

Spir1
This protein belongs to the family of Wiskott-Aldrich homology region (WH2) proteins involved in actin nucleation and organization.

Syndapins
Dynamin-binding proteins that act in the endocytic (syndapin I) and secretory (syndapin II) pathways.

teins that confirm the unexpected *cis*-side localization, cortactin could be assumed to substitute for N-WASP in the recruitment of the Arp2/3 complex at the TGN. Therefore, the *cis*-to-*trans* segregation of some fundamental components of the actin machinery in the Golgi would facilitate the efficiency and fidelity of transport carrier budding and fission at individual Golgi subdomains. Thus, at the TGN, post-Golgi protein transport is mediated by the dynamin II/cortactin/Arp2/3 and syndapin II/dynamin II interactions [42•,43•]. In contrast, Cdc42/N-WASP/Arp2/3 mediates protein transport at the ER/Golgi interface [39•,40••,41,50••].

Actin comets and actin motors in the biogenesis and locomotion of Golgi-derived transport carriers

The actin nucleation activity in Golgi membranes can also result in the formation of actin comets [52]. Despite the fact that actin tails have been observed in raft-enriched TGN-derived vesicles [53], actin comets are not used by transport carriers as a common physiological mechanism to move long distances, unlike some pathogenic microorganisms [54]. However, it is possible that actin comets may be transiently formed once the Golgi-derived transport carrier has already been pinched off the cisterna. The force generated by the Arp2/3-induced actin polymerisation on the transport carrier membrane propels it away into the cytoplasm (Figure 2). The presence of some components of the Arp2/3 complex in peri-Golgi transport carriers [40••,55••] endorses this possibility, which is consistent with the aforementioned role of actin in the transport carrier budding process occurring at the lateral portions of cisternae.

In addition to actin polymerization, actin motor proteins (myosins) also generate force, which can promote the formation of transport carriers and/or their movement away from Golgi cisternae. We have shown that a myosin activity mediates the actin-based Golgi-to-ER protein transport, and demonstrated that non-muscle myosin II is involved in this process [56]. Non-muscle myosin II is a non-processive motor, whose involvement in post-Golgi protein transport was initially controversial [57]. However, recent biochemical evidence demonstrates its interaction with Golgi membranes *in vitro* [58•], suggesting a model in which myosin II is tethered to the cisterna by its tail and to actin filaments by its head. Its subsequent translocation along actin filaments could provide the necessary force to extend Golgi-derived transport carriers away from the cisterna. This cisterna membrane exten-

Figure 2

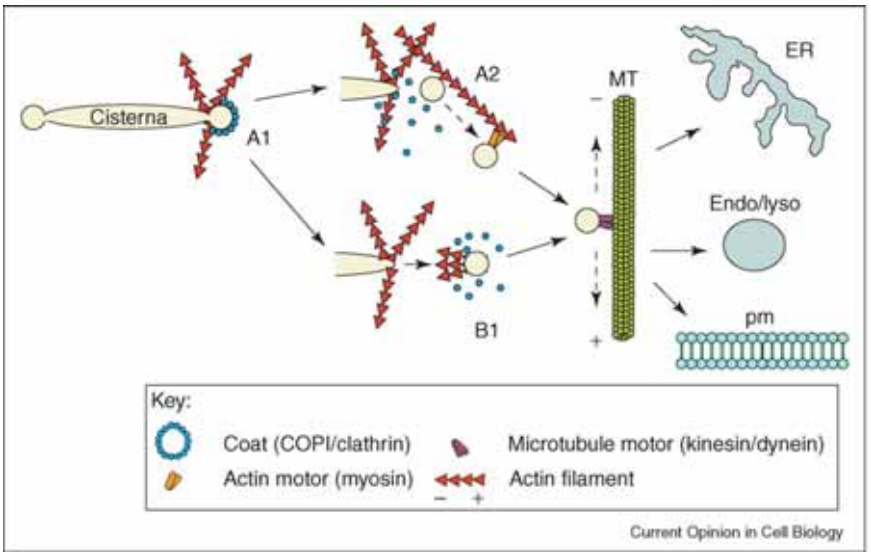

Possible involvement of actin in transport carrier budding, scission and/or locomotion processes at the Golgi: cooperative process involving microfilaments and microtubules. (A) Concomitantly to the budding process occurring at the lateral regions of the cisterna and regardless of whether it is mediated by COPI (*cis*/middle) or clathrin (*trans*/TGN) coats, the ARF1-dependent recruitment of actin regulators (Cdc42/N-WASP) and effectors (cortactin) stimulates the Arp2/3-induced actin nucleation/polymerisation (A1). Consequently, the *de novo* formed (dendritic) actin filaments (with the potential participation of non-muscle myosin II) could either help to elongate membrane (facilitating the subsequent coupling of fission proteins, for example dynamin II or CtBP3/BARS) and/or to collect the transport carrier to be subsequently transported a short distance by processive myosins (for example myosin VI) (A2) to adjacent microtubules tracks (MT). (B) Another possibility is that either concomitantly to the budding process or once the transport carrier formation is already completed, the Arp2/3-induced de novo actin polymerization would lead to the formation of short-lived actin comets (B1), which would propel the transport carrier to microtubules. Both possibilities (A,B) imply a cooperative process that consists of the capture of the transport carrier and/or its local movement in the cisternal actin-rich periphery driven by myosin motor activity coupled to long-range bidirectional microtubule-dependent movement to other (endo)membrane systems, such as the endoplasmic reticulum (ER), the endosome/lysosome (endo/lyso) system and the plasma membrane (pm).

sion induced by non-muscle myosin II could facilitate the subsequent coupling and function of the molecular machinery involved in membrane scission, leading to the complete release of the transport carrier. The binding of the tropomyosin isoform Tm5NM-2 to Golgi-associated short filaments [59••] could facilitate the recruitment of non-muscle myosin II and its interaction with these actin filaments. Myosin VI is another myosin motor located at the Golgi apparatus [60]. It differs from other processive myosins as it moves transport carriers towards the minus-pointed end of actin filaments. Therefore, myosin VI could provide force and directionality for the Golgi-derived transport carrier movement away from cisternae according to the expected fast-growing plus-end polarization of the Golgi-associated actin polymerisation (G Egea *et al.*, unpublished). This would occur concurrently with the biogenesis of the transport carriers at the cisternal lateral portions (Figure 2).

Rab proteins play an additional role in this process by linking endomembranes to cytoskeletal motors, which facilitates the long-range movement of transport carriers [61]. Up to now, the best-characterized localization of Rab proteins at the Golgi relies on Rab6. This small GTPase interacts with the kinesin-like motor rabkinesin-6 [62] and regulates the recruitment of the dynein/dynactin complex to Golgi membranes [63], hence engaging microtubules in both plus-end and minus-end locomotion of Golgi-derived transport carriers. Unlike Rab27, which tethers melanosomes to the actin cytoskeleton at the cell cortex through myosin Va [64], there is no clear evidence that Rab proteins interact with actin filaments or myosins at the Golgi complex. However, this possibility is now open thanks to the recently reported direct interaction between myosin VI and optineurin, a partner of Rab8 [65].

Control mechanisms of actin-associated transport carrier events occurring at the Golgi

Tight coupling of the timing and intensity of local actin polymerization to Golgi-membrane-associated budding and fission reactions is essential, as happens in the initial steps of clathrin-mediated endocytosis [66,67]. At the Golgi, one possibility is that this control could partially be achieved by the regulation of phosphatidylinositol 4,5-biphosphate (PIP_2) levels, which at the steady-state are very low [68]. PIP_2 synergizes with Cdc42–N-WASP [69] and cortactin [70] in Arp2/3-induced actin nucleation/polymerisation. It is reasonable to hypothesize that PIP_2 is generated in the lateral portions of cisternae and concomitantly with the ARF1-induced recruitment of COPI, Cdc42 and cortactin. Interestingly, the Golgi fragmentation in response to diminished PIP_2 synthesis correlates with the phosphorylation of the Golgi-associated βIII spectrin and its subsequent translocation to the cytoplasm [71]. Another possibility involves the presence of Cdc42 GAP (GTPase-activating protein) and GEF (guanine nucleotide exchange factor) proteins. ARHGAP4 and ARHGAP10 [72,73], plus the Cdc42 GEF proteins Fgd1 [74], are located in the Golgi. At the cell cortex, Fgd1 interacts directly with cortactin and mAbp1 and through Cdc42 indirectly activates N-WASP, leading to Arp2/3-directed actin polymerization [75]. As all these molecular components are also present in Golgi membranes [40••,42•,76], it is tempting to hypothesize that Fgd1 regulates actin dynamics at the Golgi in a similar manner to what occurs at the plasma membrane. A third possibility involves coronin 7 (crn7), whose phosphorylation triggers its recruitment to the Golgi [77]. Coronin proteins regulate cytoskeleton and/or membrane trafficking [78]. In yeast, some members of the coronin family directly interact with the Arp2/3 complex, inhibiting its actin nucleation activity [79]. Although disruption of actin cytoskeleton does not affect the Golgi localization of crn7 [77], this is consistent with its potential negative regulatory role in Golgi-associated Arp2/3 nucleation activity and transport carrier biogenesis.

In addition to the role of actin in mediating the membrane scission process, actin filaments and/or the actin-based cytoskeleton could spatially organize the Golgi-associated secretory molecular machinery by forming a physical barrier at the lateral and/or central regions of cisternae. Thus, in the flat central region of cisternae, the conjunction of the actin–spectrin-based cytoskeleton with a particular lipid and protein (glycosyltransferase) membrane composition could create a physical barrier, resulting in an area of the membrane that is permanently inhibitory to transport carrier biogenesis. Like the plasma membrane, Golgi membranes have an associated specialized actin–spectrin cytoskeleton [26], which probably has the same structural and biophysical properties as the erythrocyte plasma membrane cytoskeleton [80]. This Golgi-associated actin–spectrin cytoskeleton could partially determine the characteristic flat morphology of the central portion of cisternae (see above).

Actin–Golgi interaction in neuronal cells: a peculiar case among mammalian cells

As previously indicated, actin toxins invariably produce a compacted Golgi in most mammalian cell lines. However, in neurons, the disruption of actin filaments with CyD leads to the Golgi fragmentation [81]. On the other hand, in non-neuronal cells, a variety of independent experimental approaches show that, unlike Cdc42, neither RhoA nor Rac1 are endogenously located to Golgi membranes, nor are they involved in Golgi-associated protein transport [25,76,82,83]. This leaves Cdc42 as the only Rho GTPase with specific functions in the Golgi complex in mammalian cell lines. However, the neuronal cells seem to be also an exception. Citron-N (a RhoA-binding protein) and ROCKinase-II are both seen in the neuronal Golgi apparatus [81]. Likewise, LIMK1, a kinase that

specifically phosphorylates the actin turnover regulator ADF-cofilin, is localised to Golgi membranes. This Golgi localisation correlates with the ability of LIMK1 to regulate axon formation [84]. PAK4, a downstream effector of Cdc42 also present at the Golgi [85], specifically interacts with LIMK1, stimulating its intrinsic ability to phosphorylate cofilin [86]. This interaction probably takes place in the Golgi. Cdk35–p35 (another Cdc42 downstream effector necessary for neural morphogenesis) is also present in neural Golgi membranes and the inhibition of the kinase activity prevents the formation of Golgi-derived transport carriers [87]. Therefore, at the neuronal Golgi complex, Cdk5-p35 and LIMK1 probably function as physiological couplers of Rho-GTPase signaling, post-Golgi trafficking, actin dynamics and neuronal process outgrowth. This molecular coupling could also be involved in the polarization of developing neurons as the clustering of the Golgi complex, the centrosome and the endosomes precedes the first neurite outgrowth (the future axon) [88,89]. Thus, experimental treatments that impair either microtubule and actin polymerisation or protein trafficking prevent this centrosome-directed neuronal polarity [89]. The unrestricted presence of Rho-GTPase family members and their respective numerous downstream effectors at neuronal Golgi membranes could improve the coupling between membrane trafficking and the actin cytoskeleton, which is important given the requirement for high-capacity, high-speed membrane trafficking in neurons. In accordance with this possibility, syndapin I, unlike syndapin II, is highly enriched in brain tissue, and, like clathrin and dynamin, is highly accumulated in synaptic compartments. Therefore, syndapin II might provide the necessary fast, functional coupling between (synaptic) vesicle trafficking and actin dynamics [90].

Finally, a potentially interesting connection between actin, syndapins and post-Golgi trafficking could occur in Huntington's disease. This disease is characterized by the cytoplasmic accumulation of mutant huntingtin protein containing extended polyglutamine stretches. Huntingtin associates with numerous factors of the clathrin-mediated endocytic molecular machinery including, among others, huntingtin-interacting protein 1 (Hip1), Hip1-related protein (Hip1r), endophilin and syndapin I. The length of the polyglutamine repeat modulates the affinity of some of these interactions both *in vivo* and *in vitro*, as is the case with syndapin I [91], which directly inhibits endocytic membrane trafficking. Hip1r and the Arp2/3 complex are directly involved at the TGN in the post-Golgi trafficking of targeting proteins to late endosomes/lysosomes through the coordination of the actin assembly and the clathrin-mediated budding [55••]. This observation, plus the recently reported Golgi localization of CIP4 [92], which in addition to N-WASP and microtubules [93] also binds huntingtin [94], strongly suggests that Golgi-associated membrane trafficking defects, directly or indirectly triggered by extended polyglutamine stretches, also participate in the pathology of Huntington's disease.

Conclusions

The correct functioning of the Golgi complex is the result of a wide and complex interplay between the molecular machineries that determine the fidelity of transport events, those that determine Golgi architecture and those that integrate signals coming from outside and inside the cell. Cytoskeletal elements help to integrate all these processes. Therefore, the association and coordination of microtubules and microfilaments is necessary for correct Golgi positioning, architecture and trafficking. This is consistent with the strong evidence that the Golgi complex functions as a microtubule- and actin-nucleating organelle [39•,95••]. Over the past decade, numerous actin players have been located in the Golgi, and, in most cases, they participate in Golgi-associated transport events (Table 1). The prevailing view is that actin-based cytoskeleton molecular components, which participate in the structural organization of the plasma membrane and endocytosis, are also present in endomembrane systems. This is undoubtedly helping to clarify the function of actin filaments and their components, effectors and regulators in Golgi-derived protein transport. However, there are small but significant differences between both membrane systems [96]. Furthermore, there is an active and highly regulated actin-based molecular machinery at the Golgi that couples transport carrier budding, scission and locomotion processes at the ER/Golgi interface and at the TGN. Actin filaments are also involved in the modelling of the Golgi architecture, as they participate in the maintenance of the characteristic flattened morphology of cisternae, directly by providing mechanical stability to cisternae and indirectly through regulation of the activities of ion pumps and exchangers, and/or channels either resident in or transiting through the Golgi. Consequently, the ion and pH homeostasis of the Golgi complex is regulated together with the actin assembly state. However, a more detailed understanding of the role of actin in these Golgi functions requires knowing, first, where Golgi-associated spectrin, ankyrin and 4.1 proteins are precisely located in Golgi membranes (*cis*/*trans* polarity and central/lateral cisternae regions); second, which structural and functional impairments cause their silencing; and third, whether actin dynamics and actin-based cytoskeleton components participate in intra-Golgi transport (which could possibly regulate the progressive disappearance of fenestrations in the *cis*-to-*trans* direction). In the meantime, actin dynamics and actin effectors and regulators enable us to visualize the Golgi complex as an endomembrane system in which architecture, ion homeostasis, cargo transport and signalling are efficiently integrated.

Acknowledgements

Thanks to Rosa Ríos, Erwin Knech and Susana E. Martínez for comments on the manuscript. This work received financial support from the

Ministerio de Educación y Ciencia (SAF and BMC programmes), the European Commission (contract RTN2002-259), and the Generalitat de Catalunya-DURSI (Distinció per la Recerca). Dedicated to the everlasting memory of Valentí Costa (1963-2005) and Senén Vilaró (1956-2005).

References and recommended reading

Papers of particular interest, published within the annual period of review, have been highlighted as:

- • of special interest
- •• of outstanding interest

1. Thyberg J, Moskalewski S: **Role of microtubules in the organization of the Golgi complex**. *Exp Cell Res* 1999, **246**:263-279.
2. Rios RM, Bornens M: **The Golgi apparatus at the cell centre**. *Curr Opin Cell Biol* 2003, **15**:60-66.
3. Murshid A, Presley JF: **ER-to-Golgi transport and cytoskeletal interactions in animal cells**. *Cell Mol Life Sci* 2004, **61**:133-145.
4. Musch A: **Microtubule organization and function in epithelial cells**. *Traffic* 2004, **5**:1-9.
5. Vaughan KT: **Microtubule plus ends, motors, and traffic of Golgi membranes**. *Biochim Biophys Acta* 2005, **1744**:316-324.
6. Palmer KJ, Watson P, Stephens DJ: **The role of microtubules in transport between the endoplasmic reticulum and Golgi apparatus in mammalian cells**. *Biochem Soc Symp* 2005, **72**:1-13.
7. Engqvist-Goldstein AE, Drubin DG: **Actin assembly and endocytosis: from yeast to mammals**. *Annu Rev Cell Dev Biol* 2003, **19**:287-332.
8. Stamnes M: **Regulating the actin cytoskeleton during vesicular transport**. *Curr Opin Cell Biol* 2002, **14**:428-433.
9. Gao Y, Sztul E: **A novel interaction of the Golgi complex with the vimentin intermediate filament cytoskeleton**. *J Cell Biol* 2001, **152**:877-894.
10. Toivola DM, Tao GZ, Habtezion A, Liao J, Omary MB: **Cellular integrity plus: organelle-related and protein-targeting functions of intermediate filaments**. *Trends Cell Biol* 2005, **15**:608-617.
11. Eitzen G: **Actin remodeling to facilitate membrane fusion**. *Biochim Biophys Acta* 2003, **1641**:175-181.
12. Bader MF, Doussau F, Chasserot-Golaz S, Vitale N, Gasman S: **Coupling actin and membrane dynamics during calcium-regulated exocytosis: a role for Rho and ARF GTPases**. *Biochim Biophys Acta* 2004, **1742**:37-49.
13. Niedergang F, Chavrier P: **Signaling and membrane dynamics during phagocytosis: many roads lead to the phagos(R)ome**. *Curr Opin Cell Biol* 2004, **16**:422-428.
14. Pruyne D, Legesse-Miller A, Gao L, Dong Y, Bretscher A: **Mechanisms of polarized growth and organelle segregation in yeast**. *Annu Rev Cell Dev Biol* 2004, **20**:559-591.
15. Wada M, Suetsugu N: **Plant organelle positioning**. *Curr Opin Plant Biol* 2004, **7**:626-631.
16. Samaj J, Baluska F, Voigt B, Schlicht M, Volkmann D, Menzel D: **Endocytosis, actin cytoskeleton, and signaling**. *Plant Physiol* 2004, **135**:1150-1161.
17. Kepes F, Rambourg A, Satiat-Jeunemaitre B: **Morphodynamics of the secretory pathway**. *Int Rev Cytol* 2005, **242**:55-120.
18. Valderrama F, Babia T, Ayala I, Kok JW, Renau-Piqueras J, Egea G: **Actin microfilaments are essential for the cytological positioning and morphology of the Golgi complex**. *Eur J Cell Biol* 1998, **76**:9-17.
19. Valderrama F, Duran JM, Babia T, Barth H, Renau-Piqueras J, Egea G: **Actin microfilaments facilitate the retrograde transport from the Golgi complex to the endoplasmic reticulum in mammalian cells**. *Traffic* 2001, **2**:717-726.
20. Short B, Haas A, Barr FA: **Golgins and GTPases, giving identity and structure to the Golgi apparatus**. *Biochim Biophys Acta* 2005, **1744**:383-395.
21. Puthenveedu MA, Linstedt AD: **Subcompartmentalizing the Golgi apparatus**. *Curr Opin Cell Biol* 2005, **17**:369-375.
22. Jackson CL: **Brefeldin A revealing the fundamental principles governing membrane dynamics and protein transport**. *Subcell Biochem* 2000, **34**:233-272.
23. Vetterlein M, Ellinger A, Neumuller J, Pavelka M: **Golgi apparatus and TGN during endocytosis**. *Histochem Cell Biol* 2002, **117**:143-150.
24. Heimann K, Percival JM, Weinberger R, Gunning P, Stow JL: **Specific isoforms of actin-binding proteins on distinct populations of Golgi-derived vesicles**. *J Biol Chem* 1999, **274**:10743-10750.
25. Valderrama F, Luna A, Babia T, Martinez-Menarguez JA, Ballesta J, Barth H, Chaponnier C, Renau-Piqueras J, Egea G: **The Golgi-associated COPI-coated buds and vesicles contain β/γ-actin**. *Proc Natl Acad Sci USA* 2000, **97**:1560-1565.
26. De Matteis MA, Morrow JS: **Spectrin tethers and mesh in the biosynthetic pathway**. *J Cell Sci* 2000, **113**:2331-2343.
27. Holappa K, Suokas M, Soininen P, Kellokumpu S: **Identification of the full-length AE2 (AE2a) isoform as the Golgi-associated anion exchanger in fibroblasts**. *J Histochem Cytochem* 2001, **49**:259-269.
28. Demaurex N: **pH Homeostasis of cellular organelles**. *News Physiol Sci* 2002, **17**:1-5.
29. Axelsson MA, Karlsson NG, Steel DM, Ouwendijk J, Nilsson T, Hansson GC: **Neutralization of pH in the Golgi apparatus causes redistribution of glycosyltransferases and changes in the O-glycosylation of mucins**. *Glycobiology* 2001, **11**:633-644.
30. Palokangas H, Ying M, Vaananen K, Saraste J: **Retrograde transport from the pre-Golgi intermediate compartment and the Golgi complex is affected by the vacuolar H^+-ATPase inhibitor bafilomycin A1**. *Mol Biol Cell* 1998, **9**:3561-3578.
31. Sonawane ND, Verkman AS: **Determinants of [Cl^-] in recycling and late endosomes and Golgi complex measured using fluorescent ligands**. *J Cell Biol* 2003, **160**:1129-1138.
32. Holappa K, Munoz MT, Egea G, Kellokumpu S: **The AE2 anion exchanger is necessary for the structural integrity of the Golgi apparatus in mammalian cells**. *FEBS Lett* 2004, **564**:97-103.
33. Nordeen MH, Jones SM, Howell KE, Caldwell JH: **GOLAC: an endogenous anion channel of the Golgi complex**. *Biophys J* 2000, **78**:2918-2928.
34. Thompson RJ, Nordeen MH, Howell KE, Caldwell JH: **A large-conductance anion channel of the Golgi complex**. *Biophys J* 2002, **83**:278-289.
35. Moriyama Y, Nelson N: **H^+-translocating ATPase in Golgi apparatus. Characterization as vacuolar H^+-ATPase and its subunit structures**. *J Biol Chem* 1989, **264**:18445-18450.
36. Nakamura N: **Shingo Tanaka, Yoshinori Teko, Keiji Mitsui, and Hiroshi Kanazawa: four Na^+/H^+ exchanger isoforms are distributed to Golgi and post-Golgi compartments and are involved in organelle pH regulation**. *J Biol Chem* 2005, **280**:1561-1572.
37. Upadhyaya A, Sheetz MP: **Tension in tubulovesicular networks of Golgi and endoplasmic reticulum membranes**. *Biophys J* 2004, **86**:2923-2928.
38. Kerkhoff E, Simpson JC, Leberfinger CB, Otto IM, Doerks T, Bork P, Rapp UR, Raabe T, Pepperkok R: **The Spir actin organizers are involved in vesicle transport processes**. *Curr Biol* 2001, **11**:1963-1968.
39. • Chen JL, Lacomis L, Erdjument-Bromage H, Tempst P, Stamnes M: **Cytosol-derived proteins are sufficient for Arp2/3 recruitment and ARF/coatomer-dependent actin polymerization on Golgi membranes**. *FEBS Lett* 2004, **566**:281-286.

Using an *in vitro* reconstitution vesicle budding assay, Arp2/3 and N-WASP are recruited onto Golgi membranes in a Cdc42- and ARF1-dependent manner. The recruitment of Arp2/3 and actin is also obtained in liposomes without requiring either membrane or cytosolic proteins.

40. •• Matas OB, Martinez-Menarguez JA, Egea G: **Association of Cdc42/N-WASP/Arp2/3 signaling pathway with Golgi membranes**. *Traffic* 2004, **5**:838-846.
By quantitative cryoimmunogold electron microscopy, Cdc42, N-WASP and the Arp2/3 complex are shown to have a *cis*-to-*trans* polarised distribution in the Golgi stack. Cdc42 is present in all Golgi compartments but enriched in *cis*/middle cisternae. N-WASP is absent from the TGN and Arp2/3 is highly enriched in the *cis* cisterna and at the TGN. Furthermore, the activation of Cdc42 induces the rearrangement of Cdc42, N-WASP and Arp2/3 to the lateral regions of cisternae.

41. Luna A, Matas OB, Martinez-Menarguez JA, Mato E, Duran JM, Ballesta J, Way M, Egea G: **Regulation of protein transport from the Golgi complex to the endoplasmic reticulum by CDC42 and N-WASP**. *Mol Biol Cell* 2002, **13**:866-879.

42. • Cao H, Weller S, Orth JD, Chen J, Huang B, Chen JL, Stamnes M, McNiven MA: **Actin and Arf1-dependent recruitment of a cortactin-dynamin complex to the Golgi regulates post-Golgi transport**. *Nat Cell Biol* 2005, **7**:483-492.
This paper describes the presence of cortactin in Golgi membranes and associated buds and vesicles. Arf activation triggers the recruitment of actin, cortactin and dynamin II to the Golgi membranes. Disrupting the cortactin–dynamin interaction by expressing truncated cortactins results in the retention of VSV-G at the TGN.

43. • Kessels MS, Dong J, Leibig W, Westermann P, Qualmann B: **Syndapin/dynamin II complexes promote vesicle formation at the trans-Golgi network**. *J Cell Sci* 2006. in press.
This paper reveals that syndapin/dynamin complexes are sufficient to promote vesicle formation from the TGN. Syndapin II isoform, which is associated with Golgi membranes, interacts with the proline-rich domain (PRD) of dynamin II via its SH3 domain. The relevance of syndapin II in Golgi vesicle formation is shown, as anti-syndapin-II antibodies and overexpression of the syndapin-II SH3 domain blocks post-Golgi trafficking of VSVG–GFP.

44. Corda D, Hidalgo-Carcedo C, Bonazzi M, Luini A, Spano S: **Molecular aspects of membrane fission in the secretory pathway**. *Cell Mol Life Sci* 2002, **59**:1819-1832.

45. Praefcke GJ, McMahon HT: **The dynamin superfamily: universal membrane tubulation and fission molecules?** *Nat Rev Mol Cell Biol* 2004, **5**:133-147.

46. Ghanekar Y, Lowe M: **Protein kinase D: activation for Golgi carrier formation**. *Trends Cell Biol* 2005, **15**:511-514.

47. Martinez-Alonso E, Egea G, Ballesta J, Martinez-Menarguez JA: **Structure and dynamics of the Golgi complex at 15 degrees C: low temperature induces the formation of Golgi-derived tubules**. *Traffic* 2005, **6**:32-44.

48. Nardini M, Spano S, Cericola C, Pesce A, Massano A, Millo E, Luini A, Corda D, Bolognesi M: **CtBP/BARS: a dual-function protein involved in transcription co-repression and Golgi membrane fission**. *EMBO J* 2003, **22**:3122-3130.

49. Yang JS, Lee SY, Spano C, Gad H, Zhang L, Nie Z, Bonazzi M, Corda D, Luini A, Hsu VW: **A role for BARS at the fission step of COPI vesicle formation from Golgi membrane**. *EMBO J* 2005, **24**:4133-4143.

50. •• Chen JL, Fucini RV, Lacomis L, Erdjument-Bromage H, Tempst P, Stamnes M: **Coatomer-bound Cdc42 regulates dynein recruitment to COPI vesicles**. *J Cell Biol* 2005, **169**:383-389.
This article reports that dynein associates with COPI vesicles both *in vitro* and *in vivo*. The addition of constitutively activated forms of both Cdc42 and Arf1 to a vesicle budding reaction *in vitro* decreases the amount of dynein present in COPI-coated vesicles. This is indicative that dynein is a Cdc42-sensitive component of isolated Golgi vesicles. Cytochalasin D at low concentrations stimulates dynein/dynactin binding. Finally, dynein-mediated ER-to-Golgi protein transport is blocked by the constitutively activated Cdc42(Q61L) mutant.

51. Lee MC, Miller EA, Goldberg J, Orci L, Schekman R: **Bi-directional protein transport between the ER and Golgi**. *Annu Rev Cell Dev Biol* 2004, **20**:87-123.

52. Welch MD, Mullins RD: **Cellular control of actin nucleation**. *Annu Rev Cell Dev Biol* 2002, **18**:247-288.

53. Rozelle AL, Machesky LM, Yamamoto M, Driessens MH, Insall RH, Roth MG, Luby-Phelps K, Marriott G, Hall A, Yin HL: **Phosphatidylinositol 4,5-bisphosphate induces actin-based movement of raft-enriched vesicles through WASP-Arp2/3**. *Curr Biol* 2000, **10**:311-320.

54. Gruenheid S, Finlay BB: **Microbial pathogenesis and cytoskeletal function**. *Nature* 2003, **422**:775-781.

55. •• Carreno S, Engqvist-Goldstein AE, Zhang CX, McDonald KL, Drubin DG: **Actin dynamics coupled to clathrin-coated vesicle formation at the trans-Golgi network**. *J Cell Biol* 2004, **165**:781-788.
Using deconvolution and time-lapse confocal microscopy, the authors show that huntingtin interacting protein 1 (Hip1R) is present in clathrin-coated vesicles exiting from the TGN. These vesicles contain proteins destined to the endosomal/lysosomal system and the Arp2/3 complex. The depletion of Hip1R leads to abnormal actin formations at the Golgi, and to the accumulation of lysosomes, clathrin-coated buds and vesicles, which suggests the involvement of Hip1R in coupling actin dynamics and transport carrier fission.

56. Duran JM, Valderrama F, Castel S, Magdalena J, Tomas M, Hosoya H, Renau-Piqueras J, Malhotra V, Egea G: **Myosin motors and not actin comets are mediators of the actin-based Golgi-to-endoplasmic reticulum protein transport**. *Mol Biol Cell* 2003, **14**:445-459.

57. Stow JL, Fath KR, Burgess DR: **Budding roles for myosin II on the Golgi**. *Trends Cell Biol* 1998, **8**:138-141.

58. • Fath KR: **Characterization of myosin-II binding to Golgi stacks *in vitro***. *Cell Motil Cytoskeleton* 2005, **60**:222-235.
Using isolated Golgi and purified brush border myosin II (BBM-II), the author shows that BBM-II dimers tightly bind in a saturable manner to Golgi peripheral membrane proteins, regardless of actin. Moreover, the rod but not the head of the BBM-II binds to Golgi membranes. The casein-kinase-II-induced phosphorylation of the BBM-II rod domain prevents this binding.

59. •• Percival JM, Hughes JA, Brown DL, Schevzov G, Heimann K, Vrhovski B, Bryce N, Stow JL, Gunning PW: **Targeting of a tropomyosin isoform to short microfilaments associated with the Golgi complex**. *Mol Biol Cell* 2004, **15**:268-280.
Only the tropomyosin isoform Tm5NM-2 is specifically associated to the Golgi complex in a brefeldin-A-sensitive and cytochalasin-D-resistant manner. Furthermore, the authors give evidence for the existence of a population of short actin filaments that interact with both Golgi membranes and Golgi-derived vesicles. Tm5NM-2 is found in these Golgi-associated short actin filaments.

60. Buss F, Luzio JP, Kendrick-Jones J: **Myosin VI, an actin motor for membrane traffic and cell migration**. *Traffic* 2002, **3**:851-858.

61. Jordens I, Marsman M, Kuijl C, Neefjes J: **Rab proteins, connecting transport and vesicle fusion**. *Traffic* 2005, **6**:1070-1077.

62. Echard A, Jollivet F, Martinez O, Lacapere JJ, Rousselet A, Janoueix-Lerosey I, Goud B: **Interaction of a Golgi-associated kinesin-like protein with Rab6**. *Science* 1998, **279**:580-585.

63. Short B, Preisinger C, Schaletzky J, Kopajtich R, Barr FA: **The Rab6 GTPase regulates recruitment of the dynactin complex to Golgi membranes**. *Curr Biol* 2002, **12**:1792-1795.

64. Wu X, Rao K, Bowers MB, Copeland NG, Jenkins NA, Hammer JA III: **Rab27a enables myosin Va-dependent melanosome capture by recruiting the myosin to the organelle**. *J Cell Sci* 2001, **114**:1091-1100.

65. Sahlender DA, Roberts RC, Arden SD, Spudich G, Taylor MJ, Luzio JP, Kendrick-Jones J, Buss F: **Optineurin links myosin VI to the Golgi complex and is involved in Golgi organization and exocytosis**. *J Cell Biol* 2005, **169**:285-295.

66. Merrifield CJ, Feldman ME, Wan L, Almers W: **Imaging actin and dynamin recruitment during invagination of single clathrin-coated pits**. *Nat Cell Biol* 2002, **4**:691-698.

67. Merrifield CJ, Qualmann B, Kessels MM, Almers W: **Neural Wiskott Aldrich Syndrome Protein (N-WASP) and**

the Arp2/3 complex are recruited to sites of clathrin-mediated endocytosis in cultured fibroblasts. *Eur J Cell Biol* 2004, **83**:13-18.

68. De Matteis MA, Di Campli A, Godi A: **The role of the phosphoinositides at the Golgi complex**. *Biochim Biophys Acta* 2005, **1744**:396-405.

69. Rohatgi R, Ho HY, Kirschner MW: **Mechanism of N-WASP activation by CDC42 and phosphatidylinositol 4,5-bisphosphate**. *J Cell Biol* 2000, **150**:1299-1310.

70. Schafer DA, Weed SA, Binns D, Karginov AV, Parsons JT, Cooper JA: **Dynamin2 and cortactin regulate actin assembly and filament organization**. *Curr Biol* 2002, **12**:1852-1857.

71. Siddhanta A, Radulescu A, Stankewich MC, Morrow JM, Shields D: **Fragmentation of the Golgi apparatus. Arole for bIII spectrin and synthesis of phosphatidylinositol 4,5-biphosphate**. *J Biol Chem* 2003, **17**:1957-1965.

72. Foletta VC, Brown FD, Young WS III: **Cloning of rat ARHGAP4/C1, a RhoGAP family member expressed in the nervous system that colocalizes with the Golgi complex and microtubules**. *Brain Res Mol Brain Res* 2002, **107**:65-79.

73. Dubois T, Paleotti O, Mironov AA, Fraisier V, Stradal TE, De Matteis MA, Franco M, Chavrier P: **Golgi-localized GAP for Cdc42 functions downstream of ARF1 to control Arp2/3 complex and F-actin dynamics**. *Nat Cell Biol* 2005, **7**:353-364.

74. Estrada L, Caron E, Gorski JL: **Fgd1, the Cdc42 guanine nucleotide exchange factor responsible for faciogenital dysplasia, is localized to the subcortical actin cytoskeleton and Golgi membrane**. *Hum Mol Genet* 2001, **10**:485-495.

75. Hou P, Estrada L, Kinley AW, Parsons JT, Vojtek AB, Gorski JL: **Fgd1, the Cdc42 GEF responsible for Faciogenital Dysplasia, directly interacts with cortactin and mAbp1 to modulate cell shape**. *Hum Mol Genet* 2003, **12**:1981-1993.

76. Fucini RV, Chen JL, Sharma C, Kessels MM, Stamnes M: **Golgi vesicle proteins are linked to the assembly of an actin complex defined by mAbp1**. *Mol Biol Cell* 2002, **13**:621-631.

77. Rybakin V, Stumpf M, Schulze A, Majoul IV, Noegel AA, Hasse A: **Coronin 7, the mammalian POD-1 homologue, localizes to the Golgi apparatus**. *FEBS Lett* 2004, **573**:161-167.

78. Rybakin V, Clemen CS: **Coronin proteins as multifunctional regulators of the cytoskeleton and membrane trafficking**. *Bioessays* 2005, **27**:625-632.

79. Humphries CL, Balcer HI, D'Agostino JL, Winsor B, Drubin DG, Barnes G, Andrews BJ, Goode BL: **Direct regulation of Arp2/3 complex activity and function by the actin binding protein coronin**. *J Cell Biol* 2002, **159**:993-1004.

80. Bennett V, Baines AJ: **Spectrin and ankyrin-based pathways: Metazoan inventions for integrating cells into tissues**. *Physiol Rev* 2001, **81**:1353-1392.

81. Camera P, da Silva JS, Griffiths G, Giuffrida MG, Ferrara L, Schubert V, Imarisio S, Silengo L, Dotti CG, Di Cunto F: **Citron-N is a neuronal Rho-associated protein involved in Golgi organization through actin cytoskeleton regulation**. *Nat Cell Biol* 2003, **5**:1071-1078.

82. Prigozhina NL, Waterman-Storer CM: **Protein kinase D-mediated anterograde membrane trafficking is required for fibroblast motility**. *Curr Biol* 2004, **14**:88-98.

83. Matas OB, Fritz S, Luna A, Egea G: **Membrane trafficking at the ER/Golgi interface: functional implications of RhoA and Rac1**. *Eur J Cell Biol* 2005, **84**:699-707.

84. Rosso S, Bollati F, Bisbal M, Peretti D, Sumi T, Nakamura T, Quiroga S, Ferreira A, Caceres A: **LIMK1 regulates Golgi dynamics, traffic of Golgi-derived vesicles, and process extension in primary cultured neurons**. *Mol Biol Cell* 2004, **15**:3433-3449.

85. Abo A, Qu J, Cammarano MS, Dan C, Fritsch A, Baud V, Belisle B, Minden A: **PAK4, a novel effector for Cdc42Hs, is implicated in the reorganization of the actin cytoskeleton and in the formation of filopodia**. *EMBO J* 1998, **17**:6527-6540.

86. Dan C, Kelly A, Bernard O, Minden A: **Cytoskeletal changes regulated by the PAK4 serine/threonine kinase are mediated by LIM kinase 1 and cofilin**. *J Biol Chem* 2001, **276**:32115-32121.

87. Paglini G, Peris L, Diez-Guerra J, Quiroga S, Caceres A: **The Cdk5-p35 kinase associates with the Golgi apparatus and regulates membrane traffic**. *EMBO Rep* 2001, **2**:1139-1144.

88. Lefcort F, Bentley D: **Organization of cytoskeletal elements and organelles preceding growth cone emergence from an identified neuron *in situ***. *J Cell Biol* 1989, **108**:1737-1749.

89. De Anda FC, Pollarolo G, Da Silva JS, Camoletto PG, Feiguin F, Dotti CG: **Centrosome localization determines neuronal polarity**. *Nature* 2005, **436**:704-708.

90. Kessels MM, Qualmann B: **The syndapin protein family: linking membrane trafficking with the cytoskeleton**. *J Cell Sci* 2004, **117**:3077-3086.

91. Modregger J, DiProspero NA, Charles V, Tagle DA, Plomann M: **PACSIN 1 interacts with huntingtin and is absent from synaptic varicosities in presymptomatic Huntington's disease brains**. *Hum Mol Genet* 2002, **11**:2547-2558.

92. Larocca MC, Shanks RA, Tian L, Nelson DL, Stewart DM, Goldenring JR: **AKAP350 interaction with cdc42 interacting protein 4 at the Golgi apparatus**. *Mol Biol Cell* 2004, **15**:2771-2781.

93. Tian L, Nelson DL, Stewart DM: **Cdc42-interacting protein 4 mediates binding of the Wiskott-Aldrich syndrome protein to microtubules**. *J Biol Chem* 2000, **275**:7854-7861.

94. Holbert S, Dedeoglu A, Humbert S, Saudou F, Ferrante RJ, Neri C: **Cdc42-interacting protein 4 binds to huntingtin: neuropathologic and biological evidence for a role in Huntington's disease**. *Proc Natl Acad Sci USA* 2003, **100**:2712-2717.

95. •• Rios RM, Sanchis A, Tassin AM, Fedriani C, Bornens M: **GMAP-210 recruits gamma-tubulin complexes to *cis*-Golgi membranes and is required for Golgi ribbon formation**. *Cell* 2004, **118**:323-335.

The *cis*-Golgi microtubule binding protein GMAP-210 recruits γ-tubulin to Golgi membranes. The targeting of GMAP-210 to mitochondria also triggers γ-tubulin recruitment to this organelle. GAMP-210 overexpression induces the formation of short microtubules onto Golgi membranes. The silencing of GMAP-210 leads to Golgi fragmentation, indicating the importance of GAMP-210 in the Golgi ribbon-like structure around the centrosome.

96. Kessels MM, Qualmann B: **Extending the court for cortactin: from the cortex to the Golgi**. *Nat Cell Biol* 2005, **7**:448-449.

97. Stankewich MC, Tse WT, Peters LL, Ch'ng Y, John KM, Stabach PR, Devarajan P, Morrow JS, Lux SE: **A widely expressed βIII spectrin associated with Golgi and cytoplasmic vesicles**. *Proc Natl Acad Sci U S A* 1998, **95**:14158.

98. Holleran EA, Ligon LA, Tokito M, Stankewich MC, Morrow JS, Holzbaur EL: **βIII spectrin binds to the Arp1 subunit of dynactin**. *J Biol Chem* 2001, **276**:36598-36605.

99. Gough LL, Fan J, Chu S, Winnick S, Beck KA: **Golgi localization of Syne-1**. *Mol Biol Cell* 2003, **14**:2410-2424.

100. Devarajan P, Stabach PR, Mann AS, Ardito T, Kashgarian M, Morrow JS: **Identification of a small cytoplasmic ankyrin (AnkG119) in the kidney and muscle that binds βI sigma spectrin and associates with the Golgi apparatus**. *J Cell Biol* 1996, **133**:819-830.

101. Beck KA, Buchanan JA, Nelson WJ: **Golgi membrane skeleton: identification, localization and oligomerization of a 195 kDa ankyrin isoform associated with the Golgi complex**. *J Cell Sci* 1997, **110**:1239-1249.

102. Lin CM, Chen HJ, Leung CL, Parry DA, Liem RK: **Microtubule actin crosslinking factor 1b: a novel plakin that localizes to the Golgi complex**. *J Cell Sci* 2005, **118**:3727-3738.

103. Kakinuma T, Ichikawa H, Tsukada Y, Nakamura T, Toh BH: **Interaction between p230 and MACF1 is associated with transport of a glycosyl phosphatidyl inositol-anchored**

protein from the Golgi to the cell periphery. *Exp Cell Res* 2004, **298**:388-398.

104. Fucini RV, Navarrete A, Vadakkan C, Lacomis L, Erdjument-Bromage H, Tempst P, Stamnes M: **Activated ADP-ribosylation factor assembles distinct pools of actin on golgi membranes**. *J Biol Chem* 2000, **275**:18824-18829.

105. Stephens DJ, Banting G: **Direct interaction of the trans-Golgi network membrane protein, TGN38, with the F-actin binding protein, neurabin**. *J Biol Chem* 1999, **274**:30080-30086.

106. Holleran EA, Holzbaur EL: **Speculating about spectrin: new insights into the Golgi-associated cytoskeleton**. *Trends Cell Biol* 1998, **8**:26-29.

107. Musch A, Cohen D, Rodriguez-Boulan E: **Myosin II is involved in the production of constitutive transport vesicles from the TGN**. *J Cell Biol* 1997, **138**:291-306.

108. Buss F, Kendrick-Jones J, Lionne C, Knight AE, Cote GP, Paul Luzio J: **The localization of myosin VI at the golgi complex and leading edge of fibroblasts and its phosphorylation and recruitment into membrane ruffles of A431 cells after growth factor stimulation**. *J Cell Biol* 1998, **143**:1535-1545.

109. Warner CL, Stewart A, Luzio JP, Steel KP, Libby RT, Kendrick-Jones J, Buss F: **Loss of myosin VI reduces secretion and the size of the Golgi in fibroblasts from Snell's waltzer mice**. *EMBO J* 2003, **22**:569-579.

110. Magdalena J, Millard TH, Etienne-Manneville S, Launay S, Warwick HK, Machesky LM: **Involvement of the Arp2/3 complex and Scar2 in Golgi polarity in scratch wound models**. *Mol Biol Cell* 2003, **14**:670-684.

111. Erickson JW, Zhang C, Kahn RA, Evans T, Cerione RA: **Mammalian Cdc42 is a brefeldin A-sensitive component of the Golgi apparatus**. *J Biol Chem* 1996, **271**:26850-26854.

112. Michaelson D, Silletti J, Murphy G, D'Eustachio P, Rush M, Philips MR: **Differential localization of Rho GTPases in live cells: regulation by hypervariable regions and RhoGDI binding**. *J Cell Biol* 2001, **152**:111-126.

113. Nalbant P, Hodgson L, Kraynov V, Toutchkine A, Hahn KM: **Activation of endogenous Cdc42 visualized in living cells**. *Science* 2004, **305**:1615-1619.

114. Kroschewski R, Hall A, Mellman I: **Cdc42 controls secretory and endocytic transport to the basolateral plasma membrane of MDCK cells**. *Nat Cell Biol* 1999, **1**:8-13.

115. Musch A, Cohen D, Kreitzer G, Rodriguez-Boulan E: **cdc42 regulates the exit of apical and basolateral proteins from the trans-Golgi network**. *EMBO J* 2001, **20**:2171-2179.

116. Cohen D, Musch A, Rodriguez-Boulan E: **Selective control of basolateral membrane protein polarity by cdc42**. *Traffic* 2001, **2**:556-564.

117. Cau J, Hall A: **Cdc42 controls the polarity of the actin and microtubule cytoskeletons through two distinct signal transduction pathways**. *J Cell Sci* 2005, **118**:2579-2587.

118. Kanzaki M, Watson RT, Hou JC, Stamnes M, Saltiel AR, Pessin JE: **Small GTP-binding protein TC10 differentially regulates two distinct populations of filamentous actin in 3T3L1 adipocytes**. *Mol Biol Cell* 2002, **13**:2334-2346.

Trabajo 5

DINÁMICA DE UN AGRESOMA DE ACTINA FILAMENTOSA INDUCIDO POR EL AGENTE ESTABILIZADOR DE ACTINA JASPLAKINOLIDE

En numerosas enfermedades el citoesqueleto está alterado y es frecuente la formación de CIs por la agregación de péptidos y proteínas integrantes o relacionadas con el citoesqueleto como consecuencia de alteraciones en su ensamblaje, mutaciones o interacciones anómalas con otras proteínas. Por ejemplo, los enfermos de Alzheimer y alcohólicos crónicos presentan en el soma de las neuronas del hipocampo agregaciones paracristalinas de actina filamentosa en los CHs.

En este trabajo generamos un modelo celular para la formación de agresomas de actina filamentosa similares a los CHs. La toxina de actina Jpk que provoca la estabilización/polimerización amorfa de la actina produce la formación de agregados de F-actina dispersos citoplasmáticamente que son agrupados y transportados hasta el centrosoma de manera MT-dependiente formando un agresoma cuya morfología y composición molecular es muy similar a la de los CHs. Una vez caracterizado el mecanismo de formación en distintos tipos celulares, mofología/ultraestructura y composición molecular para estos agresomas de actina filamentosa se realizaron diversos ensayos para determinar si la presencia de este tipo de estructuras compromete la viabilidad/proliferación celular así como su funcionalidad en cuanto al transporte intracelular asociado al AG. En este sentido, no observamos alteración alguna en la dinámica de membranas asociada al AG pero si una alteración en la proliferación celular. También estudiamos la participación de los mecanismos o sistemas de proteolisis celular implicados en la degradación de este agresoma. En este caso, se pudo observar la participación directa del sistema lisosomal/autofagia y del proteasoma en la disolución del agresoma. Por último, observamos también la coexistencia de dos agresomas de naturaleza molecular distinta sin que tenga lugar ningún tipo de fusión o mezcla de sus componentes.

DYNAMICS OF A FILAMENTOUS ACTIN AGGRESOME GENERATED BY THE ACTIN STABILINZING TOXIN JASPLAKINOLIDE

Francisco Lázaro-Diéguez[1-3], Carmen Aguado[4], Eugenia Mato[1,2], Yován Sánchez-Ruíz[1], Inmaculada Esteban[4], Jordi Alberch[1,2], Erwin Knecht[4], and Gustavo Egea[1-3,*]

[1]Departament de Biologia Cel·lular i Anatomia Patològica, Facultat de Medicina, [2]Institut d'Investigacions Biomèdiques August Pi i Sunyer (IDIBAPS), [3]Institut de Nanociència i Nanotecnologia (IN[2]UB), Universitat de Barcelona, E-08036 Barcelona, Spain; [4]Laboratorio de Biología Celular, Centro de Investigación Príncipe Felipe and CIBERER, E-46013 Valencia, Spain.

In this study we report the formation of several cytoplasmic inclusion bodies composed of filamentous actin and generated by experimental treatments using depolymerizing or stabilizing actin toxins in neuronal and non-neuronal mammalian cell lines. The actin-stabilizing toxin jasplakinolide induced, in a microtubule-dependent manner, a single, large F-actin aggregate, which contained β/γ-actin, ADF/cofilin, cortactin, and the actin nucleator Arp2/3. This aggregate is tightly associated with the Golgi apparatus and mitochondria and is surrounded by vimentin intermediate filaments, microtubules and MAP4. Therefore, the Jpk-induced single, large F-actin aggregate fits the established criteria for being considered an aggresome. Lysosomes/autophagic vacuoles, proteasomes and microtubules directly participate in the dissolution of this F-actin aggresome. Finally, the model reported here is simple, highly reproducible and reversible, and it provides an opportunity to test pharmacological agents that interfere with the formation, maintenance and/or disappearance of filamentous actin-enriched pathological inclusion bodies.

Keywords: actin, aggresome, autophagy, inclusion bodies, cytoskeleton, huntingtin, jasplakinolide, microtubules, proteasome

*Corresponding author:
Gustavo Egea, Dept. de Biologia Cel·lular i Anatomia Patològica, Facultat de Medicina, Universitat de Barcelona, C/ Casanova 143, E-08036 Barcelona, Spain. Tel.: +34-93-4021909. Fax: +34-93-4021907. E-mail: gegea@ub.edu

INTRODUCTION

Alterations in the structure and dynamics of the cytoskeleton have been reported in many diseases like cancer (Suresh, 2007) and neurodegenerative disorders (Weissmann and Brandt, 2007). One of their common characteristics is that cytoskeleton disruption usually leads to peptide or protein deposits that aggregate abnormally due to misfolding or abnormal protein-protein interactions. These aggregates form cytoplasmic and non-membranous structures called inclusion bodies (IBs). Other IBs, generically named aggresomes, are usually composed of aggregated misfolded proteins or mutant proteins resulting from their expression or over-expression (Garcia-Mata et al., 1999; Johnston et al., 1998; Kopito, 2000). Several cytoskeleton components such as vimentin intermediate filaments (Kopito, 2000) and the minus-end-directed microtubular dynein motor (Johnston et al., 2002) are involved in the formation of IBs, regardless of their molecular composition. Filamentous actin (F-actin) is of particular interest as it interacts with the amyloid precursor, presenilin and Tau proteins of IBs in Alzheimer's disease (Santa-Maria et al., 2007; Maloney et al., 2005) and it strongly accumulates in other IBs termed Hirano bodies seen in post-mortem neurological histological preparations as indicators of Alzheimer's (and other neurodegenerative disorders) (Hirano, 1994) and of chronic alcoholism (Lass and Hagel, 1994). Aggregation of F-actin has been also described in some myopathies (Schroder, 1990; Podlubnaia and Nowak. 2006). The biological significance and molecular mechanisms involved in the formation, composition, and proteolysis of these F-actin enriched IBs and their precise relation to (neuro)diseases are unknown. Cellular models that reproduce the formation and composition of the F-actin enriched IBs are required in order to perform detailed examinations of the molecular mechanisms involved in their structural and functional dynamics. In this regard, cells cultured under heat shock, osmotic stress or cofilin overexpression experimental condition induce the formation of actin-containing structures called ADF/cofilin-actin rods (Nishida et al., 1987 and references herein; Minamide et al., 2000, Bernstein et al., 2006; Jang et al., 2005). Recently, it has been reported a model for formation of Hirano bodies in mammalian cell cultures by expression of a fragment of a 34 kDa actin-bundling protein (Davis et al., 2008).

One of the fastest and most effective methods of perturbing actin dynamics involves the use of actin toxins which induce the disruption of the actin cytoskeleton. Most natural actin toxins such as

cytochalasins, latrunculins, and some botulinum toxins depolymerize F-actin. Far fewer F-actin stabilizers are known and the most commonly used is the cell membrane-permeable toxin jasplakinolide (Spector et al., 1999; Holzinger 2001; Fenteany and Zhu, 2003; Allingham et al., 2006). Cytochalasins and latrunculins are widely used to study the involvement of actin in cellular events, for example in endo/exocytosis, cell motility and migration, cell polarity and differentiation, and axonal transport and neuritogenesis. Therefore, actin toxins could also be useful to find out the molecular processes impaired in neurological and non-neurological disorders in which actin is thought to play an essential role.

In this study we perturbed the actin cytoskeleton dynamics in a variety of mammalian cells using actin toxins. We report the formation of F-actin IBs, in which we highlight the single, large F-actin aggregate induced by jasplakinolide. This IB fits the criteria of an aggresome, and we provide evidence of the molecular mechanisms involved in its formation and clearance.

RESULTS

Structural dynamics (formation, maintenance and clearance) of a large F-actin-aggregate induced by jasplakinolide

We examined the way in which actin cytoskeleton is perturbed by actin toxins. Vero cells were treated with actin-depolymerizing toxins such as cytochalasin D (CyD), latrunculin B (LtB), and mycalolide B (MyB), or with the actin-stabilizing toxin jasplakinolide (Jpk) (Supplementary Table). They all induced the disruption of the actin cytoskeleton visualized by the loss of actin stress fibres and the rounding-up of cells (Fig. 1B-D). NRK and HeLa cells also showed highly similar alterations (not shown). Next, we studied the reversibility of these impairments following toxin washout (Supplementary Table). The removal of LtB or CyD early led to the formation of numerous, F-actin puntae (arrowheads and inset in Fig. 1E). The cell shape and the actin cytoskeleton organization were completely restored at 60/90 minutes (Fig. 1F). After MyB or Jpk removal, the normal cell shape and actin stress fibre organization were seen 48 hours (Fig. 1H) or 32 hours (Fig. 1J), respectively. MyB-washout cells showed juxtanuclear accumulations of F-actin puntae after 24/32 hours (arrowheads and inset in Fig. 1G). Interestingly, after 6/8 hours of Jpk removal, cells contained a single, large F-actin aggregate (FAG) (Fig. 1I and inset), which localized in the centrosomal region (identified with anti-γ-tubulin antibodies; green in the inset of Fig. 1I). Notably FAG, was also generated when cells were incubated in the continuous presence of Jpk, but at lower concentration. Using this other strategy, no cellular rounding-up was observed and, moreover, we could follow in detail the kinetics of the formation and clearance of FAG. Thus, in the continuous presence of Jpk, the coalescence of F-actin puntae (arrowheads in Fig. 2B-D) and F-actin amorphous aggregates (arrows in Fig. 2B-E) to the centrosomal region formed FAG (Fig. 2F). Over time, FAG fragmented to multiple F-actin amorphous aggregates (arrows in Fig. 2G-I) and F-actin puntae, that were dispersed throughout the cytoplasm (arrowheads in Fig. 2G-K) and finally disappeared (Fig. 2L). FAG was maintained larger and even increased in size when the culture medium was replaced every 12 hours by other medium containing new Jpk. In this case, cells showed a much larger FAG, which sometimes completely enclosed the nucleus (Supplementary Fig. 1).

Taking into account its ellipsoid morphology and filamentous actin content, F-actin puntae/F-actin amorphous aggregates and FAG resembles respectively in some degree to rod-shaped actin bundles and Hirano bodies (Minamide et al., 2000; Hirano, 1994). Therefore, we next studied its potential formation in neural cells, which included a mouse c17.2 neural stem cells (NSC) and primary cultures of rat astrocytes and mouse hippocampal neurons. The majority of NSC, astrocytes and, to a lesser extent, hippocampal neurons also showed FAG. Strikingly, neurons required higher concentrations of Jpk to generate FAG, which was indistinguishable from that seen in Vero cells (Supplementary Fig. 2). FAG was also generated when neuronal cells were incubated in the continuous presence of Jpk at lower concentrations (not shown).

Cell viability is not compromised by the presence of the F-actin aggregate

Interestingly, most Vero cells were binucleate after either MyB or Jpk withdrawal, which indicates that cells were transiently arrested in cytokinesis. The two nuclei and FAG were always tightly associated (Fig. 1G,I). As soon as FAG disappeared, binucleate cells were no longer observed (Fig. 1H,J). We tested whether FAG impaired the viability of Jpk-washout Vero cells using either trypan blue exclusion (not shown) or MTT reduction assays (Supplementary Fig. 3A). There were no significant differences between control cells and either those that contained FAG (+Jpk/6 hours and 24 hours, and -Jpk/8 h and 24 hours) or those in which FAG had already disappeared (+Jpk/48 hours and -Jpk/48 hours). Strikingly, no binucleate neural cells were seen at any point, but unlike in non-neural cells, apoptotic nuclei appeared in hippocampal neurons at 24/48 hours after the Jpk washed out (Supplementary Fig. 3B).

Organelle association and ultrastructure of the F-actin aggregate

Next, we analysed the morphology of FAG. We obtained first a 3D model from confocal serial images of Jpk-washout Vero cells. In most cases, FAG was slightly ellipsoid and curiously, the Golgi apparatus invariably housed it (Fig. 3A). A large accumulation of mitochondria around FAG was also observed (Fig. 3B). Under the electron microscope, FAG was seen as

a large electron-lucent body (Fig. 3C). In some regions, a more electron-dense material was occasionally seen (asterisks in Fig. 3D), which in some cases when examined at higher magnification showed a regular structure made-up of aligned and tightly compacted F-actin or actin bundles (Fig. 3E,F). FAG lacked of membrane, but intermediate filaments accumulated at its periphery (arrowheads in Fig. 3G). As already observed under the fluorescence microscope, numerous mitochondria (Fig. 3C,D), autophagic vacuoles and lysosomes (Fig. 3D,G), endoplasmatic reticulum, and the Golgi apparatus (Fig. 3D,G) with peri-Golgi COPI-coated vesicles (arrows in Fig. 3G) accumulated around FAG. The use of brefeldin A and the steady-state distribution of the KDELr in FAG-containing cells showed that the tight morphological association between the Golgi apparatus and FAG did not lead to any alteration in the ER/Golgi interface membrane trafficking (not shown).

Molecular composition of the F-actin aggregate

In Vero cells, FAG contained β- and γ-actin isoforms (not shown), ADF/cofilin (Fig. 4A), the p21-Arc subunit of the actin nucleator multiprotein complex Arp2/3 (Fig. 4B), and cortactin (Fig. 4C). However, it lacked N-WASP, the small Rho GTPases Cdc42, RhoA, and Rac (not shown), and myosins IIA (Fig. 4D) and IIB (not shown). FAG was surrounded by spectrin (not shown), vimentin intermediate filaments (Fig. 4E), and microtubules (MTs) (Fig. 4F). The MT-associated protein MAP4 was only present at the periphery of FAG (Fig. 4F, inset). In hippocampal neurons, neither MAP4 (Fig. 4H) nor Tau (not shown) nor synapsin (Fig. 4I) was seen in FAGs. In contrast, we observed a significant accumulation of cortactin (Fig. 4G) and spinophilin (Fig. 4J).

We also determined the distribution of several proteins in nuclei-free homogenates from Vero cells containing FAG. Cell homogenates were separated by centrifugation in discontinuous sucrose density gradients and fractions were subsequently immunoblotted for β-actin, the Arp3 component of the Arp2/3 complex, ADF/cofilin, and myosin IIA isoform. In untreated cells, the immunoreactivity of these proteins was broadly distributed along the gradient (supplementary Fig. 4A, Control). However, in Jpk-treated cells, β-actin, Arp3 and ADF/cofilin were redistributed to the densest membrane fractions along the gradient (supplementary Fig. 4A, +Jpk). In contrast, myosin IIA maintained a broader distribution in the density profile. These results indicate a restricted distribution of endogenous actin and some actin-binding/associated proteins in subcellular structures, which is consistent with the results from confocal microscopy (Fig. 4). We also used immunofluorescence microscopy to assess the F-actin reactivity in the sucrose fractions (Supplementary Fig. 4B). Unlike low- (1-3 fractions; left panel) and mid- (4-6 fractions; middle panel) density fractions, those with higher densities (7-10 fractions; right panel) were enriched in FAGs with an altered and heterogeneous morphology as a consequence of the mechanical stress produced during its isolation.

Actin dynamics in the F-actin aggregate

We first examined the dynamics of actin inside FAG. Vero cells transiently expressing YFP-actin were treated with Jpk to induce the formation of FAG, and then equal areas of cytoplasm and FAG were photobleached. The fluorescence emitted by the YFP-actin from the cytoplasm area was rapidly recovered but not that from FAG (Supplementary Fig. 5A, Control and +Jpk, respectively).

Next, we examined whether the F-actin from FAG was sensitive to LtB treatment. As expected, LtB induced the shrinkage of cells and actin stress fibres completely disappeared in the control cells and Jpk-treated cells, but FAG remained apparently unaltered (Supplementary Fig. 5B, +LtB). Next, we examined whether the presence of FAG perturbs the restoration of the actin cytoskeleton organization, which takes place after removal of LtB. In these conditions, a normal cell shape and actin stress fibre organization was observed both in control cells and in cells containing FAG (Supplementary Fig. 5B, -LtB). Finally, control and FAG-containing cells cultured in DMEM without FBS and stimulated with phorbol myristate acetate or lysophosphatidic acid quickly formed lamellipodia and stress fibres, respectively (Supplementary Fig. 6) (Ridley et at., 1992; Ridley and Hall, 1992). Therefore, actin in FAG is not dynamic and it does not perturb the induced formation of other actin cytoskeleton rearrangements such as lamellipodia and stress fibres.

Microtubules are essential for the formation and clearance of the F-actin aggregate

Next, we assessed the degree of MT dependence of the formation and clearance of FAG in Vero cells. To this end, we used nocodazole to depolymerize MTs or taxol to stabilize them (Fig. 5A, +NZ and +TX, respectively). In cells treated with NZ and then co-incubated with Jpk, instead of FAG, a large number of F-actin puntae and F-actin amorphous aggregates structures were formed throughout the cytoplasm (Fig. 5B and inset). When NZ was removed in the continuous presence of Jpk, F-actin puntae and F-actin amorphous aggregates repositioned to the centrosomal region producing FAG (Fig. 5D and inset). Similar results were obtained when cells were treated with TX (Fig. 5C,E, and respective insets). Therefore, results indicate that the formation and positioning of FAG is MT-dependent. However, when cells were incubated with Jpk and then with NZ, FAG remained unaltered despite the disruption of microtubules (Fig. 5F). This indicates that FAG integrity is MT-independent.

We then tested the role of MTs in the clearance of FAG. As indicated above, it is not a permanent structure and it disappeared in Vero cells 32/48 h after

its generation (Figs 1, 2). Cells were incubated with Jpk to form FAG and then treated with either NZ or TX for 48 h in the continuous presence of Jpk. At this time, and unlike cells treated with Jpk alone, co-incubation with NZ or TX did not altered FAG structure and increased its life-span (Supplementary Fig. 7). Therefore, this indicates that intact MTs are necessary for the dissolution of FAG.

Proteolysis of the F-actin aggregate

IBs usually contains chaperones, transcription factors, proteasomal subunits, and polyubiquitinated misfolded/unfolded proteins (Kopito, 2000; Taylor et al., 2003; Bennet et al., 2005). The formation of IBs activates the ubiquitin-proteasomal system (UPS) and can also induce lysosomal degradation (García-Mata et al., 2002; Ross and Pickart, 2004; Betarbet et al., 2005). Therefore, we examined in Vero cells the contribution of both protein degradation systems to the disappearance of FAG. First, we examined the subcellular distribution of lysosomes. In some FAG-containing cells, lysosomes partially reorganized around the aggregate (Fig. 6B, arrow). Interestingly, in Jpk-treated cells in which FAG had already disappeared, we observed an invariable stronger lysosomal staining (Fig. 6C). Next, we tested whether lysosomal activity was required for clearance of FAG. Cells were treated with bafilomycin A (Baf) or pepstatin A (Pep). The former inhibits vacuolar H^+-ATPase raising the intralysosomal pH (Drose and Altendorf, 1997; Gagliardi et al., 1999), the latter inhibits lysosomal proteases (Dean, 1977; Tanida et al., 2004 and 2005). Either Baf (Fig. 6D) or Pep (Fig. 6F) increased the life-span of FAG. Unlike Pep, Baf induced a juxtanuclear accumulation of lysosomes that were trapped by a filamentous actin network (Fig. 6E, asterisks) with a structure completely different from FAG (Fig. 6F, arrowhead). This F-actin network was also observed in cells treated with Baf alone (data not shown).

We also examined the participation of the autophagic pathway, which includes the induction and maturation of autophagosomes and autolysosomes (resulting from the fusion of lysosomes and autophagosomes) (Shintani and Klionsky, 2004; Reggiori and Klionsky, 2005; Fortun, 2007). We first used the localization of the autophagosome marker GFP-LC3 (Kabeya et al., 2000; Mizushima, 2004; Tanida et al., 2005). Since in the presence of complete medium autophagic activity is low (Fuertes et al., 2003), GFP-LC3-transfected Vero cells were cultured in the absence of FBS (for 4 hours) and in the presence of the lysosomal inhibitors Pep and E-64-d (Tanida et al., 2005). GFP-LC3-containing vesicular structures were seen in more than 80 % of transfected cells (Fig. 7A). Importantly, GFP-LC3-transfected Vero cells cultured in the presence of FBS and containing FAG showed an increased number of GFP-labeled autophagosomes in the vicinity of the aggregate (Fig. 7B). However, it has been recently reported that under certain conditions LC3 is incorporated into protein aggregates independently of autophagy (Kuma et al., 2007). Thus, we examined the conversion of the endogenous LC3-I to LC3-II forms of LC3, since LC3-II is the only protein marker that is widely accepted to be reliably associated with mature autophagosomes, and its relative amount can be used to estimate autophagy biochemically (Kabeya et al., 2004; Tanida et al., 2004; Mizushima and Yoshimori, 2007). As shown in Fig. 7C, ratio of membrane-bound (LC3-II) to tubulin was higher in cells containing FAG regardless the presence or absence of FBS (values indicated in the figure legend). Ultrastructurally, autophagic vacuoles were seen tightly associated with FAG (Fig. 7D). Autophagy in FAG-containing cells was also monitored with monodansilcadaverine (MDC) dye. We observed around FAG brighter and numerous MDC-containing vesicles (Fig. 7E), which markedly increased during the dissolution process of FAG (Fig. 7F,G). To stimulate autophagy, cells were treated with rapamycin (Rpc) because it inhibits mTOR (Meijer and Codogno, 2007). We observed a higher MDC vesicular staining and an accelerated dissolution of FAG (Fig 7H,I). Interestingly, during its clearance, there was a tight association and partial colocalization of F-actin puntae with lysosomes/MDC-containing vesicles (inset in Fig. 7H). The ultrastructural analysis of FAG clearance showed proliferation of autophagic vacuoles (Fig. 7J), which in some cases contained a highly ordered filamentous structure resembling F-actin together with glycogen particles. (Fig. 7K-L). Therefore, altogether strongly suggest that autophagy is induced in cells containing FAG and that this lysosomal process participates in its clearance.

We next checked whether chaperones are also involved in the dissolution of FAG, since the association of heat shock proteins (HSPs) with IBs could represent in our particular case an attempt of chaperons to favour FAG dissolution. To this end, Vero cells containing FAG were treated with the geldanamycin derivate 17-DMAG. This reagent binds to the ATPase site of human Hsp90 and thus prevents its interaction with HS factor 1, which in turn results in the activation and synthesis of HSPs (Muchowski and Wacker, 2005; Chiosis, 2006; Herbst and Wanker, 2007). 17-DMAG accelerated the fragmentation of FAG and its subsequent clearance (compare panels in Supplementary Fig. 8A-D).

Next, we examined the involvement of the UPS system, which plays an important role in the degradation of certain neurodegenerative IBs (Hol et al., 2006; Rubinsztein, 2006). Double immunolabelling (Fig. 8A) and western blot analysis (not shown) showed that FAG did not contain polyubiquitinated proteins. In contrast, FAG contained proteasomes (Fig. 8B). In addition, in cells treated with the proteasome inhibitor lactacystin, FAG remained longer in the cytoplasm (compare panels in Fig. 8C-F). Moreover, lactacystin delayed the effect of 17-DMAG and therefore normalized FAG clearance

kinetics (Supplementary Fig. 8E,F). To assess the functionality of proteasomes in cells containing FAG, we measured the chymotrypsin activity of proteasomes in the supernatant of lysates from cells treated with Jpk for different periods of time (Fig. 8G) because the proteasome activity of pellets (which contained FAG) could not be reliably measured due to their incomplete solubilization. We observed a significant decrease in proteasome activity in Jpk-treated cells. This was not a direct effect of Jpk, since its addition to the enzymatic reaction did not affect the proteasome activity (not shown). This decrease could be caused by the tight association of proteasomes with FAG. It is noteworthy that the decreased proteasome activity in the supernatant lasted longer (Fig. 8, +Jpk/48 and 96 hours) than the presence of FAG in the cytoplasm (Fig. 8G, 6 and 24 hours).

Cells can generate separate large inclusion bodies with segregated molecular identities

Finally, we examined whether cells can generate only a single aggresome containing different altered proteins or whether aggresomes with a different content can be formed and maintained separately. We analyzed the structural dynamics (formation and disappearance) of FAG in Vero cells expressing GFP-tagged exon 1 of mutant huntingtin (htt^m) containing a 103 trinucleotide CAG repeat expansion within its coding region that expresses a polyglutamine repeat (Canals et al., 2004). In Vero cells expressing GFP-tagged exon 1 htt^m and treated with Jpk, two large IBs were generated, one containing F-actin and the other the GFP-htt^m protein. Importantly, no IBs containing both molecular components were seen at any time (Fig. 9). Similar results were also obtained using striatal neuronal precursors M213 and HeLa (not shown). Therefore, cells can generate more than one IB, but the respective molecular inducers and components remain completely segregated.

DISCUSSION

Here we report the formation of F-actin-enriched IBs using actin toxins. The IB produced by the F-actin stabilizer jasplakinolide is particularly interesting due to its similarities with F-actin inclusion bodies of (neuro)diseases, and to its presence in the totality of cells and reversibility. The latter opens the possibility to examine in detail the proteolytic mechanisms involved in its clearance. The use of Jpk to induce a single, large F-actin aggregate was previously reported in *Dictyostelium discoideum* amoebae (Lee et al., 1998). Here we extend this study and report: (i) the formation and disappearance of this aggregate both in neuronal and non-neuronal mammalian cells, (ii) the identification of some molecular components, (iii) its ultrastructure and (iv) the proteolytic processes involved in its clearance.

The single, large F-actin aggregate produced by jasplakinolide is an aggresome

In Jpk-treated cells, three different F-actin IBs were observed: F-actin puntae, F-actin amorphous aggregates and FAG (single, large F-actin aggregate). This suggests that FAG arises from the coalescence of F-actin puntae and F-actin amorphous aggregates as a result of active MT-dependent retrograde transport (Garcia-Mata, 2002; Johnston et al., 2002). Our results are consistent with this hypothesis since they demonstrate that the formation of FAG is MT-dependent. However, FAG structure became MT-independent once it was completely formed. Therefore, on the basis of its structure, MT-dependent formation and pericentriolar positioning, the rearrangement of vimentin intermediate filaments and the accumulation of mitochondria (Johnston et al., 2002; Bauer and Richter-Landsberg, 2006; Muqit et al., 2006; Grenier et al., 2006), FAG fits criteria for being considered an aggresome (Johnston et al., 1998; Garcia-Mata et al., 2002). We also show that cells can produce several IBs whose respective molecular content and structure is totally segregated. This suggests that, although the cell generates subcellular structures (aggresomes) in response to the alteration and/or accumulation of abnormal (mutant, unfolded, etc) proteins, the resulting aggresomes are kept separated.

The F-actin aggresome as a potential experimental model for examining the cell biology of F-actin-enriched inclusion bodies associated with (neuro)disorders

The appearance of nuclear and cytoplasmic IBs is a frequent feature in numerous (neuro)diseases, but their physiological significance in terms of being harmful or protective remains a matter of debate (Ciechanover and Brundin, 2003; Ross and Poirier, 2004). F-actin has been described in various IBs present in some neurodegenerative disorders and in other diseases (Selkoe, 2004; Hirano, 1994; Lass and Hagel, 1994; Schroder, 1990; Podlubnaia, Z.A. and Nowak. 2006), the most representative being ADF/cofilin-actin rods (Nishida et al., 1987 and references herein; Minamide et al., 2000) and Hirano bodies (Cartier et al., 1985; Hirano, 1994). In fact, since both structures are highly enriched in ADF/cofilin (Nishida et al., 1987; Maciver and Harrington, 1995), it has been postulated that actin rods present in neurites of hippocampal neurons are the precursors of Hirano bodies (Minamide et al., 2000). In this regard, the Jpk-induced F-actin aggresome also contains ADF/cofilin (see below), as well as cortactin and Arp2/3, which are involved in the nucleation and polymerization of actin (Weaver et al., 2003). Therefore, this aggresome may simply represent the aberrant accumulation of multiple fragments of F-actin trapped in the cytoplasm as a result of the reported actin-crosslinking stabilization and/or the aberrant actin nucleation activity generated by Jpk (Bubb et al., 2000). The localization of cortactin, Arp2/3 and ADF/cofilin in F-actin aggresome in astrocytes, neuroblastoma cells, and/or

hippocampal neurons as well as in Hirano bodies (Galloway et al., 1987a; Galloway et al., 1987b; Goldman, 1983; Maciver and Harrington 1995; Schmidt et al., 1989) suggests that the molecular machinery involved in actin dynamics and its subcellular organization is also perturbed in neural cells and in some IBs-containing (neuro)diseases. Importantly, actin rods and Hirano bodies are actin paracrystal-like intracellular structures (Hirano et al., 1968; Izumiyama et al., 1991; Hirano, 1994; Minamide et al., 2000). However, an ordered structure is usually not present in F-actin aggresome although it is occasionally seen in some areas, which by size and morphology most likely corresponds to parallel arrays of microfilaments or actin bundles. The general absence of an ordered F-actin structure in the whole F-actin aggresome may be attributable to the mode of action of Jpk. Jpk used at the here reported concentrations (50 or 500 nM) stabilizes F-actin and, at the same time, promotes its polymerization (Bubb et al., 2000). The final result is the formation of small F-actin masses (F-actin puntae and F-actin amorphous aggregates) throughout the cytoplasm and their juxtanuclear coalescence gives rise to F-actin aggresome. Therefore, this aggresome simply represent the accumulation of multiple fragments of stable and aberrant F-actin trapped in the cytoplasm as a result of actin-crosslinking stabilization and/or aberrant actin nucleation activity generated by Jpk. In this respect, photobleaching results indicate that the actin of F-actin aggresome is not dynamic. Moreover, the presence in the aggregate of proteins that can sever F-actin without capping (ADF/cofilin) could further facilitate the intrinsic Jpk-induced actin polymerization.

Another difference with Hirano bodies described in histological preparations from brain is the absence of Tau in F-actin aggresome, but notice that this marker has been detected in only 20 % of Hirano bodies (Galloway et al., 1987b). It is proposed that the formation of Hirano bodies is either a cellular response of the actin cytoskeleton or a consequence of its aberrant function (Fechheimer et al., 2002). This postulate rises from the Hirano body-like formation observed in *Dictyostelium* and mammalian cell lines by the expression of the carboxy-terminal fragment of the *Dictyostelium* 34 kDa actin cross-linking protein (Maselli et al., 2002 and 2003; Davis et al., 2008). Mammalian cells containing model Hirano bodies showed normal growth, morphology, and motility (Davis et al., 2008).

Cell viability, actin dynamics, and proteolysis in cells containing the F-actin aggresome

Despite the perturbed subcellular distribution of mitochondria in cells containing F-actin aggresome, the assay of mitochondrial activity was normal. It is possible that the clustering of mitochondria around F-actin aggresome provide the high requirements of ATP for the proteolytic systems involved in its clearance. Strikingly, while F-actin aggresome remained in the cytoplasm, most cells were binucleate, which indicates that they were arrested in cytokinesis, probably because these cells lack enough functional (unperturbed) G-actin/F-actin to complete cell division (Glotzer, 2005). Similarly, F-actin aggresome may also hinder the formation of the myosin contractile ring, which would prevent cell cleavage. However, cells progress normally as soon as F-actin aggresome disappears and hence its presence is apparently not harmful to cells. Importantly, in neurons the appearance of F-actin aggresome requires greater Jpk concentration and a longer treatment than in non-neuronal cells. This suggests that the former are more resistant to the formation of F-actin-enriched IBs, but that once are generated, they trigger apoptosis. Therefore, the appearance of disease-associated IBs in neuronal cells could render them more sensitive than other cell types, compromising their survival and leading to apoptosis. On the other hand, intrinsic differences in the actin cytoskeleton dynamics and/or regulation between neuronal and non-neuronal cells may also explain the reported differences in response to Jpk treatment.

The actin contained in F-actin aggresome is not dynamic according to the photobleaching results with YFP-actin and to its insensitivity to LtB treatment. The latter is consistent with previous results in which actin filaments made by the addition of equimolar Jpk was resistant to depolymerization (Bubb et al., 1994). Moreover, the stimulation of actin polymerization through the reconstitution of normal cell shape and actin stress fibre organization and cell shape occurring after LtB withdrawal and the induced formation of plasma membrane ruffling or actin stress fibres do not produce any alteration in the structure of the formed F-actin aggresome. Moreover, the presence of F-actin aggresome does not interfere either in the induced formation of these actin-based structures.

The high amount of F-actin contained in the aggregate suggests that it cannot be immediately chaperoned or degraded. Consequently, the cell strongly activates proteolysis mediated by proteasomes and autophagy (Fortum, 2007). The involvement of autophagy is supported by the spatial association of GFP-labeled autophagosomes with F-actin aggresome and the visualization by light and electron microscopy of autophagic vacuoles in their vicinity. Moreover, the presence of F-actin aggresome increases the levels of LC3 II, the lipidated form bound to the autophagosome membrane and MDC-containing vesicles, almost all of which are localized around F-actin aggresome. Finally, the autophagy induced by Rpc as well as chaperones stimulated by 17-DMAG decreased the life-span of F-actin aggresome. The use of pharmacological agents that impair the normal activity of proteasomes or lysosomes also increased the life-span of F-actin aggresome, suggesting their involvement in theist clearance. The disruption of MTs also caused the aggregate to remain longer in the

cytoplasm. This may be because (i) lysosomes and autophagic vacuoles depend on MTs for their redistribution to aggresomes (García-Mata et al., 2002; Murray and Wolkoff, 2003; Iwata et al., 2005) and (ii) autophagosome-lysosome fusion also depends on MTs and dynein motor activity (Rubinsztein et al., 2005; Webb et al., 2004)). On the other hand, proteasomal activity may also depend on the integrity of cytoskeleton networks, since ubiquitination enzymes and/or proteasomes could be transported along cytoskeleton towards aggresomes (Wojcik and De Martino, 2003). Therefore, results taken together indicate that the lysosomal/autophagic system is strongly activated for the dissolution of the F-actin aggresome.

Finally, the F-actin aggresome model reported here offers numerous advantages: (i) it works in neuronal and non-neuronal mammalian cell lines, (ii) it is simple, highly reproducible and reversible, and (iii) it provides an opportunity to test pharmacological agents that could interfere with the formation, maintenance, and/or disappearance of pathological F-actin enriched IBs.

MATERIAL AND METHODS

Antibodies, plasmids, and reagents

Monoclonal antibodies to β- and γ-tubulin, cofilin, myosin IIA, and vimentin were purchased from Sigma (St. Louis, MO, USA). Monoclonal antibodies to cortactin, p21-Arc, RhoA, Rac, and Cdc42 were obtained from BD Biosciences (Erembodegem, Belgium). Monoclonal antibody to LC3 (clone 5F10) was from Nanotools (Teningen, Germany). Monospecific rabbit polyclonal antibodies to β and γ-actin, and KDELr were kindly provided by C. Chaponnier (University of Geneva) and H-D Söling (University of Göttingen). Monoclonal antibodies to giantin and MAP4 were supplied by H.P. Hauri (Biozentrum, Basel University) and J. Avila (CSIC-UAM, Madrid), respectively. Polyclonal antibodies to N-WASP, spectrin, and lamp-2 were a gift from M. Way (MRC, London), J.S. Morrow (Yale University), and Minoru Fukuda (La Jolla, CA, USA), respectively. Mouse monoclonal antibodies which recognize ubiquitinated proteins (clone FK2) were purchased from Affiniti (Exeter, Devon, UK), while those which recognize the α-subunit C9 of the 20S proteasome have been described previously (Fuertes et al., 2003). Secondary Alexa Fluor 546 $F(ab')_2$ fragments of goat anti-rabbit IgG, MitoTracker CM-H2XRos, DAPI, and Jasplakinolide were obtained from Invitrogen, (Carlsbad, CA). Goat anti-mouse-Cy2 IgG, $F(ab')_2$ fragments were purchased from Jackson ImmunoResearch (West Baltimore, PA, USA). pEGFP-LC3 encoding plasmid was a gift from T. Yoshimori and N. Mizushima (National Institute of Genetics, Japan). GFP-htt^m encoding plasmid was used as previously reported (Canals et al., 2004). TRITC- and FITC-phalloidin, monodansilcadaverine, cytochalasin D, taxol, brefeldin A, and N-Succinyl-Leu-Leu-Val-Tyr-α-4-Methyl-Coumaryl-7-Amide (N-Suc-LLVY-MCA), phorbol myristate acetate, and lysophosphatidic acid were acquired from Sigma. Latrunculin B, mycalolide B, nocodazole, lactacystin, bafilomycin A1, pepstatin A, leupeptin, E-64-d, rapamycin, and 17-DMAG were from Calbiochem (EMD Biosciences, Inc., Darmstadt, Germany). The EMbed-812 embedding media kit and the reagents used in the electron microscopy experiments were provided by Electron Microscopy Sciences (Hatfield, PA, USA).

Cell culture and actin toxins treatments

NRK, HeLa, Vero, and M213 cells were grown in Dulbecco's modified Eagle's medium (DMEM) supplemented with 10% fetal bovine serum (FBS), penicillin (100 U/ml), streptomycin (100 µg/ml), L-glutamine (2 mM), and MEM sodium pyruvate (1 mM). Cell cultures were maintained at 37°C in a humidified CO_2 (5%) atmosphere.

Primary cultures of astrocytes from cortical hemispheres of rat fetuses were prepared as described (Renau-Piqueras et al., 1989). Mouse neural stem c17.2 cells were grown in DMEM supplemented with 10% FBS, 5% horse serum, 2 mM glutamine, and 20 µg/ml gentamicin as described previously (Snyder, 1992). Primary cultures of mouse hippocampal neurons (E16 brains) were obtained and cultured as previously reported (Urena et al., 2005)

Fluorescence microcopy and indirect immunofluorescence

Indirect immunofluorescence was performed as previously described (Valderrama et al., 2001) with the following antibody dilutions: anti-giantin, 1:500; cofilin 1:1000; anti-vimentin, 1:100; anti-β-tubulin, 1:50; anti-γ-tubulin, 1:5000; anti-RhoA, Rac, and Cdc42, 1:100; anti-p21Arc (Arp2/3), 1:50; anti-cortactin: 1:500; anti-MAP4, 1:20; anti- β- and anti-γ-actin, 1:100; anti-myosin IIA and B, 1:100. Secondary antibodies were used at the following concentrations: Alexa Fluor 546-conjugated goat anti-rabbit, 1:500 and goat anti-mouse-Cy2, 1:50. TRITC- and FITC-phalloidin were used at 1:500 and DAPI at 1:100. For MDC-containing vesicles or mitochondria staining, cells were respectively incubated with MDC 200 nM or MitoTracker 100 nM for 30 minutes. Microscopy was performed with a BX60 epifluorescence microscope (Olympus, Tokyo, Japan) equipped with an Orca-ER cooled CCD camera (Hamamatsu Photonics, Japan) or with a TCS SL confocal microscope with argon and helium-neon lasers attached to a Leica DMIRE2 inverted microscope (Leica Microsystems, Heerbrugg, Switzerland). For 3D reconstruction of FAG and the Golgi apparatus, the entire three-dimensional stack of images was obtained using the Z drive present in the Leica TCS-SL microscope and the size of the confocal image between sections was 0.1 µm. The images were processed using Adobe Photoshop CS (Adobe

Systems, San Jose, CA), ImageJ 1.33 (National Institutes of Health, Bethesda, MD), and IMOD 3.5.5 (Colorado, USA) 3D modeling software.

Transmission electron microscopy

Control and treated Vero cells were processed as previously described (Lazaro-Dieguez et al., 2006). Ultrathin sections were stained with 2% uranyl acetate for 30 minutes, then with lead citrate for 10 minutes and observed with a JEOL 1010 transmission electron microscope operating at 80 kV and provided with a Gatan BioScan model 792 module for acquisition of digital images with Digital. Micrograph 3.4.3 acquisition software (Gatan, Inc., Pleasanton,. CA, USA).

Cell viability assay

Cell viability was measured either using the methylthiazol tetrazolium MTT reduction assay (which is indicative of mitochondrial function) or the trypan blue exclusion method. The reduction assay was performed using the Cell Proliferation Kit (Boehringer Mannheim, Germany) and MTT protein levels were measured spectrophotometrically at 550 nm. In the second method, cells were removed from Petri dishes and aliquots (50 µL) of the cells were mixed with PBS (40 µL) and 0.04% trypan blue (10 µL). Live (trypan blue-excluding) cells were counted. Results are expressed as the percentage of surviving cells respect to controls (100%). Statistical significance was evaluated by the Student's *t*-test.

Subcellular fractionation and immunoblotting

Vero cells containing FAG were washed in PBS, scraped and centrifuged at 300 *g* at 4 ºC for 5 minutes. Cells were washed twice in PBS and cell pellets were homogenized with a potter (10 strokes) in cold buffer A (50 mM Tris-HCl, pH 7.5 containing 150 mM NaCl, 100 mM, sodium orthovanadate, 10 mM, sodium fluoride and 10 µM leupeptin, 1 µg/mL pepstatin, and 2 mM phenylmethylsulfonyl fluoride). After further centrifugation of the suspension, the supernatant was removed. The pellet was resuspended in buffer A containing 2.5 M sucrose, which was overlaid with 630 µL of buffer A containing different sucrose concentrations (35, 30, 25, 20, 15, 10 and 5%). The discontinuous gradient was centrifuged at 130,000 *g* for 16 h at 4 ºC in the SW55-Ti rotor. Subsequently, 10 fractions were collected from the top (#1) to the bottom (#10). The capture of FAGs in the different fractions was checked by fluorescent microscopy using TRITC-phalloidin. The cytoskeleton components present in each fraction were analyzed by SDS-PAGE and immunoblotting.

Sucrose fractions (#1 to #10) were prepared for SDS-PAGE by boiling in sample buffer. Proteins were electrophoretically transferred onto nitrocellulose membranes. Blots were blocked in 5% non-fatty dry milk in Tris-buffered saline (TBS) with Tween-20 (v/v) (TBST) for 2 h at room temperature. Primary antibody incubations were performed in TBS containing 1.5% BSA for 2 h at room temperature and used at 1:10,000 for anti-cofilin, 1:500 for anti-Arp3, 1:1000 for anti-myosin II and anti-actin. Secondary antibody incubations were performed in TBST containing 5% non-fat dry milk at 1:10,000 for 1 h at room temperature. Protein bands were visualized using a Supersignal West Pico Chemiluminescence Substrate Kit from Pierce (Rockford, IL). Immunoblotting procedure for endogenous LC3 forms was carried out as previously described (Esteban et al., 2007) using the following antibody dilutions: anti-LC3, 1:500 and secondary antibody anti-mouse IgG-HRP, 1:10,000. To calculate the LC3-II fold increase, densitometry measurements of the LC3-II bands were divided by the LC3-II/tubulin ratio obtained in control cells (Jpk-, FBS+).

Gene transfections

Cells grown on 10 mm glass coverslips at 2 x 10^6 cell/mL were transfected with, GFP-LC3, GFP-htt^m or YFP-actin using the FuGene6 (Roche) and expressed for 4-48 hours.

Fluorescence recovery after photobleaching

For FRAP experiments, Vero cells transfected with YFP-actin were viewed using the Leica confocal microscope described above and equipped with an incubation system with temperature and CO_2 control. Cells (4 x 10^5) were seeded on 22 mm glass coverslip (Micro cover glass; Electron Microscopy Sciences, Fort Washington, PA). After 24 hours cells were transfected with 1 µg of YFP-actin construct. Twenty-four hours after transfection the glass coverslip was mounted in the video confocal chamber, keeping the cells at 37 °C in a 5% CO_2 atmosphere. For visualization of YFP, images were acquired using a 63x oil immersion objective lens (numerical aperture, 1.32), 488 nm laser line, excitation beam splitter RSP 500, 500-600 nm emission range detection and the confocal pinhole set at 2-3 Airy units to minimize changes in fluorescence efficiency due to the movement of YFP proteins away from the plane of focus. The same FAG or cytoplasmic area was photobleached using 40 scans with the 488 nm laser line at full power. To detect the fast component of the recovery, the first 30 images were taken every 0.5 seconds and the rest every 5 seconds for 5 minutes.

Proteasomal activity

We determined the chymotrypsin-like activity of proteasomes in the supernatants from crude cell extracts centrifuged at 10,000 *g* for 15 minutes at 4 ºC using N-Suc-LLVY-MCA (Stratford et al., 2006). The reaction mixture contained (in a final volume of 200 µL) 20 mM Tris-HCl, pH 7.8, 50 µM of N-Suc-LLVY-MCA and different amounts of the cell extract (5-20 µg) with or without 10 µM lactacystin. Activity against the fluorogenic peptide substrate was determined by continuously monitoring the

fluorescence (excitation, 355 nm; emission, 460 nm) of the released α-4-methyl-coumaryl-7-amide using a VICTOR plate reader (WALLAC VICTOR^2 V1420 Multilabel HTS Counter, Perkin Elmer, Life Sciences). Assays carried out in COSTAR 96-well plates were kinetically controlled several times at 5 minutes intervals at 37 ºC, under conditions in which a linear relation of the time-dependent product generation was obtained. Values were expressed as relative arbitrary fluorescence units (RFU) per minutes and per mg of protein.

Acknowledgements

We thank Bernat Crosas and David Andreu for helpful discussions, Eduardo Soriano and Ana La Torre for primary cultures of mouse hippocampal neurons, Evan Y. Snyder for mouse multipotent c17.2 neural stem cells, Maria Calvo (SCT-UB) for help with FRAP experiments and Robin Rycroft for editorial assistance. This study was funded by grants BFU2006-00867/BMC and Consolider CSD2006-00012 to G.E, SAF2005-1335 to J.A., and BFU2005-00087 to E.K.

REFERENCES

Allingham, J. S., Klenchin, V. A. and Rayment, I. (2006). Actin-targeting natural products: structures, properties and mechanisms of action. Cell Mol. Life Sci. 63, 2119-2134.

Bauer, N.G. and Richter-Landsberg, C. (2006). The dynamic instability of microtubules is required for aggresome formation in oligodendroglial cells after proteolytic stress. J. Mol. Neurosci. 29, 153-168.

Bennett, E. J., Bence, N. F., Jayakumar, R. and Kopito, R. R. (2005). Global impairment of the ubiquitin-proteasome system by nuclear or cytoplasmic protein aggregates precedes inclusion body formation. Mol. Cell 17, 351-365

Betarbet, R., Sherer, T. B. and Greenamyre, J. T. (2005). Ubiquitin-proteasome system and Parkinson's diseases. Exp. Neurol. 191, Suppl 1, S17-S27.

Bernstein, B.W., Chen, H., Boyle, J.A., and Bamburg, J.R. (2006). Formation of actin-ADF/cofilin rods transiently retards decline of mitochondrial potential and ATP in stressed neurons. Am. J. Physiol Cell Physiol 291, C828-C839.

Bubb, M. R., Senderowicz, A. M., Sausville, E. A., Duncan, K. L. and Korn, E. D. (1994). Jasplakinolide, a cytotoxic natural product, induces actin polymerization and competitively inhibits the binding of phalloidin to F-actin. J. Biol. Chem. 269,14869-14871.

Bubb, M. R., Spector, I., Beyer, B. B. and Fosen, K. M. (2000). Effects of jasplakinolide on the kinetics of actin polymerization. An explanation for certain in vivo observations. J. Biol. Chem. 275(7), 5163-70.

Canals, J. M., Pineda, J. R., Torres-Peraza, J. F., Bosch, M., Martin-Ibanez, R., Munoz, M. T., Mengod, G., Ernfors, P. and Alberch, J. (2004). Brain-derived neurotrophic factor regulates the onset and severity of motor dysfunction associated with enkephalinergic neuronal degeneration in Huntington's disease. J. Neurosci. 24, 7727-7739.

Cartier, L., Galvez, S. and Gajdusek, D. C. (1985). Familial clustering of the ataxic form of Creutzfeldt-Jakob disease with Hirano bodies. J. Neurol. Neurosurg. Psychiatry 48, 234-238.

Chiosis, G., Caldas, L.E., and Solit, D. (2006). Heat shock protein-90 inhibitors: a chronicle from geldanamycin to today's agents. Curr. Opin. Investig. Drugs 7, 534-541.

Ciechanover, A. and Brundin, P. (2003). The ubiquitin proteasome system in neurodegenerative diseases: sometimes the chicken, sometimes the egg. Neuron 40, 427-446.

Davis, R.C., Furukawa, R., and Fechheimer, M. (2008). A cell culture model for investigation of Hirano bodies. Acta Neuropathol. 115, 205-217.

Dean, R. T. (1977). Lysosomes and protein degradation. Acta Biol. Med. Ger. 36, 1815-1820.

Drose, S. and Altendorf, K. (1997). Bafilomycins and concanamycins as inhibitors of V-ATPases and P-ATPases. J. Exp. Biol. 200, 1-8.

Esteban, I., Aguado, C., Sanchez, M. and Knecht, E. (2007). Regulation of various proteolytic pathways by insulin and amino acids in human fibroblasts. FEBS Lett. 581, 3415-3421.

Fechheimer, M., Furukawa, R., Maselli, A. and Davis, R. C. (2002). Hirano bodies in health and disease. Trends Mol. Med. 8, 590-591.

Fenteany, G. and Zhu, S. (2003). Small-molecule inhibitors of actin dynamics and cell motility. Curr. Top. Med. Chem. 3, 593-616.

Fortun, J., Verrier, J. D., Go, J. C., Madorsky, I., Dunn, W. A. and Notterpek, L. (2007). The formation of peripheral myelin protein 22 aggregates is hindered by the enhancement of autophagy and expression of cytoplasmic chaperones. Neurobiol. Dis. 25, 252-265.

Fuertes, G., Martin De Llano, J. J., Villarroya, A., Rivett, A. J. and Knecht, E. (2003). Changes in the proteolytic activities of proteasomes and lysosomes in human fibroblasts produced by serum withdrawal, amino-acid deprivation and confluent conditions. Biochem. J. 375, 75-86.

Gagliardi, S., Rees, M. and Farina, C. (1999). Chemistry and structure activity relationships of bafilomycin A1, a potent and selective inhibitor of the vacuolar H+-ATPase. Curr. Med. Chem. 6, 1197-1212.

Galloway, P. G., Perry, G. and Gambetti, P. (1987a). Hirano body filaments contain actin and actin-associated proteins. J. Neuropathol. Exp. Neurol. 46, 185-199.

Galloway, P. G., Perry, G., Kosik, K. S. and Gambetti, P. (1987b). Hirano bodies contain tau protein. Brain Res. 403, 337-340.

Garcia-Mata, R., Bebok, Z., Sorscher, E. J. and Sztul, E. S. (1999). Characterization and dynamics of aggresome formation by a cytosolic GFP-chimera. J. Cell Biol. 146, 1239-1254.

Garcia-Mata, R., Gao, Y. S. and Sztul, E. (2002). Hassles with taking out the garbage: aggravating aggresomes. Traffic 3, 388-396.

Glotzer, M. (2005). The molecular requirements for cytokinesis. Science 307, 1735-1739.

Goldman, J. E. (1983). The association of actin with Hirano bodies. J. Neuropathol. Exp. Neurol. 42, 146-152.

Grenier, C., Bissonnette, C., Volkov, L., and Roucou, X. (2006). Molecular morphology and toxicity of cytoplasmic prion protein aggregates in neuronal and non-neuronal cells. J. Neurochem. 97, 1456-1466.

Herbst, M. and Wanker, E.E. (2007). Small molecule inducers of heat-shock response reduce polyQ-mediated huntingtin aggregation. A possible therapeutic strategy. Neurodegener. Dis. 4, 254-260.

Hirano, A. (1994). Hirano bodies and related neuronal inclusions. Neuropathol. Appl. Neurobiol. 20, 3-11.

Hirano, A., Dembitzer, H. M., Kurland, L. T. and Zimmerman, H. M. (1968). The fine structure of some intraganglionic alterations. Neurofibrillary tangles, granulovacuolar bodies and "rod-like" structures as seen in Guam amyotrophic lateral sclerosis and parkinsonism-dementia complex. J. Neuropathol. Exp. Neurol. 27, 167-182.

Hol, E. M., Fischer, D. F., Ovaa H. and Scheper, W. (2006). Ubiquitin proteasome system as a pharmacological target in neurodegeneration. Expert. Rev. Neurother. 6, 1337-1347.

Holzinger, A. (2001). Jasplakinolide. An actin-specific reagent that promotes actin polymerization. Methods Mol. Biol. 161, 109-120.

Iwata, A., Riley, B. E., Johnston, J. A. and Kopito, R. R. (2005). HDAC6 and microtubules are required for autophagic degradation of aggregated huntingtin. J. Biol. Chem. 280, 40282-40292.

Izumiyama, N., Ohtsubo, K., Tachikawa T. and Nakamura, H. (1991) Elucidation of three-dimensional ultrastructure of Hirano bodies by the quick-freeze, deep-etch and replica method. Acta Neuropathol. (Berl) 81, 248-254.

Jang, D.H., Han, J.H., Lee, S.H., Lee, Y.S., Park, H., Lee, S.H., Kim, H., and Kaang, B.K. (2005). Cofilin expression induces cofilin-actin rod formation and disrupts synaptic structure and function in Aplysia synapses. Proc. Natl. Acad. Sci. U. S. A 102, 16072-16077.

Johnston, J. A., Ward, C. L. and Kopito, R. R. (1998). Aggresomes: a cellular response to misfolded proteins. J. Cell Bio. 143, 1883-1898.

Johnston, J. A., Illing, M. E. and Kopito, R. R. (2002). Cytoplasmic dynein/dynactin mediates the assembly of aggresomes. Cell Motil. Cytoskeleton 53, 26-38.

Kabeya, Y., Mizushima, N., Ueno T., Yamamoto A., Kirisako T., Noda, T., Kominami, E., Ohsumi Y. and Yoshimori, T. (2000). LC3, a mammalian homologue of yeast Apg8p, is localized in autophagosome membranes after processing. EMBO J. 19, 5720-5728.

Kabeya, Y., Mizushima, N., Yamamoto, A., Oshitani-Okamoto, S., Ohsumi, Y. and Yoshimori, T. (2004). LC3, GABARAP and GATE16 localize to autophagosomal membrane depending on form-II formation. J. Cell Sci. 117, 2805-2812.

Kopito, R. R. (2000). Aggresomes, inclusion bodies and protein aggregation. Trends Cell Biol. 10, 524-530.

Kuma, A., Matsui M. and Mizushima, N. (2007). LC3, an Autophagosome Marker, Can be Incorporated into Protein Aggregates Independent of Autophagy: Caution in the Interpretation of LC3 Localization. Autophagy 3, 323-328.

Laas, R. and Hagel, C. (1994). Hirano bodies and chronic alcoholism. Neuropathol. Appl. Neurobiol. 20, 12-21.

Lazaro-Dieguez, F., Jimenez, N., Barth, H., Koster, A. J., Renau-Piqueras, J., Llopis, J. L., Burger, K. N. and Egea, G. (2006). Actin filaments are involved in the maintenance of Golgi cisternae morphology and intra-Golgi pH. Cell Motil. Cytoskeleton 63, 778-791.

Lee, E., Shelden, E. A. and Knecht, D. A. (1998). Formation of F-actin aggregates in cells treated with actin stabilizing drugs. Cell Motil Cytoskeleton 39, 122-133.

Maciver, S. K. and Harrington, C. R. (1995). Two actin binding proteins, actin depolymerizing factor and cofilin, are associated with Hirano bodies. Neuroreport. 6, 1985-1988.

Maloney, M.T., Minamide, L.S., Kinley, A.W., Boyle, J.A. and Bamburg, J.R. (2005). Beta-secretase-cleaved amyloid precursor protein accumulates at actin inclusions induced in neurons by stress or amyloid beta: a feedforward mechanism for Alzheimer's disease. J. Neurosci. 25, 11313-11321.

Maselli, A. G., Davis, R., Furukawa, R. and Fechheimer, M. (2002). Formation of Hirano bodies in Dictyostelium and mammalian cells induced by expression of a modified form of an actin-crosslinking protein. J. Cell Sci. 115, 1939-1949.

Maselli, A., Furukawa, R., Thomson, S. A., Davis, R. C. and Fechheimer, M. (2003). Formation of Hirano bodies induced by expression of an actin cross-linking protein with a gain-of-function mutation. Eukaryot. Cell 2, 778-787.

Meijer, A. J. and Codogno, P. (2007). AMP-activated protein kinase and autophagy. Autophagy 3, 238-240.

Minamide, L. S., Striegl, A. M., Boyle, J. A., Meberg, P. J. and Bamburg, J. R. (2000). Neurodegenerative stimuli induce persistent ADF/cofilin-actin rods that disrupt distal neurite function. Nat. Cell Biol. 2, 628-636.

Mizushima, N. (2004). Methods for monitoring autophagy. Int. J. Biochem. Cell Biol. 36, 2491-2502.

Mizushima, N. and Yoshimori, T. (2007). How to Interpret LC3 Immunoblotting. Autophagy 3, 542-545.

Muchowski, P. J. and Wacker, J. L. (2005). Modulation of neurodegeneration by molecular chaperones. Nat. Rev. Neurosci. 6, 11-22.

Muqit, M.M., Abou-Sleiman, P.M., Saurin, A.T., Harvey, K., Gandhi, S., Deas, E., Eaton, S., Payne,S., Venner,K., Matilla,A., et al. (2006). Altered cleavage and localization of PINK1 to aggresomes in the presence of proteasomal stress. J. Neurochem. 98, 156-169.

Murray, J. W. and Wolkoff, A. W. (2003). Roles of the cytoskeleton and motor proteins in endocytic sorting. Adv. Drug. Deliv. Rev. 55, 1385-1403.

Nishida, E., Iida, K., Yonezawa, N., Koyasu, S., Yahara, I. and Sakai, H. (1987). Cofilin is a component of intranuclear and cytoplasmic actin rods induced in cultured cells. Proc. Natl. Acad. Sci. U. S. A. 84, 5262-5266.

Podlubnaia, Z. A. and Nowak, E. (2006). The C-terminal fragment of thymopoietin forms F-actin bundles: electron microscopic data. Biofizika 51, 804-809.

Reggiori, F. and Klionsky, D. J. (2005). Autophagosomes: biogenesis from scratch?. Curr. Opin. Cell Biol. 17, 415-422.

Renau-Piqueras, J., Zaragoza, R., De Paz, P., Baguena-Cervellera, R., Megias, L. and Guerri, C. (1989). Effects of prolonged ethanol exposure on the glial fibrillary acidic protein-containing intermediate filaments of astrocytes in primary culture: a quantitative immunofluorescence and immunogold electron microscopic study. J. Histochem. Cytochem. 37, 229-240.

Ridley, A. J. and Hall. A. (1992). The small GTP-binding protein rho regulates the assembly of focal adhesions and actin stress fibers in response to growth factors. Cell 70, 389-399.

Ridley, A. J., Paterson, H. F., Johnston, C. L., Diekmann, D. and Hall. A. (1992). The small GTP-binding protein rac regulates growth factor-induced membrane ruffling. Cell 70, 401-410.

Ross, C. A. and Pickart, C. M. (2004). The ubiquitin-proteasome pathway in Parkinson's disease and other neurodegenerative diseases. Trends Cell Biol. 14, 703-711.

Ross, C. A. and Poirier, M. A. (2004). Protein aggregation and neurodegenerative disease. Nat. Med. 10, Suppl, S10-S17.

Rubinsztein, D. C. (2006). The roles of intracellular protein-degradation pathways in neurodegeneration. Nature 443, 780-786.

Rubinsztein, D.C., Ravikumar, B., Acevedo-Arozena, A., Imarisio, S., O'Kane, C.J., and Brown, S.D. (2005). Dyneins, autophagy, aggregation and neurodegeneration. Autophagy. 1, 177-178.

Santa-Maria, I., Hernandez, F., Del Rio, J., Moreno, F.J., and Avila, J. (2007). Tramiprosate, a drug of potential interest for the treatment of Alzheimer's disease, promotes an abnormal aggregation of tau. Mol. Neurodegener. 2, 17.

Schmidt, M. L., Lee, V. M. and Trojanowski, J. Q. (1989). Analysis of epitopes shared by Hirano bodies and neurofilament proteins in normal and Alzheimer's disease hippocampus. Lab. Invest. 60, 513-522.

Schroder, J. M., Sommer, C. and Schmidt, B. (1990). Desmin and actin associated with cytoplasmic bodies in skeletal muscle fibers: immunocytochemical and fine structural studies, with a note on unusual 18- to 20-nm filaments. Acta Neuropathol. (Berl) 80, 406-414.

Shintani, T. and Klionsky, D. J. (2004). Autophagy in health and disease: a double-edged sword. Science 306, 990-995.

Snyder, E. Y. (1992). Neural transplantation: an approach to cellular plasticity in the developing central nervous system. Semin. Perinatol. 16, 106-121.

Spector, I., Braet, F., Shochet, R. and Bubb, M. R. (1999). New anti-actin drugs in the study of the organization and function of the actin cytoskeleton. Microsc. Res. Tech. 47, 18-37.

Stratford, F. L., Chondrogianni, N., Trougakos, I. P., Gonos, E. S. and Rivett, A. J. (2006). Proteasome response to interferon-gamma is altered in senescent human fibroblasts. FEBS Lett. 580, 3989-3994.

Suresh, S. (2007). Biomechanics and biophysics of cancer cells. Acta Biomater. 3, 413 438.

Tanida, I., Ueno, T. and Kominami, E. (2004). LC3 conjugation system in mammalian autophagy. Int. J. Biochem. Cell Biol. 36, 2503-2518.

Tanida, I., Minematsu-Ikeguchi, N. Ueno, T. and Kominami, E. (2005). Lysosomal turnover, but not a cellular level, of endogenous LC3 is a marker for autophagy. Autophagy 1, 84-91.

Taylor, J. P., Tanaka, F., Robitschek, J., Sandoval, C. M., Taye, A., Markovic-Plese, S. and Fischbeck, K. H. (2003). Aggresomes protect cells by enhancing the degradation of toxic polyglutamine-containing protein. Hum. Mol. Genet. 12, 749-757.

Urena, J. M., La Torre, A., Martinez, A., Lowenstein, E., Franco, N., Winsky-Sommerer, R., Fontana, X., Casaroli-Marano, R., Ibanez-Sabio, M. A., Pascual, M., et al. (2005). Expression, synaptic localization, and developmental regulation of Ack1/Pyk1, a cytoplasmic tyrosine kinase highly expressed in the developing and adult brain. J. Comp. Neurol. 490, 119-132.

Valderrama, F., Duran, J. M., Babia, T., Barth, H., Renau-Piqueras, J. and Egea, G. (2001). Actin microfilaments facilitate the retrograde transport from the Golgi complex to the endoplasmic reticulum in mammalian cells. Traffic 2, 717-726.

Weaver, A. M, Young, M. E, Lee, W. L and Cooper, J. A. (2003). Integration of signals to the Arp2/3 complex. Curr. Opin. Cell. Biol. 15, 23-30.

Webb, J.L., Ravikumar, B., and Rubinsztein, D.C. (2004). Microtubule disruption inhibits autophagosome-lysosome fusion: implications for studying the roles of aggresomes in polyglutamine diseases. Int. J. Biochem. Cell Biol. 36, 2541-2550.

Weissmann, C. and Brandt, R. (2007). Mechanisms of neurodegenerative diseases: Insights from live cell imaging. J. Neurosci. Res. 86, 504-511.

Wojcik, C. and DeMartino, G. N. (2003). Intracellular localization of proteasomes. Int. J. Biochem. Cell Biol. 35, 579-589.

Date sent: Thu, 31 Jan 2008 02:09:11 -0800 (PST)
From: jcs@biologists.com
Subject: JOCES/2007/017665 - Manuscript Decision
To: Gustavo Egea <gegea@ub.edu>

MS ID#: JOCES/2007/017665

MS TITLE: DYNAMICS OF A FILAMENTOUS ACTIN AGGRESOME GENERATED BY THE ACTIN STABILINZING TOXIN JASPLAKINOLIDE
AUTHORS: Francisco Lázaro-Diéguez, Carmen Aguado, Eugenia Mato, Yován Sánchez-Ruíz, Inmaculada Esteban, Jordi Alberch, Erwin Knecht, and Gustavo Egea
ARTICLE TYPE: Research Article

Dear Gustavo,

I am happy to tell you that your manuscript has been accepted for publication in Journal of Cell Science. If we require anything further from you in terms of source files, we will be in touch shortly. Otherwise, you will receive proofs in due course. If you wish to see the details we hold about your manuscript or would like to view any of the files that you have submitted, decision letters or reviewer's reports on the manuscript, please click on the 'Author history' link in our Manuscript Tracking System (http://submit-jcs.biologists.org/).

Best wishes

Michael Way
Monitoring Editor
Journal of Cell Science

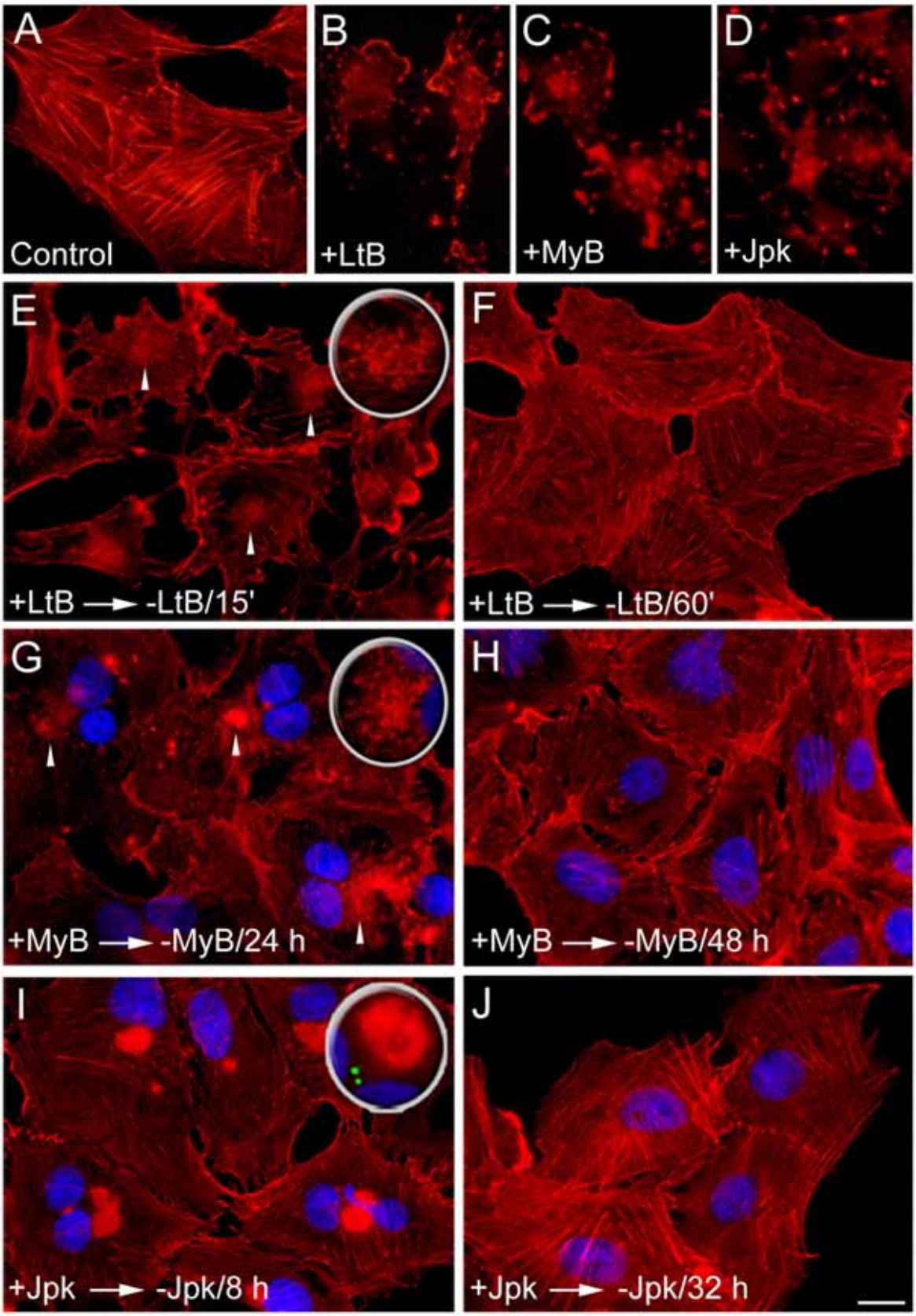

Fig. 1. Actin cytoskeleton disruption by actin toxins is reversible: formation of different F-actin aggregates/inclusion bodies. Vero cells were incubated with LtB (500 nM/45 minutes; B), MyB (100 nM/60 minutes; C), or Jpk (500 nM/45 minutes; D). To examine the reversibility, actin toxins were washed out from the culture medium and cells were left to recover for different times (-LtB, E, F; -MyB, G, H; -Jpk, I, J). Cells were stained with TRITC-phalloidin for F-actin (A-J, red) and DAPI for nuclei (G-J, blue) or the centrosome with anti-γ-tubulin antibodies (inset in I, green). Bar, 10 μm.

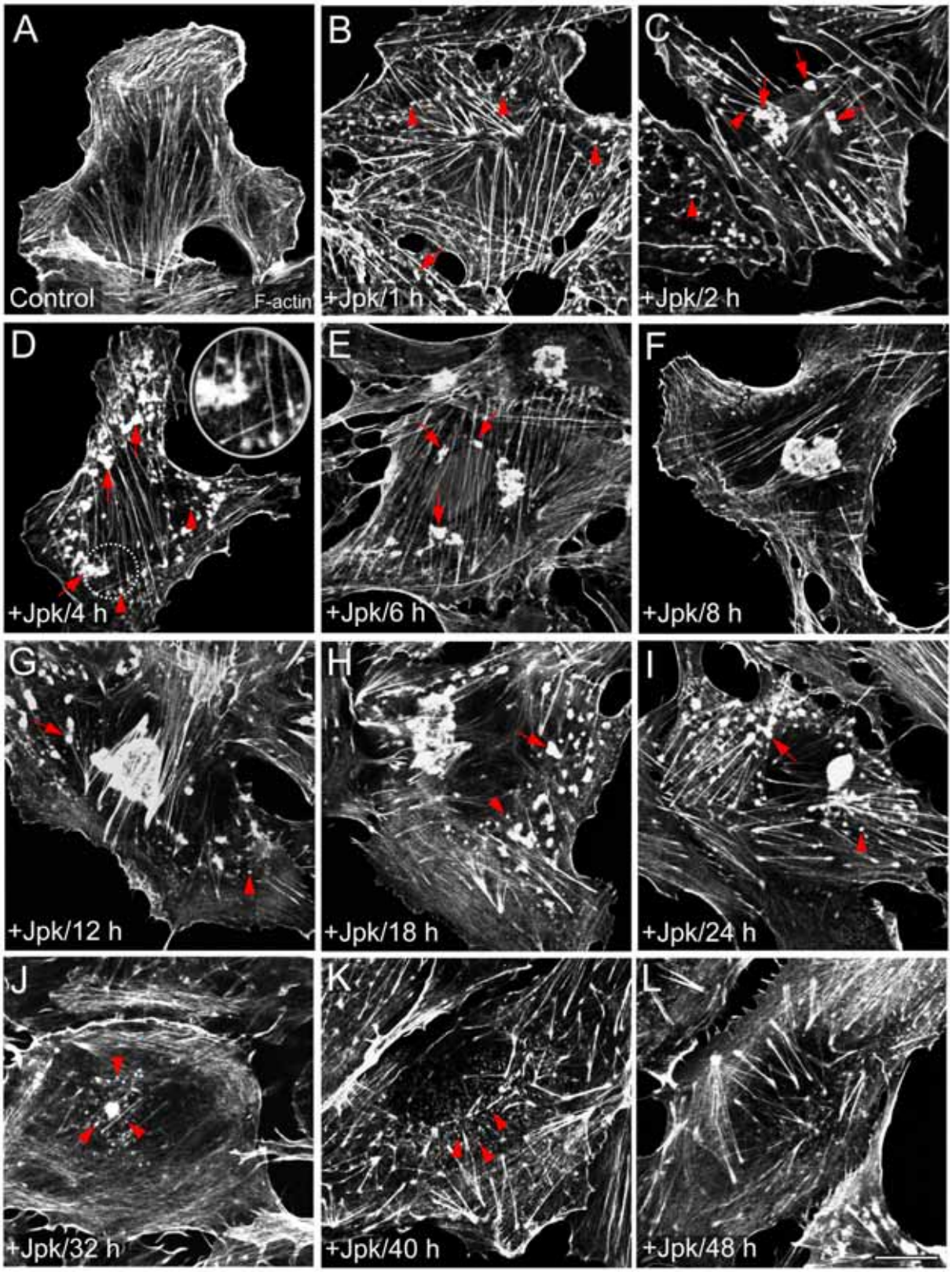

Fig. 2. Formation and clearance of the single, large F-actin aggregate produced by the continuous presence of Jpk in the culture medium. Vero cells were treated with low concentrations of Jpk (50 nM), and at different times fixed and stained with TRITC-phalloidin. Examples of F-actin puntae (B-D,G-K, arrowheads), F-actin amorphous aggregates (B-E,G-I, arrows) and FAG (F). Inset in D is an enlargement of the circle area to visualize better F-actin puntae and F-actin amorphous aggregates structures. Bar, 10 μm.

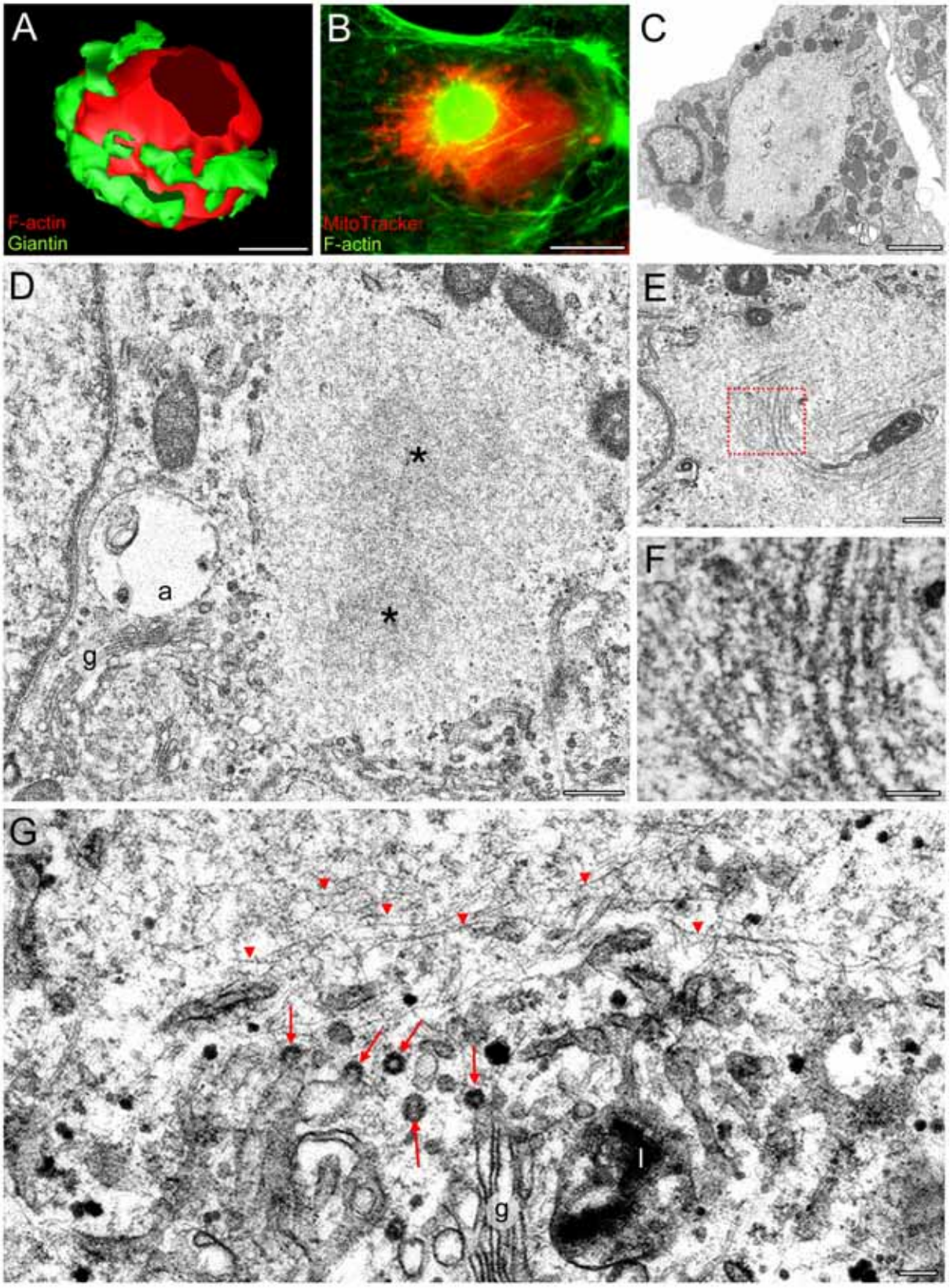

Fig. 3. Organelle association and ultrastructure of the F-actin aggregate. (A) 3D model of FAG and the Golgi apparatus in Vero cells co-stained with TRITC-phalloidin (red) and anti-giantin antibodies (green). (B) Co-staining with FITC-phalloidin (green) and the mitochondrial marker MitoTracker (red). (C-G) Ultrastructure of FAG. FAG is invariably surrounded by mitochondria (C,D), autophagic vacuoles (D), lysosomes (G), the Golgi apparatus (D,G), and intermediate filaments (arrowheads in G). In some FAGs (E), there are regions containing highly ordered F-actin or actin bundles (F, enlargement of the squared area shown in E). Autophagic vacuoles (a), lysosome (l), Golgi cisternae (g), and peri-Golgi COPI-coated transport carriers (arrows in G). Bars, 10 µm (B), 3 µm (A,C), 300 nm (D,E), 100 nm (F,G).

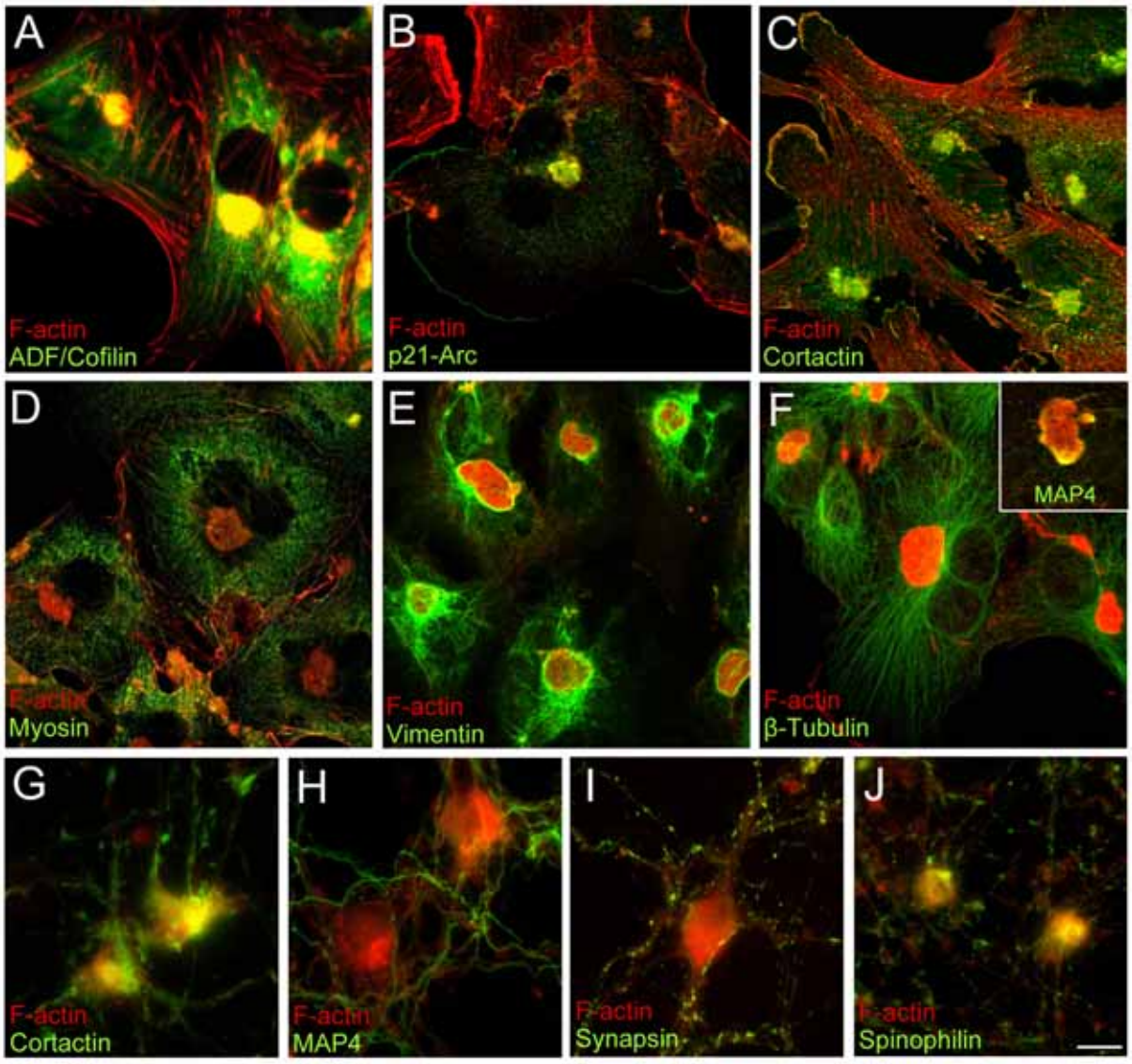

Fig. 4. Molecular composition of the F-actin aggregate in different cell types assessed by immunofluorescence. Vero cells (A-F) and mouse hippocampal neurons (G-J) were treated with Jpk (50 nM/6 hours and 500 nM/24 hours, respectively), fixed and double stained with TRITC-phalloidin (red) and with a variety of antibodies to different cytoskeleton/cytoskeleton-associated proteins and neuronal markers (indicated in each panel; green). Bar, 10 μm.

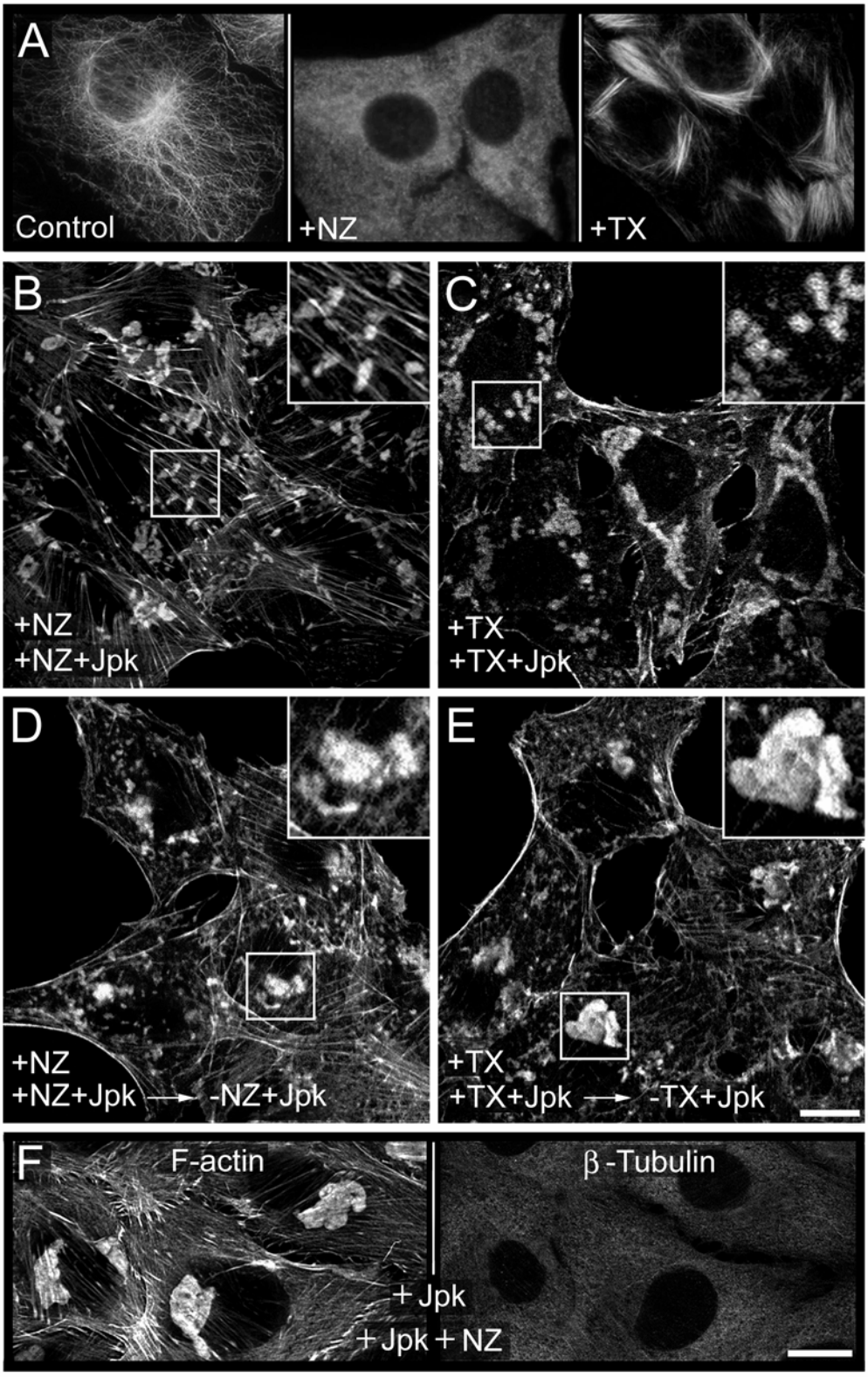

Fig. 5. Microtubules in the formation and location of the F-actin aggregate. Vero cells were treated with NZ (30 μM/6 hours) (A, +NZ) or TX (30 μM/6 hours) (A, +TX) alone or subsequently co-incubated with Jpk (50 nM/6 hours) (B,C). In NZ+Jpk-treated cells, no FAG was formed. Instead, numerous F-actin puntae and F-actin amorphous aggregates were dispersed throughout the cytoplasm (B and inset). Similar results were obtained in TX+Jpk-treated cells (C and inset). When NZ and TX were washed-out but Jpk remained (D and E, respectively), FAG was formed (D,E and insets). (F) When cells were incubated with Jpk (50 nM/6 hours) and then with NZ (30 μM/6 hours), the structural integrity of FAG (left panel) remained unaltered despite the disruption of microtubules (right panel). Cells were stained with anti-β-tubulin antibodies (A and F/right panel) or TRITC-phalloidin (B-E and F/left panel). Bars, 10 μm.

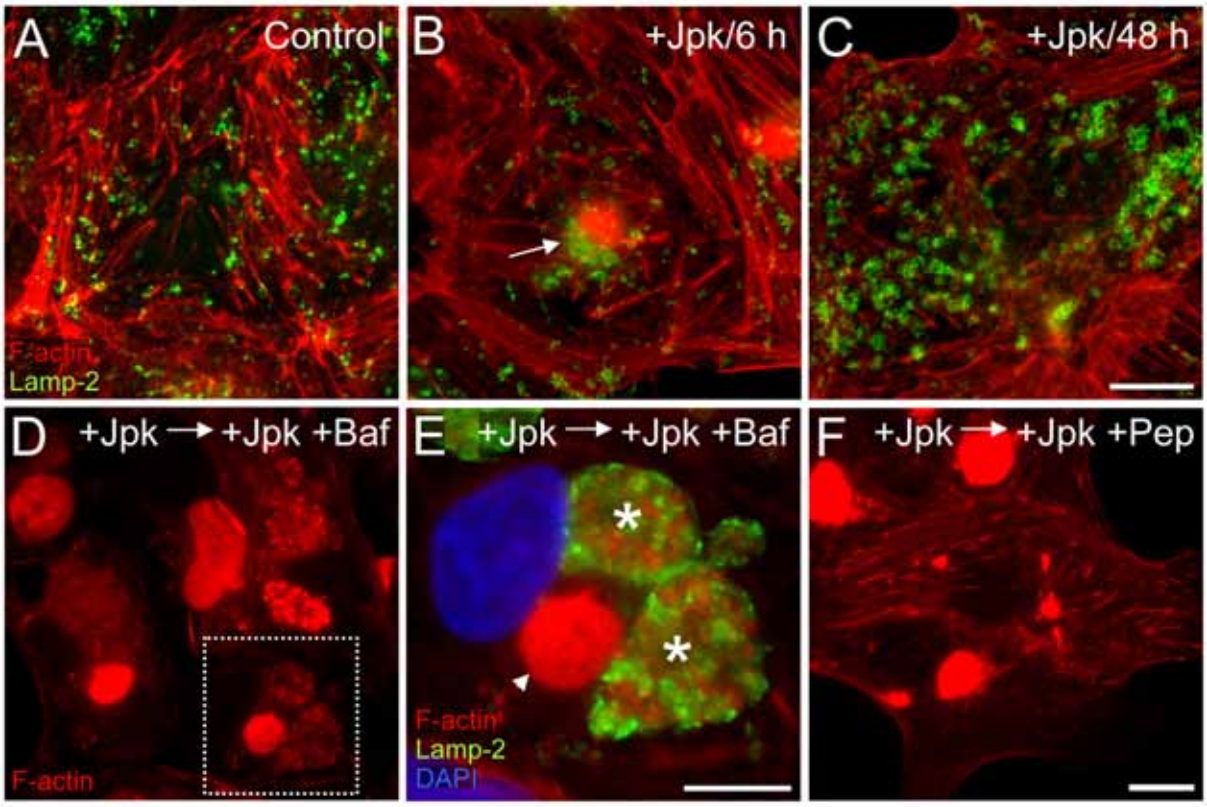

Fig. 6. Lysosomal distribution and function during the formation and/or clearance of the F-actin aggregate. (A-C) Vero cells were treated with Jpk (+Jpk, 50 nM) for different time periods, as indicated in the panels. Cells were double stained with TRITC-phalloidin (red) and anti-lamp-2 antibodies (green). Lysosomes in cells containing FAG show either a uniform distribution or accumulate around FAG (arrow in B). 48 h after Jpk treatment, an increase in lysosomal staining was observed despite the absence of FAG. (D-F) Vero cells were treated with Jpk (+Jpk, 50 nM/6 hours) and then co-incubated with bafilomycin A1 (Baf, 100 mM; +Jpk +Baf) (D,E) or pepstatin A (Pep, 10 μM; +Jpk +Pep) (F). Notice that the dysfunction of the lysosomal activity prolonged the life-span of FAG. (E) Enlargement of the squared area in D where the co-staining with TRITC-phalloidin and anti-lamp-2 antibodies revealed that Baf treatment traps lysosomes in an F-actin net (asterisks) that is structurally different from FAG (arrowhead). Bar, 10 μm

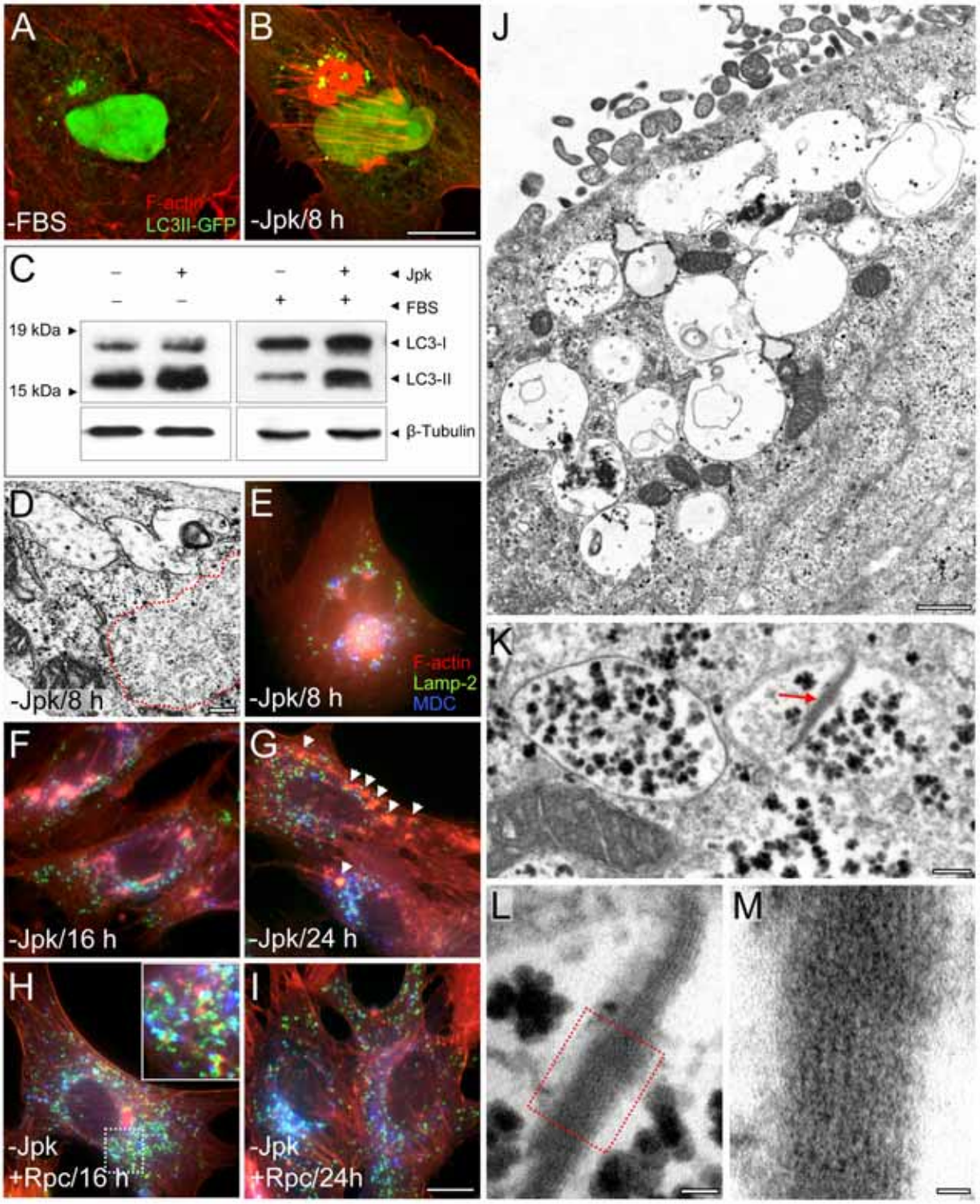

Fig. 7. Autophagy in cells containing the F-actin aggregate. (A) Vero cells were transfected with LC3-GFP plasmid and cultured in medium without FBS, but containing pepstatin A (Pep, 10 μM) plus E-64-d (10 μM). (B) LC3-GFP accumulated around FAG in transfected cells cultured in complete medium without lysosomal inhibitors. (C) Representative experiment of an immunoblot using anti-LC3 antibody in cells treated with or without jasplakanolide (+/-Jpk) to induce FAG and grown in medium with or without (4 h) serum (+/-FBS) in the presence of lysosomal inhibitors. Positions of endogenous LC3-I and LC3-II are indicated. Ratios of LC3-II to tubulin were 2.0, 3.2, 1.0 and 2.1 for the respective experimental condition. (D) Ultrastructure of a cell containing FAG (limited by dashed line) in which autophagic vacuoles appeared tightly associated with FAG. (E-I) MDC-containing vesicles accumulated around FAG (E). During the clearance of FAG occurring after Jpk removal (-Jpk/16 or 24 hours; F,G), MDC-containing vesicles and lysosomes (stained with MDC and/or anti-lamp-2 antibodies) increased and were associated with F-actin puntae and F-actin amorphous aggregates (arrowheads in G). Rpc (200 nM) added after Jpk removal accelerated the dissolution of FAG (compare panels H with F and I with G). Inset in H shows the tight association and partial colocalization of F-actin puntae (red) with lysosomes/MDC-containing vesicles (green/blue). (J) Autophagic vacuoles increased during the dissolution of FAG (-Jpk/36 hours). (K-M) Some autophagic vacuoles contained fragments of microfilaments arranged in parallel (arrow in K; high magnification in L, and M enlargement of the squared area shown in L). Bar, 10 μm (A,B,E-I), 1 μm (J), 200 nm (D), 100 nm (K), 30 nm (L), 10 nm (M).

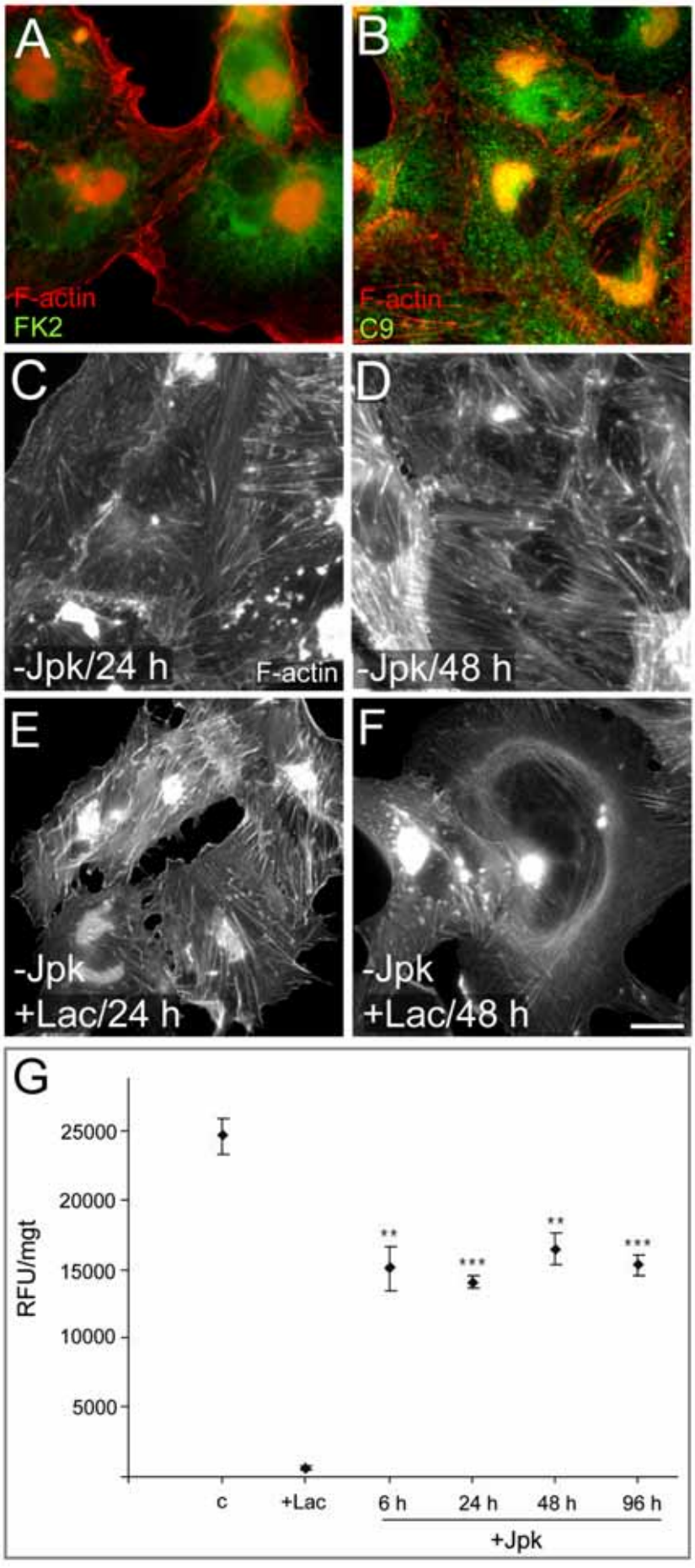

Fig. 8. Proteasomes and proteasomal function in the F-actin aggregate. (A-B) Vero cells containing FAG (red) co-stained with FK2 antibodies to show (poly)ubiquitinated proteins (A, green) or with C9 antibodies to reveal the presence of proteasomes (B, green), indicating that FAG contains proteasomes but not polyubiquitinated proteins. (C-G) FAG clearance was delayed in cells treated with lactacystin (compare panels E with C and F with D). (G) Proteasome activity measured in clarified lysates from untreated Vero cells (control), cells treated with lactacystin (+Lac, 10 μM), or cells treated with Jpk (+Jpk, 50 nM) for different times. Results are the mean ± s.d. from three independent experiments. Differences from control (c) significant at $p \leq 0.01$ (**) and $p \leq 0.001$ (***). Bar, 10 μm.

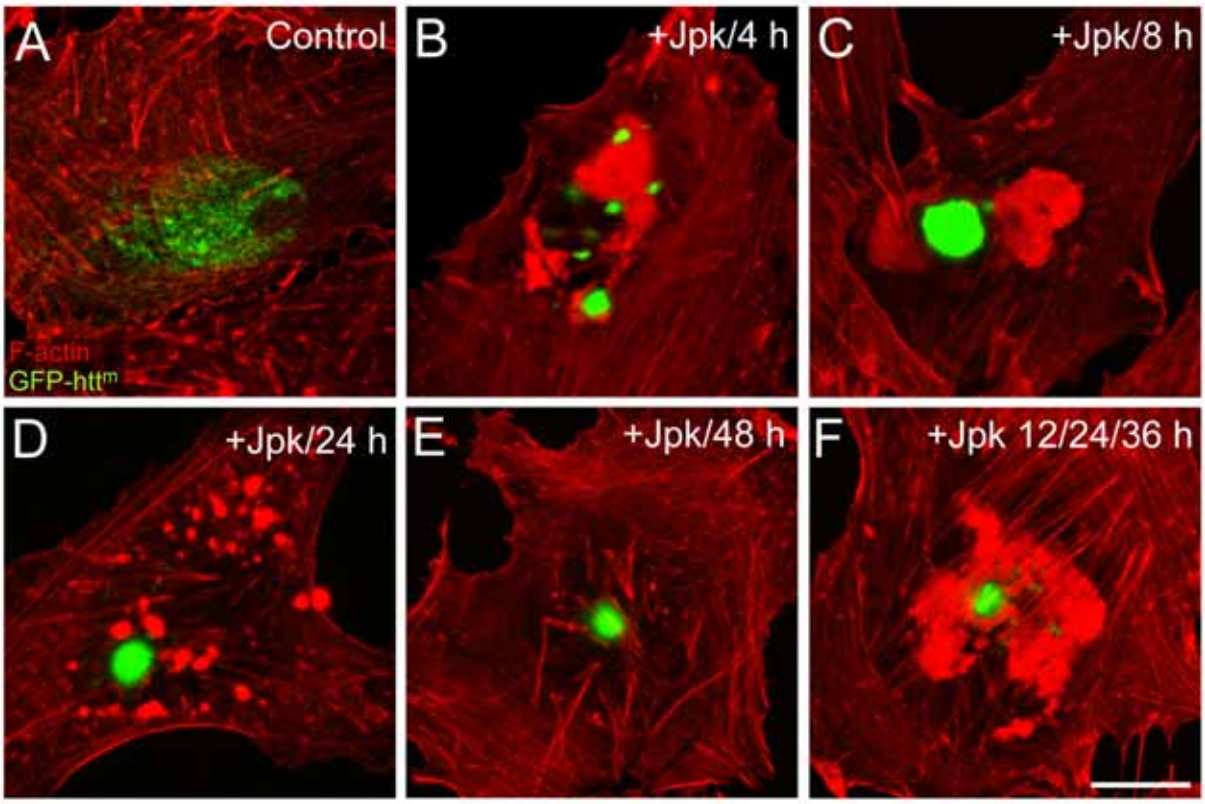

Fig. 9. Cells can generate segregated aggresomes with different molecular composition. Vero cells were transfected with a GFP-huntingtin mutant plasmid (GFP-htt^m). At early expression times of GFP-htt^m (4 hours), a diffuse cytoplasmic staining was seen (green; A). (B-E) Subsequent treatment with Jpk (+Jpk, 50 nM) produced F-actin amorphous aggregates and FAG (B,C, red) as long as the GFP-htt^m aggresome was also forming (B,C, green). At longer Jpk treatment, FAG is fragmented in F-actin amorphous aggregates and F-actin puntae (D, red) until its complete clearance (E), but the GFP-htt^m aggresome (E, green) remained in the cytoplasm. Notice that the two aggresomes one containing GFP-htt^m (green) and the other F-actin (red) remain all the time morphologically and molecularly segregated, even when cells were submitted to various Jpk pulses (F, see supplementary Fig. 1). Bar, 10 µm.

Supplemetary Figures

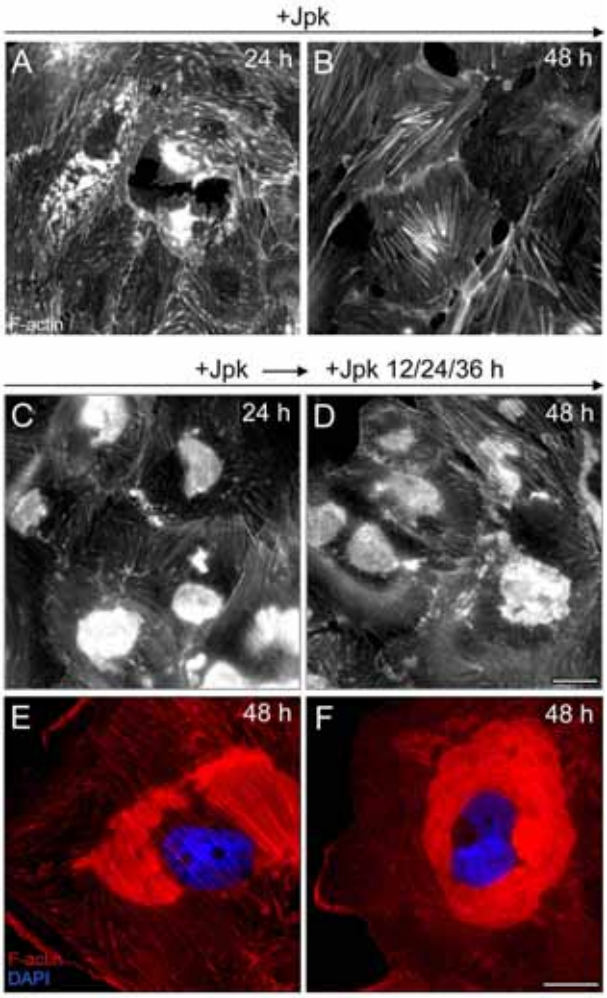

Supplementary Fig. 1. Maintenance and enlargement of the jasplakinolide-induced F-actin aggregate. (A,B) Vero cells were treated with a single pulse of Jpk at low concentration (50 nM) for 24 hours and 48 hours. FAG was not observed after 48 hours. (C-F). When the culture medium of these Jpk-treated cells was replaced every 12 hours (+Jpk 12/24/36 hours) by new medium containing Jpk, FAG lasted longer and was larger (compare C with A and D with B). Cells were stained with TRITC-phalloidin (A-F) and DAPI (blue) (E,F). Bars, 10 µm.

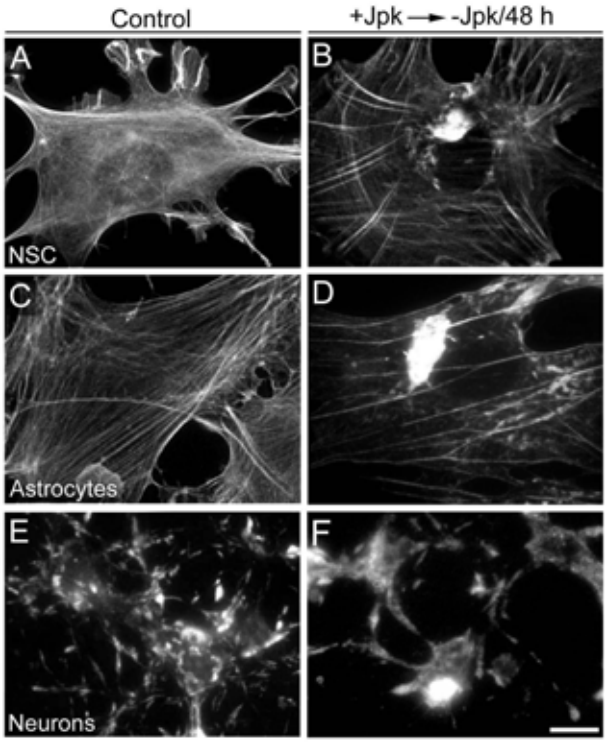

Supplementary Fig. 2. The formation of the F-actin aggregate in neural cells. Mouse c17.2 neural stem cells cells (NSC) (A,B) and primary cultures of rat astrocytes (C,D) or hippocampal neurons (E,F) were treated with Jpk (+Jpk, 500 nM/45 minutes for NSC and astrocytes, or 5 µM/45 minutes for neurons) and Jpk was then washed out (-Jpk/48 hours). Cells were stained with TRITC-phalloidin. Bar, 10 µm.

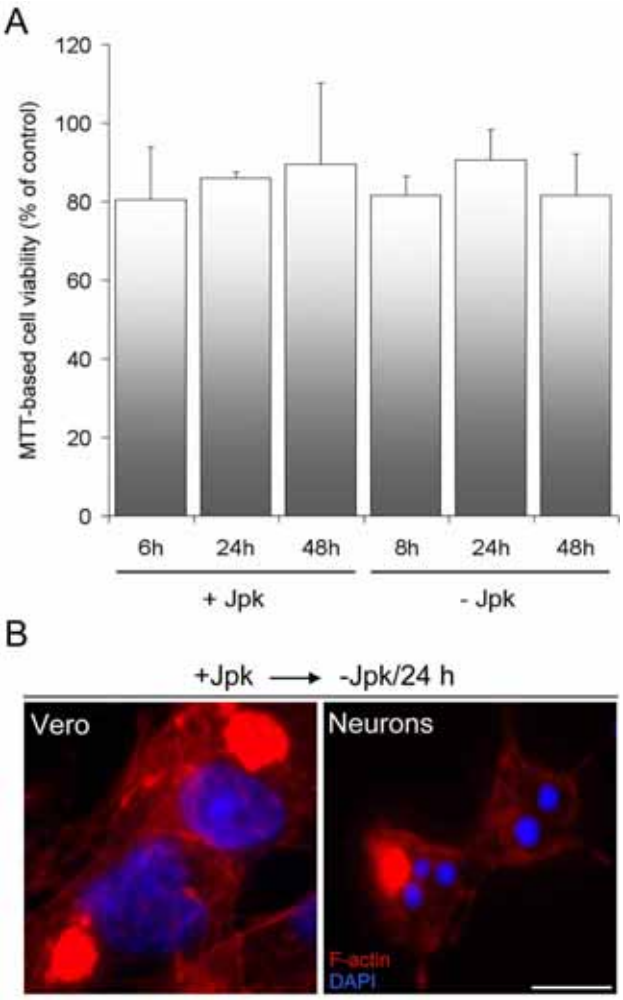

Supplementary Fig. 3. (A) Cell viability is not compromised by the presence of the F-actin aggregate. Cell viability was examined by determining the mitochondrial function (MTT reduction ability) of Jpk (50 nM)-treated (+Jpk) and Jpk (500 nM/45 minutes)-washout (-Jpk) Vero cells for the indicated times. No significant differences were observed. Data represent means ± s.d. for three independent experiments. **(B) The F-actin aggregate triggers apoptosis in hippocampal neurons but not in Vero cells.** FAG was generated by treating Vero and hippocampal neurons first with Jpk at higher concentrations (+Jpk, 5 µM/45 minutes) and then the actin toxin was washed out for 24 hours (-Jpk). Cells were double stained with TRITC-phalloidin (red) and DAPI (blue). Bar, 10 µm.

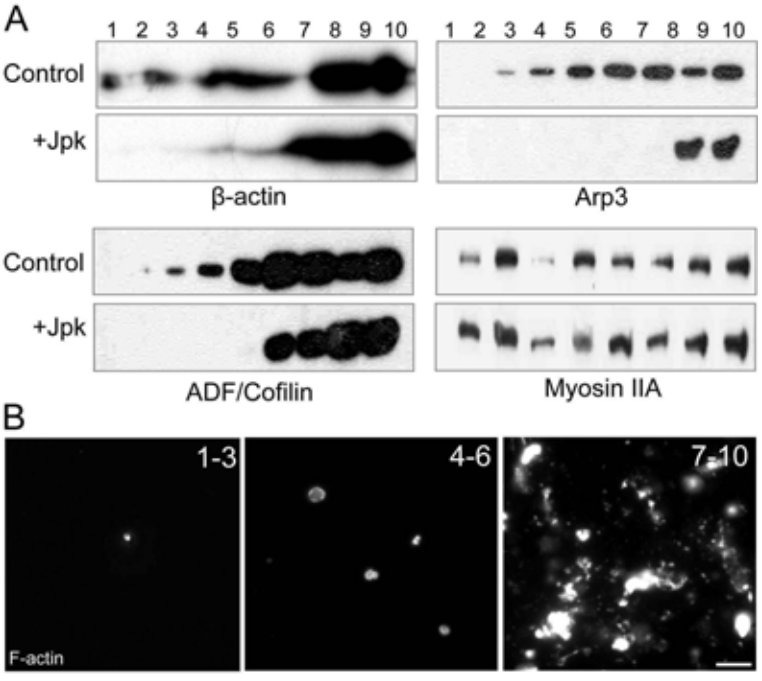

Supplementary Fig. 4. Distribution of cytoskeletal proteins from cell homogenates containing the F-actin aggregates in a discontinuous sucrose density gradient. (A) Homogenates were separated by centrifugation in a discontinuous sucrose density gradient (see Material and Methods). Fractions were collected from the top (#1) to the bottom (#10). Each fraction was immunoblotted for β-actin, Arp3, ADF/cofilin and myosin IIA. (B) TRITC-phalloidin staining of gathered sucrose fractions (indicated at the top of each panel). Bar, 10 µm.

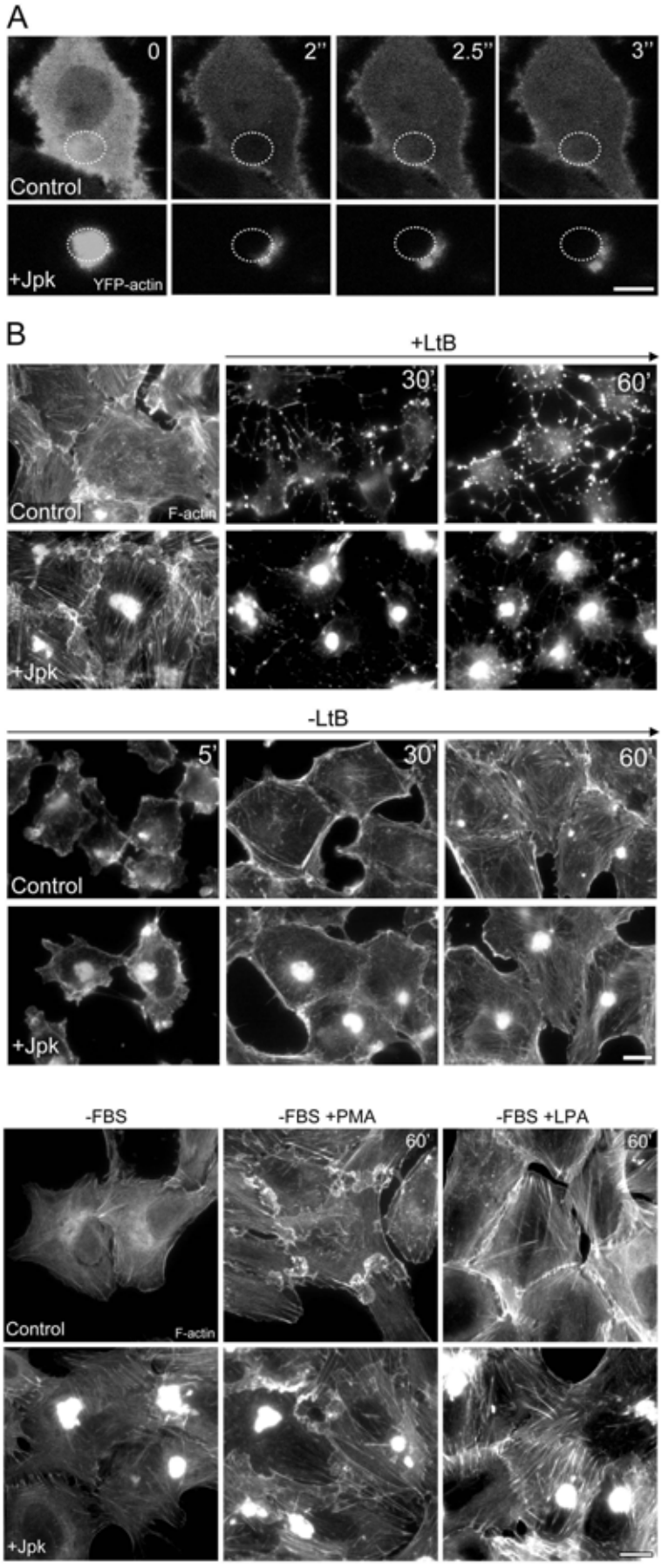

Supplementary Fig. 5. (A) Actin in the F-actin aggregate is non-dynamic. Vero cells were transfected with YFP-actin plasmid. After 24 hours, cells were treated with Jpk (+Jpk, 50 nM/6 hours) to induce the formation of FAG. Subsequently, FAG (B, white circle) or an equivalent portion of the cytoplasm in untreated cells (A, white circle) was subjected to FRAP and movies were recorded to visualize the recovery of fluorescence over time (see movie). Figure shows epresentative frames obtained from videos (time indicated in seconds). **(B) The Jpk-induced F-actin aggregate is resistant to latrunculin B and does not interfere with the reassembly of actin stress fibres that occurs after removal of the toxin.** Untreated Vero cells (Control) or cells treated with Jpk (+Jpk, 50 nM/6 hours) containing FAG were incubated with LtB (+LtB, 500 nM/30 and 60 minutes). In Vero cells without or with FAG the actin toxin was washed out (-LtB, 5, 30, and 60 minutes). Bars, 10 μm.

Supplementary Fig. 6. The presence of the F-actin aggregate does not alter the formation of lamellipodia and stress fibres. Untreated Vero cells (Control) or cells treated with Jpk (+Jpk, 50 nM/6 hours) containing FAG were cultured for 4 hours in the absence of FBS to clarify the cytoplasm of stress fibres (-FBS). The subsequent addition of phorbol myristate acetate (PMA) (1 μM/60 seconds) or lysophosphatidic acid (LPA) (1 μM/60 seconds) quickly induced the formation of lamellipodia and stress fibres, respectively. Cells were stained with TRITC-phalloidin. Bar, 10 μm.

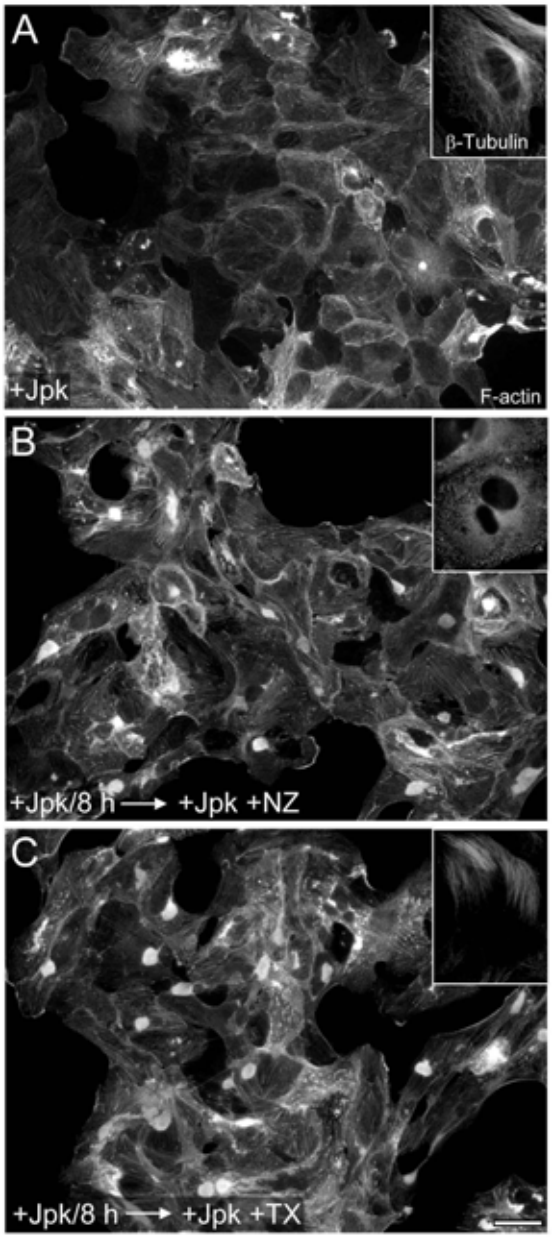

Supplementary Fig. 7. Disruption of microtubules prolongs the life-span of the F-actin aggregate. Vero cells were treated with Jpk (+Jpk, 50 nM/48 hours) alone (A) or pre-treated with Jpk (+Jpk, 50 nM/6 hours) and then co-incubated with nocodazole (30 μM) (+Jpk +NZ) (B) or taxol (30 μM) (+Jpk +TX) until 48 hours (C). Cells were stained with TRITC-phalloidin (A-C). Insets show the MT organization stained with anti-β-tubulin antibodies in untreated (A), NZ (B)- or TX (C)-treated cells after 48 hours. Bar, 20 μm.

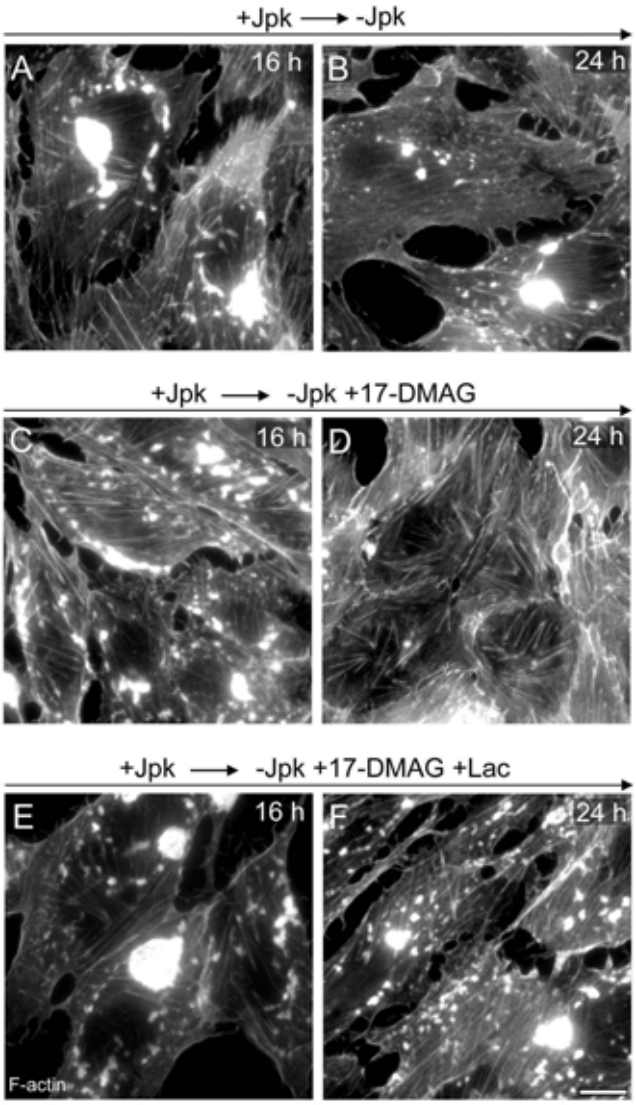

Supplementary Fig. 8. The activation of heat shock proteins accelerates the dissolution of the F-actin aggregate. Vero cells were treated with Jpk (+Jpk, 500 nM/45 minutes) and then the toxin was removed for 16 or 24 hours (A,B). 17-DMAG (10 μM) (C,D) or 17-DMAG plus lactacystin (10 μM) (E,F) was added when Jpk was washed-out and maintained for the same times. Note that 17-DMAG accelerated the dissolution of FAG, which in contrast was normalized by the presence of lactacystin. Bar, 10 μm

Supplementary Table

		Treatment		Withdrawal	
Toxin	***Working concentration***	***T(+)***	***ACSK***	***T (-)***	***ACSK***
CyD	1µM 100 nM	+60' +2/6h	D d, FAP	-15' -60/90' n.d.	d, FAP n n.d.
LtB	500 nM 50 nM	+45' n	D n	-15' -60/90' n.a.	d, FAP n n.a.
MyB	100 nM 10 nM	+60' +2/6 h	D d, FAP	-60/90' -24/32 h -48/56 h n.d.	D d, FAP N n.d.
Jpk	500 nM 50 nM	+45' +1/4 h +6/8 h +12/24 h +32/40 h +48 h	D d, FAP, FAM d, FAG d, FAG, FAM d, FAM, FAP N	-60/90' -3/5 h -6/8 h -16/24 h -32/48 h n.d. n.d. n.d. n.d. n.d.	D d, FAP, FAM d, FAG d, FAM, FAP n n.d. n.d. n.d. n.d. n.d.

Supplementary Table. Effects of treatment and subsequent withdrawal of several actin toxins on the actin cytoskeleton organization of Vero cells. ***Toxins***: cytochalasin D (CyD), latrunculin B (LtB), mycalolide B (MyB), jasplakinolide (Jpk). ***T(+)/T(-)***: time or time interval (/) of treatment (+) or withdrawal (-) of actin toxin in minutes (') or hours (h). ***ACSK*:** actin cytoskeleton organization (n, normal; D, fully disrupted without stress fibres; d, partially disrupted with some stress fibres) or F-actin aggregates/inclusion bodies (FAP: F-actin punctae; FAM: F-actin amorphous aggregates; FAG: single, large F-actin aggregate). n.d. (not determinated). n.a. (not applicable).

Supplementary Movies

Movie 1: FRAP confocal recording of YFP-actin in untreated Vero cells (Control) and in cells containing FAG (Jpk).

Trabajo 5

RESULTADOS ADICIONALES NO PUBLICADOS

5.1. Alteraciones de la red de filamentos de actina en tratamientos prolongados con toxinas de actina a su concentración mínima efectiva

La incubación de células con las toxinas de actina CyD, MyB y Jpk por debajo de su concentración mínima efectiva (ver discusión) en donde se mantiene la morfología celular provoca la formación de agregaciones de actina filamentosa. Cuando las células son expuestas a las toxinas de actina CyD, LtB, MyB y Jpk a la concentración la mínima efectiva se produce la perturbación y el colapso de la arquitectura celular que se refleja por la pérdida de las fibras de estrés y redondeamiento celular. La formación de agregaciones de actina filamentosa también se puede observar tras la retirada de las toxinas de actina MyB y Jpk en células tratadas con estas toxinas. Sorprendentemente observamos agregaciones de actina filamentosa incluso manteniendo en el medio de cultivo 24 h a la concentración mínima efectiva las toxinas CyD, LtB y Jpk, Tras este tiempo se aprecia con claridad la presencia de células binucleadas así como una alteración en la localización del AG.

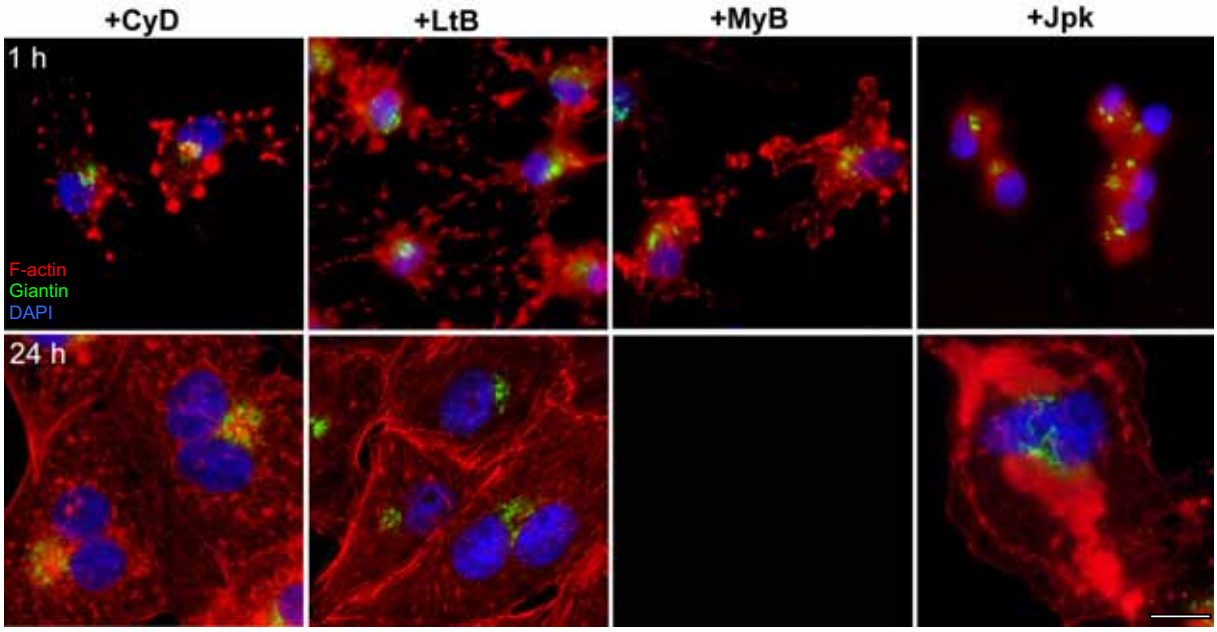

Alteraciones de la red de filamentos de actina en tratamientos prolongados con toxinas de actina a la concentración mínima efectiva. Células Vero fueron incubadas con CyD (1µM/1-24 h), LtB (500 nM/1-24 h), MyB (100 nM/1-24 h) y Jpk (500 nM/1-24 h). Tras ello fueron fijadas y marcadas frente a los MFs con faloidina-TRITC, núcleo con DAPI y AG con giantina. Barra: 10 µm.

5.2. Análisis del flujo de membranas inducido por brefeldina A y distribución subcelular del receptor KDEL en la región retículo endoplasmático-aparato de Golgi en células que presentan un agresoma de actina filamentosa

El agresoma de actina inducido por Jpk (FAG) condiciona la posición del AG, lo cual plantea la posibilidad de que el flujo de membranas entre el ER y el AG estuviese alterado. Tanto el desensamblaje del AG inducido por BfA (A) como el reensamblaje del el AG (B) no están alterados en las células que contienen el FAG. La distribución subcelular del KDELr tampoco se encuentra alterada en las células que presentan el FAG (C). Por consiguiente el FAG no condiciona el flujo de membranas en la zona ER-AG.

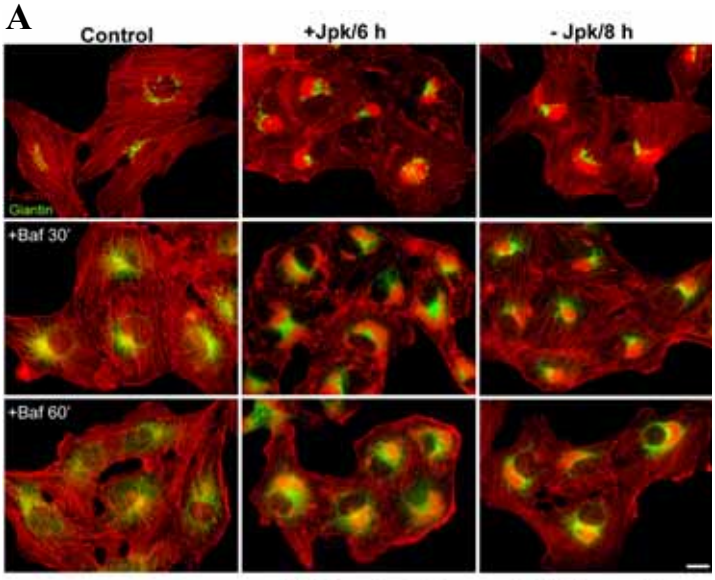

Cinética del desensamblaje del AG inducido por la BfA en células conteniendo el FAG inducido por Jpk. Células Vero se incubaron con Jpk (50 nM/6 h), o (500 nM/1h tras lo cual se elimina la toxina de actina dejándose recuperar 8 h). En este punto, se incubaron con BfA 1 μg/ml 15 y 30 min. El desensamblaje del AG fué visualizado mediante anticuerpos frente a la giantina, los MFs se detectaron con faloidina-TRITC. Barra: 10 μm.

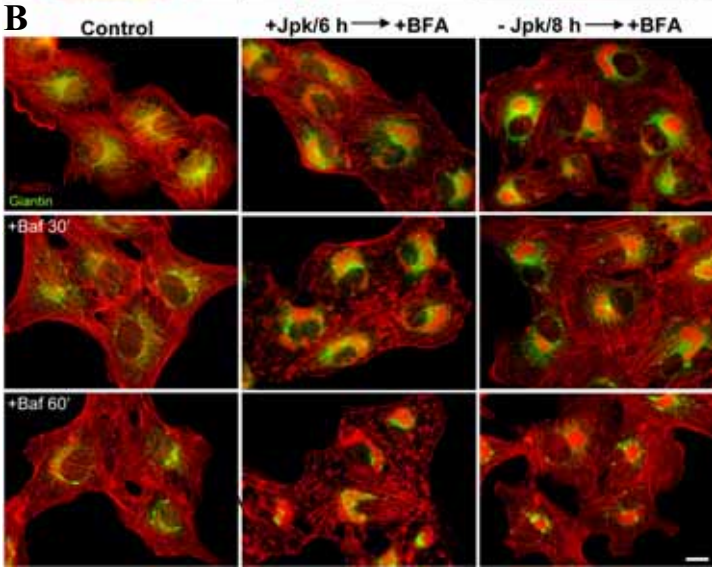

Cinética del reseensamblaje del AG tras la retirada de la BfA en células conteniendo el FAG inducido por Jpk. Células Vero se incubaron con BfA (1 μg/ml /30 min) para inducir el desensamblaje del AG. A continuación fueron coincubadas con Jpk (50 nM/6 h), o (500 nM/1h tras lo cual se elimina la toxina de actina dejándose recuperar 8 h). En este punto, se lava el medio de cultivo y se dejan recuperar 15 y 30 min. El reensamblaje del AG fue visualizado mediante anticuerpos frente a la giantina, los MFs se detectaron con faloidina-TRITC. Barra: 10 μm.

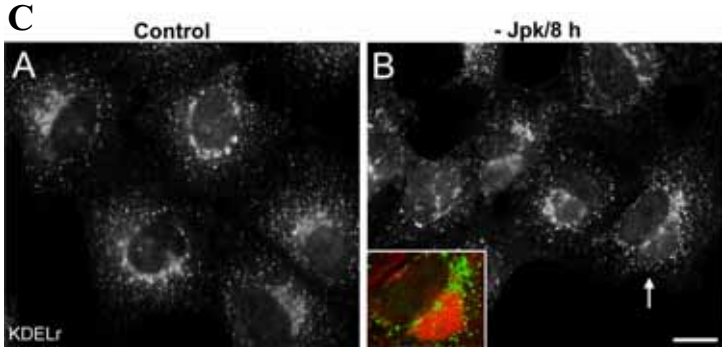

Distribución subcelular del receptor KDEL en células que presentan el FAG inducido por Jpk. Células Vero se incabron con Jpk (50 nM/6 h), o bien (500 nM/1h y tras lo cual se elimina la toxina de actina dejándose recuperar 8 h). Tras ello fueron fijadas y marcadas frente al receptor de KDEL. La flecha señala la zona aumentada en el anexo en la que se muestra la asociación entre la distribución del KDELr y el FAG detectado con faloidina-TRITC. Barra: 10 μm.

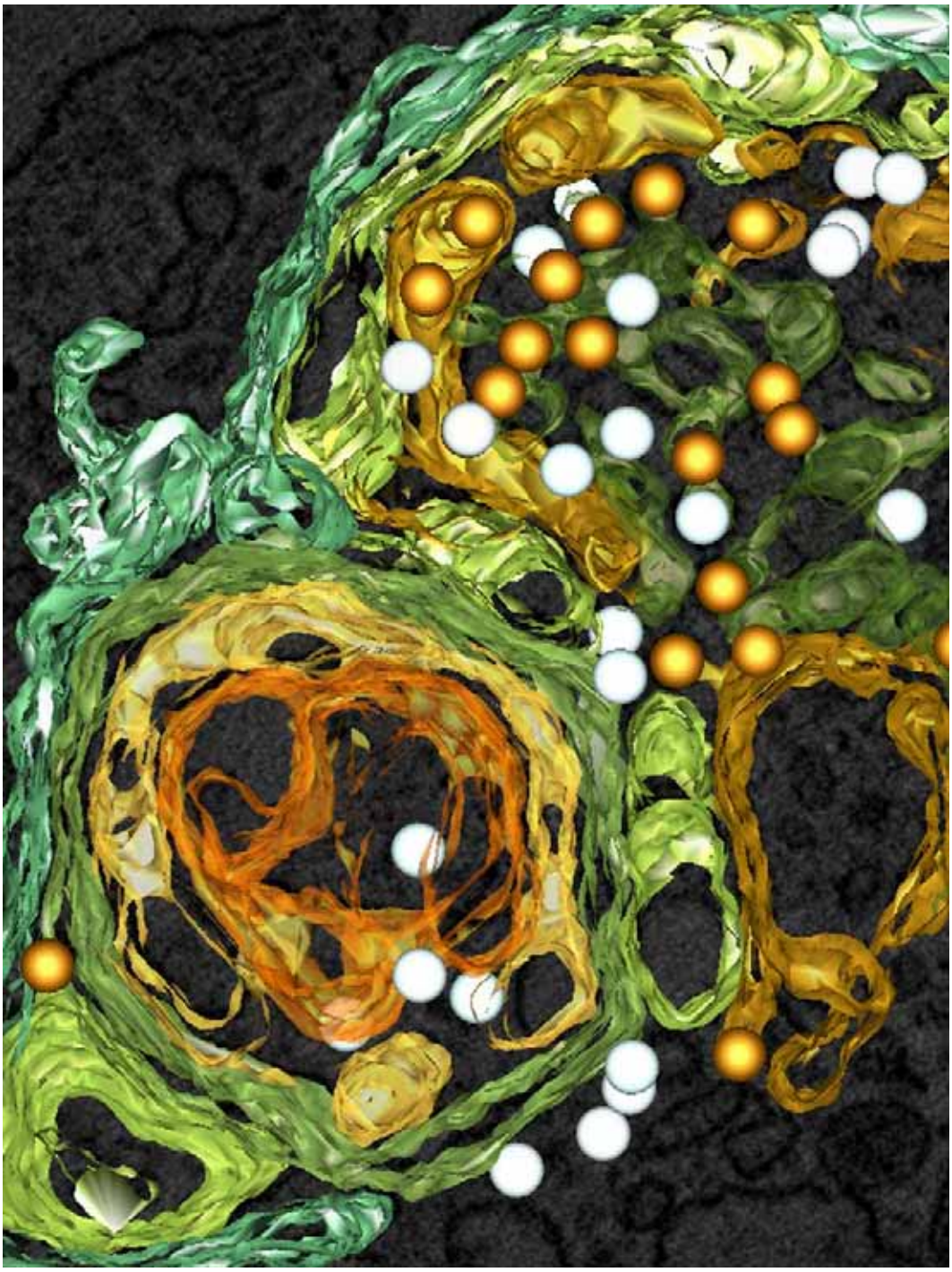

- RESUMEN DE LOS RESULTADOS Y DISCUSIÓN -

El citoesqueleto de actina está implicado en el movimiento, la división celular y en el mantenimiento de la morfología celular. En los últimos años multitud de evidencias experimentales han implicado también a los MFs en las distintas rutas del tráfico intracelular. Nuestro laboratorio ha centrado su investigación en el papel de los MFs en las etapas tempranas del tráfico secretor a nivel de la región RE-AG obteniendo resultados que implican a los MFs y a la maquinaria molecular que regula su dinámica en el transporte desde el AG al RE. Hemos descrito que los MFs son necesarios para mantener la morfología del AG (di Campli et al., 1999; Valderrama et al., 1998) y la presencia de β/γ actina en la zona distal/lateral no compacta de las cisternas del AG y en los ITs de tipo COPI (Valderrama et al., 2000). También hemos localizado en las cisternas del AG los elementos de la maquinaria implicada en la polimerización de actina Cdc42, N-WASP y Arp2/3 (Luna et al., 2002; Matas et al., 2004). A la vista de estos datos nos planteamos que el citoesqueleto de actina no sólo tuviese un papel estructural en el mantenimiento de la morfología del AG sino que también estuviese implicado en su funcionalidad. Así, vimos que los MFs facilitan el transporte desde el RE al AG (Valderrama et al., 2001) en donde participa la miosina II (Duran et al., 2003).

A partir estos resultados nos planteamos realizar un estudio ultraestructural exhaustivo de las alteraciones que acontecen en las cisternas del AG como consecuencia de la perturbación de la dinámica de actina. Estos experimentos podrían aportarnos datos relevantes del papel de la dinámica de actina en la morfo-funcionalidad del AG. Para ello, en primer lugar realizamos un estudio del uso de distintas toxinas de actina en varios tipos celulares que empleamos con frecuencia para estudios del tráfico intracelular. Nos familiarizamos con concentraciones y tiempos de exposición a distintas toxinas de actina analizando sus efectos sobre la morfología célular. El empleo de las toxinas de actina no es trivial y los resultados dependen del tipo celular, concentración de uso y tiempo de exposición (Trabajo 1). A continuación, aplicando esta experiencia, comparamos las alteraciones que provocan estas toxinas de actina sobre la arquitectura del AG estableciendo un modelo que interrelaciona la dinámica de actina con la morfología y homeostasis del pH_G (Trabajos 2 y 4). Siguiendo con las toxinas de actina, posteriormente estudiamos la implicación de los MFs en salida del *cargo* del AG o transporte post-Golgi (Trabajos 3 y 4). Por último, el conocimiento exhaustivo del empleo de las distintas toxinas de actina nos ha permitido generar un modelo celular que mimetiza la formación de agresomas de actina filamentosa sobre el que hemos estudiado la participación de los mecanismos implicados en su formación y posterior desaparición (Trabajo 5).

Implicación de los filamentos de actina en la arquitectura y homeostasis del pH del aparato de Golgi.

Por extensión de lo que ocurre en la formación de un compartimento biológico elemental como las micelas o bicapas lipídicas, la estructura originada de forma espontánea y favorable desde un punto de vista termodinámico que tendría una célula o compartimento subcelular en un entorno acuoso sería de naturaleza esférica. Sin embargo, tanto la célula como la mayoría de compartimentos y/o orgánulos intracelulares adoptan morfologías diversas, lo cual representaría un mecanismo de adaptación celular destinado a la mejora funcional del compartimento. Por ejemplo, las cisternas del AG presentan una morfología aplanada en forma de discos o sáculos apilados, lo cual va en contra de la esperada morfología esférica debida a la hiperosmoticidad del lumen por la cantidad de *cargo* que atraviesa continuamente este orgánulo. La morfología en sáculos apilados probablemente facilite la formación de ITs en las regiones no compactas de la cinta o *ribbon* del AG y/o en la zona no compacta distal/lateral o *lateral rims* de las cisternas de los dictiosomas, facilitando el estrangulamiento y fisión de los mismos. La proximidad y densidad de superficie de membrana accesible entre las cisternas en este tipo de estructuras apiladas facilitaría la modificación y transporte del *cargo* en un espacio menor que en un sistema constituido por cisternas esféricas. En este sentido, el AG es capaz de generar continuidades de naturaleza tubular entre las cisternas del AG, probablemente transitorias como consecuencia de una situación de elevada actividad secretora la cuales revelan la plasticidad morfológica y dinamismo de este compartimento (Marsh et al., 2004; Trucco et al., 2004).

En ausencia de interacciones con fuerzas extracelulares, el citoesqueleto de actina es el principal componente celular que gobierna la morfología tanto de la célula como de los orgánulos intracelulares. En distintas líneas célulares como HeLa, NRK y Vero incubaciones a la concentración mínima efectiva (en la tiene lugar la pérdida de fibras de estrés y adhesión a sustrato con el subsecuentre redondeamiento celular) con toxinas de actina que bloquean/despolimerizan los MFs como la CyD, LtB, MyB y C2 provocan la desaparición de las fibras de estrés y el redondeamiento de la célula al igual que ocurre con el agente polimerizador/estabilizador Jpk. Estas alteraciones se reflejan a nivel de la superficie celular con la formación de estructuras de tipo vesicular/burbuja o *blebs* (Trabajo 1 Figs. 2,3) probablemente debidas a una relajación en cuanto a las fuerzas de tensión ejercidas por la red de F-actina del córtex sobre la membrana plasmática (Charras et al., 2005).

La perturbación de la dinámica del citoesqueleto de actina provocada por estas toxinas induce en todos los casos la compactación del AG cuando las células son analizadas mediante microscopía óptica (Trabajo 2 Supplementary Fig. 1). A nivel de TEM la CyD provoca básicamente la dilatación de las cisternas del AG (Valderrama et al., 1998) con pérdida de la continuidad intra-cisterna pero se mantiene su apilamiento. LtB, MyB provocan la misma alteración fenotípica (Trabajo 2 Fig. 1) observándose además como en el caso de exposiciones a LtB más prolongadas o bien con la toxina C2 la estructura del AG aparece muy desorganizada con una fenotipo electrodenso en el que no se puede distinguir la separación entre cisternas (Trabajo 2 Fig. 1E,G). Este resultado podría representar el estadio final de una serie de cambios sucesivos que acontecen en la morfología del AG en función del grado de despolimerización de los MFs cuya asociación con la membrana de las cisternas del AG resultaría imprencisdible para el mantenimiento de su estructura. Efectivamente, detectamos una bajada progresiva en los niveles de F-actina a lo largo del tiempo para un tratamiento con LtB a la concentración mínima efectiva (Trabajo 2 Resultados adicionales no publicados 2.1 B,C). Por el contrario, el tratamiento con Jpk únicamente provoca la pérdida de continuidad intra-cisterna incluso en exposiciones prolongadas (Trabajo 2 Resultados adicionales no publicados 2.1 D). Así, no solamente se necesita la presencia física de los MFs en torno a la membrana del AG sino también su dinamismo para mantener la integridad estructural del AG en cuanto a la continuidad intra-cisterna. Por otro lado, tanto la depolimerización/bloqueo como la estabilización/polimerización aberrante de los MFs provoca un notable incremento en el número de perfiles vesiculares en la región peri-Golgi, lo cual podría reflejar una alteración en el transporte de los ITs derivados del AG. Estas alteraciones fenotípicas del AG provocadas por las toxinas de actina se cuantificaron determinámdose un incremento significativo en cuanto a la densidad de volumen ($Vv_{cist\text{-}G}$) y superficie ($Sv_{cist\text{-}G}$) de las cisternas respecto al dictiosoma provocada por la despolimerización de los MFs, así como un aumento significativo en el número de perfiles vesiculares peri-Golgi ($Nv_{ves\text{-}G}$) originados tanto por la depolimerización/bloqueo como por la estabilización/polimerización aberrante de los MFs (Trabajo 2 Table I). Mediante tomografía electrónica/reconstrucción 3D, se observó cómo las discontinuidades entre cisternas correponden en realidad a perforaciones/fragmentaciones de las mismas. También se observó un incremento en el número de vesículas o ITs en la región peri-Golgi no asociados a las cisternas del AG (Trabajo 2 Fig. 2, Movies 1-6). Ésto último ratifica las observaciones bidimensionales observadas a nivel de TEM y podría ser indicativo de la necesidad de MFs dinámicos (aquellos en los que no hay alteraciones en el recambio de monómeros de actina) en la región

peri-Golgi, para promover el movimientro de ITs pero no para su fisión de la cisterna del AG. Por otro lado el fenotipo de cisternas desorganizadas electrodensas consecuencia de la despolimerización drástica de los MFs provocada por la C2 o exposiciones prolongadas a la LtB podría ser consecuencia de la acumulación del *cargo* en las cisternas debida a la alteración en el tráfico celular derivado del AG. Resumiendo, la estabilización de la dinámica de los MFs inducida por el Jpk provoca la pérdida de la continuidad intra-cisterna observándose la aparición de perforaciones/fragmentaciones de cisterna, mientras que la despolimerización de los MFs comportará un serie de cambios fenotípicos en la morfología de AG en función del grado de despolimerización de los MFs, originando tras la perforación/fragmentación de las cisternas su dilatación y posteriormente su total desorganización/colapso manteniéndose en todos los casos la posición centrosomal yuxtanuclear y el apilamiento de los dictiosomas. Las mismas observaciones descritas sobre los dictiosomas del AG se observaron a nivel de los minidictiosomas generados tras despolimerizar el citoesqueleto de MTs (Trabajo 2 Supplementary Fig. 2). Según esto, los MFs estarían implicados en el mantenimiento de la morfología aplanada y continuidad intra-cisterna, mientras que los MTs gobernarían el posicionamiento y confluencia centrosomal perinuclear de los dictiosomas manteniendo la integridad de la cinta o *ribbon* del AG. El apilamiento de las cisternas del AG parece ser independiente del citoesqueleto de MTs o MFs, en este sentido el citoesqueleto de espectrina-anquirina asociado al dictiosoma (Beck, 2005) así como por las interaciones entre proteínas de matriz de cisternas del AG, bien entre sí o bien con elementos del citoesqueleto (Short et al., 2005) podrían ser determinantes para el apilamiento de las cisternas del AG.

¿Cómo actuarían los MFs para mantener la forma aplanada de las cisternas?

Nos plantemos dos posibles mecanismos que no son mutuamente excluyentes. Por un lado los MFs, probablemente en conjunción con otros elementos del citoesqueleto como la espectrina-anquirina podrían proporcionar estabilidad mecánica a las cisternas ejerciendo fuerzas de tensión/centrípetas sobre las cisternas del AG que contrarrestarían la dilatación espontánea de éstas debida al elevado contenido proteíco presente en el lumen. La despolimerización de los MFs y la subsecuente dilatación podría incrementar la tensión de membrana de las cisternas (Morris and Homann, 2001; Sheetz, 2001) y por tanto reducir las diferencias de tensión descritas entre el AG y el RE (Upadhyaya and Sheetz, 2004) disminuyendo así el flujo de membrana entre estos compartimentos. Consistente con esta hipótesis, la LtB y toxina C2 provocan un retraso en el desensamblaje del AG inducido por BfA (Valderrama et al., 2001).

Otro posible mecanismo que explicaría las alteraciones provocadas en la arquitectura del AG al perturbar la integridad de la red de MFs estaría en relación con el desacoplamiento entre los MFs y los elementos implicados en la regulación de la homeostasis iónica intracelular como son las H^+-ATPasas vacuolares y los intercambiadores iónicos AEs y NHEs. Se sabe que los MFs interaccionan con estos elementos implicados en la regulación de la homeostasis del pH intracelular. Así, la G/F-actina interacciona directamente con las H^+-ATPasas vacuolares a nivel de la subunidades B y C del dominio V_0 (Holliday et al., 2005; Vitavska et al., 2003; Vitavska et al., 2005). En cuanto a los NHEs las isoformas NHE6, NHE7 y NHE9 interaccionan con la quinasa RACK1 y ésta con las proteínas Src y PKC, ambas implicadas en la polimerización de actina. La supresión de la actividad RACK1 provoca la alcalinización del lumen en los endosomas (Ohgaki et al., 2007). También se ha descrito una asociación entre los NHEs con las proteínas SCAMPs (Lin et al., 2005; Aharonovitz et al., 2000) y PIP_2, el cual está directamente implicado en polimerización de actina (Liao et al., 2007). En cuanto a la interacción de los AEs con los MFs, la isoforma AE1 interacciona con el citoesqueleto de actina-espectrina a través de la anquirina. Por otro lado, se ha descrito la presencia tanto de la H^+-ATPasa vacuolar como de las isoformas AE2 y NHE7 en el AG y/o TGN (Trabajo 2 Resultados adicionales no publicados 2.2) probablemente asociados a microdominios de membrana (Dettmer et al., 2006; Gkantiragas et al., 2001; Nakamura et al., 2005; Holappa and Kellokumpu, 2003; Holappa et al., 2004).

Hay que tener en cuenta también que la actividad de los elementos implicados en la regulación del pH intracelular resulta crucial para el transporte derivado del AG. En este sentido, la inhibición de la H^+-ATPasa vacuolar, de los AEs o NHEs con Baf, NaGlu o Benz, respectivamente, provoca alteraciones en el flujo de membrana en la región RE-AG y un cambio en la distribución del KDELr (Trabajo 2 Resultados adicionales no publicados 2.3). Según esto la alteración de la red de MFs asociados a la membrana de las cisternas del AG podría comportar una alteración en la funcionalidad de los elementos implicados en la regulación del pH_G con las consecuentes alteraciones en la glicosilación de lípidos y proteínas y el tráfico intracelular (Axelsson et al., 2001; Palokangas et al., 1998). En línea con esta hipótesis resulta interesante que tanto la perturbación de la actividad H^+-ATPasa vacuolar (Yilla et al., 1993) como la despolimerización de actina (Jacob et al., 2003; Cobbold et al., 2004) provocan una alteración del transporte post-Golgi. Consistente con estos datos es la observación del incremento significativo de ITs alrededor de las cisternas en las células

tratadas con las toxinas de actina, los cuales probablemente requieran la presencia de MFs dinámicos para su transporte. Alternativamente, la retención de los ITs podría ser consecuencia de un retraso en su transporte provocado por un impedimento físico o barrera de actina filamentosa amorfa producto de la polimerización aberrante de actina inducida por el Jpk.

Analizando el AG a nivel ultraestructural observamos como la incubación de células con inhibidores específicos de la H^+-ATPasa vacuolar como la Baf o la ConA provocan la fragmentación, dilatación y estructura difusa electrodensa de cisternas al igual que ocurre al despolimerizar los MFs con LtB. Por su parte la alteración de la actividad de los AEs o NHEs provoca, respectivamente, la disminución en el número de cisternas integrantes del dictiosoma o bien la pérdida de continuidad intra-cisterna pero nunca la dilatación de las cisternas (Trabajo 2 Fig. 4, Resultados adicionales no publicados 2.4). Este resultado sitúa a la H^+-ATPasa vacuolar como el principal candidato para mediar el efecto de la despolimerización de los MFs sobre el fenotipo del AG. Teniendo en cuenta que a las cocentraciones de Baf utilizadas no se observaron alteraciones en el estado estacionario de la redes de los distintos elementos del citoesqueleto, las hipotéticas fuerzas de tensión/centrípetas ejercidas por los MFs en la estructura de las cisternas serían insuficientes para contrarrestrar el desequilibrio homeostático/osmótico generado por la Baf y mantener la integridad de las cisternas a no ser que la ésta actuase precisamente en el punto de anclaje entre las cisternas y los MFs, lo cual podría provocar la pérdida de su interacción y por tanto una relajación en las fuerzas de tensión/centrípetas. En este sentido la estabilización de los MFs podría prevenir el efecto de la Baf sobre la arquitectura del AG solamente en el caso de que exista una diferencia en cuanto a la hipotética regulación de la actividad de la H^+-ATPasa vacuolar entre MFs dinámicos y estabilizados por el Jpk ya que la Baf actúa igualmente en presencia de MFs dinámicos. Es importante destacar que tanto la Baf, como el NaGlu y el Benz provocan un incremento notable del número de perfiles túbulo-vesiculares en la zona peri-Golgi, resultado que está en concordancia con las alteraciones en el flujo de membrana provocadas por estos agentes en la región RE-AG. En este sentido la inhibición de la actividad de la H^+-ATPasa vacuolar podría estar afectando tambíen de alguna manera la formación de los ITs, ya que al menos en endosomas tempranos, se ha establecido una interacción entre proteínas implicadas en la formación de estos y las subunidades c, a del dominio V_0 de la H^+-ATPasa vacuolar en los endosomas tempranos (Hurtado-Lorenzo et al., 2006).

Concomitantemente a las alteraciones ultraestructurales observadas en el AG detectamos un incremento significativo en el pH_G como consecuencia bien de la inhibición específica de la H^+-ATPasa vacuolar o bien de la despolimerización los MFs (Trabajo 2 Tabla II). Se pudo observar como tras retirar las toxinas de actina del medio de incubación se restaura simultáneamente tanto la estructura del AG como los niveles del pH_G (Trabajo 2 Fig. 3, Suplementary Fig. 3, Tabla II). Así, los efectos similares sobre la estructura del AG y el pH_G provocados por la despolimerización de actina o la inhibición de la H^+-ATPasa vacuolar sugieren una asociación entre la red de MFs y las H^+-ATPasas vacuolares destinada al mantenimiento de la morfología aplanada de las cisternas del AG.

La H^+-ATPasa vacuolar hidroliza ATP en el dominio V_1 provocando la rotación de un complejo rotatorio relativo a la parte estacionaria de la enzima, lo cual induce la translocación del H^+ a través de un dominio integral V_0. El hecho de que el Jpk no provoque dilatación de cisternas podría interpretarse como un requerimiento fisico de MFs no necesariamente dinámicos por parte de las H^+-ATPasas vacuolares para ejercer su actividad. Así, los MFs probablemente actuarían como puntos de anclaje para la H^+-ATPasa vacuolar, bien para retenerla en zonas concretas de la membrana o bien para aportarle la estabilidad mecánica requerida por la parte estacionaria de la H^+-ATPasa vacuolar para permitir la rotación del complejo rotatorio. En este sentido, la subunidad B de la H^+-ATPasa vacuolar, la cual interaciona con los MFs, ha sido descrita en zonas "rígidas" de membrana a nivel de microdominios ricos en colesterol y esfingomielina (Gkantiragas et al., 2001) y en balsas lipídicas obtenidas de células B (Mielenz et al., 2005). Esta observación estaría en relación con la asociación encontrada para el citoesqueleto de actina-espectrina con el AE2 en la membrana del eritrocito en donde la adición de ácido palmítico a la anquirina constituiría una señal para la retención de ésta en las balsas lipídicas. Así, tanto la H^+-ATPasa vacuolar como el AE2 se localizarían en las balsas lipídicas, representando estos domínios de membrana una región donde se establecerían puntos de anclaje entre la red del citoesqueleto de actina con la membrana. Probablemente la retención de elementos implicados en la homeostasis iónica en las balsas lipídicas constituye un mecanismo para asegurar de estos elementos en los ITs derivados de balsas lipídicas y/o destinado a la preservación del balance iónico de un determinado compartimento en los ITs derivados de éste. En este sentido, se ha descrito la implicación de la H^+-ATPasa vacuolar en la formación de ITs (Geyer et al., 2002; Hurtado-Lorenzo et al., 2006; Ying et al., 2000). En conjunto los resultados presentados demuestran

que los MFs estan implicados en el mantenimiento de la estructura aplanada de las cisternas del AG en donde, probablemente participan regulando la actividad de las ATPasas vacuolares presentes en el AG.

Implicación de los filamentos de actina en la salida de *cargo* del aparato de Golgi

Teniendo en cuenta que el desensamblaje de los MFs comporta una alteración en el transporte desde el AG y el RE, no planteamos estudiar si el transporte post-Golgi desde el TGN a la membrana plasmática se encuentra comprometido al perturbar la dinámica del citoesqueleto de actina con la LtB o el Jpk, concretamente a nivel de la salida del cargo del AG/TGN. Para ello, empleamos la técnica de FRAP inverso, la cual nos permite estudiar la cinética de salida del cargo del AG/TGN de distintas proteínas con destino apical o basolateral asociadas o no a balsas lipídicas. En las proteínas no asociadas a balsas lipídicas con destino basolateral (VSV-G) o su mutante con destino apical (VSV-G mut) se observó un comportamiento variable en cuanto al requerimieto físico y/o dinámico los MFs. La estabilización y despolimerización de los MFs comporta un retraso significativo en la salida del VSV-G con destino basolateral, mientras que en el caso del VSV-G mut con destino apical solamente la despolimerización de los MFs retrasa su salida del TGN. (Trabajo 3 Fig. 2). Así, la salida de *cargo* del AG/TGN no asociado a balsas lipídicas con destino basolateral y apical requiere de la presencia de los MFs aunque únicamente el *cargo* con destino basolateral requiere de MFs dinámicos.

También se observó como la salida del *cargo* con destino basolateral es más rápida que el destinado apicalmente como se puede apreciar en las curvas de pérdida de fluorescencia en el área del AG del VSV-G y el VSV-G mut, respectivamente (Trabajo 3 Fig. 2A,B). En este sentido la fracción móvil (porcentaje de pérdida de fluorescencia en el AG) para el VSV-G es mayor que para el VSV-G mut en el tiempo medio $T_{1/2}$ (tiempo en el que el 50% de la fluorescencia correspondiente a la fracción móvil se pierde) (Trabajo 3 Tabla 1). Se ha de destacar que el retraso provocado en la salida del VSV-G por el Jpk es incluso mayor que lo observado con la LtB, es decir la disminución o ausencia de MFs provoca un retraso menor que su estabilización o polimerización amorfa. Esto podría interpretarse en el sentido de que los MFs facilitarían el la salida del AG de *cargo* con destino basolateral, su disminución o ausencia frenaría la salida del éste mientras que su estabilización o polimerización amorfa supondría una barrera o impedimento fisico para la formación/fisión del IT. Sin embargo,

según el estudio a nivel de TEM y tomografía electrónica/reconstrucción 3D (Trabajo 2 Fig. 2, Movies 1-6) la exposición a Jpk provoca el acúmulo de vesículas en la región peri-Golgi pero no una alteración en su formación/físión ya que no se observarón gemas a nivel de las cisternas del AG. Con lo cual, suponiendo válido el modelo descrito en el trabajo 4, la F-actina estable o amorfa de la región peri-Golgi producto de la exposición al Jpk, representaría una barrera fisica para los ITs con destino basolateral que frenaría su llegada hasta los MTs. La ausencia de MFs frenaría su salida pero no interferiría en su formación/físión ya que tampoco se observó un incremento de gemas en las cisternas en los estudios ultraestructurales.

Paralelamente se estudió la salida del AG de otra proteína no asocida a balsas lipídicas con destino apical, el receptor de neurotrofinas p75 (p75NTR). A diferencia de lo ocurrido en la salida del VSV-G mut, tanto la LtB como el Jpk provocan un retraso en su transporte. Comparando la curva de pérdida de fluorescencia para el p75NTR en células expuestas o no a las toxinas de actina (Trabajo 3 Fig. 3A), los MFs no participarían en la salida de los ITs conteniendo ésta proteína puesto que el retraso aparece aproximadamente tras 10 minutos de seguimiento observando a este tiempo una clara disminución de la fracción móvil tanto para la LtB como el Jpk respecto al control (Trabajo 3 Tabla 1). Por el contrario, como se acaba de comentar, los MFs si que podrían participar en la salida inicial de los ITs conteniendo *cargo* con destino apical ya que desde el principio se observa una diferencia significativa en la salida del VSV-G mut entre las células incubadas con LtB respecto al control, lo cual es mucho más evidente en la salida del VSV-G (Trabajo 3 Fig. 2AB). La sensibilidad del p75NTR al Jpk respecto al VSV-G mut podría ser debida a que el p75NTR contiene tres motivos di-leucina en su secuencia que podrían ser los responsables de su respuesta similar frente al Jpk en cuanto a la salida del AG/TGN observada para el VSV-G (Jespersen et al., 2004; Johnson et al., 1986).

Por último se estudió la salida con destino apical de YFP-GPI asociada a balsas lipídicas con destino apical. En este caso la perturbación del citoesqueleto de actina con la LtB o el Jpk no provocó ninguna alteración en la salida del AG/TGN de esta proteína. Según esto, la salida del AG de ITs con destino apical asociados a balsas lipídicas sería independiente de la presencia y/o dinámica de los MFs (Trabajo 3 Fig. 3B). Este resultado fue inesperado teniendo en cuenta la asociación descrita entre las balsas lipícas y los MFs a nivel de la membrana plasmática (Caroni, 2001). Una posible explicación a este hecho es que las balsas lipídicas a nivel de AG/TGN presentan una concentración mucho menor de PIP_2 en

comparación con la membrana plasmática (De Matteis and Godi, 2004; Minogue et al., 2006). Además se sabe que a diferencia de lo que ocurre con la salida del *cargo* con destino apical no asociado a balsas lipídicas la oligomerización de proteínas ancladas al GPI es suficiente para mediar su salida del AG/TGN (Paladino et al., 2007; Polishchuk et al., 2004). Resumiendo el transporte post-Golgi de ITs a nivel de la salida de *cargo* en el AG/TGN para proteínas asociadas a balsas lipídicas con destino apical sería independiente del citoesqueleto de MFs mientras que el transporte de *cargo* no asociado a balsas lipídicas sería dependiente en mayor o menor medida de la presencia y dinámica de los MFs.

Estudio de la formación y degradación de un agresoma de actina filamentosa

Una característica común a multitud de enfermedades en las que tiene lugar la perturbación del citoesqueleto es la formación de CIs debida a la agregación de péptidos y proteínas integrantes o relacionadas con el citoesqueleto como consecuencia de alteraciones en su ensamblaje, mutaciones o interacciones anómalas con otras proteínas. La relevancia fisiológica de los CIs es desconocida en cuanto a si estas estructuras tienen una función protectora o son perjudiciales para la célula (Ciechanover and Brundin, 2003; Ross and Poirier, 2004). Los enfermos de Alzheimer y alcohólicos crónicos presentan en el soma de neuronas del hipocampo agregaciones paracristalinas de actina filamentosa en los CHs, los cuales se ha postulado que se forman como consecuencia de la agregación centrosomal (en forma de agresoma) de agregados dispersos citoplasmáticamente de F-actina conocidos como barras de actina o *actin rods* (Minamide et al., 2000).

Manipulando el citoesqueleto de actina con las toxinas CyD, LtB, MyB y Jpk se originan agregados de actina en la región centrosomal o bien agregados dispersos por el citoplasma. Tanto el efecto como la reversión de las toxinas de actina a las concentraciones mínimas efectivas promueven la aparición de estos agregados que también son generados realizando incubaciones con estas toxinas por debajo de la concentración mínima efectiva. Situación en la que no se produce el típico colapso/redondeamiento celular (Trabajo 5 Fig 1,2, Supplementary Fig. 1, Supplementary Table, Resultados adicionales no publicados 5.1). La actividad estabilizadora de MFs y/o de nucleación/polimerización aberrante de actina inducida por el Jpk (Bubb et al., 2000) provoca la formación de pequeños agregados de actina filamentosa (F-actin puntae), los cuales se agrupan formando agregados amorfos de F-actina

que finalmente se concentran de manera MT-dependiente en la región centrosomal (Trabajo 5 Fig. 5) dando lugar a un único gran agregado de F-actina no dinámica o FAG (Trabajo 5 Supplementary Fig. 5, Movie 1). En este sentido, la actina filamentosa contenida en el FAG probablemente presente una estructura aberrante consecuente de la polimerización amorfa inducida por el Jpk lo cual explicaría la relativa escasez de estructuras filamentosas detectadas a nivel de TEM (Trabajo 5 Fig. 3) así como la falta de dinamismo de los MFs.

De forma similar a la acumulación de barras de actina para originar un CH, el FAG también se forma a partir de la acumulación de agregados menores de actina filamentosa. Este comportamiento junto con la distribución de FIs y la acumulación de mitocondrias alrededor del FAG nos permiten definir a éste como un agresoma de actina filamentosa (Bauer and Richter-Landsberg, 2006; Garcia-Mata et al., 2002; Grenier et al., 2006; Johnston et al., 1998; Muqit et al., 2006). En este sentido, también se observó una alteración en el posicionamiento celular del AG inducida por el FAG (Trabajo 5 Fig. 3A,B). Sin embargo, la presencia del FAG no perturbaría el tráfico intracelular ya que no se observaron alteraciones en el flujo de membrana entre el AG y el RE inducidas por BfA o en la distribución subcelular del KDELr (Trabajo 5 Resultados adicionales no publicados 5.2). Por otro lado, también se observó que la presencia del FAG no interfiere con otros procesos celulares en los que se requiere la polimerizacion de actina como son la formación de lamelipodios y/o fibras de estrés (Trabajo 5 Supplementary Fig. 6).

La localización de cortactina, Arp2/3 y ADF cofilina en los FAGs *in situ* o aislados de células Vero o bien en astrocitos, células de neuroblastoma y neuronas de hipocampo (Trabajo 5 Fig. 4 y Supplementary Figs. 2,4) así como en los CHs (Galloway et al., 1987; Maciver and Harrington, 1995) sugiere que la maquinaria implicada en la dinámica de polimerización de actina se encuentra alterada en las células neurales de aquellas enfermedades en las que se detectan CIs de actina filamentosa como el CH en la enfermedad de Alzeheimer. En este sentido se ha propuesto que la formación de los CHs debida a la sobreexpresión de fragmento C-terminal de una proteína de entrecruzamiento de actina de 34 kDa de *D. discoideum* es consecuencia de la función aberrante del citoesqueleto de actina. Sin embargo, el CH obtenido por esta aproximación no altera ni la morfología ni el crecimiento o movilidad de las células que lo contienen (Davis et al., 2008).

Es importante destacar que el FAG no compromete la viabilidad celular (Trabajo 5 Supplementary Fig. 3), lo cual estaría a favor de su función como una estructura "protectora" (al menos inicialmente). Probablemente un agresoma no constituya en sí mismo una estructura citoprotectora sino que es el producto de la acción distintos sistemas/mecanismos celulares "citoprotectores" destinados al mantenimiento de la homeostasis proteica celular. Estos mecanismos actuarían frente a la presencia de proteínas anómalas etiquetándolas y concentrándolas/posicionándolas en una determinada localización citoplamática seguramente favorable y/o accesible a los sistemas/mecanismos de proteólisis intracelular. Por otro lado, se observaron gran cantidad de células no neurales binucleadas conteniendo el FAG, lo cual puede ser indicativo de una parada de la división celular en la fase citoquinesis y por tanto interfiriendo en la proliferación. Esto se explicaría bien por una deficiencia en la disponibilidad de F-actina dinámica necesaria para la formación del anillo contráctil de actomiosina que media la división celular o bien debido a que el FAG representaría un impedimento fisico que obstaculizaría con la formación del anillo contráctil de actomiosina. A diferencia de las células Vero (Trabajo 5 Supplementary Fig. 3B), se detectaron núcleos apoptóticos en neuronas que contenían el FAG. Así, las neuronas resultan más vulnerables al efecto del Jpk debido probablemente a diferencias en cuanto a la dinámica intrínseca de los MFs, con lo que la exposición al Jpk a una misma concentración podría inducir apoptosis o no en función del tipo celular estudiado. En este sentido, no podemos descartar que la apoptosis de las neuronas sea consecuencia de la exposición propia exposición al Jpk y no por la presencia del FAG en el soma celular. Según este razonamiento los agresomas no constituirían un elemento citotóxico para la célula (al menos inicialmente). Esta idea es apoyada por los resultados observados en cuanto a la función mitocondrial/viabilidad celular y tráfico intracelular, los cuales no se ven alterados por la presencia del FAG.

El elevado contenido de actina filamentosa en el FAG, estabilizada o aberrante, sugiere que no puede ser inmediatamente degradado por los sistemas de degradación proteíca celular. Consecuentemente la célula intensifica la proteólisis celular con la finalidad de eliminar el agresoma. La acumulación de mitocondrias en torno al FAG podría interpretarse como un mecanismo celular destinado a proporcionar localmente niveles de ATP elevados para ser consumidos probablemente por los sistemas de degradación proteica. En este sentido, detectamos la presencia del proteasoma, (Trabajo 5 Fig. 8) lisosomas (Trabajo 5 Fig 6) y autofagosomas/vacuolas autofágicas (Trabajo 5 Fig 7) asociados con los F-actin puntae, agregados amorfos de F-actina y el FAG. Además la estimulación de la autofagia o las

chaperonas provoca una aceleleración en la degradación del FAG (Trabajo 5 Fig 7 y Supplementary Fig. 8) mientras que el uso de fármacos que interfieren en la función del proteasoma o sistema lisosomal y autofagia provoca un retraso en su degradación (Trabajo 5 Figs. 6,8). Curiosamente la despolimerización de los MTs retrasa la desaparición del FAG (Trabajo 4 Supplementary Fig. 7), lo cual podría ser debido a la redistribución de los lisosomas y autofagosomas/vacuolas autofágicas (Iwata et al., 2005) o bien debido a una alteración en la fusión de los autofagosomas con los lisosomas (Rubinsztein et al., 2005). Por otro lado, la ausencia poliubicuitina en la actina filamentosa contenida en el FAG junto con la presencia de la partícula 20S del proteasoma (Asher et al., 2006) indica que el SUP actúa sobre el FAG de manera ubicuitina-independiente. En este sentido, la degradación del FAG podría ser promovida por el antizima, que se localizada en el centrosoma y que está implicado en la degradación proteosomal de proteínas implicadas en la proliferación celular de manera ubicuitina-independiente (Mangold et al., 2008). Por último cabe mencionar a las calpaínas, las cuales han sido asociadas con la degradación de elementos de citoesqueleto de actina como la cortactina por lo que también podrían estar implicadas en la degradación del FAG y éstas a su vez promover la autofágia (Hoyer-Hansen et al., 2007).

La formación de FAGs conjuntamente a los agresomas de huntingtina mutada revela como la célula es capaz de concentrar en una misma región dos agresomas de distinta composición molecular sin meclar sus componentes (Trabajo 5 Fig. 9). La ausencia de fusión entre estos dos tipos de agresomas constituiría una evidencia alternativa a favor de la falta de dinamismo intrínseco en los agresomas ya que de ser estructuras dinámicas probablemente tendría lugar la mezcla de sus componentes debido a que sendos agresomas se concentran yuxtanuclearmente en una misma región. Así, los agresomas corresponderían a estructuras inertes acumuladas en el centrosoma, donde posteriormente la célula promueve su degradación. Esta localización no parece ser circunstancial y podría interpretarse como un mecanismo celular destinado a incrementar la accesibilidad y/o eficiencia de actuación sobre el agresoma de los distintos sistemas/orgánulos implicados en su eliminación. El centrosoma representaría el punto de confluencia de estos sistemas/orgánulos siendo su reclutamiento/centralización eficientemente mediada por la red de MTs y motores asociados. La prevalencia en el tiempo del agresoma de huntingtina frente al FAG sería consecuencia de la contínua expresión de la huntingtina mutada frente al tratamiento putual o pulso de Jpk. Por el contrario, la aplicación repetida de Jpk mantiene el FAG en el citoplasma aumentando su tamaño y observándose como éste preserva su identidad molecular sin mezclarse con la

huntingtina mutada que en principio se sintetiza continuamente. El aporte contínuo de proteína aberrante en el agresoma de hungtintina mutada podría comprometer la viabilidad celular ya que los mecanismos/sistemas de degradación proteica no serían capaces de contrarrestar la cantidad de proteína aberrante originada. En este punto el agresoma podría convertirse en una estructura citotóxica ya que escaparía al control o regulación de la homeostasis proteíca intracelular, lo cual desencandenaría la apoptosis de la célula.